New indium Lewis acids for catalysis

Cotgreave, Jamie Howard

Award date:
2004

Awarding institution:
University of Bath

NEW INDIUM LEWIS ACIDS FOR CATALYSIS

Jamie Howard Cotgreave

A thesis submitted for the degree of Doctor of Philosophy

University of Bath

Department of Chemistry

October 2004

ProQuest LLC
789 East Eisenhower Parkway
P.O. Box 1346
Ann Arbor, MI 48106-1346

Dedicated to Mum, Dad,

Anna and Robin

Contents

Acknowledgements

I would like to thank Dr Chris Frost and particularly Dr Andrew Weller for all their encouragement, support and enthusiasm throughout my PhD. I would also like to thank Dave Colclough for his support and advice. Thanks also to Dr Gus Ruggerio for DFT calculations on complex **(7)** and Gabriele Kociok-Köhn and Mike Ingleson without whom I would not have any crystal structures to report. GlaxoSmithKline and the EPSRC are thanked for funding.

On a social note I would like to thank Nico, Mark, Nathan and Adem in the Weller lab. More importantly thanks to Susie for her never ending supply of tea bags and amusing laboratory moments, Graham and Cheryl for being great housemates and Mike for his dazzling football skills and "comic genius" which have contributed to making the last 3 years a highly enjoyable experience. Lastly and most importantly, immense thanks to Jane for her love and understanding.

Abbreviations

NMR	Nuclear Magnetic Resonance
Hz	Hertz
Å	angstrom (1×10^{-10}metres)
δ	Chemical Shift
ppm	Parts per million
R	alkyl
Me	methyl
Et	ethyl
Bu	butyl
Ph	phenyl
Ac	acyl
o	ortho
m	meta
p	para
s	singlet
d	doublet
t	triplet
Mes	mesityl (2,4,6-trimethylphenyl)
(iMes)	1,3-dimesitylimidazol-2-ylidene
(iMes)Cl	1,3-dimesitylimidazolium chloride
$(iMes)^+$	1,3-dimesitylimidazolium cation
$H(NTf_2)$	bistrifluoromethanesulfonimide
H(OTf)	trifluoromethanesulfonic acid
Tf	trifluoromethanesulfonyl
1D	one-dimensional
L	ligand
TMS	trimethylsilyl
$MeNO_2$	nitromethane

Abstract

The stoichiometric reaction of trimethylindium with bulky β-ketoimine ligands (which contain a single acidic proton) provides a clean pathway to new indium complexes. The reactions result in elimination of one equivalent of methane gas and a range of bismethylindium β-ketoimine products which have been spectroscopically and structurally characterised. Manipulation of these complexes in methyl substitution reactions resulted in complex decomposition via cleavage of the β-ketoimine bonds with the indium metal so the capping ligand was replaced with the bulky *N*-heterocyclic carbenes which coordinate to the metal more strongly.

The reaction of trimethylindium with the carbene (iMes) and (iMes)Cl provides a new high yield route to a pair of air stable compounds. These two compounds: $Me_2ClIn(iMes)$ and $Me_3In(iMes)$, are ideal precursors to more reactive indium triflate and triflamide complexes and are produced by their reaction with TMS(OTf), H(OTf) and $H(NTf)_2$. The structurally and spectroscopically characterised complexes $Me(OTf)_2In(iMes)$ and $Me(NTf_2)_2In(iMes)$ have good solubility and are active as catalysts in the Friedel-Crafts acylation of activated aromatics. The complexes' spectroscopic handles provide a means to identify the active catalyst in the catalytic cycle which our studies with $Me(NTf_2)_2In(iMes)$ suggest is a Lewis assisted Brønsted acid. We postulate that this species is formed by coordination of acetic acid to indium, resulting in $H(NTf_2)$ formation which has been shown to be an active Brønsted acid catalyst in the reaction.

Chapter 1 - Introduction

1.1 Indium and its Applications

Since the early 1990s, there has been a marked increase in the number of publications documenting indium's application in organic transformation reactions. One area that made significant impact was the discovery that indium metal can react with an organic substrate to generate an organoindium species *in situ*. This has meant that the use of sensitive, toxic or expensive organometallic compounds can be avoided. Organic catalysis reactions where indium is employed often exploit indium(III) complexes as Lewis acids. Most commonly, indium(III) triflate and indium(III) chloride are used, although they remain structurally and spectroscopically ill-defined. Conversely, the properties and behaviour of indium complexes synthesised as precursors for MOCVD (Metallo-Organic Chemical Vapour Deposition) are often overlooked, although in many cases they have been very well identified structurally.

The aim of this thesis is to model indium(III) triflate and indium(III) triflamide using well-defined complexes and uncover structure/activity relationships. Synthesis of new indium complexes containing spectroscopic handles and incorporating the triflate moiety should prove extremely useful toward this end. Determination of solid state structures and monitoring the role of the complexes in catalysis via their spectroscopic handles should yield previously hidden information.

In this introduction a brief overview of indium, indium(III) complexes and their use in organic catalysis will be described. This is not an exhaustive review but should provide a good background of the relevant areas and establish the foundations for this work.

1.2 Indium in Organic Catalysis

1.2.1 Indium Metal in Catalysis

Until recently, research into indium chemistry was primarily devoted to the electronics industry due to the significance of indium semiconductors and other related materials.[1] Indium metal's relatively late emergence as a useful reagent in organic synthesis can perhaps be attributed to its low natural abundance. Due to improved purification techniques and the resulting significantly lower costs, its use is now common in organic chemistry.

The chemical properties of indium lead to its superiority over other metals in organic synthesis. For example:

- Indium metal can tolerate air or oxygen and does not readily form oxides at ambient temperatures. This is a major advantage over most other metal reagents.
- Indium is practically unaltered in water unlike, for example, sodium and potassium.
- The first ionisation potential of indium (5.8eV) is on a par with the alkali metals e.g. lithium and sodium (~5eV) which is low when compared to zinc (9.4eV), tin (7.3eV) and magnesium (7.6eV). This makes it an ideal candidate for SET (single electron transfer) reactions.
- Indium metal exhibits low heterophilicity in organic reactions. This, when coupled with its ability to tolerate oxygen and nitrogen functionalities, makes it a suitable C-C bond-forming mediator. Indium reagents also display low

nucleophilicity, thus permitting chemoselective transformations at groups with similar reactivity.

- Its organo-compounds are non-toxic - a major advantage over the highly toxic organolead and less toxic organotin reagents.

It was not until the late 1980s that indium metal was first used as a synthetically useful reagent in organic chemistry.[2] Since then, indium has been used to mediate a range of reactions. Several exhaustive reviews exist which describe the area. Among these are a review covering most of the literature upto 1995,[3] and a review of reactions mediated by indium metal and indium compounds in aqueous media in 1999.[4] In 2000, reviews involving more specific areas of indium chemistry were published.[5,6] While a systematic review of indium-mediated chemistry was also released in 2001.[7] Lastly, a review of indium mediated carbon-carbon bond forming reactions has been published this year.[8] These reviews offer an extremely thorough analysis of this area and as indium metal catalysis chemistry is not directly linked to this report it will not be discussed further. The following section will look at In(III) salts in organic catalysis specifically.

1.2.2 Indium Halides in Catalysis

Together with the development of indium metal chemistry, indium(III) halides have also materialised as useful Lewis acid catalysts for carbon-carbon bond formation. A distinctive characteristic of indium(III) chloride is that it is effective in both organic solvents and aqueous media. Although possessing comparatively weak electrophilicity when compared to their aluminium and boron counterparts, indium(III) salts are stable to water and are reusable.

A number of reviews of indium(III) halides in organic synthesis have been recently published.[5,6,9,10] While the most commonly used halides are indium(III) chloride and indium(III) bromide, the use of indium(III) fluoride and indium(III) iodide has also been documented.[11,12]

Transesterification of esters to corresponding analogues with higher alcohol moieties is well documented, but examples of the reverse transformation are much less common. A simple, yet effective, synthesis was discovered using indium(III) iodide.[11] Even transesterification to a tert-butyl ester, which is often found to be problematic in acid-catalysed reactions, has been successfully carried out via this method. Extending this methodology, an indium(III) iodide catalysed heteroatom acylation using ethyl acetate in a transesterification process was also documented.[13] A catalyst loading of 10mol% InI_3 was shown to selectively mediate the acylation of amines and primary alcohols in the presence of secondary and phenolic alcohols in an excess of refluxing ethyl acetate (Figure 1).

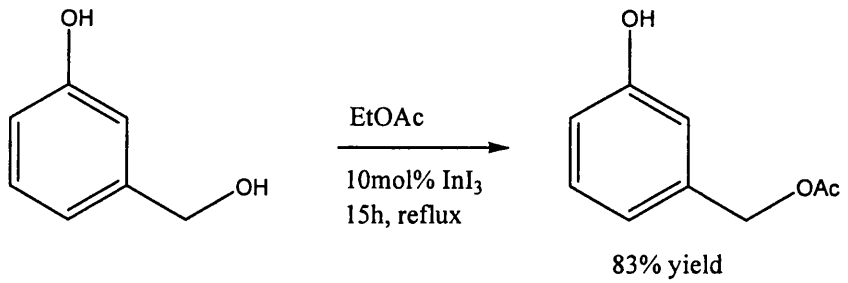

Figure 1: InI_3 selective mediated acylation of a primary alcohol [13]

The same technique has been used in the conversion of both tetrahydropyranyl- and methoxymethyl- protected alcohols to the corresponding acetates in a one pot reaction.[14,15] This reaction is chemoselective for primary alcohols, only deprotecting secondary and phenolic ethers to their parent alcohols.

While the acylation of protected alcohols by indium(III) halides has been documented, it has also been shown that indium reagents can be used as catalysts in the protecting of carbonyl groups. The indium(III) bromide (10mol%) catalysed chemoselective dithioacetalization of aldehydes in the presence of ketones in both organic and aqueous media has been reported.[16] Prior to this, limitations in the Lewis acid catalysed processes resulted in the requirement for an excess of thiols, anhydrous conditions and a stoichiometric amount of catalyst whilst still yielding poor selectivity when faced with mixtures of aldehydes and ketones.

A lower loading of indium trichloride (5mol%) also made an efficient catalyst for aldehyde thioacetalistion (Figure 2).[17] Reaction times for a range of substrates varied considerably, from 10 minutes to 28 hours. The excellent chemoselectivity was attributed to the slower reaction rate of ketones in comparison to aldehydes.

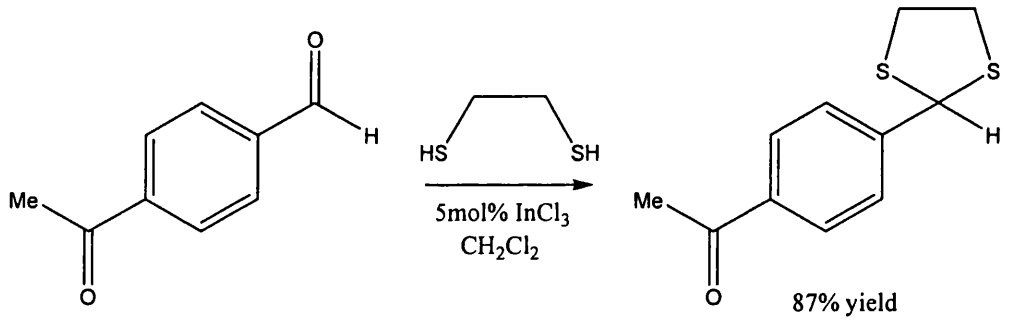

Figure 2 : $InCl_3$ chemoselective thioacetalisation of aldehydes in the presence of ketones [17]

In a related study, Indium(III) chloride has also been shown to catalyse the transthioacetalisation of *O,O*-acetals in excellent yields under mild conditions.[18] This method even bypasses the intermediate step of returning to the parent aldehyde functionality (Figure 3).

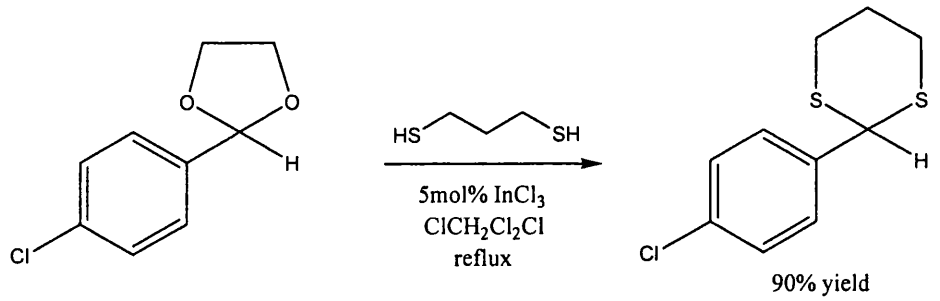

Figure 3 : Transthioacetalisation of O,O-acetals cataylsed by $InCl_3$ [18]

Other examples of indium(III) chloride catalysis with carbonyl groups involves their production from the rearrangement of a range of epoxides in THF solution to yield the corresponding ketone highly selectively (Figure 4).[19]

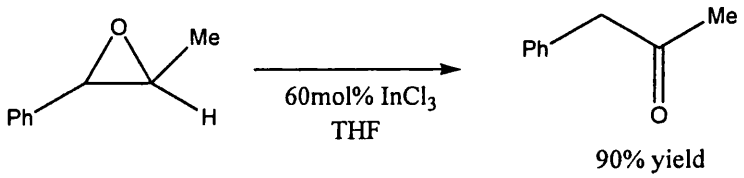

Figure 4 : $InCl_3$ catalysed rearrangement of epoxides [19]

Indium(III) chloride has also been shown to be an efficient catalyst in Mukaiyama aldol reactions of aldehydes with silyl enol ethers in water at room temperature.[20] It was found that the reaction could be enhanced further by the addition of small amounts of surfactant thereby producing a more efficient reaction media (Figure 5). [21]

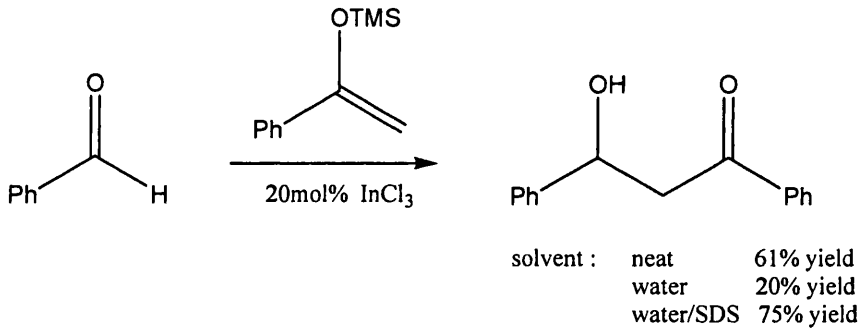

Figure 5 : $InCl_3$ catalysed aldol reaction of benzaldehyde with silyl enol ether [21]

Indium(III) fluoride (20mol%) meanwhile has been shown to be an effective catalyst to mediate the addition of TMSCN (trimethylsilyl cyanide) to aldehydes in aqueous media at ambient temperature (Figure 6).[12] The products of these reactions are versatile synthetic intermediates allowing access to α-hydroxy aldehydes, α-hydroxy ketones, α-amino acids, and β-hydroxy amines. The addition is chemoselective for aldehydes over ketones and in fact catalytic indium trifluoride is superior even to stoichiometric $InCl_3$.

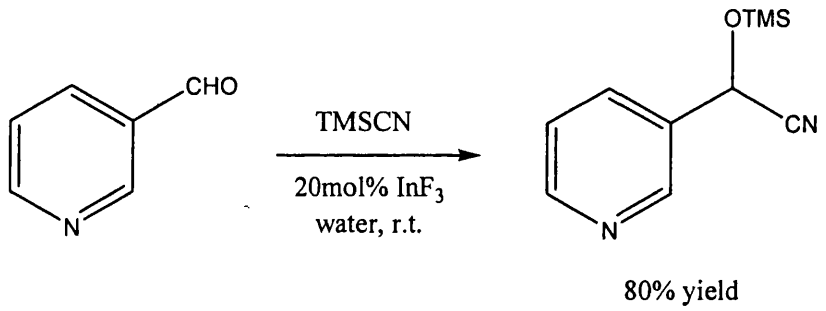

Figure 6 : InF_3 catalysed addition of TMSCN to aldehydes [12]

A further reaction comprising carbonyls was the one pot Mannich-type reaction involving the indium(III) chloride catalysed production of β-aminoketones.[22] A range of these compounds were produced using 20mol% indium(III) chloride in aqueous media at room temperature (Figure 7).

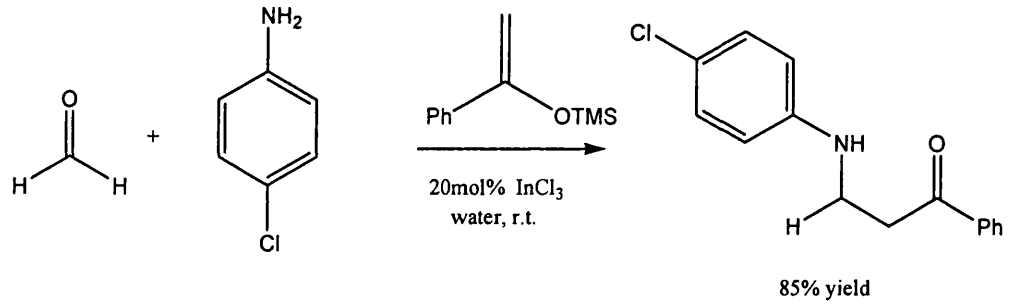

Figure 7 : A one pot Mannich type reaction producing β-aminoketones [22]

Indium(III) halides are also active catalysts for Diels Alder reactions, which are ubiquitous in the regio- and stereospecific preparation of carbocyclic and heterocyclic

ring systems. Lewis acids increase reaction rate and the regio-, endo- and π-face selectivities by coordination with the dienophile, i.e., with a conjugated C=O or C=N group. Indium(III) chloride has been shown to be an effective catalyst of the Diels-Alder reaction of cyclopentadiene and acrylates in water, and can be easily recovered and recycled (Figure 8).[23]

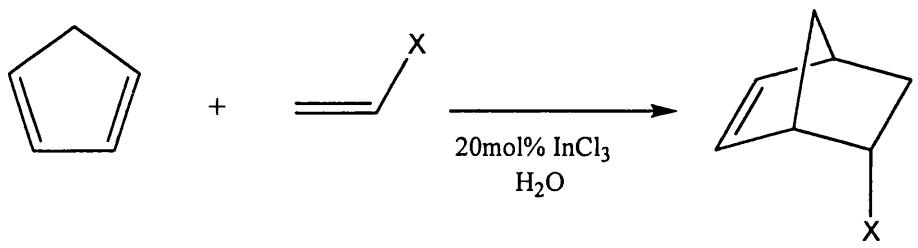

Figure 8 : $InCl_3$ catalysed Diels-Alder reaction of cyclopentadiene and acrylates [23]

Indium(III) chloride has also been used in the related imino Diels-Alder reaction for the synthesisis of quinoline and pyridine derivatives. Indium(III) chloride has a clear advantage over other Lewis acids that promote these reactions. These reactions require the addition of more than a stoichiometric equivalent of Lewis acid as a result of the strong coordination of the Lewis acid to the nitrogen atoms.[24,25] As mentioned previously, indium has a lower affinity for nitrogen functionalities and thus in contrast can be used efficiently at 20mol% loadings. An example of this is shown in Figure 9 for the reaction of Schiff bases with cyclopentadiene to afford cyclopentaquinolines.[26]

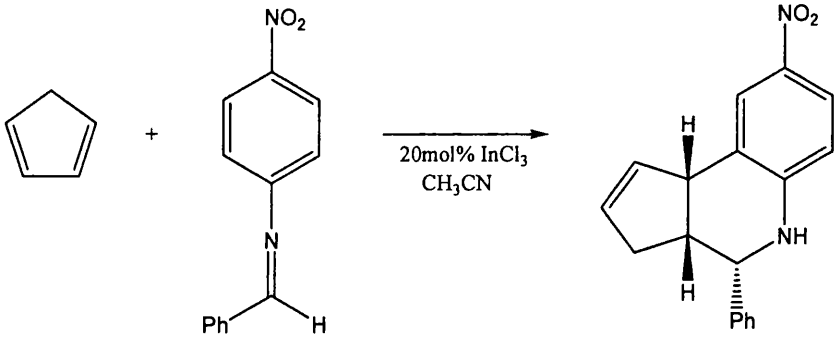

Figure 9 : Example of $InCl_3$ catalysed imino Diels-Alder reaction of a Schiff base with cyclopentadiene [26]

Along with indium(III) halides, indium(III) triflates are also well documented as active Lewis acid catalysts in a number of organic transformations.

1.2.3 Indium(III) Triflate in Catalysis

The use of indium(III) triflate in the acylation of alcohols and amines with acetic anhydride has been reported under very mild conditions.[27] It was demonstrated that only very low catalyst loadings are required to acylate heteroatoms in excellent yield at room temperature. Even polyhydroxy compounds such as D-mannitol are acylated in excellent yield (94%) (Figure 10). The use of isopropenyl acetate instead of acetic anhydride is documented and this avoids the production of acetic acid as a by-product in the acylation of alcohols. Using catalytic quantities of indium(III) triflate in tandem with stoichiometric lithium perchlorate the predominant side-product in this reaction is the more benign acetone.

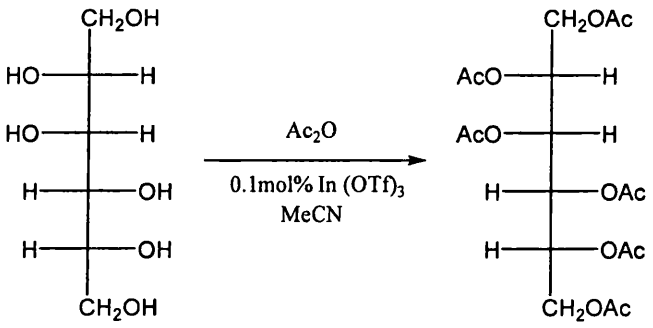

Figure 10 : $In(OTf)_3$ catalysed acylation of D-mannitol under mild conditions [27]

Indium(III) triflate's efficacy in Diels-Alder reactions has also been reported.[28] As well as activating aldehydes it can also preferentially activate imines in the presence of aldehydes using a catalyst loading of only 0.5mol% (Figure 11).

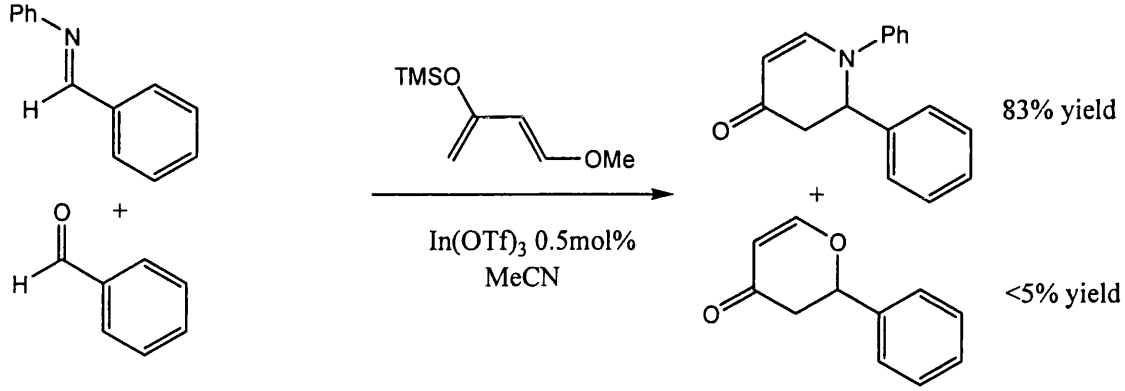

Figure 11 : Competition reaction of Danishefsky's Diene + 1:1 benzaldehyde : N-benzilideneaniline [28]

It was postulated that because indium(III) triflate can also promote imine formation, the catalyst should be able to drive a three component coupling reaction of aldehyde, amine and diene in a similar manner to that demonstrated with lanthanum and scandium triflates but at much lower catalyst loadings than 10mol%.[29] This was proved to be the case at 0.5mol% loadings, with the catalyst retaining its activity even in the presence of water and amines at these low loadings.

Indium(III) triflate like indium(III) chloride has also been successfully used in the thioacetalization and transthioacetalization of aldehydes and oxyacetals respectively. A range of catalyst loadings (8-25mol%) at ambient temperature in CH_2Cl_2 show short reaction times (5mins-4hrs) and high yields (80-95%) over a range of substrates.[30] Catalyst loadings of 5mol% or less however resulted in prolonged reaction times (~35hrs).

A simple and efficient method for tetrahydropyranylation and depyranylation of alcohols, as well as acetylation of tetrahydropyran (THP) ethers, using a catalytic amount of indium(III) triflate has also been reported.[31] The protection of 3-cyclohexene-1-methanol for example takes only 30 minutes (Figure 12), whilst the deprotection step takes 10hrs and gives a reduced yield of 60%.

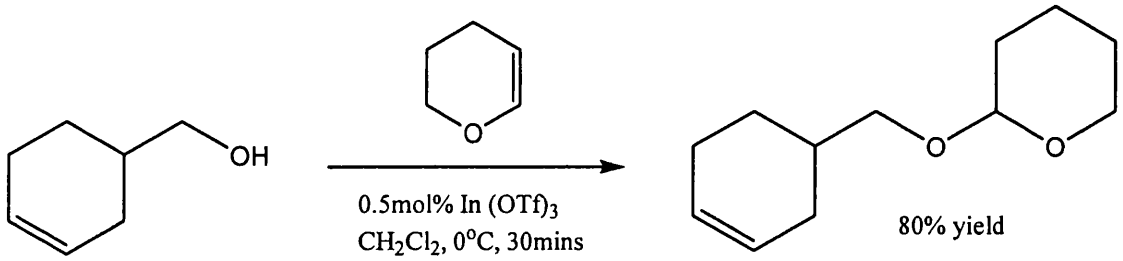

Figure 12 : The tetrahydropyranylation of a primary alcohol to its THP protected analogue [31]

An indium(III) triflate-catalyzed tandem procedure for tetrahydrofurans has also been reported.[32] It was determined that the mechanism relied on the indium(III) triflate-catalyzed (3,5) oxonium-ene type cyclization and a thermo-dynamically controlled skeletal reorganization of the cyclic ether (Figure 13).[33]

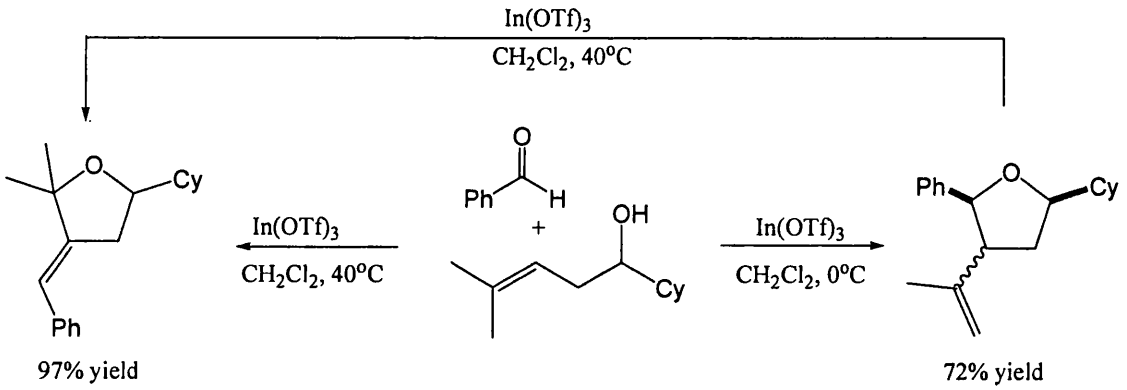

Figure 13 : Convergent formation of cyclic ethers catalysed by indium(III) triflate [33]

Meanwhile O-H insertion reactions of α-diazo ketones with aliphatic/aromatic alcohols or benzenethiol using indium(III) triflate as the catalyst (Figure 14) show that

primary and secondary alcohols react rapidly whilst tertiary alcohols required 3 hours to complete the reaction.[34]

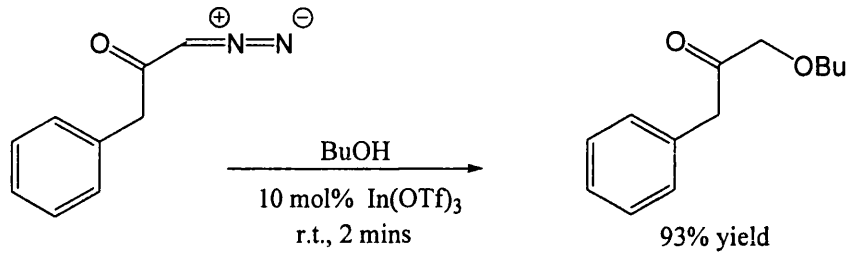

Figure 14 : $In(OTf)_3$ catalysed production of an α-alkoxy ketone from an α-diazo ketone [34]

Indium(III) triflate is also an active mediator in the (4+2)-cycloaddition of chromone Schiff's bases.[35] A simple one pot reaction from the starting amine to the final product, demonstrated that 3,4-Dihydro-*2*H-pyran reacts with a variety of chromone Schiff's bases (Figure 15). Indium(III) triflate mediates the *endo* cycloadducts regiospecifically in high yields at ambient temperature and pressure.

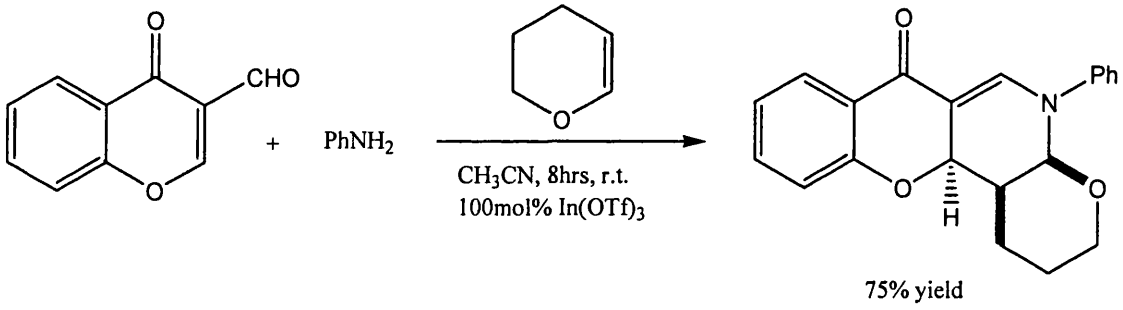

Figure 15 : one pot reaction showing (4+2)-cycloaddition of chromone Schiff bases [35]

Finally a catalytic, asymmetric synthesis of β-lactams using a bifunctional catalyst system consisting of a chiral nucleophile and indium triflate has been reported.[36] Previous work has shown that nucleophilic ketenes react with electrophilic imines in the presence of a chiral nucleophile (typically benzoylquinone) to give β-lactams in

high enantioselectivity but only moderate yield. Indium(III) triflate was the best overall Lewis acid co-catalyst with benzoylquinone for promoting the reaction of N-tosyl imine with the ketene precursor, phenylacetyl chloride, forming β-lactams in excellent yield. High enantioselectivity was achieved (>95%) and the inclusion of catalyst increased the yield from 40-60% to 92-98%.

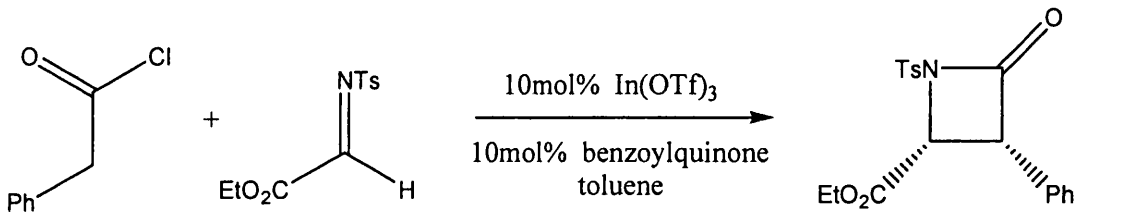

Figure 16 : $In(OTf)_3$ and benzoylquinone co-catalysed production of β-lactams [36]

Indium(III) triflamides have also recently been documented as active Lewis acid catalysts in several organic transformations.

1.2.4 Indium(III) Triflamide in Catalysis

Recently the efficacy of using indium(III) triflamide, $In(NTf_2)_3$, an indium(III) triflate analogue, in aromatic electrophilic substitution reactions was documented.[37] The compound itself was prepared by reaction of indium(III) oxide, (In_2O_3), with 3 equivalents of bis(trifluoromethanesulfonyl)imide [$H(NTf_2)$].[38] It is suggested that the more weakly coordinating nature of the triflamide over the triflate anion leads to enhanced Lewis acidity at the metal centre making it a more active species in catalysis.[37]

1.3 Indium(III) Complexes

The previous section showed the role of InX_3 in organic catalysis where (X = halide triflate or triflamide). The exact nature of the active species in solution during each of the documented reactions is unknown. To understand the behaviour of In(III) in catalysis it is useful to have structural and spectroscopic data of well defined complexes to compare with. Therefore both structural and spectroscopic handles are required. This section shows the documented stabilisation of indium(III) centres to yield structural and spectroscopic information about the metal centre.

Trivalent indium has been coordinated to a range of ligands and this section shows some of the coordination chemistry that has been documented. Generally these complexes have been synthesised just for structural interest or MOCVD. Further chemistry is rarely reported. This section contains indium(III) halide and trimethylindium adducts as well as complexes synthesised both from their adducts and from the available indium starting materials. A brief summary of the few documented structurally defined indium triflate complexes is also included.

1.3.1 Indium(III) Halide Adducts

The formation of coordination complexes between indium(III) halides and neutral ligands containing either nitrogen, phosphorus, oxygen or sulphur donor centres is now a well established area of chemistry.[39] They are usually synthesised by the general scheme shown in Figure 17.

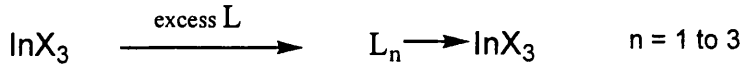

Figure 17 : The general scheme of InX_3 adduct formation
(where X = halide and L = neutral electon donor)

The steric bulk of L, the neutral electron donor determines whether it is one, two or three ligands that are coordinated to each indium centre.

1.3.1.1 Indium(III) Halide Adducts with Oxygen Donors

Adducts of indium(III) halides have been synthesised by reaction of the halides in polar solvents with strong oxygen donor ligands. For example, $InCl_3$ has been coordinated to three equivalents of tetrahydrofuran (THF) by stirring $InCl_3$ in a large excess of THF at reflux for 24 hours.[40] The resulting crystal structure showed the geometry about the indium atom to be approximately octahedral, where the THF and chloride ligands adopt a meridianal conformation about the indium. More recently the bis THF adduct $InBr_3(THF)_2$ has been synthesised by repeating the above process with indium tribromide for 48 hours.[41] The larger steric bulk of the bromine atoms stops a third molecule of THF binding to the indium centre as in $InCl_3(THF)_3$. The crystal structure revealed that the five coordinate metal centre adopts a trigonal bipyramidal geometry with the three halogen atoms in the equatorial plane and the two THF ligands in the axial positions (Figure 18).

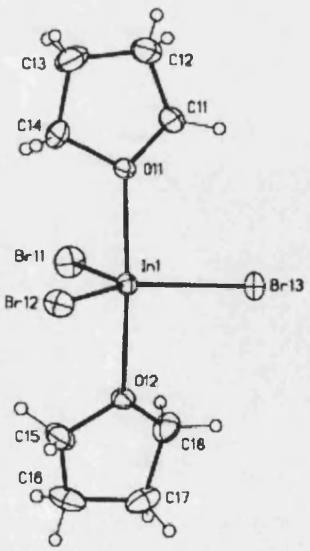

Figure 18 : Crystal structure of $InBr_3(THF)_2$ [41]

$InCl_3$ can also be readily coordinated to the oxygen donor atom of other solvent ligands, as demonstrated by the ligation of indium trichloride with dimethylformamide (DMF), dimethylacetamide (DMA) and acetophenone. [42]

1.3.1.2 Indium(III) Halide Adducts with Phosphorus Donors

Indium(III) halides have also been coordinated to various phosphines. The indium(III) halide bis-monodentate phosphine complexes $[InBr_3(PMe_2Ph)_2]$ (Figure 19) and $[InI_3(PMePh_2)_2]$ have been documented.[43] In the indium tribromide complex, the In-P bonds are equivalent at 2.614(3)Å and 2.622(3)Å and the P-In-P angle is almost linear at 177.34(8)°. In the indium triiodide complex the In-P bonds are slightly longer at 2.712(3)Å and 2.719(3)Å as expected while the P-In-P bond is slightly kinked at 169.82(9)° showing a distorted trigonal bipyramidal geometry. Other indium(III) halide monodentate phosphine complexes which have been structurally characterised include the 1:1 adducts $[InI_3(PHPh_2)]$ and $[InI_3(PH^tBu_2)]$,[44] the 2:1 adducts $[InCl_3(PPh_3)_2]$,[45] $[InCl_3(PMe_3)_2]$ and the 2:3 adduct $[(InI_3)_2(Ph_2PCH_2CH_2PPh_2)_3]$.[46] Reactivity studies of these complexes are not reported.

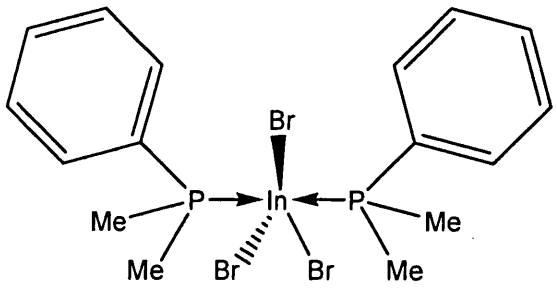

Figure 19 : Structure of $[InBr_3(PMe_2Ph)_2]$ [43]

Coordination of indium halides to bidentate phosphine ligands is also possible. Bis(diphenylphosphino)benzene has been bound to indium(III) chloride and indium(III) iodide.[47] The 1:1 reaction of InI_3 and [1,2-

Bis(diphenylphosphanyl)benzene] in toluene gave the complex shown in Figure 20. A broad singlet is observed in the $^{31}P\{^{1}H\}$ NMR spectrum due to the phosphorus coupling to the quadrupolar indium nuclei ^{113}In (4.3%, I = $^{9}/_{2}$) and ^{115}In (95.7%, I = $^{9}/_{2}$).

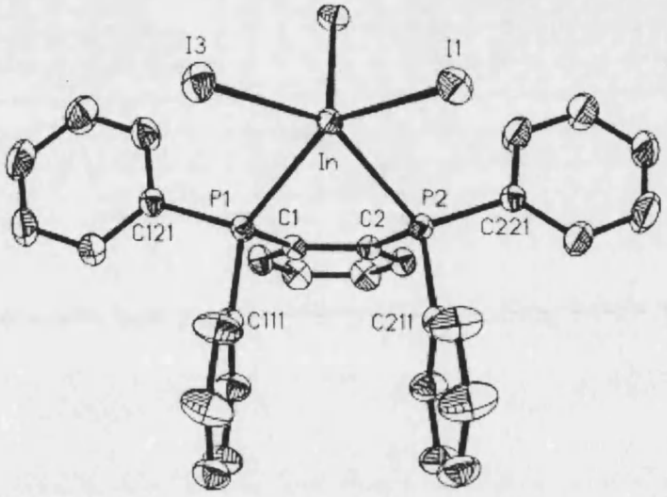

Figure 20 : Crystal structure of $[InI_3(PMePh_2)_2]$ [47]

1.3.1.3 Indium(III) Halide Adducts with Nitrogen Donors

One of the first structural examples of indium trihalides bound to nitrogen was synthesised by the reaction of trimethylamine with indium trichloride. $(Me_3N)_2InCl_3$ (Figure 21) was produced by stirring up an excess of amine with indium(III) chloride in THF.[48] Only structural studies of the complex were reported, which show the In-N bond lengths to be equivalent within errors at 2.345(19)Å and 2.320(20)Å and the N(1)-In-N(2) angle to be linear at 179.90(13)°. More recently $[(C_6H_5CH_2)_2NH)]_2InCl_3$ has been synthesised via the same technique.[49]

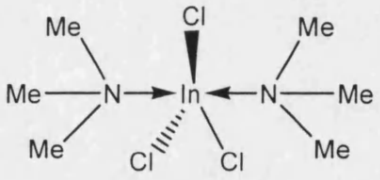

Figure 21 : Structure of $(Me_3N)_2InCl_3$ [48]

1.3.1.4 Indium(III) Halides Adducts with Sulphur Donors

Ligands containing sulphur have also been coordinated to indium trihalides. Two examples are the complex trichlorobis(N,N,N',N'-tetramethylthiourea)indium(III),[50] and the coordination of 1,3-dimethyl-2(3H)-imidazolethione (or dmit) to both indium trichloride and indium triiodide (Figure 22).[51] In each case these adducts have been synthesized and structurally assigned but no further reactivity studies were reported.

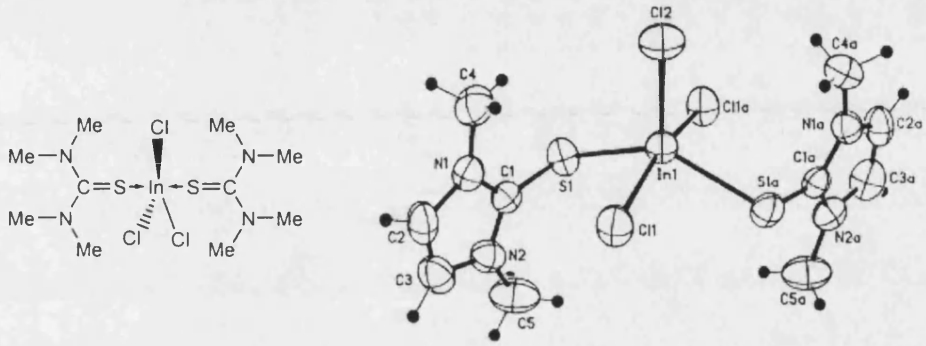

Figure 22 : Structure of trichlorobis(N,N,N',N'-tetramethylthiourea)indium(III) [50] and the crystal structure of 1,3-dimethyl-2(3H)-imidazolethione with indium(III) chloride [51]

1.3.1.5 Indium(III) Halide Adducts with N-heterocyclic Carbenes

Indium trihalides can also be stabilised by *N*-heterocyclic carbenes. For example, the reaction of $InBr_3$ with free 1,3-bis(2,6-diisopropylphenyl)imidazol-2-ylidene (^{i}Pr) carbene results in the formation of ^{i}PrInBr$_3$ (figure 23).[52] The coordination of *N*-heterocyclic carbenes to indium is discussed in detail in Chapter 3.

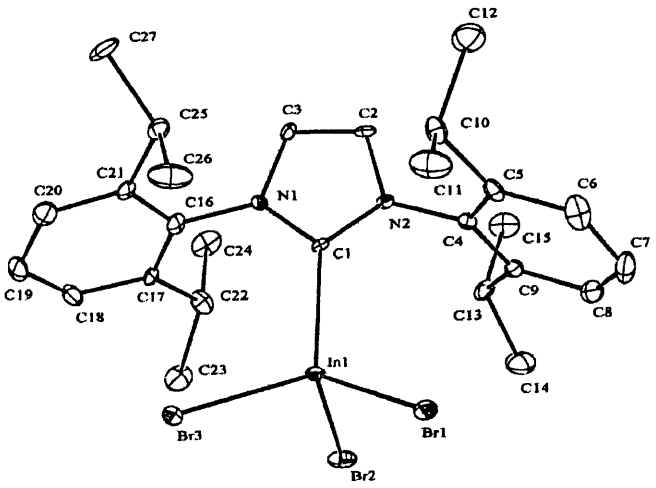

Figure 23 : Crystal structure of $^{i}PrInBr_3$ [52]

1.3.2 Reaction of Indium(III) halides to form Indium(III) complexes

While adducts of indium(III) halides are readily formed by combining indium(III) halides with suitable donor ligands, substitution reactions of halides at the indium metal centre are also possible. This section shows that use of suitable reagents including Grignards, alkyl lithiums and lithium amides results in halide substitution. The first example documents the use of a Grignard reagent to synthesise a phosphavinyl indium complex (Figure 24).[53]

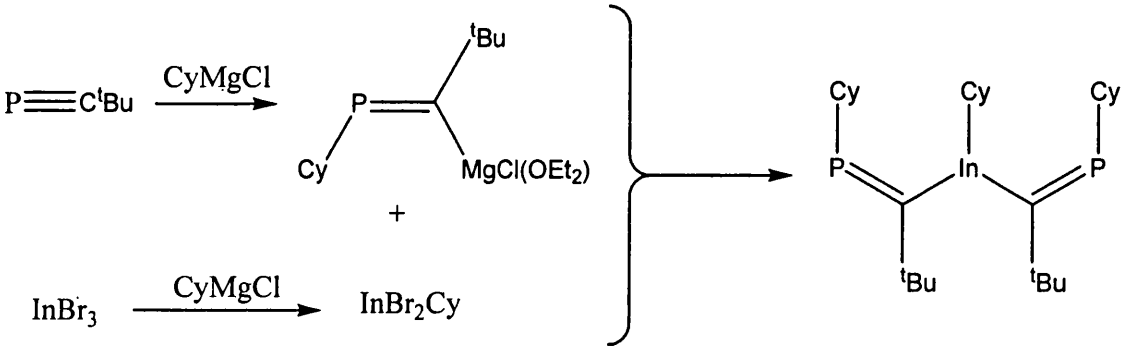

Figure 24 : Reaction scheme showing for [CyIn{C(^{t}Bu)=PCy}$_2$] synthesis [53]

The crystal structure is shown in Figure 25 and while the indium is only 3-coordinate, the compound is monomeric in the solid state as a result of the steric bulk of the ligands.

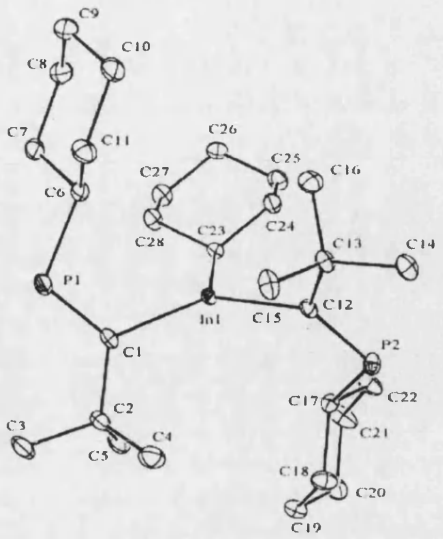

Figure 25 : Crystal structure of $[CyIn\{C(^tBu)=PCy\}_2]$ [53]

The route to indium amide compounds by reaction of indium trihalides with lithium amides has also been reported. The reaction of indium trichloride with a lithium amide reagent - $MeN(SiMe_2NMeLi)_2$ for example, results in formation of the dimer $[ClIn(NMeSiMe_2)_2NMe]_2$ by elimination of lithium chloride (Figure 26).[54] Such compounds are potentially useful for MOCVD. The structure for $[ClIn(NMeSiMe_2)_2NMe]_2$ is shown in Figure 27.

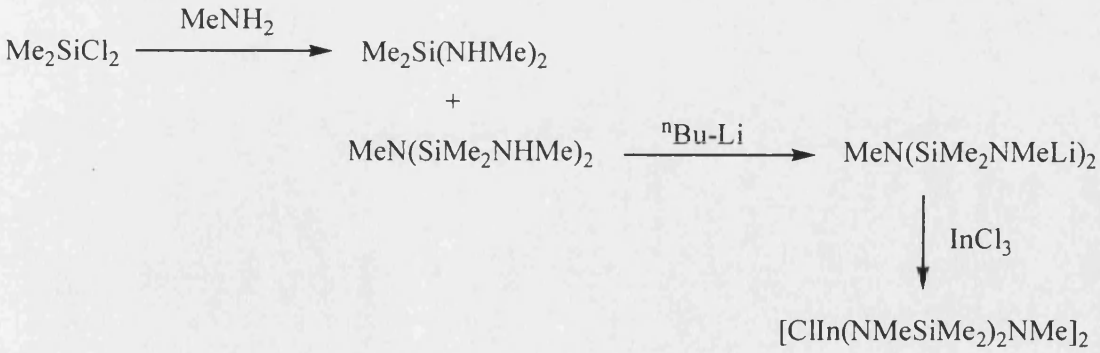

Figure 26 : $[ClIn(NMeSiMe_2)_2NMe]_2$ synthesis [54]

The compound is a dimer in the solid state where an In-N-In-N four-membered ring is formed. This is common structural motif observed in indium crystal structures where electron rich atoms (e.g. oxygen, nitrogen) either α or β to the indium act as bridges. Dimerisation can be blocked by large groups protecting the coordination sphere of the metal (see Chapter 2).

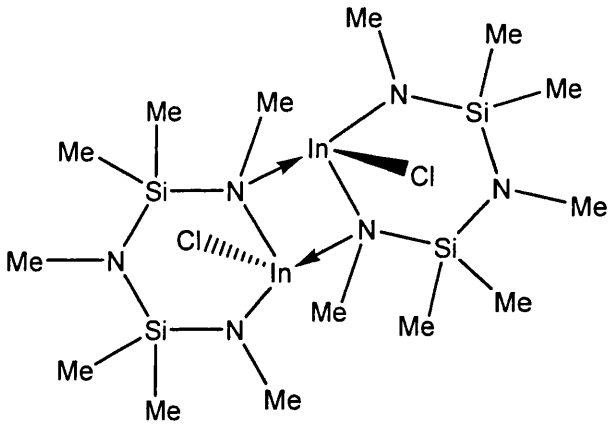

Figure 27 : Structure of $[ClIn(NMeSiMe_2)_2NMe]_2$ [54]

Research into single source indium-amide precursors for MOCVD resulted in the isolation of a stabilised intermediate in a chloride abstraction reaction. The reaction of a lithiated aniline species with indium trichloride using THF as the solvent media shows surprisingly, not chloride abstraction but formation of what was termed a dichloroindium amide.[55] The structure shown in Figure 28 can be rationalised by the fact that the three molecules of THF coordinate to the lithium, satisfying some of its desire for electron density. As a result the lithium does not require such a strong bond with the chloride and instead of being abstracted, one of the chlorides forms a bridge between the indium and the lithium.

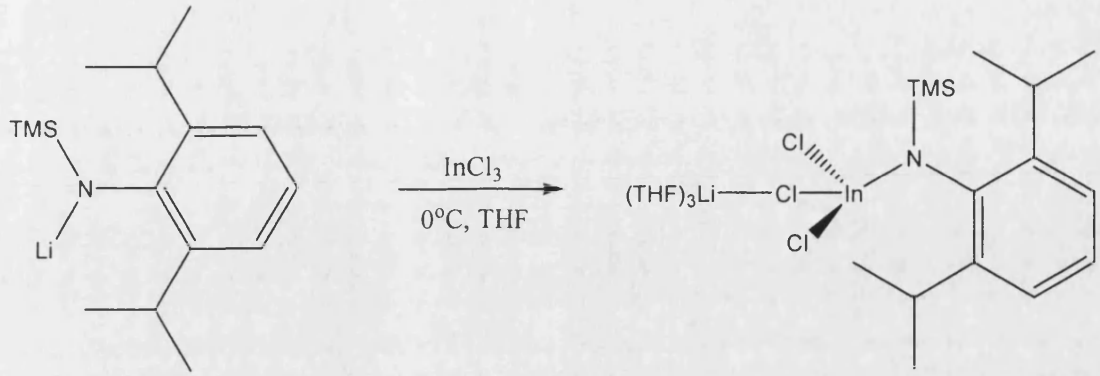

Figure 28 : $(THF)_3Li(\mu\text{-}Cl)Cl_2InN(SiMe_3)(Dipp)$ (Dipp = 2,6-diisopropylphenyl) [55]

Alkyl lithium reagents have also been shown to be useful reagents for halide substitution. Reaction of indium trichloride with two equivalents of (2,6-diphenylphenyl)lithium caused substitution of two of the chloride ligands (Figure 29).[56] In this case although the analogous gallium iodide structure is reported, despite repeated attempts at growing suitable crystals, a crystal structure of the indium compound could not be obtained. Analysis of the indium complex by ^{1}H, ^{13}C NMR spectroscopy and elemental analysis suggested it is likely to be structurally similar to the gallium iodide analogue. As the gallium structure shows, steric protection of the metal's coordination sphere ensures dimerisation of the complex cannot occur in the solid state.

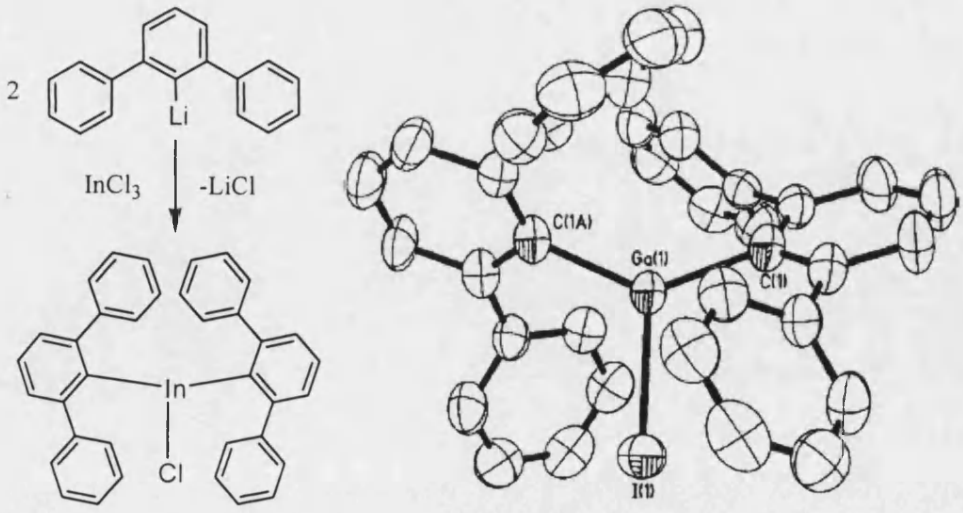

Figure 29 : Synthesis of $(Ph_2C_6H_3)_2InCl$ and crystal structure of $(Ph_2C_6H_3)_2GaI$ [56]

1.3.3 Trimethylindium Adducts

Trimethylindium itself has been found to exist as a loosely associated tetramer in the solid state.[57] Tetramer formation occurs due to intermolecular CH_3•••In interactions between the metal and a methyl group on a neighbouring metal atom. In fact a weaker interaction through 4 more neighbouring methyl group exists, linking the tetramers into an infinite three-dimensional (3D) network (Figure 30).

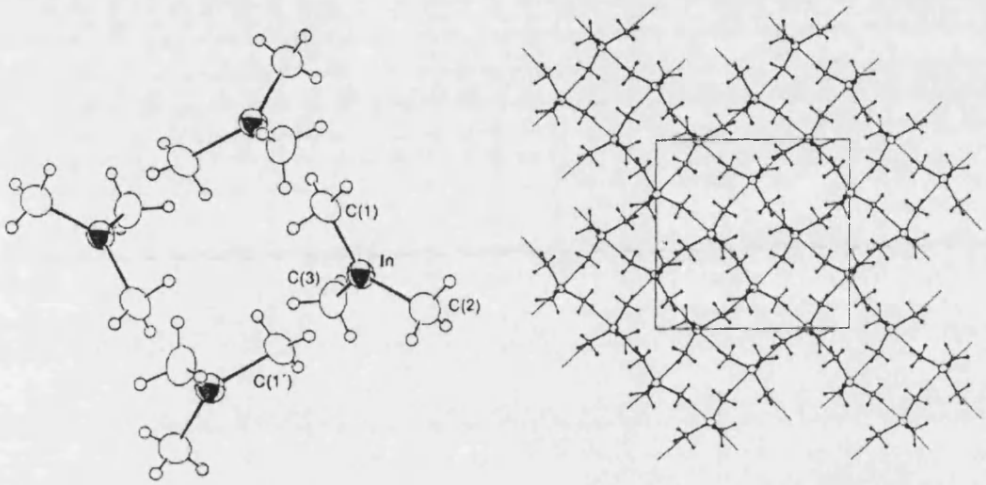

Figure 30 : The tetrameric structure of $InMe_3$ and the extended 3D network viewed along one of its planes [57]

Table 1 shows bond lengths of interest in the crystal structure. The $InMe_3$ molecules are bound into cyclic tetramers by intermolecular In•••C(1) contacts of 3.083(12)Å. These tetramers are linked into the 3D network by 4 longer intermolecular contacts of 3.558(15)Å.

	Bond lengths (Å)
In-C(1)	2.179(12)
In-C(2)	2.121(14)
In-C(3)	2.136(13)
Intermolecular In•••C(1) contacts	3.083(12)
Extended 3D In•••C network contacts	3.558(15)

Table 1 : Table of relevant bond lengths in $InMe_3$ [57]

A search of the Cambridge Structural Database (CSD) revealed that few structural examples of adducts of trimethylindium have been reported. Structurally characterised examples include adducts with tertiary amines,[58,59] trialkylphosphines,[60,61] trisilylphosphines and phosphine oxides.[62,63] The 2:1 adduct formed by reaction of $InMe_3$ and diphenylphosphinoethane (dppe) showed trimethylindium can be stabilised by phosphorus donors (Figure 31).[61]

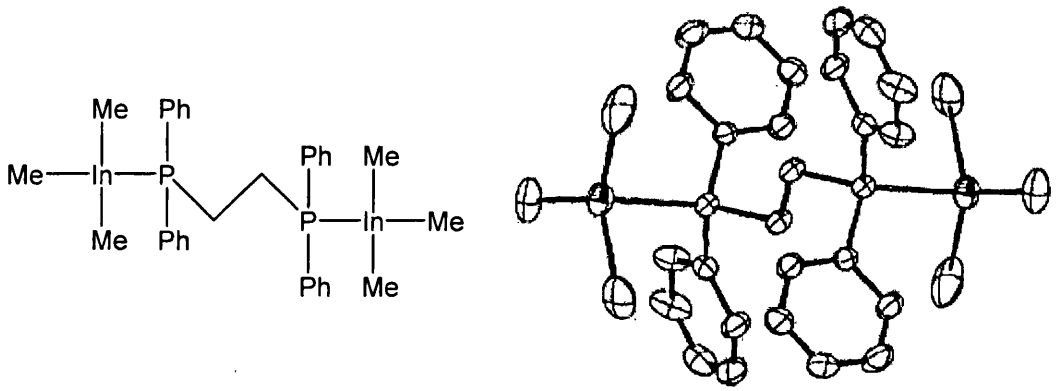

Figure 31 : Structure and crystal structure of dppe•2($InMe_3$)[61]

More recently, adducts of $InMe_3$ stabilised by the bidentate tertiary amine *N,N,N',N'*-tetramethyl-4,4'-methylenebis(aniline) (MBDA) were documented where both the 2:1 and the 1:2 adducts were formed.[59] The 2(Me_3In)•MBDA 2:1 adduct is four-coordinate and exists in a distorted tetrahedral environment (Figure 32). The In-N bond lengths are significantly shorter than those in the 1:2 adduct (Figure 33). They are 2.446(3)Å and 2.462(2)Å in length indicating a much stronger indium-nitrogen interaction than that seen in Me_3In•2(MBDA).

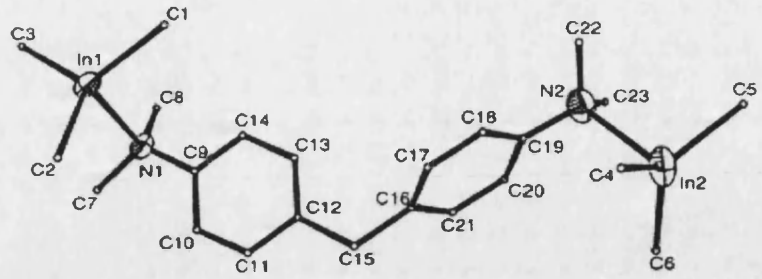

Figure 32 : Crystal structure of the 2:1 adduct $2(Me_3In)\bullet MBDA$ [59]

The structure of $Me_3In\bullet 2(MBDA)$ (Figure 33) includes the longest In-N bond lengths [2.720(4)Å and 2.865(4)Å] ever reported and is one of only a few monomeric 5-coordinate alkylindium adducts. These generally involve chelating donor ligands (eg. $Me_3In\bullet Me_2NCH_2NMe_2$ and $Me_2InCl\bullet$2,2'bipy),[64,65] and structural data is scarce. The Me_3In moiety is in a trigonal bipyramidal configuration with a linear N-In-N bond of 179.45(12)°.

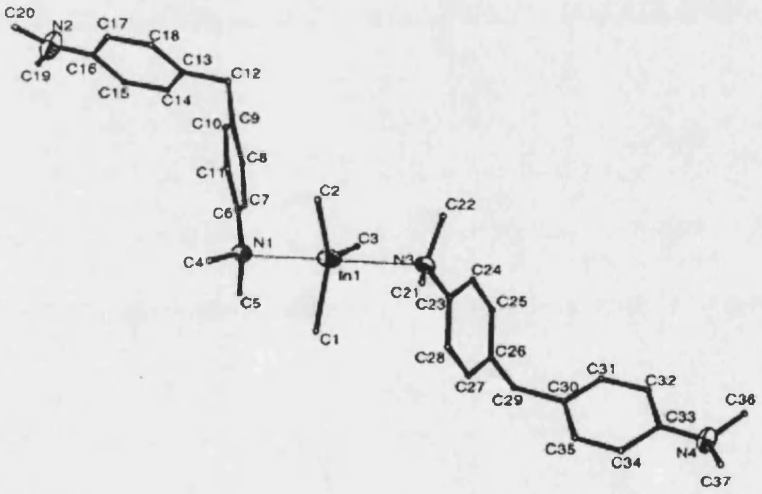

Figure 33 : Crystal structure of the 1:2 adduct $Me_3In\bullet 2(MBDA)$ [59]

While there are many examples of trimethylindium acting as a single lone pair acceptor,[66] only rarely have adducts been formed where two or more Lewis base donor atoms are present per indium atom. While one such example has already been mentioned [$Me_3In\bullet 2(MBDA)$],[59] other examples include that of trimethylindium with diaazobicyclo[2.2.2]octane (DABCO),[67] where indium is bound to two Lewis base

donor atoms, and the adduct of $InMe_3$ bound to a tridentate triisopropyl-triazocyclohexane ligand.[58] Trimethylindium adducts of the empirical formulae $InMe_3 \cdot C_3H_6N_3R_3$ where R = Me, ^iPr or ^tBu have also been reported.[68] Only $InMe_3 \bullet \{N(^iPr)\text{-}CH_2\text{-}\}_3$ was structurally characterised (Figure 34).

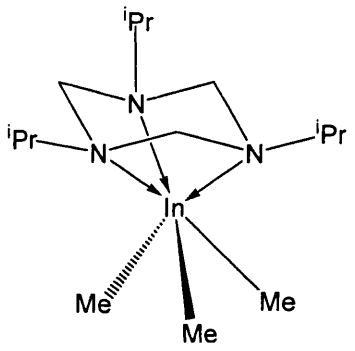

Figure 34 : Structure of $InMe_3 \cdot C_3H_6N_3(^iPr)_3$ [58]

1.3.4 Reaction of Trimethylindium to form Indium(III) Alkyl Complexes

Reaction of $InMe_3$ with functional groups containing acidic hydrogens often results in methane elimination by protonolysis. The subsequent syntheses discussed in this section occur via this reaction pathway.

$$InMe_3 \xrightarrow[-CH_4]{X\text{—}H} R\text{—}InMe_2$$

Figure 35 : The general scheme of $InMe_3$ reaction with alkyl compounds (where X = functional group)

1.3.4.1 Bismethylindium Complexed to Phosphorus Donors

Reaction of trimethylindium with diphenylphosphine in toluene at room temperature results in methane elimination.[69] The product is a trimer in the solid state (Figure 36) where each indium is 4-coordinate and takes up a position in the chair conformation of the 6-membered $[\text{-In-P-}]_3$ ring. Reactivity studies showed the compound demonstrates little reactivity toward Lewis bases such as amines, ethers or other

phosphines. Use of a more sterically demanding phosphine results in a four-membered ring dimer i.e. $[Me_2In\text{-}P(SiMe_3)_2]_2$ instead of a trimer.[70]

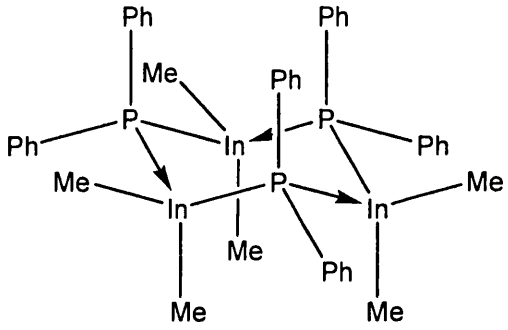

Figure 36 : Structure of $(InMe_2PPh_3)_3$ [69]

1.3.4.2 Bismethylindium Complexed to Nitrogen Donors

Structurally characterised 5- and 6-coordinate monomeric organometallic indium complexes with nitrogen ligands have also been reported.[71] The scheme in Figure 37 shows that reaction of a pyridine adduct of $InMe_3$ (formed by a 1:1 pyridine : $InMe_3$ mixture in hexane) with a bidentate diphenyltriazene ligand (Hdpt), results in the 1:1 indium bismethyl complex via loss of one equivalent of methane (Figure 38). Reaction with a second equivalent of the 1,3-diphenyltriazene ligand gave the 1:2 complex.

$$InMe_3(3,5\text{-}Me_2py) \xrightarrow[-CH_4(g)]{Hdpt} InMe_2(dpt)(3,5\text{-}Me_2py) \xrightarrow[-CH_4(g)]{Hdpt} InMe(dpt)_2(3,5\text{-}Me_2py)$$

Figure 37 : Reactions of $InMe_{3-n}(dpt)_n$ type compounds [71]

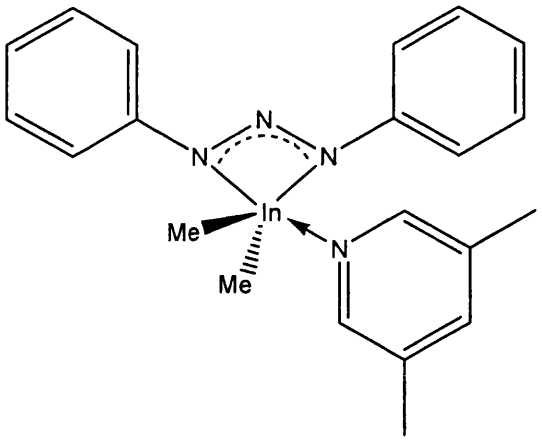

Figure 38 : Structure of $InMe_2(dpt)(3,5\text{-}Me_2py)$ [71]

Another route to these compounds, via the chloride analogues has also been reported.[71] Reaction of the lithium salt of the ligand (Lidpt) and $InCl_3$ gave the bischloride complex.[72] Its treatment with MeLi resulted in a mixture of the monomethyl and bismethyl complexes which were separated by fractional crystallisation.

$$InCl_2(dpt)(3,5\text{-}Me_2py)_2 \xrightarrow[-LiCl]{2MeLi} \begin{matrix} InMe_2(dpt)(3,5\text{-}Me_2py)\ 60\% \\ + \\ InMe(dpt)_2(3,5\text{-}Me_2py)\ 12\% \end{matrix}$$

Figure 39 : An alternative route to $InMe_{3-n}(dpt)_n$ compounds [72]

Direct reaction of trimethylindium with primary and secondary amines also results in methane elimination. Figure 40 shows the crystal structure of the product of a reaction of $InMe_3$ with benzylamine to form the dimer, $[Me_2InN(H)CH_2Ph]_2$.[73] Reactivity studies of trimethylindium with a series of five silylamines has also been reported.[74]

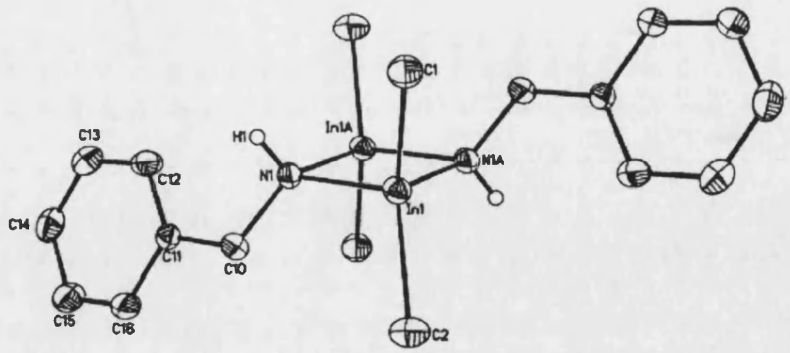

Figure 40 : Crystal structure of $[Me_2InN(H)CH_2Ph]_2$ [73]

1.3.4.3 Bismethylindium Complexed to Oxygen Donors

Indium(III) alkyls have also been reacted with oxygen donor ligands. The synthesis of $InMe_2(C_5H_5)$,[75,76] and a subsequent cyclopentadiene elimination reaction via reaction with 2,4-pentanedione (acetylacetone or acac) gave the complex $[Me_2In(acac)]_2$.[77] The synthesis of this complex had already been reported but via the reaction of dimethylindium methoxide and 2,4-pentanedione where methanol was eliminated (Figure 41).[78]

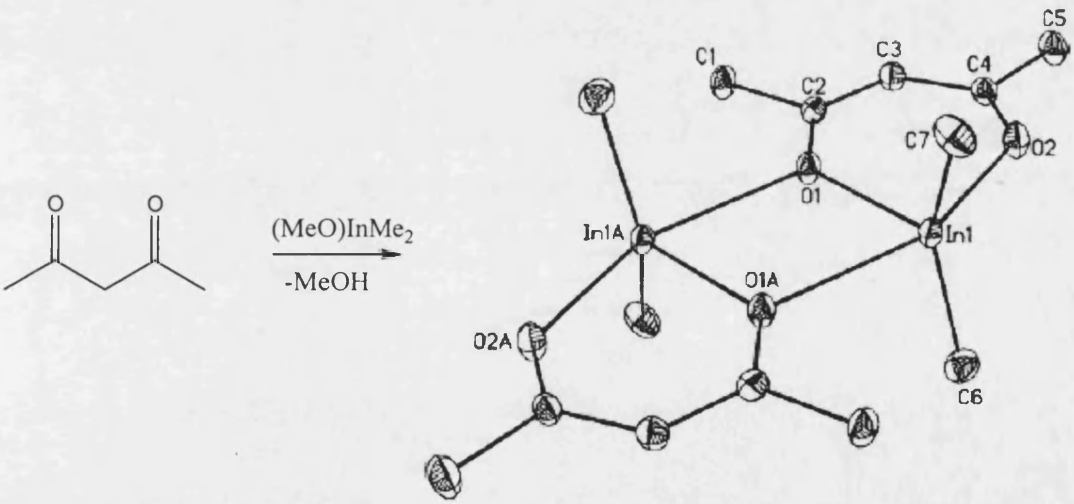

Figure 41 : Reaction of pentane-2-4-dione and $MeOInMe_2$ to give $[Me_2In(acac)]_2$ [78]

The acac chelates through its oxygen atoms to form 6-membered In-O-C-C-C-O-In rings in a π conjugated system and dimerises through 4-membered In-O-In-O rings.

These type of indium compounds and their dimeric formation will be discussed in depth in Chapter 2.

1.3.5 Structurally Defined Indium Triflate Complexes

Until recently,[79] only two structural examples of indium triflate complexes had been reported (see Chapter 3 section 3.2.1.7-8). These are an indium(I) triflate species,[80] and a mixed coordination indium(III) polymer.[81]

Indium(I) triflate is synthesised by direct reaction of Cp*In (Cp* = C_5Me_5)[82] with triflic acid (HOTf).

$$InCp^* + HOTf \longrightarrow InOTf + Cp^*H$$

Figure 42 : synthesis of indium(I) triflate

Figure 43 shows the solid state asymmetric unit consists of two independent ion pairs each having a particularly short In-O contact of 2.579(6)Å or 2.589(6)Å. The crystal structure actually consists of columns of indium(I) cations separated by columns of triflate anions 4.9834(4)Å apart. Each indium has 4 close contacts to oxygens on different triflate anions (<3Å) and a total of 12 contacts to oxygen and fluorine atoms within a 4Å radius in the solid state.

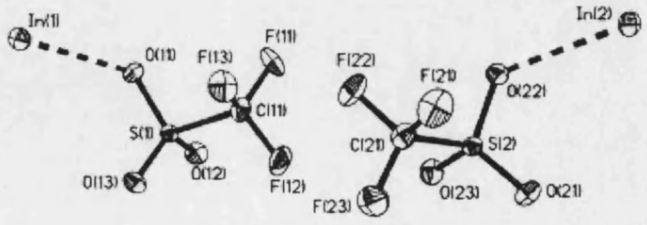

Figure 43 : Crystal structure asymmetric unit of indium(I) triflate [80]

Figure 44 shows the only other indium triflate complex, as reported by Fischer *et al.* during their research into indium-nitride thin films.[81] The structure can be interpreted as the co-crystallisation of two different monomers: $(CF_3SO_3)In[(CH_2)_3NMe_2)]_2$ and $(N_3)In[(CH_2)_3NMe_2)]_2$. The indium of interest occupies an octahedral geometry where it is bound to the triflate ligand with an In-O bond length of 2.473(2)Å while the pentacoordinate indium is weakly coordinated to the oxygen of the triflate ligand on a neighbouring molecule and a one-dimensional (1D) coordination polymer is propagated.

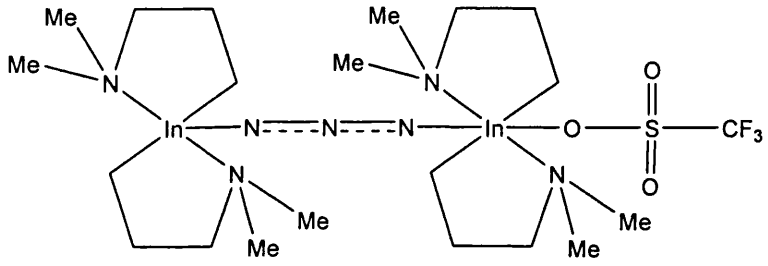

Figure 44 : Structure of $\{(CF_3SO_3)In[(CH_2)_3NMe_2)]_2(\mu\text{-}N_3)In[(CH_2)_3NMe_2)]_2\}_x$ [81]

1.4 Summary

Indium has been bound to a range of Lewis basic ligands and the available structural data shows indium can adopt a range of coordination numbers in the solid state. The commercially available indium(III) halides and trimethylindium can form adducts which are readily crystallised and can yield information about the geometry around the metal centre. They are also useful precursors to a range of complexes. Generally the adducts and indium complexes are 5-coordinate and adopt trigonal bipyramidal geometries when sterics and binding positions allow it.

1.5 Scope of Thesis

Indium(III) salts have received considerable attention as Lewis acids in recent years. Their stability to coordinating functional groups present in organic synthesis makes them excellent catalysts for a wide variety of transformations. For transformations mediated by Lewis acids, $InOTf_3$ and $InCl_3$ are particularly efficient catalysts. These catalysts are ill-defined both structurally and spectroscopically. As a result, the active species when these reagents are used as catalysts are unknown and can only be speculated at.

The goal of this thesis is to synthesise a library of new well defined molecules based on indium triflate (and related triflamide [NTf_2]) and indium (III) chloride that are suitable for single crystal X-ray analysis and NMR spectroscopy and can therefore be unambiguously structurally characterised. This should provide us with a means to ascertain vital and previously unknown information about the activity of indium(III) triflate, indium(III) triflamide and indium(III) chloride in Lewis acid catalysed organic transformation reactions.

Our intended complex design is shown in Figure 45. Introduction of a capping ligand to trimethylindium and indium(III) chloride should stabilise the metal centre. This stabilisation should make it possible to substitute some of the methyl/chloro groups for more labile ligands such as triflates and triflamides. The weakly interacting nature of the triflate and triflamide anions means they can break their bonds with the indium core to generate a vacant site at the metal centre. It is hoped that this vacant position generated will be a Lewis acidic active site to which an organic substrate can bind whereby the complex can act as a catalyst.

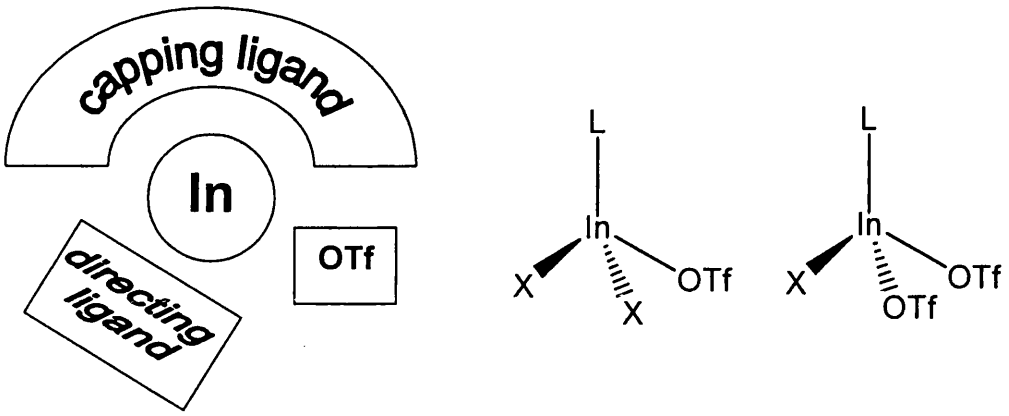

Figure 45 : General scheme for complex design (where L = capping ligand, X = Me, Cl)

It should prove possible to substitute more than one methyl or chloride ligand, so replacing two or all three methyls or chlorides with systems with higher lability will also be investigated to see how this affects catalytic activity.

1.6 References

(1) Simmonds, M. G.; Gladfelter, W. L. *The Chemistry of Metal CVD*; VCH: Weinheim, 1994.
(2) Araki, S.; Ito, H.; Butsugan, Y. *J. Org. Chem.* **1988**, *53*, 1831-1833.
(3) Cintas, P. *Synlett* **1995**, 1087-&.
(4) Li, C. J.; Chan, T. H. *Tetrahedron* **1999**, *55*, 11149-11176.
(5) Ranu, B. C. *Eur. J. Org. Chem.* **2000**, 2347-2356.
(6) Chauhan, K. K.; Frost, C. G. *J. Chem. Soc.-Perkin Trans. 1* **2000**, 3015-3019.
(7) Podlech, J.; Maier, T. C. *Synthesis* **2003**, 633-655.
(8) Nair, V.; Ros, S.; Jayan, C. N.; Pillai, B. S. *Tetrahedron* **2004**, *60*, 1959-1982.
(9) Frost, C. G.; Hartley, J. P. *Mini-Rev. Org. Chem.* **2004**, *1*, 1-7.
(10) Babu, G.; Perumal, P. T. *Aldrichim. Acta* **2000**, *33*, 16-22.
(11) Ranu, B. C.; Dutta, P.; Sarkar, A. *J. Org. Chem.* **1998**, *63*, 6027-6028.
(12) Loh, T. P.; Xu, K. C.; Ho, D. S. C.; Sim, K. Y. *Synlett* **1998**, 369-+.
(13) Ranu, B. C.; Dutta, P.; Sarkar, A. *J. Chem. Soc.-Perkin Trans. 1* **2000**, 2223-2225.
(14) Ranu, B. C.; Hajra, A. *J. Chem. Soc.-Perkin Trans. 1* **2001**, 355-357.
(15) Ranu, B. C.; Hajra, A. *J. Chem. Soc.-Perkin Trans. 1* **2001**, 2262-2265.
(16) Ceschi, M. A.; Felix, L. D.; Peppe, C. *Tett. Lett.* **2000**, *41*, 9695-9699.
(17) Muthusamy, S.; Babu, S. A.; Gunanathan, C. *Tet. Lett.* **2001**, *42*, 359-362.
(18) Ranu, B. C.; Das, A.; Samanta, S. *Synlett* **2002**, 727-730.
(19) Ranu, B. C.; Jana, U. *J. Org. Chem.* **1998**, *63*, 8212-8216.
(20) Loh, T. P.; Pei, J. A.; Cao, G. Q. *Chem. Commun.* **1996**, 1819-1820.
(21) Kobayashi, S.; Busujima, T.; Nagayama, S. *Tet. Lett.* **1998**, *39*, 1579-1582.
(22) Loh, T. P.; Wei, L. L. *Tet. Lett.* **1998**, *39*, 323-326.
(23) Loh, T. P.; Pei, J.; Lin, M. *Chem. Commun.* **1996**, 2315-2316.
(24) Weinreb, S. M. *Comprehensive Organic Synthesis*; Pergamon Press: Oxford, UK, 1991.
(25) Boger, D. L.; Weinreb, S. M.; Academic Press: New York, 1987.
(26) Babu, G.; Perumal, P. T. *Tetrahedron* **1998**, *54*, 1627-1638.
(27) Chauhan, K. K.; Frost, C. G.; Love, I.; Waite, D. *Synlett* **1999**, 1743-1744.
(28) Ali, T.; Chauhan, K. K.; Frost, C. G. *Tett. Lett.* **1999**, *40*, 5621-5624.
(29) Kobayashi, S.; Ishitani, H.; Nagayama, S. *Chem. Lett.* **1995**, 423-424.
(30) Muthusamy, S.; Babu, S. A.; Gunanathan, C. *Tetrahedron* **2002**, *58*, 7897-7901.
(31) Mineno, T. *Tetrahedron Letters* **2002**, *43*, 7975-7978.
(32) Loh, T. P.; Hu, Q. Y.; Ma, L. T. *J. Am. Chem. Soc.* **2001**, *123*, 2450-2451.
(33) Loh, T. P.; Hu, Q. Y.; Tan, K. T.; Cheng, H. S. *Org. Lett.* **2001**, *3*, 2669-2672.
(34) Muthusamy, S.; Babu, S. A.; Gunanathan, C. *Tet. Lett.* **2002**, *43*, 3133-3136.
(35) Gadhwal, S.; Sandhu, J. S. *J. Chem. Soc., Perkin Trans. 1* **2000**, 2827-2829.
(36) France, S.; Wack, H.; Hafez, A. M.; Taggi, A. E.; Witsil, D. R.; Lectka, T. *Org. Lett.* **2002**, *4*, 1603-1605.
(37) Frost, C. G.; Hartley, J. P.; Griffin, D. *Tet. Lett.* **2002**, *43*, 4789-4791.
(38) Hartley, J. P., University of Bath, 2002.
(39) Tuck, D. G. *Chemistry of aluminium, gallium, indium and thallium, ch8 and refs. therein.*; Blackie Academie: Glasgow, 1993.
(40) Wells, R. L.; Kher, S. S.; Baldwin, R. A.; White, P. S. *Polyhedron* **1994**, *13*, 2731-2735.

(41) Willey, G. R.; Aris, D. R.; Haslop, J. V.; Errington, W. *Polyhedron* **2001**, *20*, 423-429.
(42) Jin, S. C.; McKee, V.; Nieuwenhuyzen, M.; Robinson, W. T.; Wilkins, C. J. *J. Chem. Soc., Dalton Trans.* **1993**, 3111-3116.
(43) Clegg, W.; Norman, N. C.; Pickett, N. L. *Acta Crystallogr. C* **1994**, *50*, 36-38.
(44) Alcock, N. W.; Degnan, I. A.; Howarth, O. W.; Wallbridge, M. G. H. *J. Chem. Soc., Dalton Trans.* **1992**, 2775-2780.
(45) Veidis, M. V.; Palenik, G. J. *Chem. Comm.* **1969**, 586-587.
(46) Degnan, I. A.; Alcock, N. W.; Roe, S. M.; Wallbridge, M. G. H. *Acta Crystallogr. C* **1992**, *48*, 995-999.
(47) Sigl, M.; Schier, A.; Schmidbaur, H. *Eur. J. Inorg. Chem.* **1998**, 203-210.
(48) Karia, R.; Willey, G. R.; Drew, M. G. B. *Acta Crystallogr. C* **1986**, *42*, 558-560.
(49) Pauls, J.; Chitsaz, S.; Neumuller, B. *Z. Anorg. Allg. Chem.* **2001**, *627*, 1723-1730.
(50) Beddoes, R. L.; Collison, D.; Mabbs, F. E.; Temperley, J. *Acta Crystallogr. C* **1991**, *47*, 58-61.
(51) Williams, D. J.; Bevilacqua, V. L. H.; Morson, P. A.; Dennison, K. J.; Pennington, W. T.; Schimek, G. L.; VanDerveer, D.; Kruger, J. S.; Kawai, N. T. *Inorg. Chim. Acta* **1999**, *285*, 217-222.
(52) Baker, R. J.; Davies, A. J.; Jones, C.; Kloth, M. *J. Organomet. Chem.* **2002**, *656*, 203-210.
(53) Jones, C.; Richards, A. F. *J. Organomet. Chem.* **2001**, *629*, 109-113.
(54) Kim, J.; Bott, S. G.; Hoffman, D. M. *J. Chem. Soc., Dalton Trans.* **1999**, 141-146.
(55) Prust, J.; Muller, P.; Rennekamp, C.; Roesky, H. W.; Uson, I. *J. Chem. Soc., Dalton Trans.* **1999**, 2265-2266.
(56) Crittendon, R. C.; Beck, B. C.; Su, J. R.; Li, X. W.; Robinson, G. H. *Organometallics* **1999**, *18*, 156-160.
(57) Blake, A. J.; Cradock, S. *J. Chem. Soc., Dalton Trans.* **1990**, 2393-2396.
(58) Bradley, D. C.; Frigo, D. M.; Harding, I. S.; Hursthouse, M. B.; Motevalli, M. *Chem. Comm.* **1992**, 577-578.
(59) Coward, K. M.; Jones, A. C.; Steiner, A.; Bickley, J. F.; Smith, L. M.; Pemble, M. E. *J. Chem. Soc., Dalton Trans.* **2001**, 41-45.
(60) Bradley, D. C.; Chudzynska, H.; Faktor, M. M.; Frigo, D. M.; Hursthouse, M. B.; Hussain, B.; Smith, L. M. *Polyhedron* **1988**, *7*, 1289-1298.
(61) Visona, P.; Benetollo, F.; Rossetto, G.; Zanella, P.; Traldi, P. *J. Organomet. Chem.* **1996**, *511*, 59-65.
(62) Self, M. F.; McPhail, A. T.; Jones, L. J.; Wells, R. L. *Polyhedron* **1994**, *13*, 625-634.
(63) Wang, W. J.; Pan, Y.; Huang, X. Y.; Sun, H. S.; Lua, Z. B.; Sun, X. Z. *Acta Crystallogr. C* **1996**, *52*, 1661-1663.
(64) Storr, A.; Thomas, B. S. *Can. J. Chem.* **1970**, *23*, 3667.
(65) Clark, H. C.; Pickard, A. L. *J. Organomet. Chem.* **1968**, *13*, 61.
(66) Abernethy, C. D.; Cole, M. L.; Jones, C. *Organometallics* **2000**, *19*, 4852-4857.
(67) Bradley, D. C.; Dawes, H.; Frigo, D. M.; Hursthouse, M. B.; Hussain, B. *J. Organomet. Chem.* **1987**, *325*, 55-67.
(68) Bradley, D. C.; Harding, I. S. *J. Chem. Soc., Dalton Trans.* **1997**, 4637-4641.

(69) Burns, J. A.; Dillingham, M. D. B.; Hill, J. B.; Gripper, K. D.; Pennington, W. T.; Robinson, G. H. *Organometallics* **1994**, *13*, 1514-1517.
(70) Dillingham, M. D. B.; Burns, J. A.; Byershill, J.; Gripper, K. D.; Pennington, W. T.; Robinson, G. H. *Inorg. Chim. Acta* **1994**, *216*, 267-269.
(71) Leman, J. T.; Roman, H. A.; Barron, A. R. *Organometallics* **1993**, *12*, 2986-2990.
(72) Leman, J. T.; Roman, H. A.; Barron, A. R. *J. Chem. Soc., Dalton Trans.* **1992**, 2183-2191.
(73) Styron, E. K.; Lake, C. H.; Powell, D. H.; Krannich, L. K.; Watkins, C. L. *J. Organomet. Chem.* **2002**, *649*, 78-85.
(74) Styron, E. K.; Schauer, S. J.; Lake, C. H.; Watkins, C. L.; Krannich, L. K. *J. Organomet. Chem.* **1999**, *585*, 266-274.
(75) Beachley, O. T.; Robirds, E. S.; Atwood, D. A.; Wei, P. R. *Organometallics* **1999**, *18*, 2561-2564.
(76) Beachley, O. T.; MacRae, D. J.; Kovalevsky, A. Y.; Zhang, Y. G.; Li, X. *Organometallics* **2002**, *21*, 4632-4640.
(77) Beachley, O. T.; MacRae, D. J.; Churchill, M. R.; Kovalevsky, A. Y.; Robirds, E. S. *Organometallics* **2003**, *22*, 3991-4000.
(78) Park, J. H.; Horley, G. A.; O'Brien, P.; Jones, A. C.; Motevalli, M. *J. Mater. Chem.* **2001**, *11*, 2346-2349.
(79) Cotgreave, J. H.; Colclough, D.; Kociok-Kohn, G.; Ruggiero, G.; Frost, C. G.; Weller, A. S. *J. Chem. Soc., Dalton Trans.* **2004**, 1519-1520.
(80) Macdonald, C. L. B.; Corrente, A. M.; Andrews, C. G.; Taylor, A.; Ellis, B. D. *Chem. Comm.* **2004**, 250-251.
(81) Fischer, R. A.; Sussek, H.; Miehr, A.; Pritzkow, H.; Herdtweck, E. *J. Organomet. Chem.* **1997**, *548*, 73-82.
(82) Beachley, O. T.; Churchill, M. R.; Fettinger, J. C.; Pazik, J. C.; Victoriano, L. *J. Am. Chem. Soc.* **1986**, *108*, 4666-4668.

Chapter 2 - β-Ketoimine Complexes of In(III)

2.1 Introduction

To gain a better structural awareness of Lewis acidic indium complexes and study their subsequent activity, it is vital to have a system from which structural information can be readily obtained. β-ketoimine ligands and derivatives thereof suggested themselves as good candidates for preparing such complexes and currently few examples of β-ketoimine complexes of indium exist. β-ketoimines can be readily functionalised at a range of positions and should provide a good route to structurally characterised indium complexes.

Firstly an introduction to the three closely related ligand types including β-ketoimines will be briefly reviewed, including their coordination to indium. This will be followed by a report of our synthesis of a range of structurally well-defined indium β-ketoimine systems.

2.1.1 β-Ketoimine, β-Diketone and β-Diketiminate Complexes of Indium

The use of β-diketones, β-ketoimines, and β-diketiminates ligands is widespread in coordination chemistry.[1-3] The general framework of these three ligands is shown in Figure 1, and their coordination chemistry to indium will be discussed in turn.

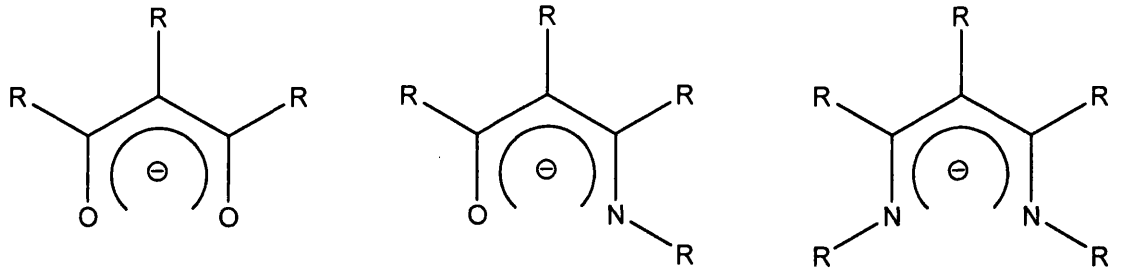

β-diketones β-ketoimines β-diketiminates

Figure 1 : The three chelating ligands (where R can be a range of alkyl groups or hydrogens)

2.1.2 β-Diketone Complexes of Indium

Much attention has been paid to the structural chemistry of β-diketones involving keto-enol tautomerism (Figure 2).[4,5]

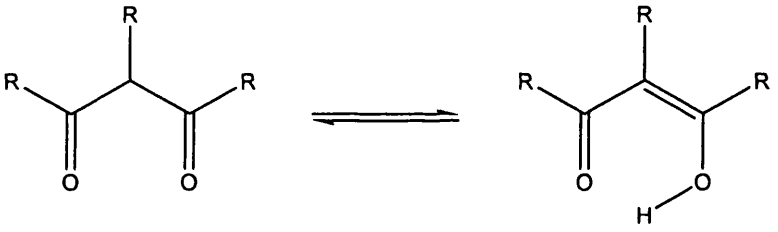

Figure 2 : Keto-enol tautomerism of β-diketones

This tautomerism allows acac to react with $InMe_3$ to produce $[Me_2In(acac)]_2$. The driving force for the reaction is methane elimination which occurs via protonolysis with the enol tautomer providing the acidic hydrogen. The loss of a proton from the enol, gives the ligand a monoanionic charge and thus on binding to the indium the metal retains it +3 oxidation state. A fluorinated derivative of $[Me_2In(acac)]_2$ has also been reported - $[Me_2In(hfac)]_2$ (where hfac = 1,1,1,5,5,5-hexafluoro-2,4-pentanedionate).[6]

Indium has also been bound to this type of ligand for ion-size recognition studies of group 13 metals with modified β-diketones.[7] It was determined that structural modification of the β-diketone chelate by introduction of bulky groups, altered ligand sterics improving selectivity between indium and aluminium. This change in sterics caused a change in the O···O distance between the oxygens of the two carbonyls in the chelate ring and the ligands could be tuned to improve selectivity towards either metal ion.

The previous two examples show indium : β-diketone 1:1 dimeric complexes, but it also possible to bind more than one equivalent of the ligand to indium as shown by the complexation of indium to dibenzoylmethanate in a 1:3 ratio.[7] Dimer formation in this case is avoided by steric protection.

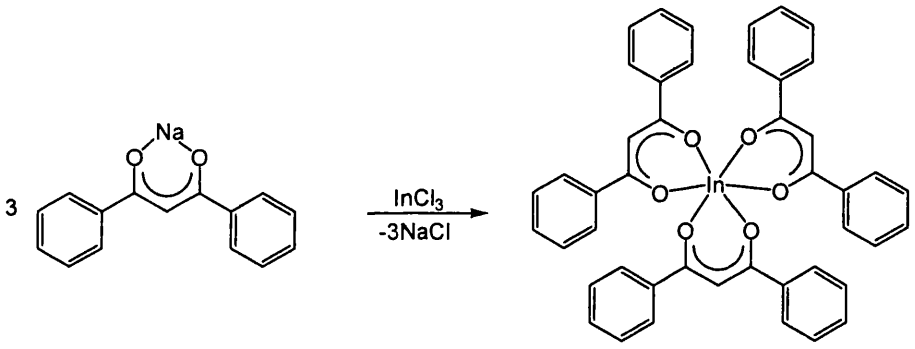

Figure 3 : Scheme showing the reaction of dibenzoylmethane with $InCl_3$ [7]

Use of salicylaldehyde compounds instead of β-diketones still results in indium β-diketonate complexes (Figure 4).[8]

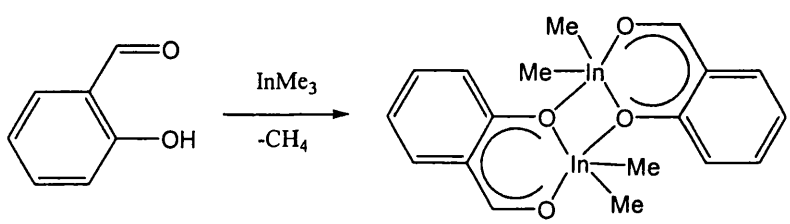

Figure 4 : Dimer formation as a result of reaction of $InMe_3$ with one equivalent of salicylaldehyde [8]

More recently, $InMe_3$ was reacted with methyl salicylate 2-$(HO)C_6H_4CO_2Me$ or (Hmesal) to give a similar compound (Figure 5).[9]

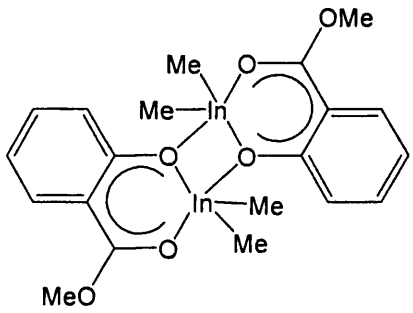

Figure 5 : Product of reaction of $InMe_3$ with Hmesal [9]

The reaction is stoichiometric and proceeds in essentially quantitative yield with one equivalent of methane eliminated.

2.1.3 β-Diketiminate Complexes of Indium

β-diketiminates have been bound to a host of main group and transition metals and lanthanides.[10,11] Recently there has been a revived interest in these bidentate, monoanionic ligands. This is particularly the case when the more sterically encumbered derivatives are concerned, especially those containing ortho-substituted aryl substitutents. The steric bulk of these ligands allows them to stabilize low coordination numbers, rare coordination geometries and low oxidation states.[12,13]

Coordination of the bulky $[dipp_2nacnac]^-$ ligand (Figure 6) to a range of metals has been reported including nickel,[14] palladium,[15] iron and copper,[16,12] as well as indium and other group 13 metals (dipp = C_6H_3-2,6-i-Pr_2 where $nacnac^-$ was so named because of its analogy to $acac^-$).[11]

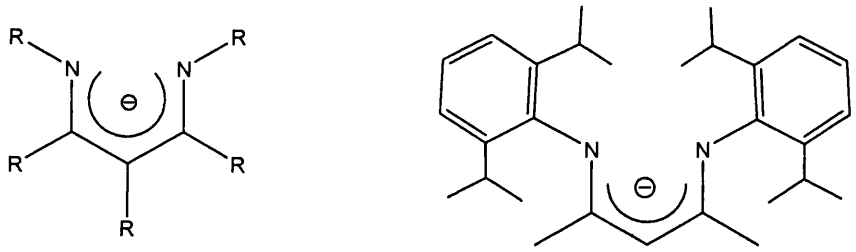

Figure 6 : General scheme for β-diketiminates and $dipp_2nacnac^-$

The synthesis of the bis-methyl, -chloro, -bromo and -iodo indium complexes of $dipp_2nacnac$ have been reported (Figure 7).[11] The formation of these 4-coordinate indium compounds occurs via a reaction of indium(III) halide precursors with lithium etherate salts of the ligand. The bis-methyl derivative is then accessible by the reaction of two equivalents of methyl Grignard with the bis-chloride complex.[17] The bulky dipp groups ensure dimerisation cannot occur and as a result all four of the indium complexes are monomeric.

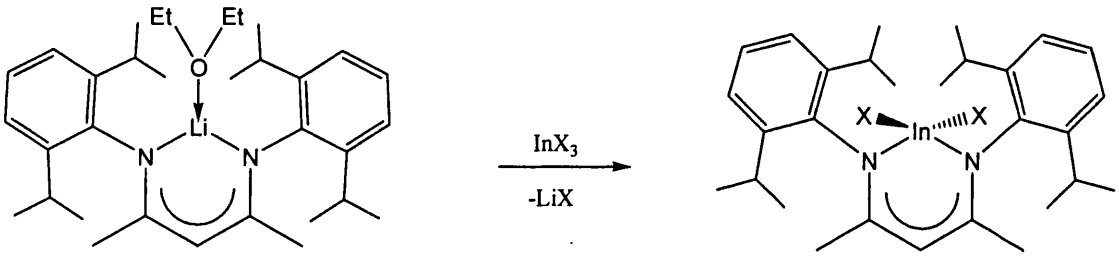

Figure 7 : Reaction scheme of $InX_2dipp_2nacnac$ (where X = Cl, Br, I) [11]

The reaction of trimethylindium with the bidentate monoanionic ligand N,N'-diisopropylaminotroponiminate ($^iPr_2$-ATI)H, a similar system to the β-diketiminates, has also been documented (Figure 8).[18]

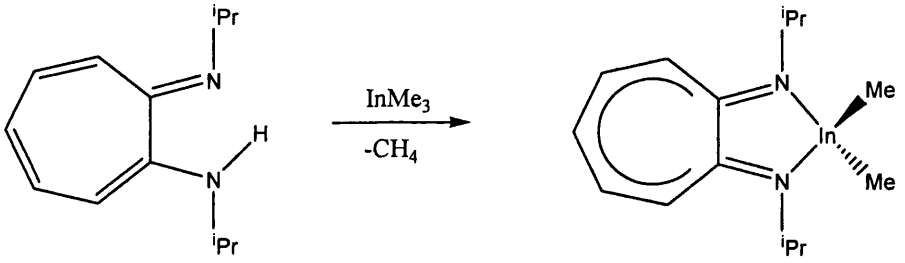

Figure 8 : Synthesis of $Me_2In(^iPr_2\text{-ATI})$ [18]

$Me_2In(^iPr_2\text{-ATI})$ is also accessible via the bis chloride congener, $Cl_2In(^iPr_2\text{-ATI})$.[18] $Me_2In(^iPr_2\text{-ATI})$ is a monomer in the solid state.

2.1.4 β-Ketoimine Complexes of Indium

β-ketoimines - Schiff-base derivatives of β-diketones - were first documented in 1927,[19] and can be considered to exist in two basic forms (Figure 9).

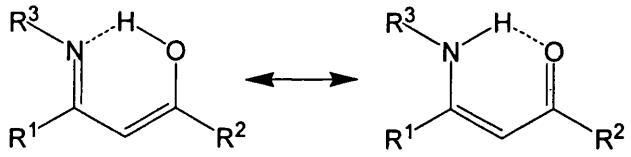

Figure 9 : The two basic forms of a β-ketoimine

β-ketoimines have been coordinated to silicon,[20] copper(I),[21] zirconium(IV) and titanium(IV),[22] but reports of their coordination to indium are scarce. However, trimethylindium and triethylindium have been reacted with the Schiff base ligands of *N*-salicylidene-2-aminopyridine and *N*-salicylidene-2-methoxyaniline (Figure 10).[23]

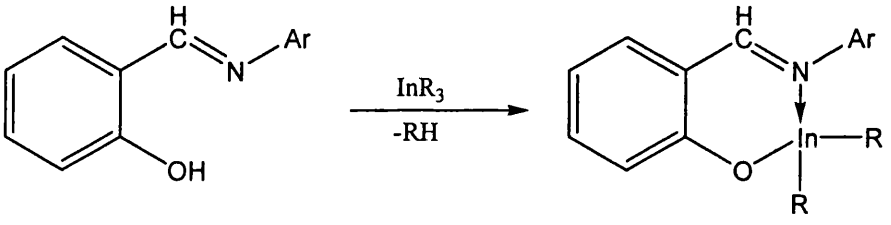

Figure 10 : Reaction scheme for the reaction of trimethyl- and triethylindium with N-salicylidenes (where Ar = 2-methoxyaniline, 2-aminopyridine and R = Me, Et) [23]

Mass spectrometry shows no peaks higher than that of M^+, implying that solid state dimerisation does not occur. The two triethylindium species **(A)** and **(B)** have been shown to be 5- and 4-coordinate respectively in the solid state (Figure 11).

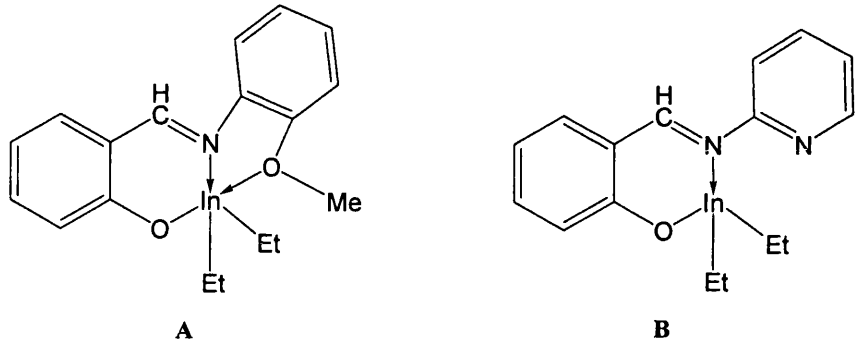

Figure 11 : The compounds of Pan *et al.* (**A** and **B**) [23]

$InMe_3$ reacts with a stoichiometric quantity of 2-(2-pyridyl)ethanol to produce indium[2-(2-pyridyl)]ethoxide (Figure 12).[24] While this is not a β-ketoimine, the reaction occurs through a similar pathway, i.e. methane elimination. The sterics of the ligand system permit dimerisation to occur and as a result the two indium metal atoms in the complex are 5-coordinate.

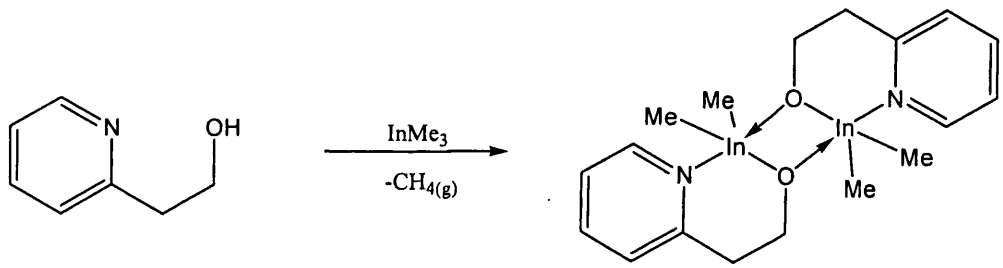

Figure 12 : Reaction of 2-(2-pyridyl)ethanol with trimethylindium [24]

Indium β-ketoimine analogues have also seen use in MOCVD. The utilization of $HOC(CF_3)_2CH_2NHR$, (R = $(CH_2)_2OMe$, Me or ^tBu) with $InMe_3$ gave the type of results shown in Figure 13.[25]

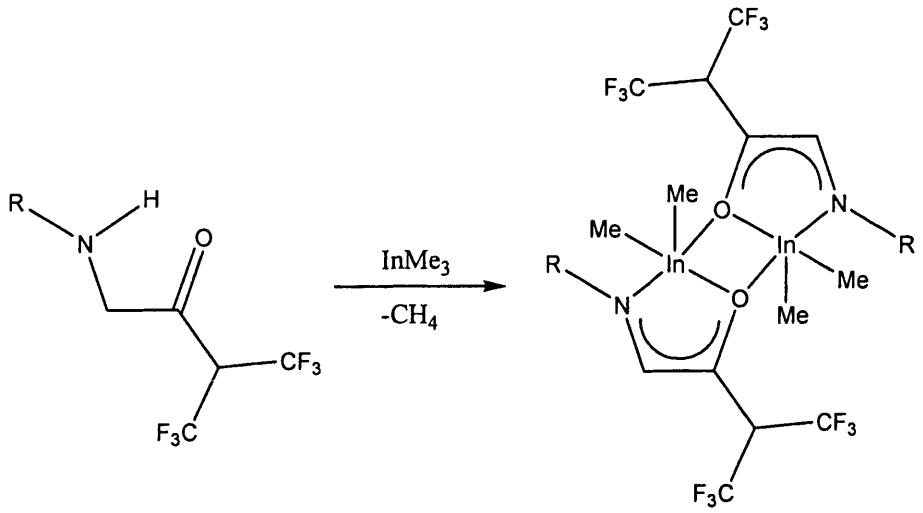

Figure 13 : Reaction of $HOC(CF_3)_2CH_2NHR$ with $InMe_3$ (where R = $(CH_2)_2OMe$, Me, or ^tBu) [25]

By altering the R group on the nitrogen to a $CH_2CH_2NMe_2$ and adding a methylene to the linker between the ketone and amine group, dimerisation was avoided. The nitrogen from the NMe_2 group stabilises the indium and makes it 5-coordinate, also blocking off coordination of a second molecule (Figure 14).

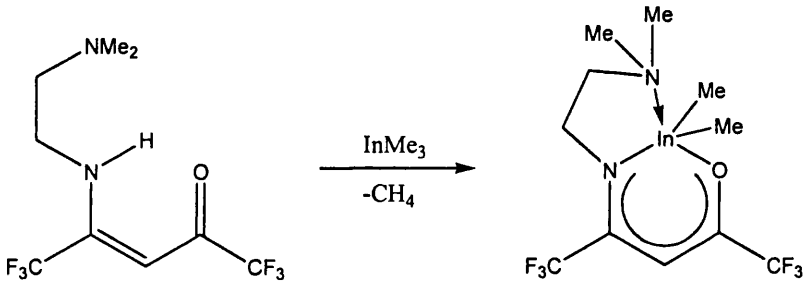

Figure. 14 : Reaction of $O=C(CF_3)CH_2C(CF_3)=NCH_2CH_2NMe_2$ with $InMe_3$ [25]

2.1.5 Summary and Scope of Chapter

In summary, there is precedent for coordinating indium to β-diketone, β-diketiminate and β-ketoimine ligands and some of these compounds have been structurally characterised. However no reactivity studies on these systems have been reported. These systems will often dimerise in the solid state by forming In_2O_2 four-membered rings unless steric protection of the metal centre prohibits it. The literature suggests

that direct reaction of trimethylindium with β-ketoimines should result in bismethyl indium complexes from which it should be possible to grow crystals suitable for single crystal X-ray diffraction.

A range of indium β-ketoimine complexes will be synthesized and structurally and spectroscopically characterized. The properties of these complexes will then be investigated with particular respect to their reactivity regarding substitution of the methyl groups with triflate ligands. Substitution of the methyl/chloro substituents for triflate/triflamide ligands should provide us with a library of indium complexes of the type shown in Figure 15, possessing an active site so they can be screened for activity as Lewis acid catalysts in organic transformations.

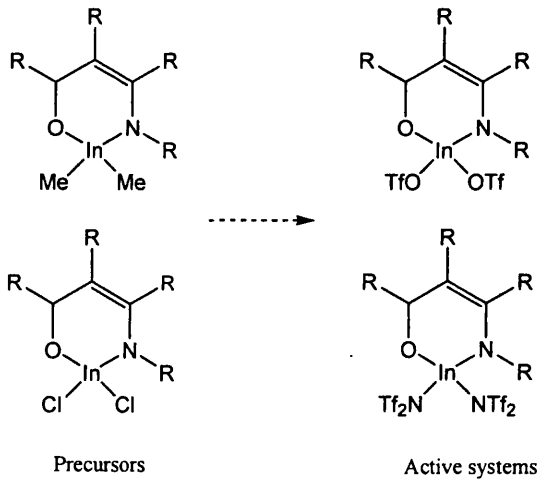

Figure 15 : Scheme showing the planned complex design

2.2 Results

2.2.1 Synthesis of $[Me_2In\{N[C_6H_5]C(CH_3)CHC(CH_3)\mu\text{-}O\}]_2$, (1)

The simple β-ketoimine 4-phenylaminopent-3-ene-2-one was synthesized by literature methods.[19,26,20] The synthesis involved overnight reflux of pentane-2-4-dione and aniline in toluene in the presence of 1mol% para-toluene sulphonic acid (PTSA), using a Dean-Stark apparatus to tap off the water-toluene azeotrope.

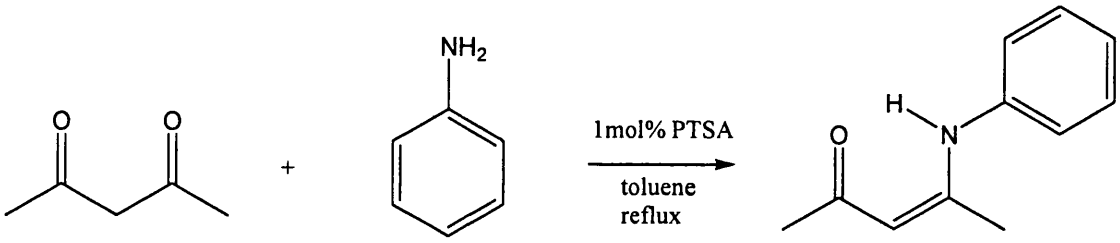

Figure 16 : Reaction of pentane-2,4-dione and aniline

Reaction of this ligand with a stoichiometric amount of $InMe_3$ in toluene followed by removal of the solvent *in vacuo* gave $[Me_2In\{N[C_6H_5]C(CH_3)CHC(CH_3)\mu\text{-}O\}]_2$, compound **(1)** shown in Figure 17. By tracking the reaction *in situ* by ^1H NMR spectroscopy a singlet resonance was observed at 0.16ppm in C_6D_6 attributed to methane production. Crystals suitable for X-ray crystallography were obtained by dissolving the compound in minimum hexane and storing the solution at 4°C.

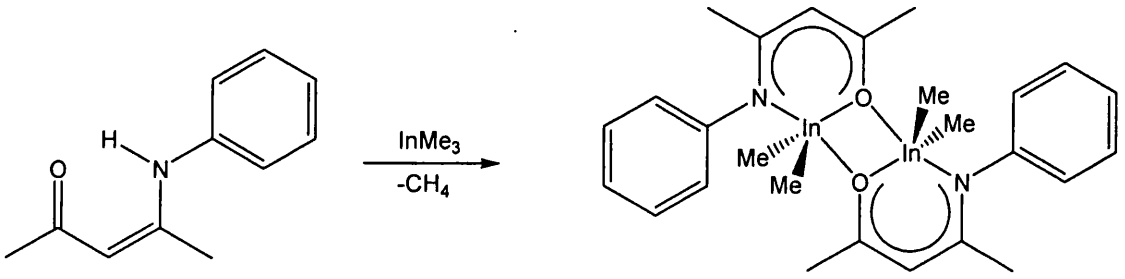

Figure 17 : Reaction of 4-phenylaminopent-3-ene-2-one and $InMe_3$ to form **(1)**

Figure 18 shows the solid state structure of compound **(1)**. The compound is a dimer in the solid state, where it forms a 4 membered In-O-In-O ring. Table 2 shows a list of relevant bond lengths and angles. The internal angles in the In_2O_2 ring (O-In-O# 73.66°, In-O-In# = 106.34°) are comparable to a similar, reported indium complex (O-In-O# = 75.4(2)°, In-O-In# = 104.6(2)°) (see dimethylindium[2-(2-pyridyl)]ethoxide in Table 1).[24] The plane defined by one indium and the carbon atoms of the two metal bound methyl groups is approximately perpendicular to the plane of the central In_2O_2 ring. The 6-membered In-O-C-C-C-N-In chelate rings are planar and sit in the same plane as the In_2O_2 4-membered ring. The In-O bond length of 2.1637(11)Å is shorter than the In-O# bond length of 2.611Å by around 0.45Å. This is in accordance with an asymmetric bridging mode in the In_2O_2 core of the dimer, with two weak or O:→In dative bonds. Table 1 shows the In-O and In-N bonds for **(1)** and two reported, structurally similar compounds.[24,27]

	Compound **(1)**	dimethyl[μ-(2-pyridinecarboxo-aldehydeoximato)]indium [27]	dimethylindium[2-(2-pyridyl)]ethoxide [24]
	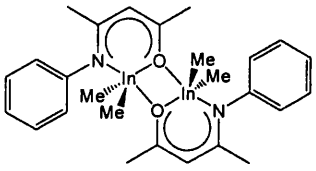	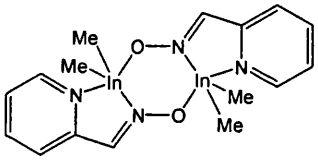	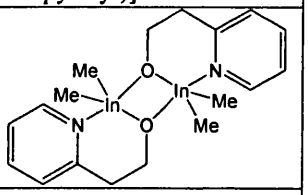
In-O	2.164(1)Å	No In-O bond present in the monomer unit	2.132(5)Å
In-O#	2.611Å	2.241(16)Å	2.240(5)Å
In-N	2.306(1)Å	2.271(16)Å & 2.228(15)Å	2.523(5)Å

Table 1: Comparisons of In-O and In-N bond lengths of complex **(1)** with similar compounds in the literature

As the data shows, the bond lengths of **(1)** are within the same range as for previously reported compounds in the literature, where there is a balance between the In-O and In-N bond lengths, i.e. compound **(1)** has a weaker In-O bond, but a stronger In-N

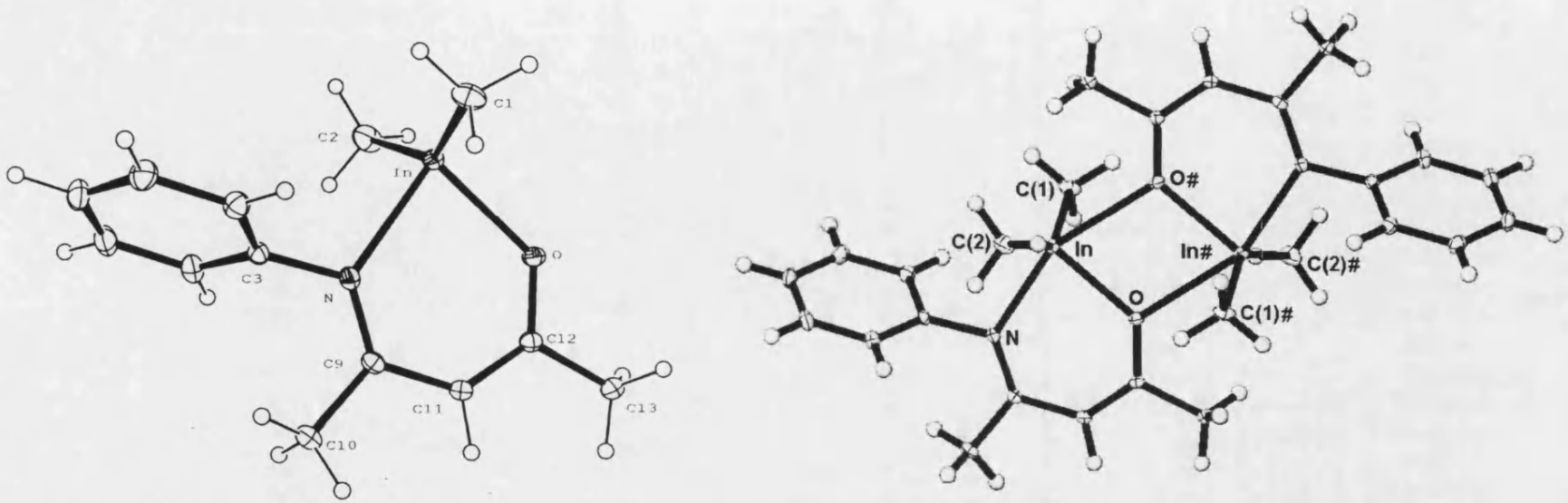

Figure 18 : Molecular structure of the asymmetric unit of $[Me_2In\{N[C_6H_5]C(CH_3)CHC(CH_3)\mu\text{-}O\}]_2$ and the solid state structure showing all In contacts in the unit cell (ellipsoids drawn at 30% probability level)

In-C(2)	2.1400(19)	C(2)-In-C(1)	143.30(8)	In-O#	2.611	In-O-In#	106.34
In-C(1)	2.1438(17)	C(2)-In-O	110.16(7)	In#-O#	2.164	O#-In-C(1)	103.70
In-O	2.1637(11)	C(1)-In-O	103.70(7)			O#-In-C(2)	110.17
In-N	2.3057(13)	C(2)-In-N	98.14(7)			O-In-O#	73.66
N-C(9)	1.305(2)	C(1)-In-N	99.05(6)				
N-C(3)	1.429(2)	O-In-N	84.01(5)				
O-C(12)	1.3079(19)	C(12)-O-In	128.70(10)				

Table 2 : Selected bond lengths (Å) and angles (°) for **(1)**

bond than dimethylindium[2-(2-pyridyl)ethoxide.[24] The bridging In-O# bonds in this compound, however, are significantly shorter (by 0.35Å) than in **(1)**.

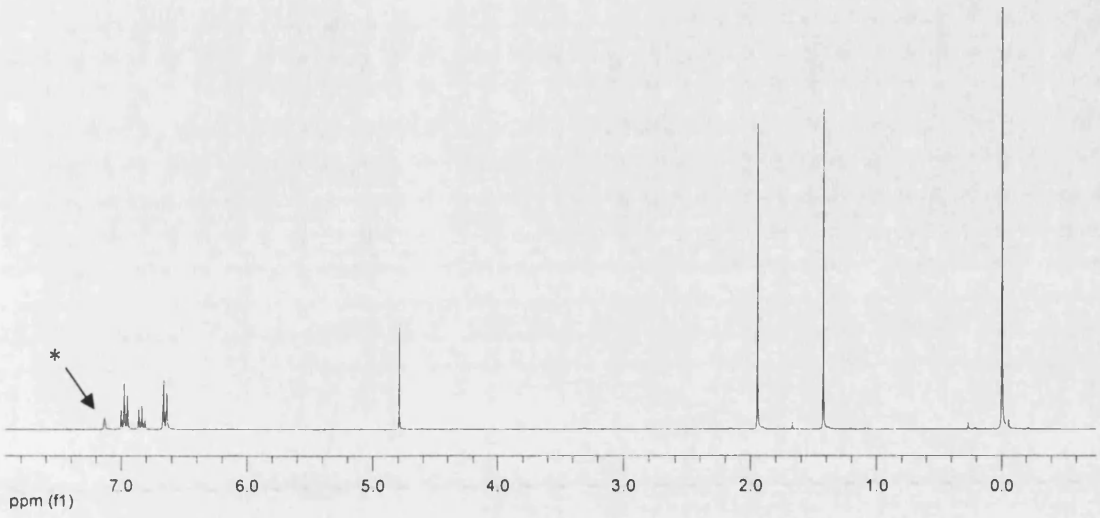

Figure 19 : ^{1}H spectrum of compound **(1)** (* = residual solvent)

Figure 19 shows the ^{1}H NMR spectrum of compound **(1)** in C_6D_6. The metal bound methyl ($InMe_2$) resonances appear as a singlet at 0.03ppm showing the two metal methyl groups are equivalent in solution consistent with the solid state structure. The two methyl groups belonging to the ligand are present as singlets at 1.45 and 1.97ppm, while the sole proton bound to a carbon in the 6-membered In-N-C(CH_3)-C(**H**)-C(CH_3)-O-In ring appears as a singlet at 4.82ppm. The peaks attributed to the aromatic protons appear in the range 6.65-7.04ppm. Comparison of the methyl resonance of $InMe_3$ in C_6D_6 (-0.23ppm) with that of the $InMe_2$ methyls in **(1)** (0.03ppm), shows there is a significant downfield shift of 0.26ppm. This downfield shift has been previously reported for other indium bismethyl compounds complexed with β-ketoimine analogues.[9,18,24] The chemical shift change is related to the electron withdrawing nature of the two metal bound atoms of the bidentate ligand, where the more electronegative the donor atoms, the more deshielded the indium methyl groups. The ^{1}H NMR spectrum of **(1)** was also run in CD_2Cl_2 to compare the $InMe_2$ proton

resonance with the methyl resonance in free $InMe_3$ in CD_2Cl_2. Table 3 shows that the chemical shift change on coordination differs greatly between the two solvents which is important to be aware of when making literature comparisons.

	Chemical Shift (ppm)	
	C_6D_6	**CD_2Cl_2**
$InMe_3$	-0.23	-0.81
Compound **(1)**	0.03	-0.23
Shift difference	**+0.20**	**+0.58**

Table 3 : Chemical shift change comparisons of **(1)** and $InMe_3$

2.2.2 Synthesis of $Me_2In\{N[C_6H_5]C(CH_3)CHC(C_6H_5)\mu\text{-}O\}$, (2)

It was envisaged that dimerisation of this type of compound might be avoided by introducing a more bulky substituent α- to the carbonyl group.[11] By avoiding dimerisation at the precursor stage, when triflate and triflamide ligands are introduced the Lewis acidity at the indium should not be reduced as it would by the larger indium coordination number inherent in dimers. Reflux of benzoylacetone and aniline in a similar manner to that for 4-phenylaminopent-3-ene-2-one, produced 1-phenyl-4-phenylaminopent-3-ene-2-one which has been previously reported (Figure 20).[20]

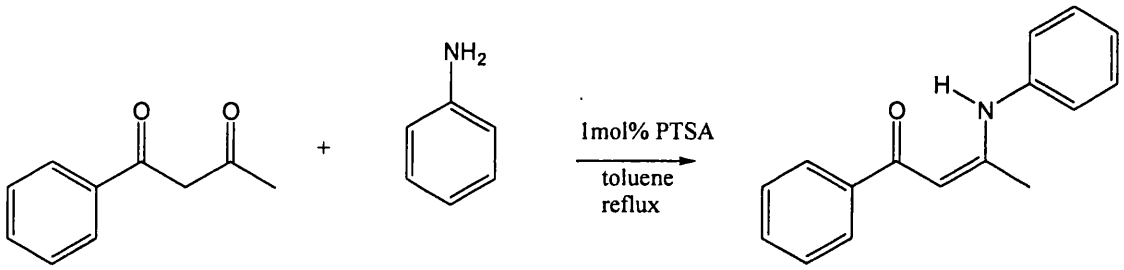

Figure 20 : reaction of benzoylacetone and aniline

Reaction of this ligand with a stoichiometric amount of $InMe_3$ in toluene gave $Me_2In\{N[C_6H_5]C(CH_3)CHC(C_6H_5)\mu\text{-}O\}$, compound **(2)** shown in Figure 21. Removal of the solvent *in vacuo* and recrystallisation of the compound in hexane yielded crystals suitable for X-ray crystallography.

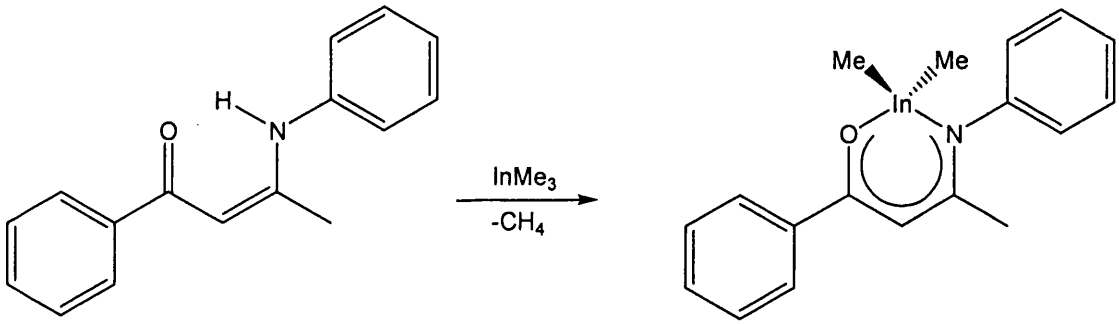

Figure 21 : Reaction of 1-phenyl-4-phenylaminopent-3-ene-2-one and $InMe_3$ to form **(2)**

The solid state structure is shown in Figure 22. Two molecules are present in the asymmetric unit and relevant bond lengths and angles are shown in Table 4. As the structure shows, introducing the more bulky phenyl group prevents dimerisation occurring in the solid state and the result is a 4-coordinate indium complex where no close intermolecular contacts to the metal within 3.6Å are observed (the closest intermolecular indium oxygen distance is 5.432Å). In the absence of dimerisation, the 4-coordinate indium in **(2)** is bound more strongly to both the oxygen and nitrogen of the ligand than in **(1)**. The In-O and In-N bond lengths of **(2)** and **(1)** are shown in Table 5.

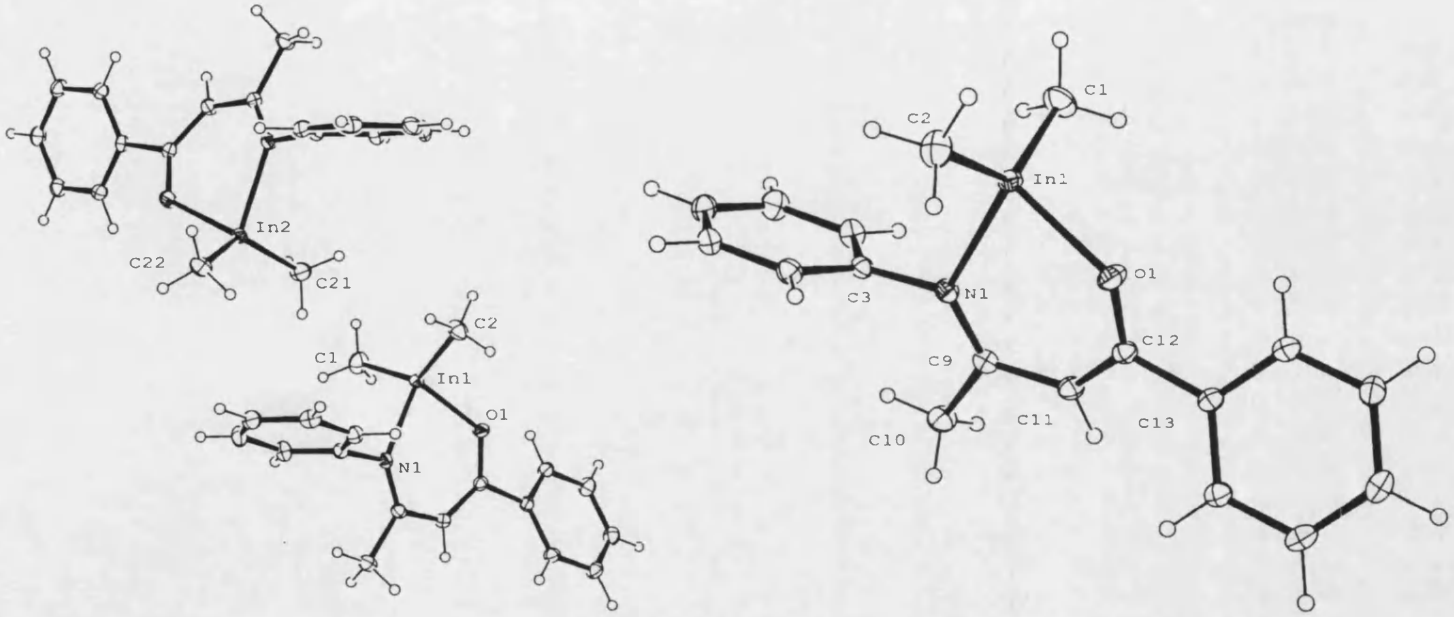

Figure 22 : The asymmetric unit of $Me_2In\{N[C_6H_5]C(CH_3)CHC(C_6H_5)\mu\text{-}O\}$ and the molecular structure of one of the crystallographically inequivalent molecules (ellipsoids drawn at 30% probability level)

In(1)-C(1)	2.142(2)	O(1)-In(1)-C(2)	105.35(8)	In(2)-O(2)	2.1333(14)	O(2)-In(2)-C(22)	105.93(8)
In(1)-C(2)	2.132(2)	O(1)-In(1)-C(1)	108.32(9)	In(2)-C(22)	2.141(2)	O(2)-In(2)-C(21)	108.21(8)
In(1)-O(1)	2.1201(14)	C(2)-In(1)-C(1)	133.12(11)	In(2)-C(21)	2.145(2)	C(22)-In(2)-C(21)	134.25(9)
In(1)-N(1)	2.2110(15)	O(1)-In(1)-N(1)	85.75(6)	N(2)-In(2)	2.2245(15)	O(2)-In(2)-N(2)	85.25(5)
O(1)-C(12)	1.294(2)	C(2)-In(1)-N(1)	110.61(8)			C(22)-In(2)-N(2)	108.57(7)
N(1)-C(9)	1.309(2)	C(1)-In(1)-N(1)	103.56(8)			C(21)-In(2)-N(2)	103.77(8)
N(1)-C(3)	1.435(2)	C(12)-O(1)-In(1)	126.74(12)				

Table 4 : Selected bond lengths (Å) and angles (°) for **(2)**

	Compound (2)	Compound (1)
	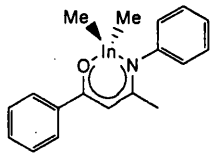	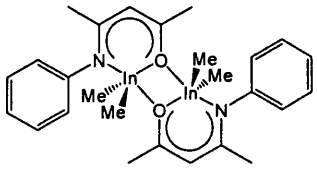
In-O	2.1201(14)Å	2.1637(11)Å
In-N	2.2110(15)Å	2.3057(13)Å

Table 5 : Comparisons of In-O and In-N bond lengths of complexes **(2)** and **(1)**

The plane defined by the indium and the carbon atoms of the two methyl groups is approximately perpendicular to the plane of the central 6-membered chelate ring. The O(1)-In(1)-N(1) bond angle is 85.75(6)° which is similar to the 84.01(5)° angle seen in **(1)**. The ^{1}H NMR spectrum of **(2)** in C_6D_6 shows a singlet for $InMe_2$ at 0.00ppm. This is a very similar chemical shift in comparison to the equivalent resonance in **(1)**, (0.03ppm).

2.2.3 Synthesis of $[Me_2In\{OC(CH_3)CHC(C_6H_5)\mu\text{-}O\}]_2$, (3)

It was unclear if dimerisation could be avoided without the presence of the steric bulk of the phenylamino group, so the commercially available benzoylacetone was reacted directly with $InMe_3$ in toluene. The reaction proceeded cleanly, eliminating methane and yielding the dimethylindiumdiketonate species $[Me_2In\{OC(CH_3)CHC(C_6H_5)\mu\text{-}O\}]_2$, **(3)** (Figure 23). The solvent was removed in vacuo and the product recrystallised in hexane to yield clear and colourless crystals suitable for X-ray crystallography.

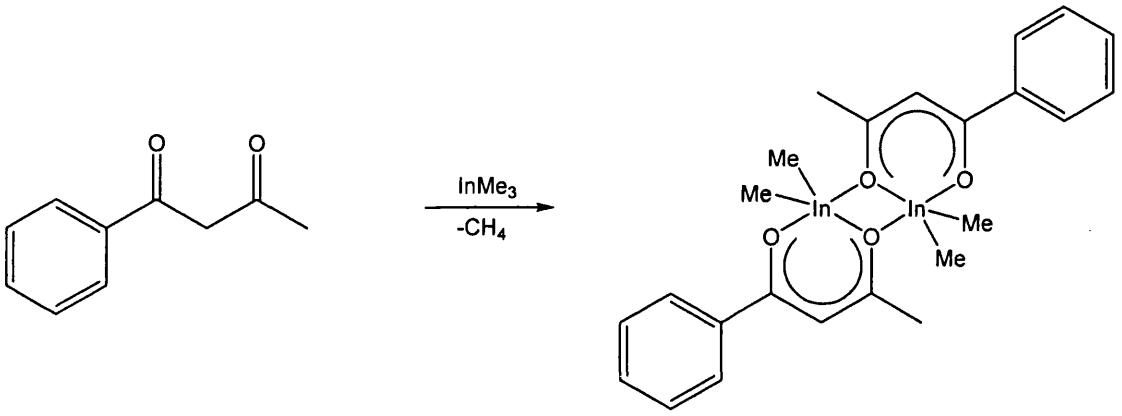

Figure 23 : Reaction of benzoylacetone and $InMe_3$ to form $[Me_2In\{OC(CH_3)CHC(C_6H_5)\mu\text{-}O\}]_2$ **(3)**

The molecular structure of **(3)** is shown in Figure 24. The absence of the phenylamino group in **(2)** does provide enough space for dimerisation to occur in the solid state. The In_2O_2 core comprises the oxygen furthest away from the phenyl group due to the fact that it is the less sterically hindered. Relevant bond lengths and angles of complex **(3)** are shown in Table 7. The In-O bond lengths of **(3)** with those of $[Me_2In(acac)]_2$ and $[Me_2In(mesal)]_2$ are shown in Table 6.[28]

	Compound **(3)**	$[Me_2In(acac)]_2$ [28]	$[Me_2In(mesal)]_2$ [9]
	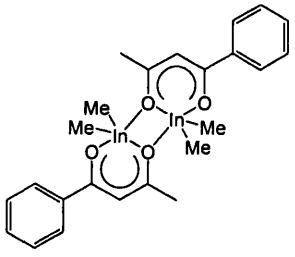	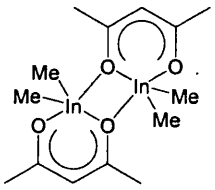	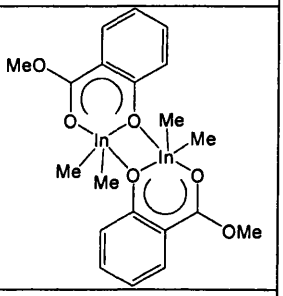
In-O(1)(Å)	2.198(7)	2.194(2)	2.165(4)
In-O(2)(Å)	2.228(7)	2.253(2)	2.332(5)
In-O(1)#(Å)	2.547(7)	2.606(3)	2.376(4)

Table 6 : Comparisons of In-O bond lengths of complex **(3)** with two similar compounds in the literature

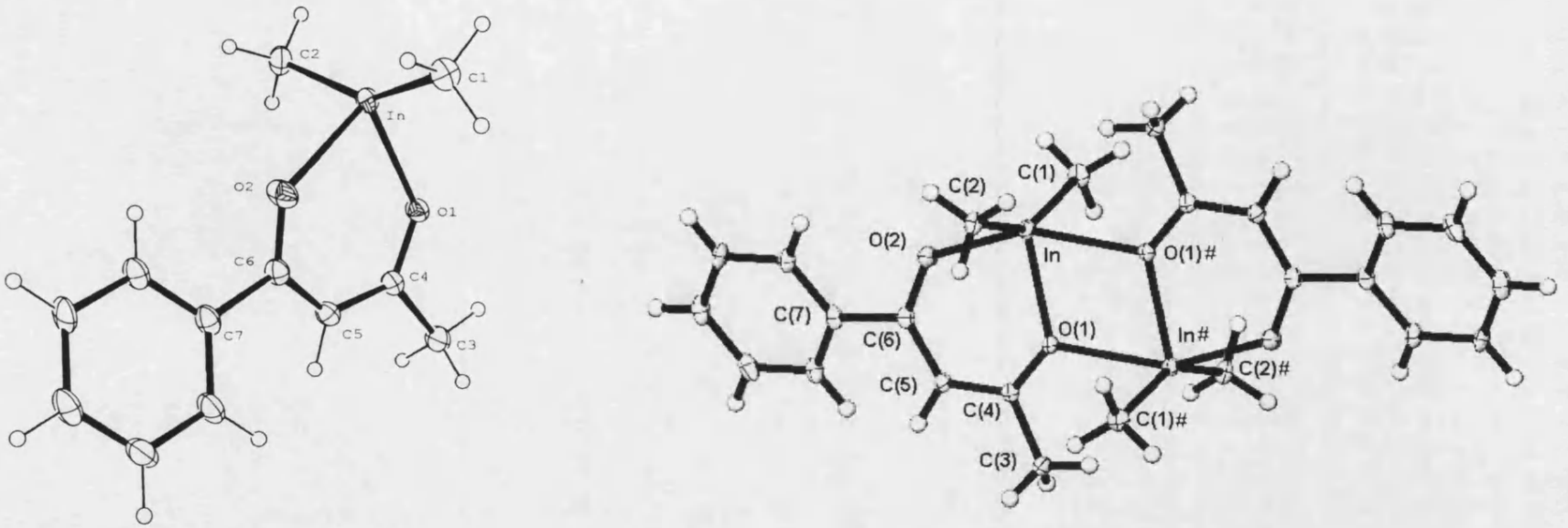

Figure 24 : Asymmetric unit of $[Me_2In\{OC(CH_3)CHC(C_6H_5)\mu\text{-}O\}]_2$ and its dimeric molecular structure (ellipsoids drawn at 30% probability level)

In-C(1)	2.134(11)	C(2)-In-C(1)	148.8(5)	In#-O(1)	2.547(7)	In-O(1)-In#1	105.9(3)
In-C(2)	2.130(11)	C(2)-In-O(1)	104.0(4)			O(1)-In-O(1)#	74.1(3)
In-O(1)	2.198(7)	C(1)-In-O(1)	106.4(4)			C(1)-In-O(1)#	92.3(4)
In-O(2)	2.228(7)	C(2)-In-O(2)	95.6(4)			C(2)-In-O(1)#	89.3(3)
O(1)-C(4)	1.295(11)	C(1)-In-O(2)	95.1(4)			O(2)-In-O(1)#	156.9(3)
O(2)-C(6)	1.272(13)	O(1)-In-O(2)	82.8(3)			C(4)-O(1)-In#	125.1(6)
C(4)-C(5)	1.387(13)	C(4)-O(1)-In	128.7(6)				
C(5)-C(6)	1.400(14)						

Table 7 : Selected bond lengths (Å) and angles (°) for **(3)**

The In-O bond lengths in complex **(3)** and $[Me_2In(acac)]_2$ are very similar in length as expected for these two very similar complexes but the two indium oxygen coordination bonds [In-O(1)#] in **(3)** are slightly shorter than those in $[Me_2In(acac)]_2$. It is clear that the position of the phenyl ring in **(3)** means the ligand is unable to offer any steric protection to the metal centre and so the compound is dimeric in the solid state. Figure 24 shows that the phenyl ring points well away from the In_2O_2 core in the molecular structure so sterically it has little effect on the indium. In the ^1H NMR spectrum the $InMe_2$ resonance of $[Me_2In(acac)]_2$ appears as a singlet at 0.11ppm while the equivalent resonance in complex **(3)** appears as a singlet at 0.10ppm as expected for these similar systems. The equivalent resonance in $[Me_2In(mesal)]_2$ however appears significantly downfield at 0.32pppm.

2.2.4 Synthesis of $[Me_2In\{N[(S)\text{-}CH(CH_3)C_5H_6]CHC(C_6H_5)\mu\text{-}O\}]_2$, (4)

An attempt was made to introduce chirality to these indium bismethyl complexes in the anticipation of synthesising chiral precatalysts. The readily available chiral amine, *(S)*-methylbenzylamine was reacted with the β-diketone, benzoylacetone to give 4-(*(S)*-methylbenzyl)aminopent-3-ene-2-one which has been previously reported,[29] (Figure 25).

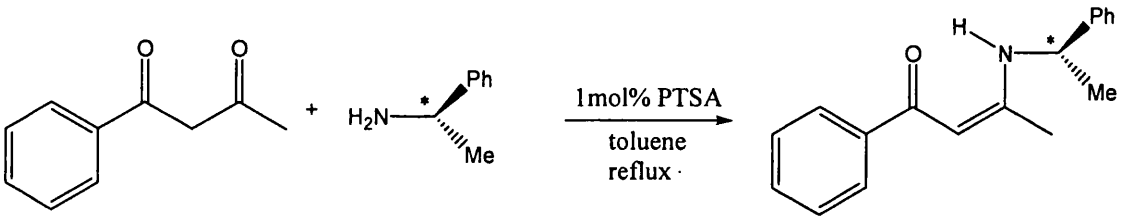

Figure 25 : Synthesis of the ligand 4-(*(S)*-methylbenzyl)aminopent-3-ene-2-one (* = chiral centre)

The ligand was then reacted with a stoichiometric quantity of trimethylindium in toluene eliminating methane and yielding complex **(4)**, $Me_2In\{N[(S)$-

$CH(CH_3)C_5H_6]CHC(C_6H_5)\mu$-O} (Figure 26). Unfortunately, despite repeated attempts crystals suitable for X-ray crystallography could not be obtained.

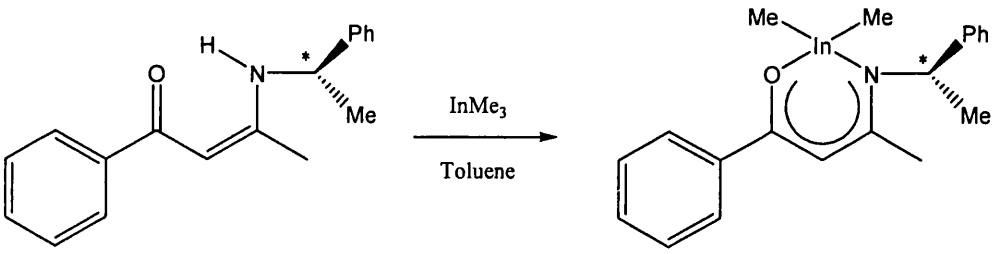

Figure 26 : Synthesis of complex (**4**), $Me_2In\{N[(S)\text{-}CH(CH_3)C_5H_6]CHC(C_6H_5)\mu\text{-}O\}$ (* = chiral centre)

The stereocentre present on the ligand in complex **(4)** is demonstrated by its ^1H and $^{13}C\{^1H\}$ NMR spectra which show two different indium-methyl environments whereas in contrast ^1H and $^{13}C\{^1H\}$ NMR spectra of complexes **(1)-(3)** show the two indium-methyls to be chemically and magnetically equivalent in solution. The ^1H NMR chemical shifts of the metal-bound methyl singlets ion **(4)** are -0.08ppm and -0.55ppm, while the $^{13}C\{^1H\}$ NMR chemical shifts are -4.6 and -6.7ppm.

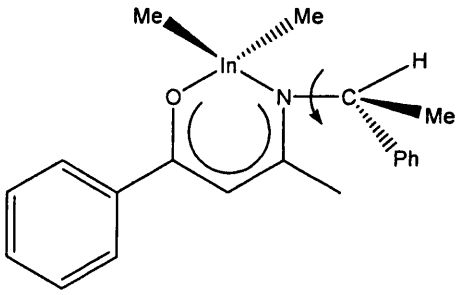

Figure 27 : The possible rotation around the C-N amino group bond in (**4**)

The chemical inequivalence of the two indium methyl groups can be clarified by viewing complex **(4)** and the rotation around the C-N bond of the amino group. The two methyl groups are prochiral due to the asymmetry of the amino group. This remains the case regardless of how much rotation occurs around the C-N bond.

2.2.5 Synthesis of $[Cl_2In\{N[o\text{-}C_6H_3(^iPr)_2]C(CH_3)CHC(CH_3)\mu\text{-}O\}]_2$, (5)

A route to the bischloride analogues of the bismethyl complexes was also investigated because chloride abstraction might provide a means to introduce triflate or triflamide ligands to the metal centre and possibly allow for the isolation of chiral pre-catalysts.

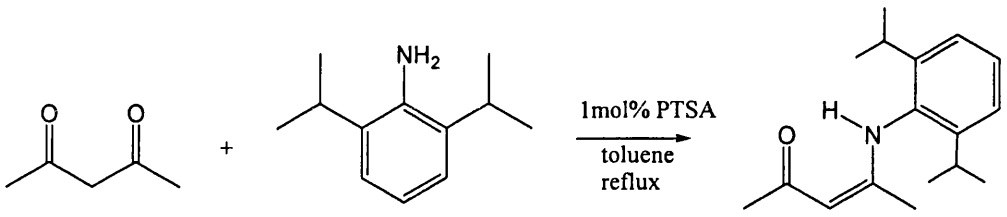

Figure 28 : Reaction of pentane-2,4-dione and 2,6-diisoproylaniline

Reflux of pentane-2,4-dione and 2,6-diisoproylaniline in a similar manner to that previously, gave 4-(2,6-diisopropylphenyl)aminopent-3-ene-2-one (Figure 28).[30] The ligand was deprotonated using butyllithium which has been previously documented (Figure 29).[31]

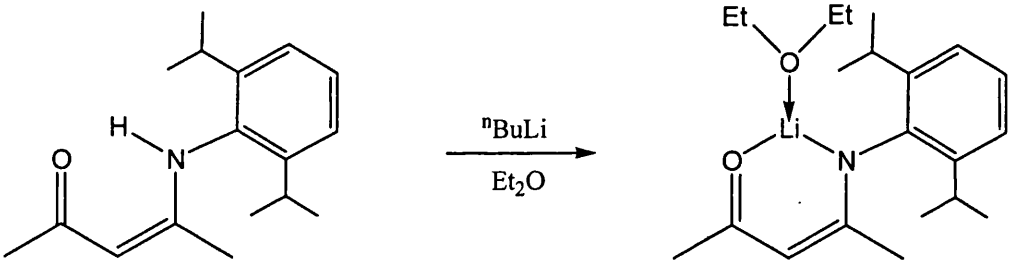

Figure 29 : Reaction of 4-(2,6-diisopropylphenyl)aminopent-3-ene-2-one with butyllithium

By reacting the lithium etherate directly with $InCl_3$ in refluxing toluene, it was possible to synthesise $[Cl_2In\{N[o\text{-}C_6H_3(^iPr)_2]C(CH_3)CHC(CH_3)\mu\text{-}O\}]_2$, **(5)** although only in low yield (36%).

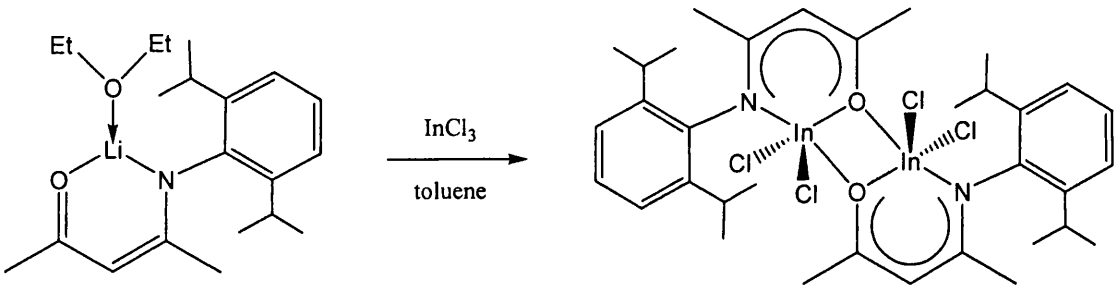

Figure 30 : Synthesis of $[Cl_2In\{N[o\text{-}C_6H_3(^iPr)_2]C(CH_3)CHC(CH_3)\mu\text{-}O\}]_2$, **(5)**

The crystal structure of **(5)** is shown in Figure 31, while relevant bond lengths and angles are shown in Table 9. Complex **(5)** is a dimer in the solid state. A molecule of co-crystallised solvent (toluene) is not shown. Table 8 shows the In-O and In-N bond lengths and the bond angles in the In_2O_2 core of both **(5)** and **(1)**.

	Compound **(5)**	Compound **(1)**
	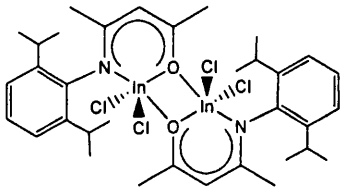	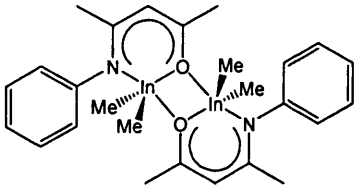
In-O(1)(Å)	2.1440(18)	2.1637(11)
In-N(Å)	2.208(2)	2.3057(13)
In-O(2)(Å)	2.2555(18)	2.611
In(1)-O(1)-In(2)(°)	109.35(8)	106.34
O(1)-In(1)-O(2)(°)	70.91(7)	73.66

Table 8 : Comparisons of In-O and In-N bond lengths and In_2O_2 core angles of complex **(5)** with complex **(1)**

The In-O, In-N and In-O# bond lengths are all shorter in **(5)** than in **(1)**. It is reasonable to conclude that this is caused by the electronegative chlorines in **(5)**. The internal angles in the In_2O_2 ring (O-In-O# 70.91°, In-O-In# = 108.34(8)°) are comparable to **(1)** (O-In-O# = 73.66(1)°, In-O-In# = 106.34°).[8] The plane defined by

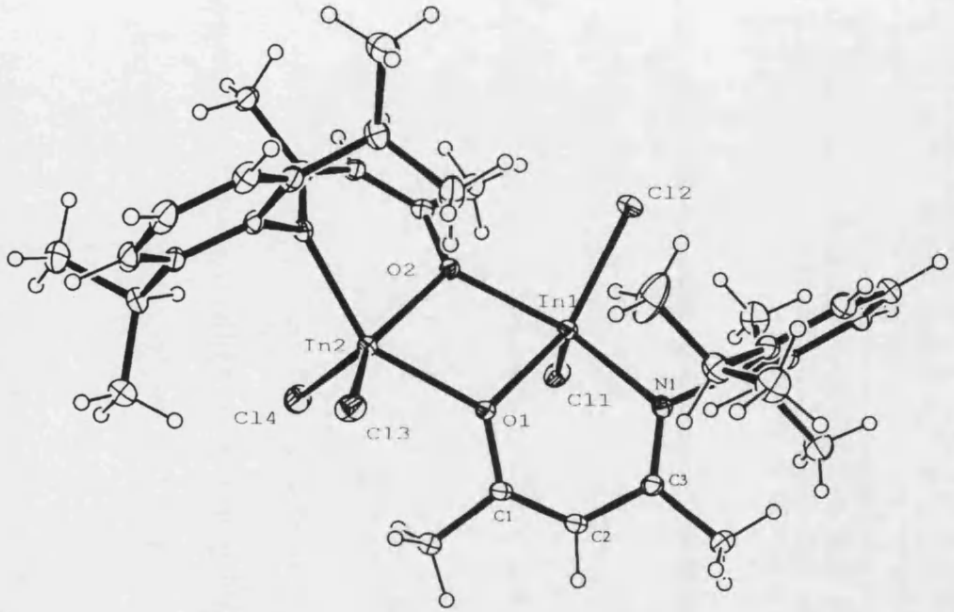

Figure 31 : Molecular structure of the asymmetric unit of $[Cl_2In\{N[o\text{-}C_6H_3(^iPr)_2]C(CH_3)CHC(CH_3)\mu\text{-}O\}]_2$ (ellipsoids drawn at 30% probability level)

In(1)-O(1)	2.1440(18)	O(1)-In(1)-Cl(2)	138.77(6)	In(2)-O(1)	2.2449(18)	In(2)-O(2)-In(1)	108.34(8)
In(1)-N(1)	2.208(2)	O(1)-In(1)-Cl(1)	99.22(6)	In(1)-O(2)	2.2555(18)	In(1)-O(1)-In(2)	109.35(8)
In(1)-O(2)	2.2555(18)	O(1)-In(1)-N(1)	85.35(8)	In(2)-O(2)	2.1613(18)	O(2)-In(2)-O(1)	70.91(7)
In(1)-Cl(2)	2.3524(7)	N(1)-In(1)-Cl(2)	96.18(6)	In(2)-Cl(3)	2.3544(8)	O(1)-In(2)-Cl(4)	101.11(6)
In(1)-Cl(1)	2.3568(7)	N(1)-In(1)-Cl(1)	104.25(6)	In(2)-Cl(4)	2.3519(8)	O(1)-In(2)-Cl(3)	89.23(5)
O(1)-C(1)	1.349(3)	C(3)-N(1)-In(1)	121.53(19)				
N(1)-C(3)	1.313(3)	C(1)-O(1)-In(1)	119.70(16)				

Table 9 : Selected bond lengths (Å) and angles (°) for **(5)**

the indium and the two chlorine atoms of the monomeric unit is approximately perpendicular to the plane of In_2O_2 core and the central 6-membered chelate ring. Of particular interest are the In-O# bonds [2.2555(18)Å] which are significantly shorter than those in **(1)** [2.611Å]. In fact, the indium-oxygen dimer bonds are even shorter than the corresponding bonds in $Me_2In(mesal)$ [2.376(4)Å] which has been shown to exist as a dimer in solution.[9] Because of the chlorides' enhanced electron withdrawing nature over methyl groups, they draw more electron density away from the metal centres encouraging dimer formation. Thus the metal centre in **(5)** pulls more electron density away from the oxygen and nitrogen atoms than the corresponding centre in **(1)**. The result is stronger indium-nitrogen and indium-oxygen bonds in **(5),** which is observed by the shorter bond lengths.

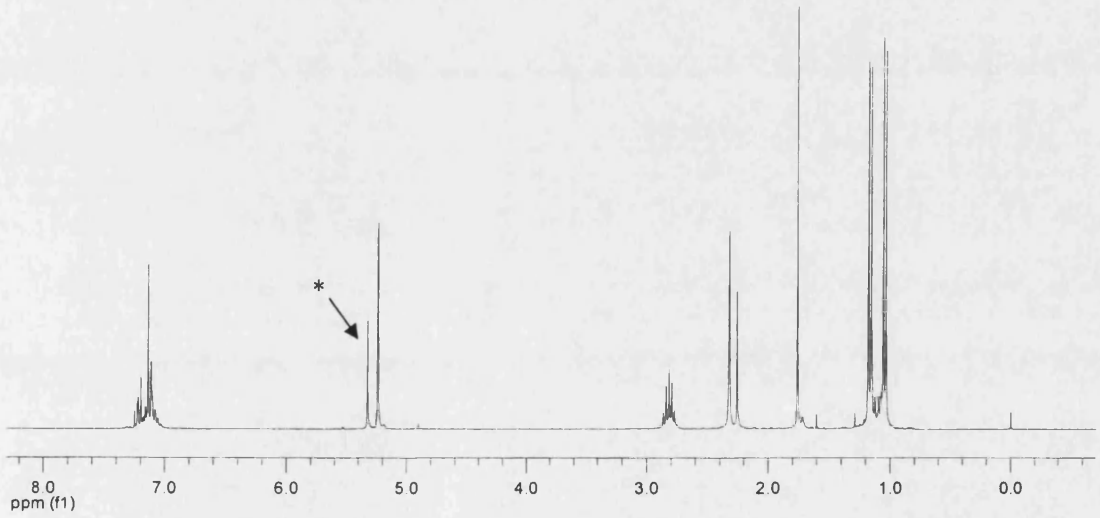

Figure 32 : ^{1}H NMR spectrum of $[Cl_2In\{N[o\text{-}C_6H_3(^iPr)_2]C(CH_3)CHC(CH_3)\mu\text{-}O\}]_2 \cdot C_6H_5CH_3$, **(5)** (* = residual solvent)

Figure 32 shows the ^{1}H NMR spectrum of compound **(5)** in CD_2Cl_2. A molecule of co-crystallised toluene in the solid state structure is also present. Assuming a dimer is retained in solution the molecule has a C_2 axis perpendicular to the centre of the In_2O_2 core. Thus the atoms in each monomer unit are equivalent by rotation and only one set of resonances are observed. The C-H of each of the four isopropyl group are

equivalent and one resononance is observed at 2.91ppm. Two resonances are observed for the two prochiral CH_3 substitutents of each isopropyl groups which are inequivalent and appear at 1.14 and 1.26ppm. Only two doublet resonances are observed for these substituents due to rotation about the C-N amino bond. The aromatic peaks attributed to the complex and the molecule of toluene are overlapped in the range 7.14-7.35 ppm, and the toluene methyl resonance can be seen at 2.35ppm. The proton bound to the carbon in the 6-membered chelate ring appears at 5.41ppm.

2.2.6 Reactivity Studies of Complexes (1)-(5)

Reactivity studies with regard to indium-methyl and -chloride substitution of **(1)-(5)** using various reagents including triflic acid and silver triflate to introduce triflate ligands resulted in complex decomposition, which was observed by ^1H NMR spectroscopy. An example of this is shown in Figure 33. The spectrum of **(1)** (top) and the spectrum of the reaction mixture after addition of two equivalents of triflic acid, HOTf (where OTf = SO_3CF_3) to **(1)** are compared. Direct observation of the reaction showed formation of metallic indium, while the remaining solution provided intractable, unidentifiable decomposition products. Similar reactions with complexes **(2)-(5)** gave the same results. Halide abstraction of **(5)** using silver triflate, Ag(OTf) also resulted in intractable/unidentifiable products. Although the products could not be identified, they may be similar to those described in the next section.

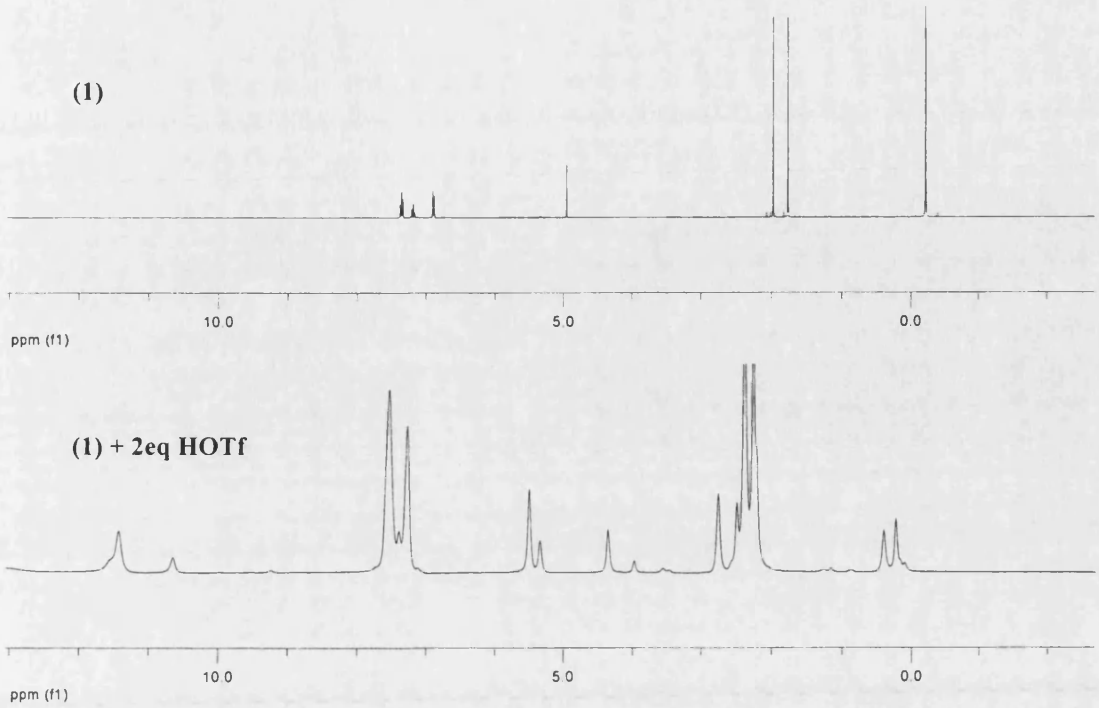

Figure 33 : ^{1}H NMR spectrum of **(1)** and **(1)** + 2 equivalents of HOTf

2.2.7 Reactivity of Indium-dipp$_2$nacnac Complexes

Although work with the β-diketiminate, dipp$_2$nacnac$^-$ did not give the desired substitution reactions, it gave an insight into complex decomposition which may explain why substitution reactions with indium β-ketoimine complexes also gave unwanted side reactions and unknown decomposition products.

Me$_2$Indipp$_2$nacnac which has already been reported by Stender *et al.*[11] was synthesised via a new route. By following their preparation for the gallium analogue, GaMe$_2$dipp$_2$nacnac, but using InMe$_3$ in place of GaMe$_3$, Me$_2$Indipp$_2$nacnac was produced in good yield matching the NMR data reported for the compound.[11]

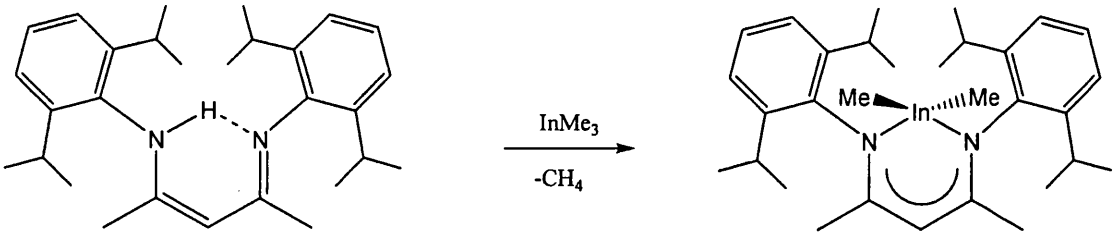

Figure 34 : Reaction of $dipp_2nacnacH$ with $InMe_3$

Our interest in this compound was based on preliminary reactivity studies and indium methyl substitution reactions. Attempts were made to substitute the metal methyl groups for triflate ligands. However the efforts to synthesise the indium mono- and bistriflate complexes by reaction with trimethylsilyltriflate, TMS(OTf) (where TMS = Me_3Si), and H(OTf) did not give the desired results. Combination of $Me_2Indipp_2nacnac$ with one and two equivalents of TMS(OTf) showed no reaction. while addition of H(OTf) caused decomposition of the complex. The main decomposition product in this case could be isolated and was analysed by X-ray crystallography. The solid-state structure is shown in Figures 35 & 36. Table 10 shows relevant bond lengths and bond angles. This clearly shows it to be protonated starting ligand and it is likely to have been produced via reprotonation of the ligand back to starting material followed by protonation of the other nitrogen to give a triflate salt of the ligand.

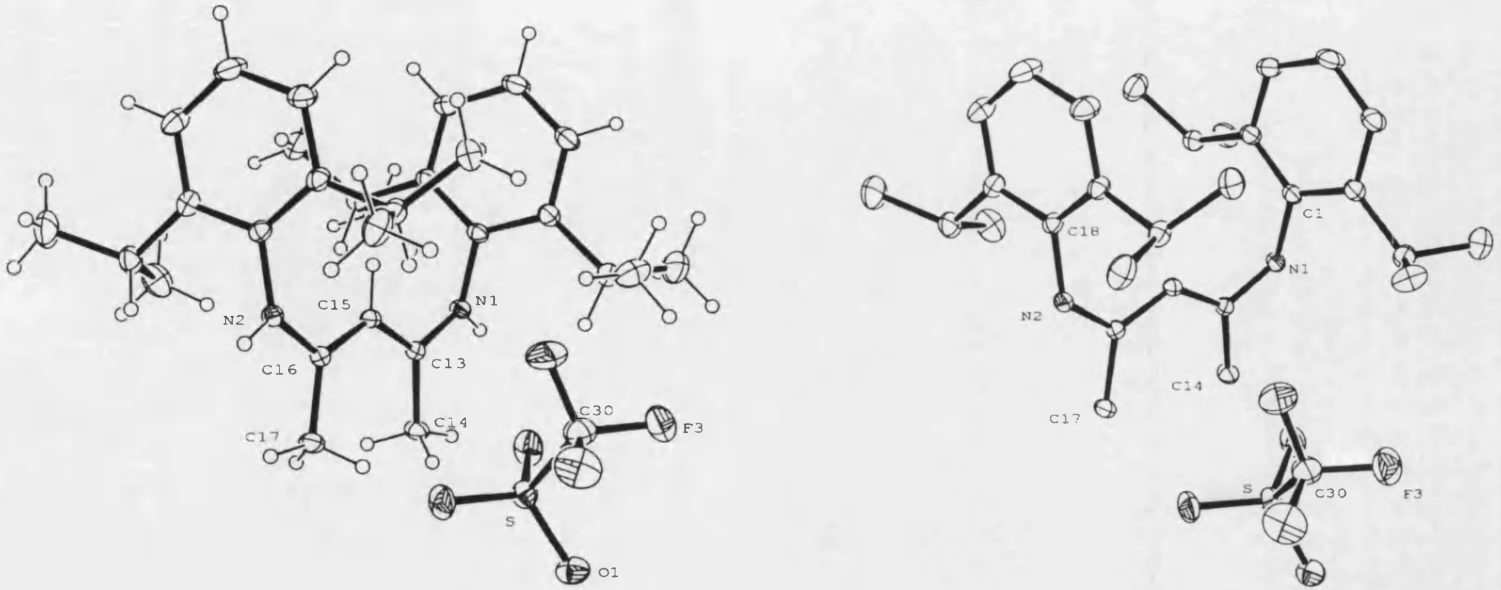

Figure 35 : Molecular structure of the asymmetric unit of $dipp_2nacnacH_2^+$ OTf^- with and without hydrogens shown (ellipsoids drawn at 30% probability level)

N(1)-C(13)	1.3342(15)	N(2)-C(16)-C(15)	120.69(11)
N(2)-C(16)	1.3363(15)	N(2)-C(16)-C(17)	113.29(11)
N(2)-C(18)	1.4414(16)	C(16)-N(2)-C(18)	126.93(11)
C(15)-C(16)	1.3927(17)	N(1)-C(13)-C(15)	120.46(11)
C(13)-C(15)	1.3967(16)	N(1)-C(13)-C(14)	113.60(11)
C(16)-C(17)	1.5041(17)	C(16)-C(15)-C(13)	127.49(11)
C(13)-C(14)	1.5032(17)		

Table 10 : Selected bond lengths (Å) and angles (°) for **(6)**

Observing the decomposition *in situ* in CD_2Cl_2, ^1H NMR spectroscopy showed the appearance of a singlet resonance at 12.15ppm for the acidic proton of dippnacnacH followed by the appearance of another singlet at 9.06ppm which can be attributed to the formation of the bis-imine salt where the imine protons bound to each nitrogen are equivalent (Figure 36). The indium species formed in the complex decomposition reaction could not be identified by NMR or mass spectrometry.

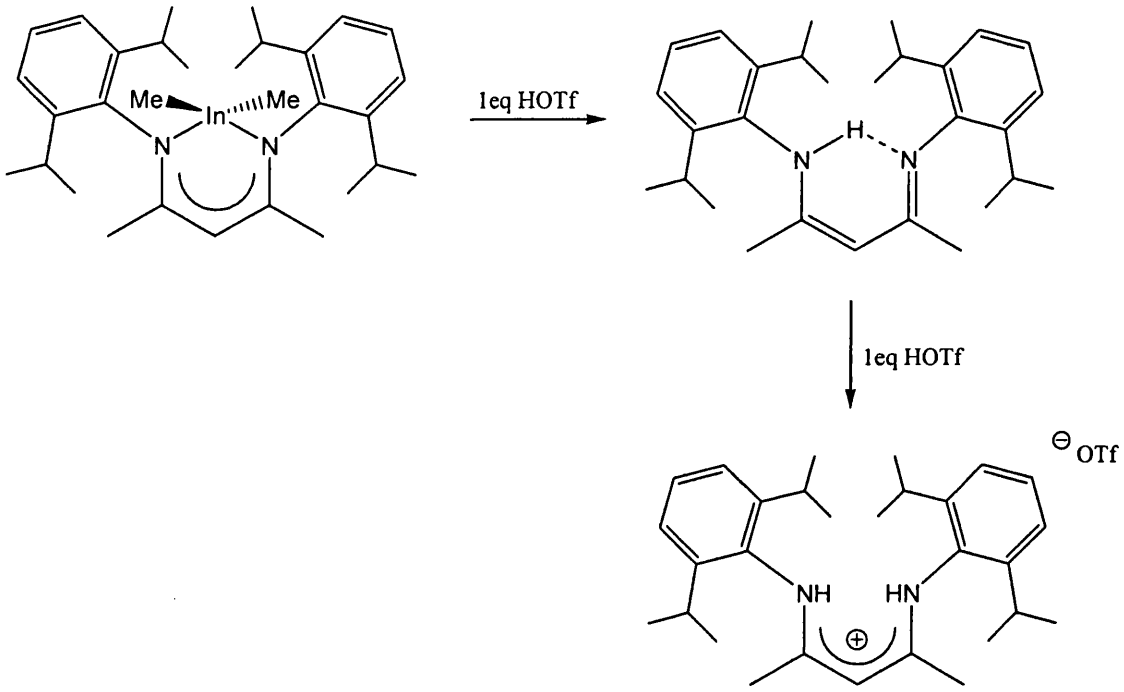

Figure 36: Reaction of $Me_2InDipp_2nacnac$ with triflic acid to form **(6)**

A similar decomposition reaction was observed on the reaction of an equivalent amount of 2M ether solution of hydrogen chloride, HCl, with $Me_2Indipp_2nacnac$ (Figure 37). It is easily identified by ^1H NMR from the appearance of the two proton imine singlet at ~9.06ppm. This is expected to be the chloride analogue of the triflate salt **(6)**.

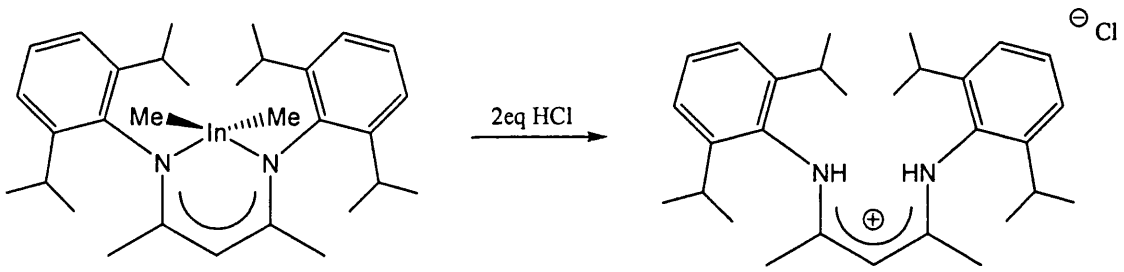

Figure 37 : Reaction of $Me_2Indipp_2nacnac$ with hydrogen chloride

The decomposition observed in these cases give an insight into the type of reactions that may have occurred when the similar substitution reactions with compounds **(1)-(4)** were attempted.

2.3 Discussion

2.3.1 Solution state studies

Cryoscopic molecular weight studies of the previously reported compound $[Me_2In(mesal)]_2$ have shown it to be a dimer in solution,[32] while $[Me_2In(acac)]_2$, a similar compound which has much weaker dimer contacts in the solid state has been proved to undergo a monomer-dimer equilibrium in solution.[33] ^1H NMR spectroscopy studies of $[Me_2In(acac)]_2$, showed sharp single resonances whose chemical shifts were independent of concentration in the range studied.[33] These peaks are likely to be time averaged and suggest that the equilibrium occurs fast on the NMR time scale. It was only via molecular weight cryoscopic studies when the degree of association decreased on dilution of the compound that the monomer-dimer equilibrium was observed. It is clear that although structurally similar in the solid state, the metal bound methyl resonances show quite different chemical shifts for the two compounds (Table 11). This may also give a measure of the solution behaviour of these

compounds. Comparison of the chemical shift of the $InMe_2$ resonances in their ^1H spectrum with those of compound **(3)** suggests that **(3)** may also undergo a monomer-dimer equilibrium in solution.

	^1H NMR chemical shift of $InMe_2$ (ppm)	Bridging In-O# bond length (Å)
$[Me_2In(mesal)]_2$	0.32	2.376(4)
$[Me_2In(acac)]_2$	0.11	2.606(3)
(3)	0.10	2.547(7)

Table 11 : Comparison of In-O# bond lengths with the $InMe_2$ chemical shifts for $[Me_2In(mesal)]_2$, $[Me_2In(acac)]_2$ and **(3)**

There appears to be a correlation between a reduction in the In-O# bond length and a downfield chemical shift. The shorter the dimeric In-O# contact in the solid state, the more likely the compound is to be a dimer in solution. Correspondingly, the shorter the In-O# contact in the solid state, the more deshielded the metal bound methyl groups and the further downfield their resonance appears in their ^1H NMR spectra in solution.

Comparison of the ^1H NMR metal bound methyl resonances of **(1)**, **(2)** and **(4)** in CD_2Cl_2 shows there is no obvious correlation between them (Table 12). Complex **(2)** has been shown to be a 4-coordinate monomer in the solid state, therefore, it is likely to also be monomeric in solution. Complex **(1)** is a dimer in the solid state but its behaviour in solution is unknown while no solid state data could be obtained for **(4)**. The stereocentre in the amino group in **(4)** causes the inequivalency of the two metal bound methyl groups resulting in two singlet resonances where for **(1)** and **(2)** only one resonance is observed. A lack of ^1H NMR spectroscopic solution state studies of

analogous compounds in the literature means that without molecular cryoscopy measurements, the solution behaviour of **(1)**, **(2)**, and **(4)** remains ambiguous.

	Bridging In-O# Distance (Å)	^{1}H NMR $InMe_2$ chemical shift (ppm) (CD_2Cl_2)
(1)	2.611	-0.23
(2)	no bridging bond	-0.14
(4)	unknown	-0.08 & -0.55

Table 12 : Comparison of In-O# bond lengths and ^{1}H NMR $InMe_2$ chemical shifts of **(1)** **(2)** and **(4)**

The solid state structure of **(5)** suggests that the complex is a dimer in solution. Comparison of the In-O# bond length in **(5)** with that of $[Me_2In(mesal)]_2$ shows the In-O# bond length in **(5)** is even shorter than that in $[Me_2In(mesal)]_2$ which has been proved to be a dimer in solution (Table 13).[32]

	Bridging In-O# Distance (Å)
(5)	2.256(2)
$[Me_2In(mesal)]_2$	2.376(4)

Table 13 : Comparison of In-O# bond lengths of **(5)** $[Me_2In(mesal)]_2$

Unfortunately, cryoscopy equipment was not available for the solution behaviour of our compounds **(1)**-**(5)** to be proved unequivocally. Further studies with these systems

seems unwarranted particularly as they decompose when substitution reactions with triflate compounds are attempted.

Satisfactory microanalyses on complexes **(1)-(4)** could not be obtained despite repeated attempts. Every analysis was low in the percentage of carbon and hydrogen by two methyl groups expected to be those methyls bound directly to the metal. This is supported by the fact that complex **(5),** which does not possess metal methyl groups but instead has two chlorides bound to each indium gives an accurate microanalysis suitable for publication. Satisfactory mass spectrometry analyses of these compounds could not be obtained despite repeated attempts. However these complexes are all pure by NMR (>99%).

2.4 Summary

A range of bidentate β-ketoimine ligands have been reacted with trimethylindium and undergo proton abstraction and methane elimination to form a group of interesting new bismethyl indium complexes which have been structurally characterised by single crystal X-ray diffraction and NMR spectroscopy. A bischlorideindium β-ketoiminate and a bismethylindium β-diketonate have also been structurally and spectroscopically characterised. Attempts to substitute the methyl and chloride ligands for triflates resulted in side reactions and decomposition products which could not be identified. Reactions of a bismethyl indium β-diketiminate complex, $Me_2Indipp_2nacnac$, showed that one of the decomposition routes of the compound involved the breaking of the indium nitrogen bonds and reprotonation of the anionic ligand to the neutral dippnacnacH followed by further protonation of the ligand to make it a bis-imine cation which was stabilised by a triflate anion. This

decomposition product was isolated and structurally characterised. This provides some idea of how decomposition of the β-ketoimine systems may occur. Clearly another robust ligand set which binds more strongly to indium set is needed. *N*-Heterocyclic carbenes form stronger L→M bonds and therefore should be more resistant to protonolysis. Such indium-carbene systems are discussed in the next chapter.

2.5 References

(1) Mehrotra, R. C.; Bohra, R.; Gaur, D. P. *Metal Beta-Diketonates and Allied Derivatives*; Academic Press: New York, 1978.

(2) Holm, R. H.; Everett, G. W.; Chakravorty, A. *Progress in Inorganic Chemistry* **1966**, *7*, 83.

(3) Calligaris, M. R., L. *Comprehensive Coordination Chemistry*; Pergamon: Oxford, U.K., 1987.

(4) Gilli, G.; Bellucci, F.; Ferretti, V.; Bertolasi, V. *J. Am. Chem. Soc.* **1989**, *111*, 1023-1028.

(5) Gilli, P.; Bertolasi, V.; Pretto, L.; Ferretti, V.; Gilli, G. *J. Am. Chem. Soc.* **2004**, *126*, 3845-3855.

(6) Xu, C. Y.; Baum, T. H.; Guzei, I.; Rheingold, A. L. *Inorg. Chem.* **2000**, *39*, 2008-2010.

(7) Le, Q. T. H.; Umetani, S.; Matsui, M. *J. Chem. Soc., Dalton Trans.* **1997**, 3835-3840.

(8) Alcock, N. W.; Degnan, I. A.; Roe, S. M.; Wallbridge, M. G. H. *J. Organomet. Chem.* **1991**, *414*, 285-293.

(9) Lewinski, J.; Zachara, J.; Starowieyski, K. B. *J. Chem. Soc., Dalton Trans.* **1997**, 4217-4222.

(10) Bourget-Merle, L.; Lappert, M. F.; Severn, J. R. *Chem. Rev.* **2002**, *102*, 3031-3065 and references therein.

(11) Stender, M.; Eichler, B. E.; Hardman, N. J.; Power, P. P.; Prust, J.; Noltemeyer, M.; Roesky, H. W. *Inorg. Chem.* **2001**, *40*, 2794-2799 and references therein.

(12) Holland, P. L.; Tolman, W. B. *J. Am. Chem. Soc.* **1999**, *121*, 7270-7271.

(13) Hardman, N. J.; Eichler, B. E.; Power, P. P. *Chem. Comm.* **2000**, 1991-1992.

(14) Eckert, N. A.; Bones, E. M.; Lachicotte, R. J.; Holland, P. L. *Inorg. Chem.* **2003**, *42*, 1720-1725.

(15) Feldman, J.; McLain, S. J.; Parthasarathy, A.; Marshall, W. J.; Calabrese, J. C.; Arthur, S. D. *Organometallics* **1997**, *16*, 1514-1516.

(16) Eckert, N. A.; Smith, J. M.; Lachicotte, R. J.; Holland, P. L. *Inorg. Chem.* **2004**, *43*, 3306-3321.

(17) Stender, M.; Wright, R. J.; Eichler, B. E.; Prust, J.; Olmstead, M. M.; Roesky, H. W.; Power, P. P. *J. Chem. Soc., Dalton Trans.* **2001**, 3465-3469.

(18) Delpech, F.; Guzei, I. A.; Jordan, R. F. *Organometallics* **2002**, *21*, 1167-1176.

(19) Roberts, E.; Turner, E. E. *J. Chem. Soc.* **1927**, 1832-1857.

(20) Singh, R. V.; Tandon, J. P. *J. Prakt. Chem.* **1979**, *321*, 151-158.

(21) Shin, H. K.; Hampdensmith, M. J.; Kodas, T. T.; Rheingold, A. L. *Chem. Comm.* **1992**, 217-219.

(22) Jones, D.; Roberts, A.; Cavell, K.; Keim, W.; Englert, U.; Skelton, B. W.; White, A. H. *J. Chem. Soc., Dalton Trans.* **1998**, 255-262.

(23) Shen, Y. Z.; Gu, H. W.; Pan, Y.; Dong, G.; Wu, T.; Jin, X. P.; Huang, X. Y.; Hu, H. W. *J. Organomet. Chem.* **2000**, *605*, 234-238.

(24) Shen, Y. Z.; Pan, Y.; Jin, X. P.; Xu, X.; Sun, X. Z.; Huang, X. Y. *Polyhedron* **1999**, *18*, 2423-2426.

(25) Chou, T. Y.; Chi, Y.; Huang, S. F.; Liu, C. S.; Carty, A. J.; Scoles, L.; Uclachin, K. A. *Inorg. Chem.* **2003**, *42*, 6041-6049.

(26) Martin, D. F.; Janusonis, G. A.; Martin, B. M. *J. Am. Chem. Soc.* **1961**, *83*, 73-75.
(27) Shearer, H. M. M.; Twiss, J.; Wade, K. *Organometallic Chemistry* **1980**, *184*, 309.
(28) Park, J. H.; Horley, G. A.; O'Brien, P.; Jones, A. C.; Motevalli, M. *J. Mater. Chem.* **2001**, *11*, 2346-2349.
(29) Cimarelli, C.; Palmieri, G. *Tetrahedron* **1998**, *54*, 915-926.
(30) Parks, J. E.; Holm, R. H. *Inorg. Chem.* **1968**, *37*, 2317.
(31) Yu, R. C.; Hung, C. H.; Huang, J. H.; Lee, H. Y.; Chen, J. T. *Inorg. Chem.* **2002**, *41*, 6450-6455.
(32) Lewinski, J.; Zachara, J.; Starowieyski, K. B. *J. Chem. Soc., Dalton Trans.* **1997**, 4217-4222.
(33) Beachley, O. T.; MacRae, D. J.; Churchill, M. R.; Kovalevsky, A. Y.; Robirds, E. S. *Organometallics* **2003**, *22*, 3991-4000.

Chapter 3 - Indium(III) N-Heterocyclic Carbene Complexes

3.1 Introduction

The capping ligand systems studied so far have been proven to form binding interactions with the indium metal centre that are too weak when methyl and chloride substitution is attempted, resulting in complex decomposition. Therefore our attention turned toward *N*-heterocyclic carbenes, which are readily accessible, form strong C-M bonds - stabilising the metal through σ-donation and have precedence for coordination to indium. Encouragingly for this study, the hydride ligands in indium trihydride carbene adducts can be substituted without breaking the indium-carbon bond of the metal carbene.[1] It was hoped that this would also prove the case when methyl groups in our target systems are substituted for triflates or other weakly binding anions. This chapter covers an introduction to *N*-heterocyclic carbenes and their coordination chemistry with indium. This will be followed by the report of successful structural and spectroscopic characterisation of indium-carbenes, including complexes containing the indium triflate and triflamide moieties. Their activity as Lewis acid catalysts will be reported in Chapter 4.

3.1.1 *N*-Heterocyclic Carbenes

The chemistry of stable carbenes is one of the fastest growing areas in both coordination and catalytic chemistry, with numerous reviews and articles available on this subject.[2,3,4] Therefore this section will only present a brief overview of the properties and synthesis of carbene ligands, along with a few examples of their main applications in coordination chemistry.

Carbenes are neutral molecules containing a divalent carbon atom. The carbon only has four valence electrons (of which two are non-bonding), making them electron deficient and highly reactive. Their electronic configuration gives rise to two different arrangements: paired or unpaired non-bonding electrons. Singlet carbenes have paired non-bonding electrons, whereas the non-bonding electrons of triplet carbenes occupy different orbitals and possess parallel spins.

Because the carbene carbon atom ($C_{carbene}$) is divalent, carbenes might be expected to possess a linear geometry with an sp-hybridisation and two degenerate non-bonding p_x and p_y orbitals around the carbene centre. Such a carbene would have to distribute two of its four electrons in two σ-orbitals while the two remaining electrons would each inhabit different degenerate p-orbitals of higher energy because of electron repulsion. Very few carbenes are in fact linear suggesting the geometry about the carbon atom is in the sp^2 hybridized state. If the carbene is sp^2 hybridized, either each of the three electron pairs occupy sp^2 orbitals as in the singlet state, or one of the electron pairs is split between an sp^2 and a p_π-orbital as in the triplet state (Figure 1).

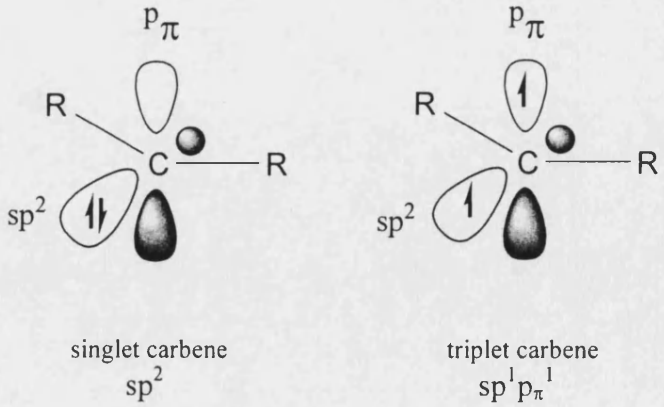

singlet carbene
sp^2

triplet carbene
$sp^1p_\pi{}^1$

Figure 1 : The electron occupancy in the sp^2 and p_π - orbitals

Carbenes can exist in either of these states but often it is the triplet state that is preferable because of the extra energy (often only about 40kJmol^{-1}) that is required to pair the two electrons together in the sp^2 orbital in the singlet state.[5] Wanzlick *et al.* showed that the singlet state is the preferred carbene configuration if the substituents in the vicinal positions, (X in Figure 2) have σ-acceptor π-donor character.[6,7] This type of carbene, having electron-donating substituents is less electrophilic than other carbenes and in fact, some carbenes, (e.g. diamino carbenes) can be quite nucleophilic.[5]

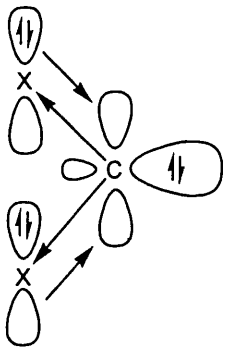

Figure 2 : Vicinal σ-acceptor π-donors stabilize the singlet state

3.1.2 Stable Singlet Carbenes

Stable *N*-heterocyclic carbenes (NHCs) were first reported in 1961, although only the dimers could be isolated (Figure 3).[7] It was recognised that carbenes with electron rich amino substituents at the 2 and 5-positions were capable of stabilising the carbene centre, $C_{carbene}$, by enhancing the carbene's nucleophilicity and thermodynamic stability.[6-8]

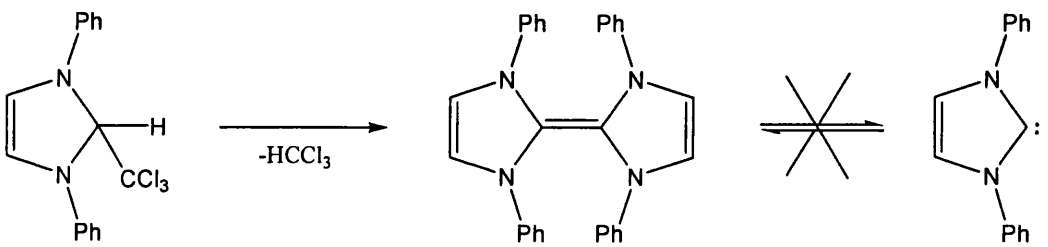

Figure 3 : Synthesis of the first *N*-heterocyclic carbene

The real breakthrough in the field of NHC chemistry occurred when the bulky adamantylamine was used to make 1,3-bis(1-adamantyl)imidazol-2-ylidene (IAd) which was successfully isolated as free carbene (Figure 4).[3,9,10]

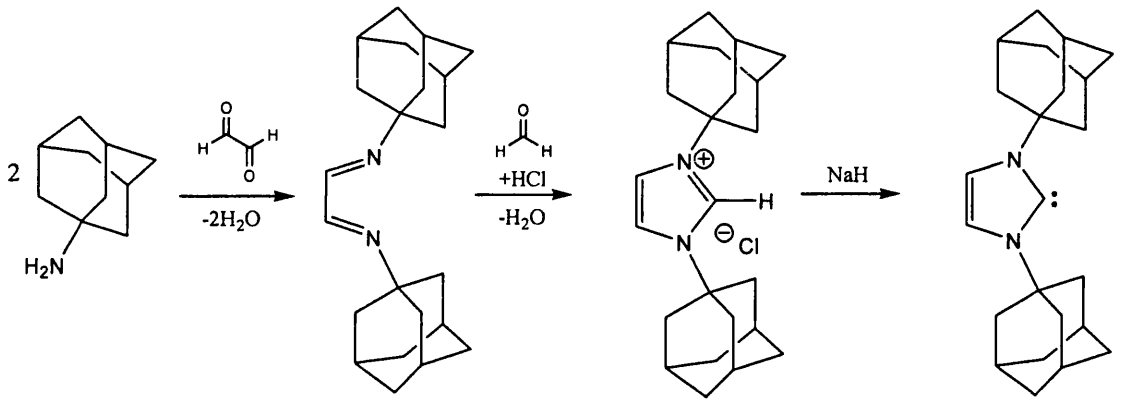

Figure 4 : Synthesis of 1,3-bis(1-adamantyl)imidazol-2-ylidene

This work caused a rapid revival in research into alternative nucleophilic carbenes and the last decade has seen numerous reports of variations in the basic imidazol-2-ylidene skeleton.

Cyclic diaminocarbenes were originally considered to be the only stable type of carbene because of the stability provided by the nitrogen when it was bound to groups with good π-donor/σ-acceptor character. Combined with steric bulk and some aromatic character, these groups also prevented dimerization.[11,12] New generations of NHC ligands range from having basic functionalised aryl groups on the nitrogen (Figure 5), to more sophisticated NHCs with N groups designed for specific purposes (where Mes = $C_6H_2Me_3$-2,4,6) (Figure 6).

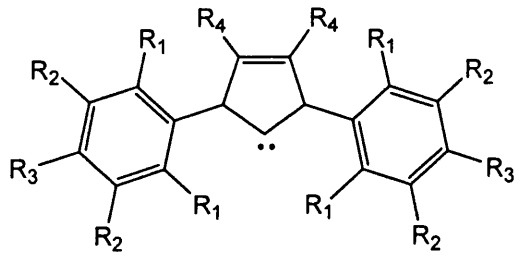

IMes [13]	R_1, R_3 = Me, R_2, R_4 = H
IPr [14]	R_1 = $CHMe_2$, R_2, R_3, R_4 = H
$IMesCl_2$ [15]	R_1, R_3 = Me, R_2 = H, R_4 = Cl

Figure 5 : Basic functionalised NHCs

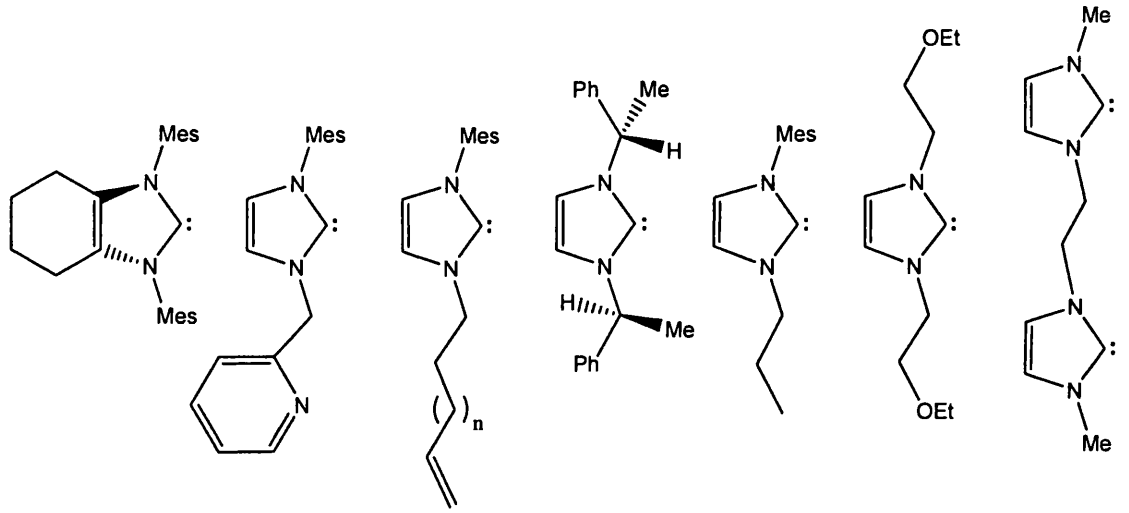

a[16] **b**[17] **c**[18] **d**[19,20] **e**[21] **f**[19,20] **g**[19,20]

Figure 6 : Examples of NHCs that have been designed and synthesised

Non-aromatic versions of the imidazol-2-ylidenes, shown in Figure 7, have also been isolated,[22,23] along with six-membered tetrahydropyrimid-2-ylidenes,[24,25] and acyclic systems.[26,27] They still possess two nitrogens vicinal to the carbene, but lack the 6π-electron 5-membered ring configuration.

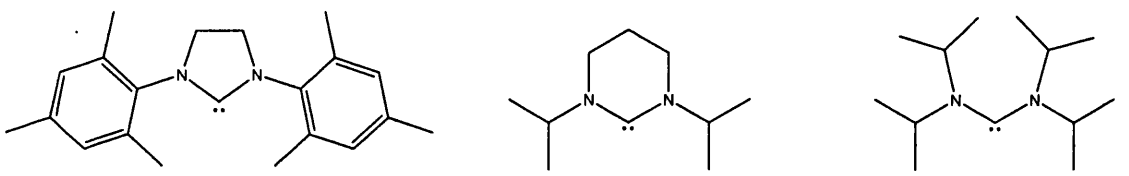

Figure 7 : Saturated imidazolid-2-ylidenes, tetrahydropyrimid-2-ylidenes and acyclic carbenes

Stable carbenes have also been reported incorporating π-donor substituents including alkoxy and arylsulfido groups.[28]

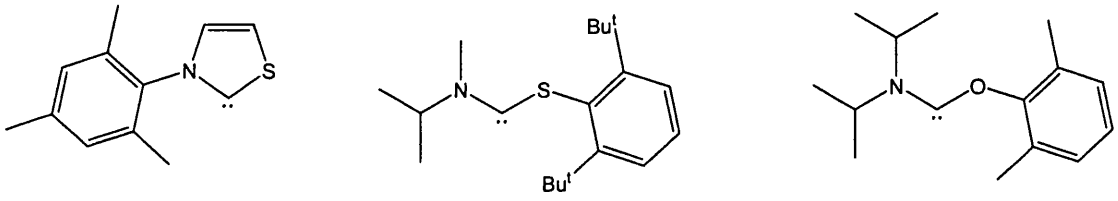

Figure 8 : Synthesised carbenes with alkoxy and arylsulfido groups

The first examples of metal NHC complexes were reported in 1968.[29,30] Nowadays these ligands' application to coordination chemistry covers a large area of the periodic table from the alkali metals,[24] alkaline earth metals,[31,32] to the transition metals.[4] Even their coordination to rare earth metals has been reported.[33,34]

3.1.3 Synthesis of *N*-Heterocyclic Carbenes

The synthesis of free *N*-heterocyclic carbenes generally starts from *N*-*N'*-disubstituted azolium salts (imidazolium salts), which are commonly deprotonated with potassium *tert*-butoxide (KO^{t}Bu) using thf as the solvent.

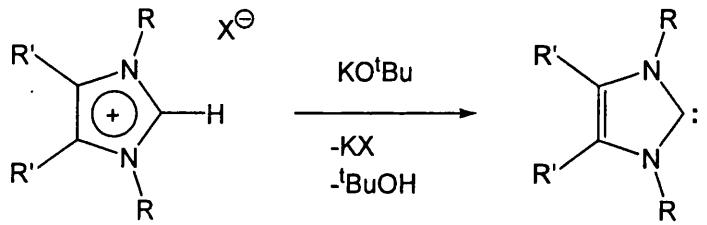

Figure 9 : Deprotonation of imidazolium salts (where X = Cl, Br and R, R' = alkyl)

Imidazolium salts are good precursors to the free carbene and are accessible by two main routes (i) and (ii). These methods have been reviewed thoroughly and will only be briefly discussed here.[4]

(i) Nucleophilic substitution at the imidazole heterocycle (Figure 10)

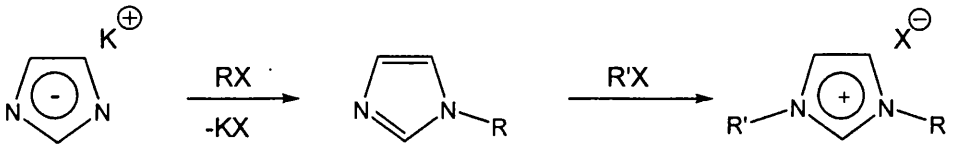

Figure 10 : Nucleophilic substitution synthesis (where X = Cl, Br and R = alkyl)

Imidazolium salts that can be prepared by this procedure, which involves alklation of imidazole, are easy to obtain and often used for metal complex synthesis.[35-38]

(ii) A multi-component reaction building up the heterocycle with the desired substitutents in one-step (Figure 11)[29,30,39-41]

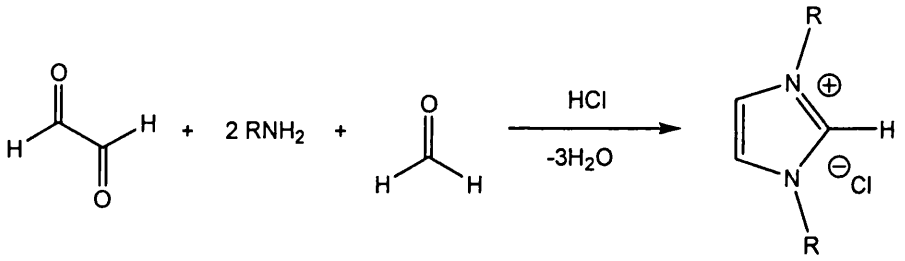

Figure 11 : Multi-component synthesis of imidazolium chloride (R = alkyl)

Other substituents may be introduced at the 1- and 3-positions of the imidazolium ring by use of different primary amines (RNH_2).[19,42,43] Variation of the amine allows the preparation of a diverse library of imidazolium salts which can be further broadened by use of different acids to change the salt anion.[44] This method was extended to the use of chiral amines in the preparation of C_2-symmetric imidazolium salts.[45] A two-step version of this synthesis has been shown to proceed via the bisimine followed by subsequent ring closure with formaldehyde and an acid.[46,39]

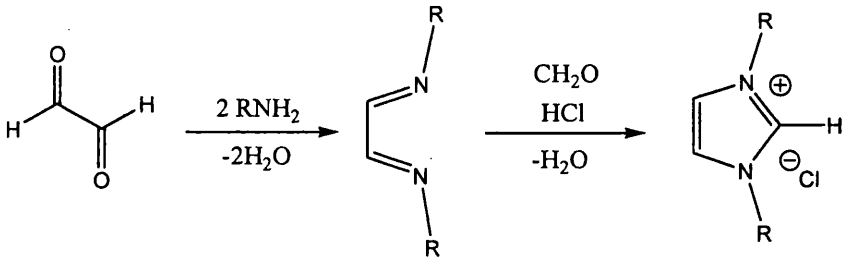

Figure 12 : Two-step imidazolium salt synthesis

3.1.4 What is the nature of the $C_{carbene}$-metal bond?

Stabilized carbenes, such as diaminocarbenes, are highly σ-donating and low π-accepting species, showing coordination properties similar to those of basic phosphorus-based ligands.[2,10] This is because the amino substituents in the vicinal positions (see Figure 2), have σ-acceptor π-donor character and thus fill the available π-orbital of the $C_{carbene}$. The poor π-acceptor nature of NHCs is comparable to that observed in the phosphorus based ligand tricyclohexylphosphine PCy_3.

3.1.5 Coordination of N-heterocyclic Carbenes to Indium

Coordination of group 13 metals to N-heterocyclic carbenes had not been significantly studied when the first instance of indium – carbene coordination was reported.[47] Prior to that, only five complexes of ratio 1:1 carbene: group 13 had been documented: two 1,3-diethylimidazol-2-ylidene - borane complexes,[48] an aluminium trihydride – (iMes) complex,[49] and finally the coordination of trimethylgallium and trimethylaluminium to 1,3-diisopropyl-4,5-dimethylimidazol-2-ylidene producing the products shown in Figure 13 in almost quantitative yield.[50]

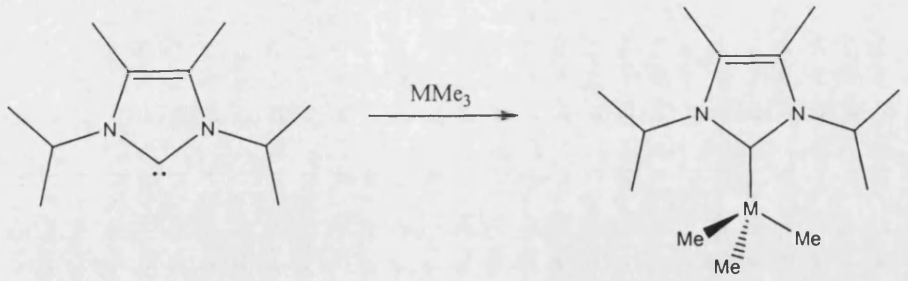

Figure 13 : Reaction of metal trimethyls with 1,3,-diisopropyl-4,5-dimethylimidazol-2-ylidene (M = Ga or Al)

Addition of one or two equivalents of the stable carbene 1,3-diisopropyl-4,5-dimethylimidazol-2-ylidene ($CN(Pr^i)C_2Me_2NPr^i$)[51] to either THF solutions of indium tribromide or indium trichloride resulted in the 1:1 and 2:1 complexes respectively.

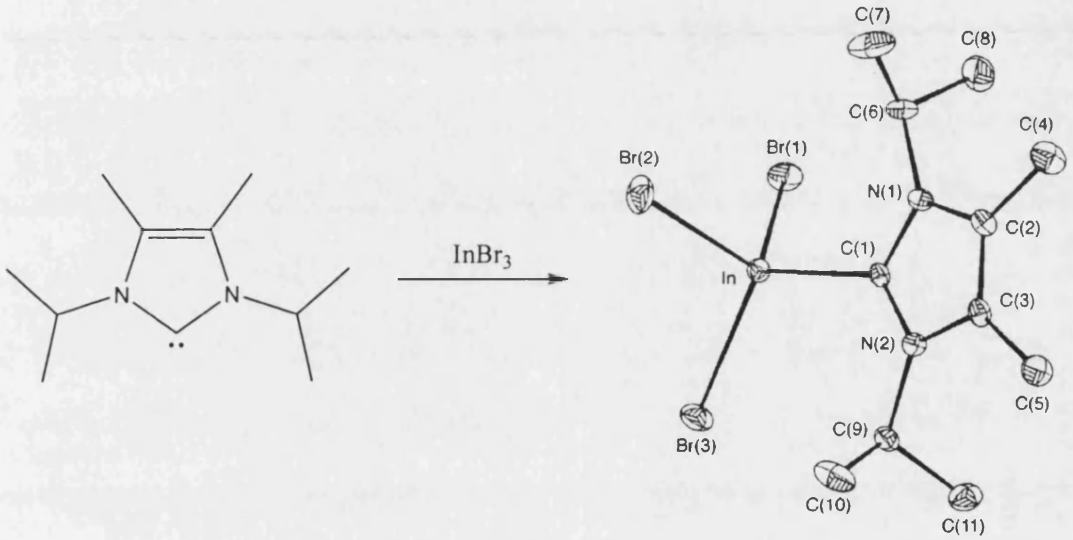

Figure 14 : Synthesis of $InBr_3[CN(Pr^i)C_2Me_2NPr^i]$ [47]

The structure of the mono-carbene adduct (Figure 14) is monomeric in the solid state with a mildly distorted tetrahedral geometry, and slightly shorter In-Br bonds than those in the 2:1 adducts. The $InCl_3$ bis-adduct is shown in Figure 15. The indium trichloride and tribromide bis-adducts are isostructural and also both monomeric. The coordination environment about the metal centres in each complex has been calculated to be distorted trigonal bipyramidal with two of the halides occupying the

apical positions while the third halide and two $C_{carbene}$ atoms occupy the equatorial positions.

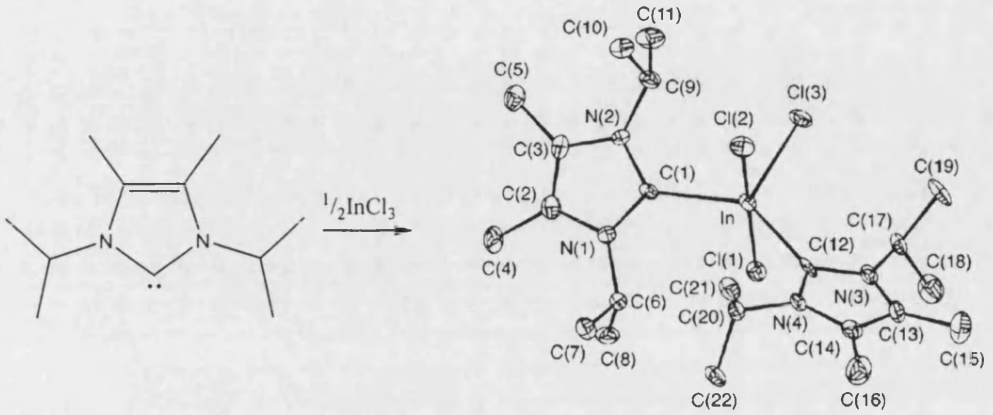

Figure 15 : Synthesis of $InCl_3[CN(Pr^i)C_2Me_2NPr^i]_2$ [47]

It was also found that treatment of InX_3 (X = Br, Cl) with one equivalent of $[CN(Pr^i)C_2Me_2NPr^i]$ and half an equivalent of water afforded the ionic compounds $[HCN(Pr^i)C_2Me_2NPr^i]^+[InX_4\{CN(Pr^i)C_2Me_2NPr^i\}]^-$ (Figure 16).[47] The ^1H and $^{13}C\{^1H\}$ NMR spectroscopic data for this compound shows only one set of heterocyclic resonances (for the imidazolium cation, $[HCN(Pr^i)C_2Me_2NPr^i]^+$), and it is postulated that a fluxional process is occurring which involves complexation and decomplexation of the carbene ligand with a concomitant proton exchange with the imidazolium cation. This process occurs faster than the NMR spectroscopy timescale even at -70°C.

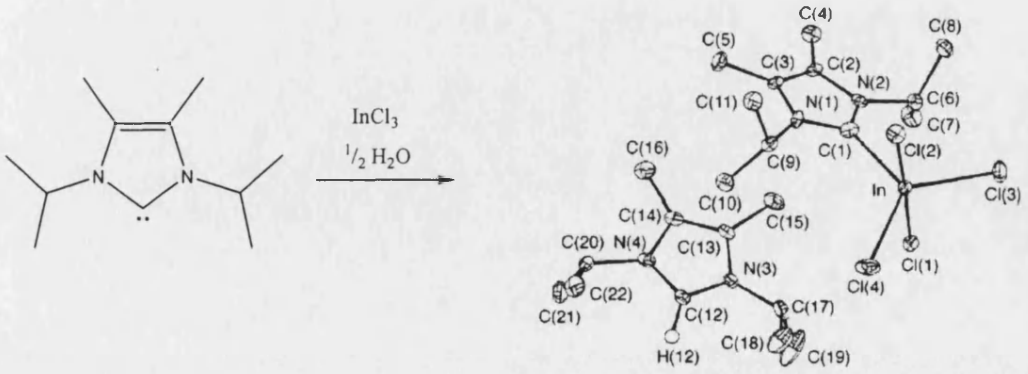

Figure 16 : Synthesis of $[HCN(Pr^i)C_2Me_2NPr^i]^+[InCl_4\{CN(Pr^i)C_2Me_2NPr^i\}]^-$ [47]

A similar type of ionic complex was synthesised this time using the more bulky (^{i}Pr) carbene resulting in the compound $[(^i\text{Pr})\text{H}]^+[\text{InBr}_4]^-$.[52] In this case however, the indium centre in the anion stabilised by the cation of $[(^i\text{Pr})\text{H}]^+$ is not bound to a molecule of carbene. The tetrahedral $[\text{InBr}_4]^-$ anion is reported has having a non-bonding interaction with the cation in the solid state (Figure 17).

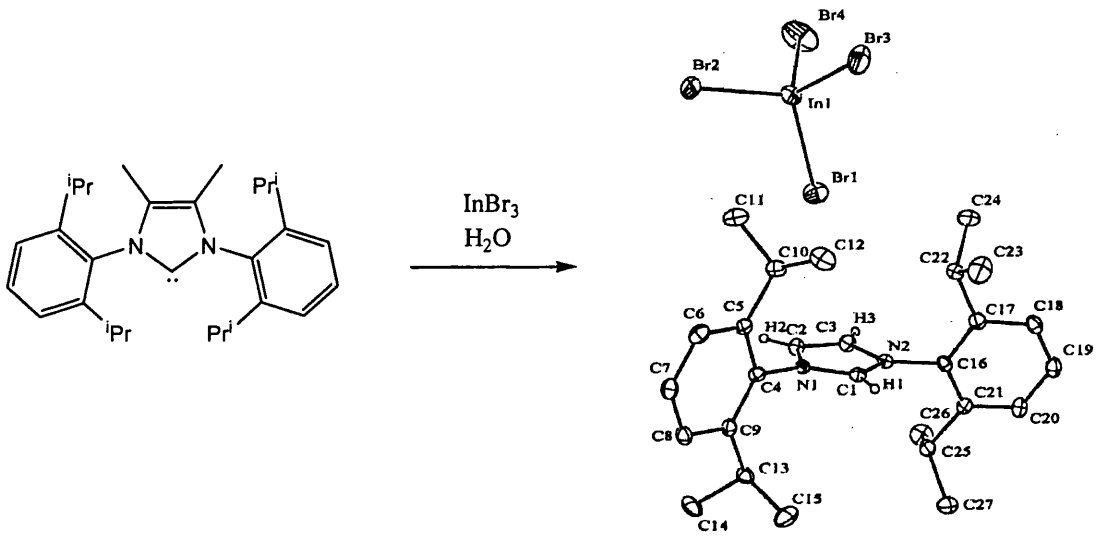

Figure 17 : Synthesis of $[^i\text{PrH}]^+[\text{InBr}_4]^-$ [52]

Having stabilised indium trihalides by carbene complexation, it was postulated that although no adducts of InH_3 had been previously synthesised (due to the weakness of the In-H bond and the decomposition it undergoes),[53] the stabilisation that the carbene provided for the indium trihalides would make them excellent precursors to carbene-InH_3 complexes. This proved to be the case with the indium trihydride analogue, $H_3In(CN(Pr^i)C_2Me_2NPr^i)$, which was successfully isolated and decomposes at -20°C in solution and -5°C in the solid state (Figure 18).[54]

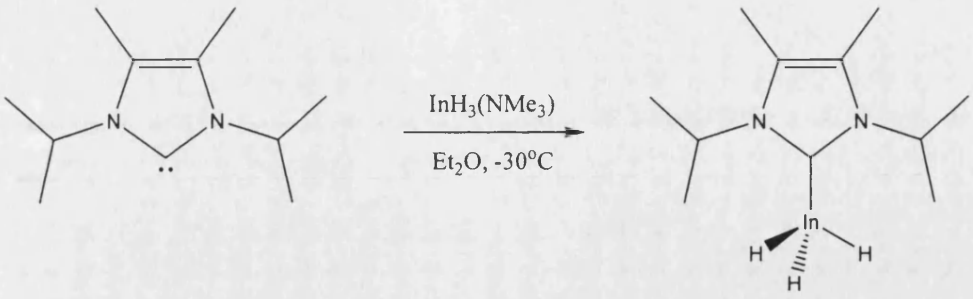

Figure 18 : Synthesis of the $H_3In[CN(Pr^i)C_2Me_2NPr^i]_2$ [54]

Despite the ease of formation of bis-carbene complexes of indium trihalides, no evidence of bis-carbene complexes of indium trihydrides has been observed. It has been suggested that this is due to the lower Lewis acidity of InH_3 with respect to InX_3 (X = Cl, Br).[54] This is demonstrated in the reaction of the bidentate NHC 1,2-ethylene-3,3'-di-*tert*-butyl-diimidazol-2,2'-diylidene, ($EtIBu^t$), with excesses of $H_3In(NMe_3)$ or indium tribromide as well as with stoichiometric amounts of each compound. Only the 1:2 four-coordinate indium trihydride and the 1:1 five-coordinate indium trihalide complexes are produced in each case (Figure 29).[55]

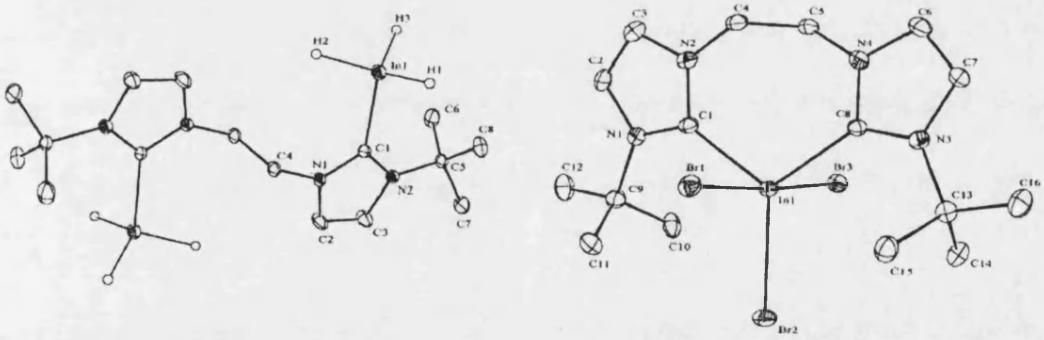

Figure 19 : Solid state structure of $(H_3In)_2(EtIBu^t)$ and $Br_3In(EtIBu^t)$[55]

The use of more bulky carbenes has been shown to produce even more stable adducts of indium trihydride. Using (iMes), a 1:1 carbene-InH_3 adduct, $H_3In(iMes)$ was synthesised that does not decompose until 115°C (Figure 20). This complex shows that substitution of the isopropyl groups for the more bulky mesityl groups greatly

enhances the stability of the system by better stabilising the metal centre.[1] This complex has been documented as being a successful reducing agent of ketones and epoxides.[56]

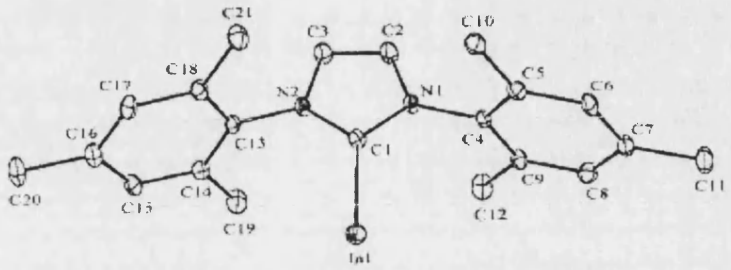

Figure 20 : Crystal structure of $H_3In(iMes)$ [1]

Similarly to its predecessor, the X-ray crystal structure of this indium complex did not reveal the hydride positions. The molecule is also monomeric and does not display any intermolecular interactions in the solid state. The chloride analogue, $Cl_3In(iMes)$ (Figure 21), was synthesised by stirring $H_3In(iMes)$ in dichloromethane producing the trichloride complex by chloride abstraction from the solvent (a common reaction for metal hydrides).[1]

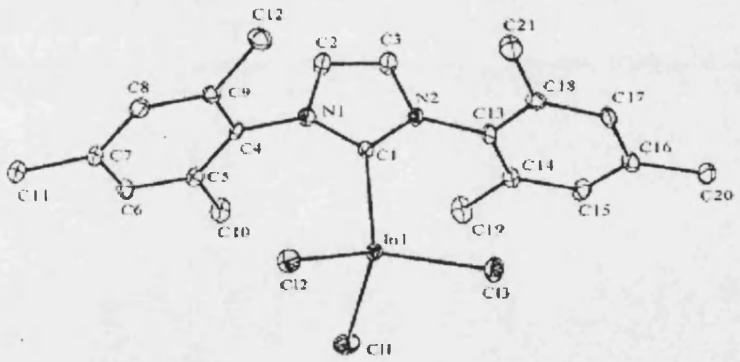

Figure 21 : Crystal structure of $Cl_3In(iMes)$ [1]

The coordination of both (iPr), and (iMes) to indium tribromide to give $Br_3In(iPr)$ and $Br_3In(iMes)$ has also been reported (Figure 22).[52] In both cases $InBr_3$ was reacted directly with the free carbene of each ligand. $Br_3In(iMes)$ was reported as being isomorphous and isostructural with $Cl_3In(iMes)$.

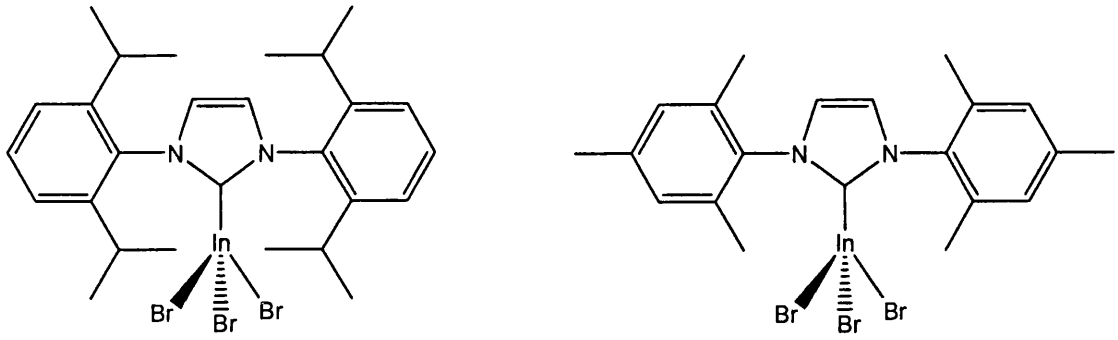

Figure 22 : Structures of $Br_3In(iPr)$ and $Br_3In(iMes)$ [52]

Recently the formation of a titanium carbene complex via a new reaction pathway has been reported.[57] This synthetic route had not been published when our work on indium carbenes commenced. It was found that direct reaction of (iMes)Cl with the tertiary amino- titanium reagent $Ti(NMe_2)_4$ produced a titanium(IV) complex by amine elimination via proton abstraction (Figure 23) – a similar mechanism to that reported in Chapter 2 and in the forthcoming results and discussion of this chapter.

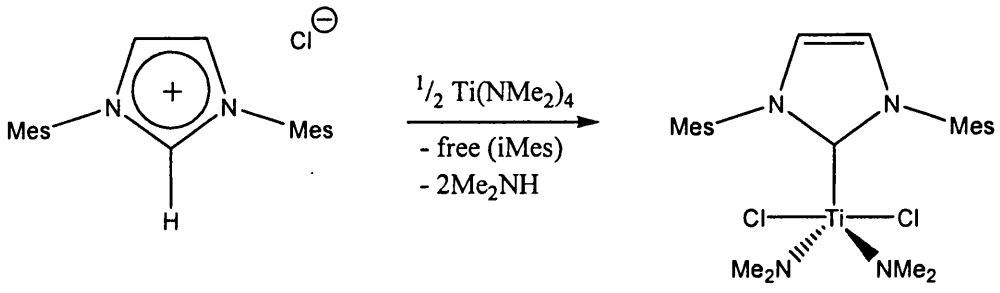

Figure 23 : Amine elimination to form a titanium carbene complex [57]

The reported yield is below 50% based on the amount of $Ti(NMe_2)_4$ used. Two equivalents of (iMes)Cl are involved in the reaction because two equivalents of amine are eliminated and two chlorides bind to the titanium centre. However, only one carbene ligand binds to the titanium, so presumably one equivalent of free (iMes)

remains in the reaction mixture after amine elimination. It may be this reactive species that inhibits a higher yield of titanium carbene.

3.1.6 Summary and Scope of Chapter

In summary, the electron rich amino substituents at the 2- and 5- positions of N-heterocyclic carbenes, stabilize the $C_{carbene}$ by donation of π-electrons to the $C_{carbene}$ vacant 2p orbitals. This stabilization means the NHCs can exist in the singlet state and as ligands are comparable to PCy_3 in terms of their strong σ-donor weak π-acceptor properties. The literature documents that a range of group 13 complexes of NHCs have been synthesized including several indium(III) carbene complexes. Simple substitution of substituents at the indium centre whilst it is stabilized by a carbene has also been reported.[1]

This chapter will show that direct reaction of trimethylindium with the acid salts of bulky NHCs has provided a new, clean route to a range of novel indium carbene complexes. Simple substitution reactions of the methyl and chloride groups with the weakly binding triflate and triflamide ligands has provided a group of potential indium catalysts which have been structurally characterized and contain spectroscopic handles. Their activity as Lewis Acid catalysts is reported further in Chapter 4.

3.2 Results

The reactions of trimethylindium with β-diketones and β-ketoimines has shown that these ligands' possession of a single acidic hydrogen provides a clean reaction pathway to indium complexes by methane elimination. It was envisaged that direct reaction of $InMe_3$ with a carbene imidazolium salt might also provide a route to indium complexes in a similar manner and in fact shortly after this work was started, a related reaction via amine elimination (instead of alkane elimination) was shown to form a titanium carbene (see Figure 23).[57]

3.2.1 Synthesis of $Me_2ClIn(iMes)$, (7)

Trimethylindium was reacted with (iMes)Cl in toluene at room temperature (Figure 24). As soon as the reagents were combined in solution, gas evolution was observed. A ^1H NMR spectroscopy scale reaction in CD_2Cl_2 showed the gas to be methane due to the appearance of the singlet at 0.20ppm. After 2 hours, the effervescence had ceased, leaving a clear yellow solution – a further indication that a new product had formed, as (iMes)Cl is only partially soluble in toluene. The solvent was removed *in vacuo* and the residue recrystallised in toluene to produce crystals of complex $Me_2ClIn(iMes)$ **(7)** in good yield (83%) suitable for X-ray crystallography. The solid state structure of **(7)** is shown in Figure 25. Table 1 shows relevant bond lengths and angles.

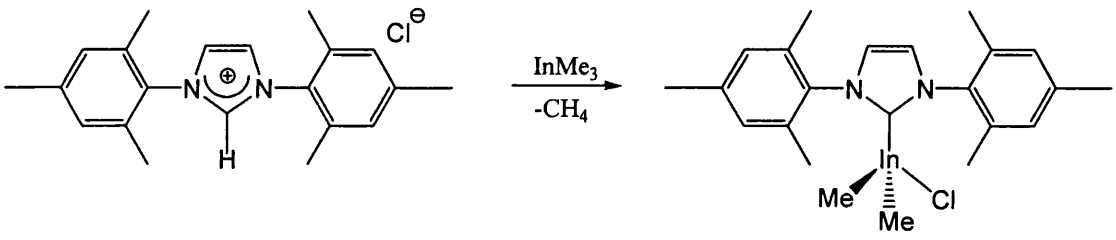

Figure 24 : Reaction of (iMes)Cl and $InMe_3$

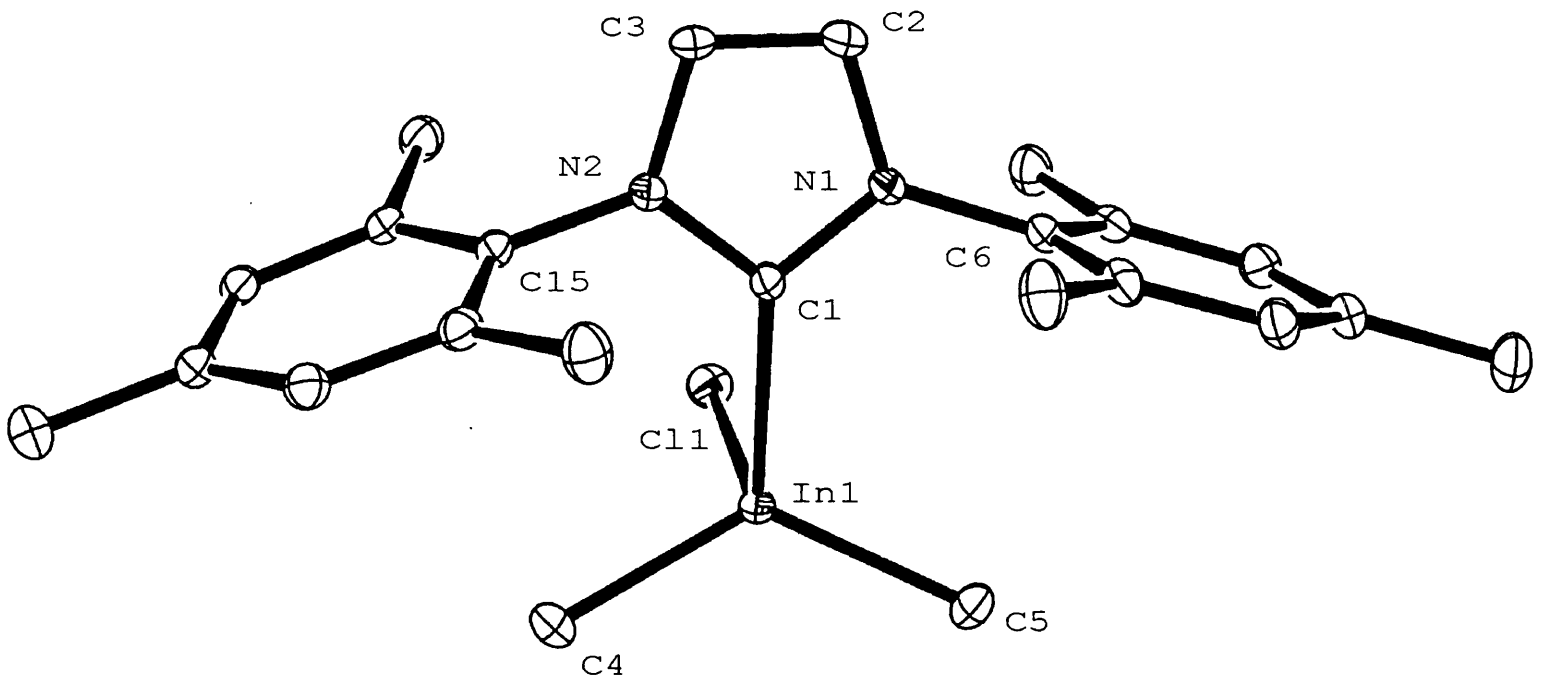

Figure 25 : Molecular structure of the asymmetric unit of $Me_2ClIn(iMes)$ (ellipsoids drawn at 30% probability level) hydrogen atoms are omitted for clarity

In(1)-C(5)	2.156(2)	N(2)-C(15)	1.447(3)	C(4)-In(1)-C(1)	112.95(9)	C(1)-In(1)-Cl(1)	91.45(5)
In(1)-C(1)	2.267(2)	N(1)-C(1)	1.352(3)	C(4)-In(1)-Cl(1)	103.13(7)	C(5)-In(1)-C(1)	110.77(9)
In(1)-C(4)	2.166(2)	N(1)-C(6)	1.453(3)	C(5)-In(1)-C(4)	124.47(10)	N(2)-C(1)-In(1)	126.11(15)
In(1)-Cl(1)	2.4807(6)	N(2)-C(3)	1.389(3)	C(5)-In(1)-Cl(1)	108.28(7)	N(1)-C(1)-In(1)	127.06(15)
N(1)-C(2)	1.387(3)	C(3)-C(2)	1.341(3)	C(1)-N(1)-C(6)	125.13(18)	C(1)-N(2)-C(15)	124.61(17)
N(2)-C(1)	1.353(3)			N(1)-C(1)-N(2)	104.64(17)		

Table 1 : Selected bond lengths (Å) and angles (°) for **(7)**

Complex **(7)** is monomeric in the solid state and no close intermolecular contacts to indium (within 4.1Å) are observed. The N(1)-C(1)-N(2) bond angle of **(7)** [104.6(4)°], like $H_3In(iMes)$[1] and $Cl_3In(iMes)$,[1] is typical for "Arduengo-type" carbenes coordinated to metal centres and lies between the normal value for free imidazol-2-ylidenes [~102°] and imidazolium cations [~108°].[49] The molecule has C_s symmetry in the solid state and the indium centre is four coordinate. However, unlike $Cl_3In(iMes)$ it does not adopt a pseudo-tetrahedral arrangement (where C-In-Cl angles of 108.7(2), 112.09(15) and 111.45(15)Å are reported).[1] Instead, the single chloride ligand lies orthogonal to the carbene ligand, [C(1)-In-(Cl(1) = 91.45(5)°]. Optimisation of complex **(7)** by density functional theory (DFT) calculations gave good agreement with the observed structure of **(7)** (discussed further in section 3.3.4).

The ^1H NMR spectrum of complex **(7)** is shown in Figure 26. This shows that the molecule retains the C_s symmetry defined by the $C_{carbene}$-In-Cl bond shown in the solid state. This symmetry accounts for some of the equivalency seen in the molecule. The olefin of the NHC appears furthest downfield as a 2H integral singlet at 7.19ppm, while the aromatic protons appear as a 4H integral singlet at 7.05ppm. The two methyl groups at the para positions in the phenylamino appear as a singlet at 2.37ppm and the four methyl groups in the ortho positions come at 2.12ppm. The two indium methyl groups are equivalent by ^1H spectroscopy and appear as a singlet at -1.03ppm. The singlet is not broadened significantly (peak width at ½ height = 1.70Hz) even though they are proximate to indium (^{115}In, 95% I = $^9/_2$ and ^{113}In, 5% I = $^9/_2$). The data shows that either rotation around the aryl rings is occurring and/or there is free rotation around the $C_{carbene}$-In bond. This is because only one singlet resonance is observed for the methyl environments attributed to the substituents in the 2- position

on the aromatic rings and only one metal bound methyl environment is observed. This data does not allow us to discriminate between the two mechanisms.

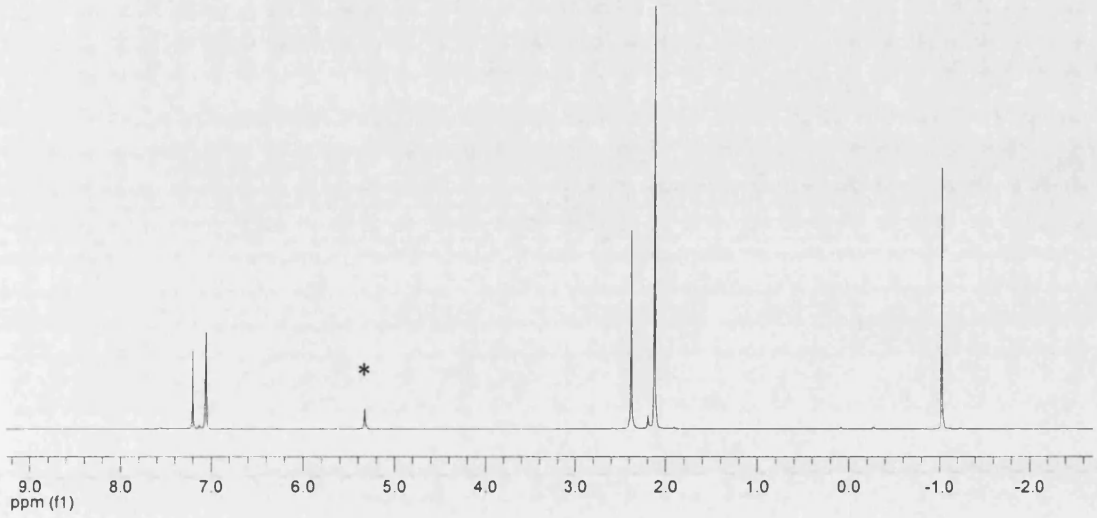

Figure 26 : ^{1}H NMR spectrum of **(7)** (* = residual solvent)

The $^{13}C\{^{1}H\}$ NMR spectrum of **(7)** is shown in Figure 27 and clearly shows 9 carbon environments. The $C_{carbene}$ resonance for complex **(7)** is not broadened substantially and appears in the range seen for aluminium and gallium carbenes, at 177.5ppm, shifted significantly upfield of the $C_{carbene}$ resonance in the free (iMes) carbene (219.9ppm in C_6D_6 and 219.7ppm in d_8-thf).[13] The equivalent carbons of the two metal bound methyl groups are observed furthest upfield at -8.1ppm, and only this resonance appears as a significantly broad peak (peak width at ½ height = 9.0Hz). The fact that a sharp peak appears (peak width at ½ height = 2.5Hz) for the $C_{carbene}$ in **(7)**, suggests the different nature of the In-$C_{carbene}$ bonding in complex **(7)** in comparison to previously reported indium carbene complexes in which no $C_{carbene}$ resonance is observed.[47,52,54,58] The observation of no $C_{carbene}$ peak has been attributed to the quadrupolar nature of the indium nuclei (^{115}In, 95% I = $^{9}/_{2}$ and ^{113}In, 5% I = $^{9}/_{2}$) and will be discussed in more detail in sections 3.3.1.

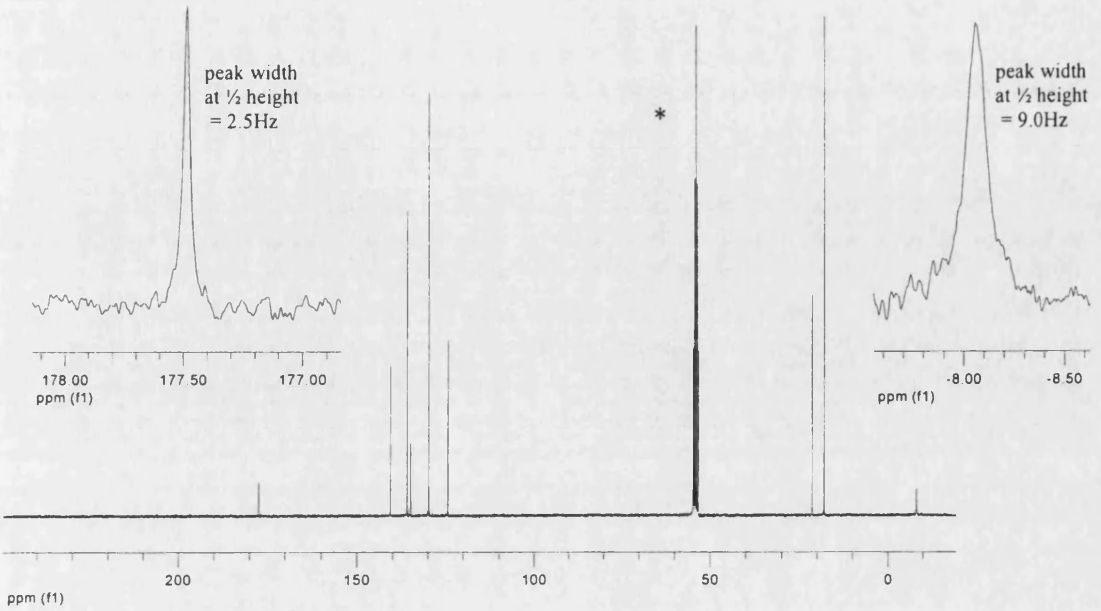

Figure 27 : $^{13}C\{^{1}H\}$ NMR spectrum of **(7)** showing expansions of the $C_{carbene}$ (left) and C_{Me}-In (right) resonances (* = residual solvent)

An alternative synthesis for complex **(7)** was developed to avoid the use of the expensive and pyrophoric trimethylindium. Instead, the cheaper and more readily available indium trichloride was used. Methylation of indium trichloride using methyllithium to generate $InMe_3$ *in situ* followed by addition of (iMes)Cl gave complex **(7)** in a slightly lower yield (67%) than that observed from the synthesis involving $InMe_3$ (83%).

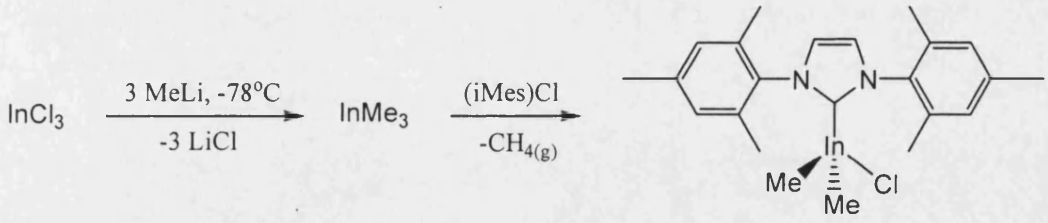

Figure 28 : Alternative synthesis of **(7)** via $InCl_3$

3.2.2 Synthesis of $Me_2ClIn(iPr)$, (8)

Trimethylindium was reacted with (iPr)Cl in toluene at room temperature following the synthesis of (7). As soon as the reagents were combined in solution, gas evolution was observed. As expected, a ^1H NMR spectroscopy scale reaction in CD_2Cl_2 showed the gas to be methane due to the appearance of the singlet at 0.20ppm. After 2 hours, the effervescence had ceased, leaving a clear yellow/brown solution - an indication that a new product had formed as (iPr)Cl is only partially soluble in toluene. The reaction that occurs is shown in Figure 29 and $Me_2ClIn(iPr)$ **(8)** is produced in good yield (86%). Crystals suitable for X-ray crystallography studies were obtained by recrystallisation in toluene at 4°C. The solid state structure is shown in Figure 30.

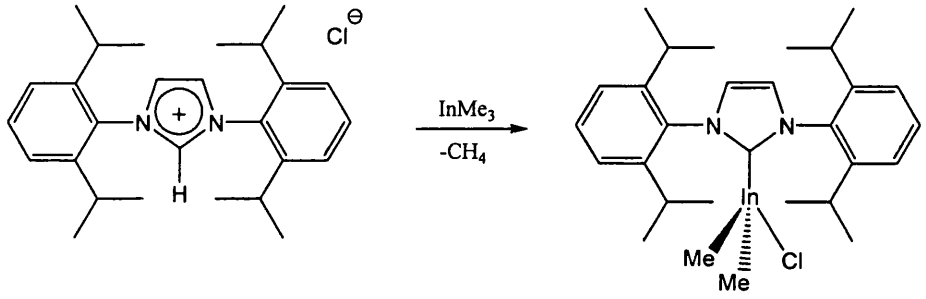

Figure 29 : Reaction of (iPr)Cl and $InMe_3$

Unlike (7), for **(8)** there are two crystallographically independent molecules in the asymmetric unit. The bond lengths and angles of the two molecules are equivalent within error so only one will be discussed which is shown in Figure 30. Table 2 shows its relevant bond lengths and angles. The N(1)-C(1)-N(2) bond angle of **(8)** [103.7(2)°] is the same of that of (7) [104.6(2)] within error. Complex **(8)** is monomeric in the solid state and no close intermolecular contacts within 3.5Å are observed. The indium centre is four coordinate, and like (7) does not adopt a pseudo-

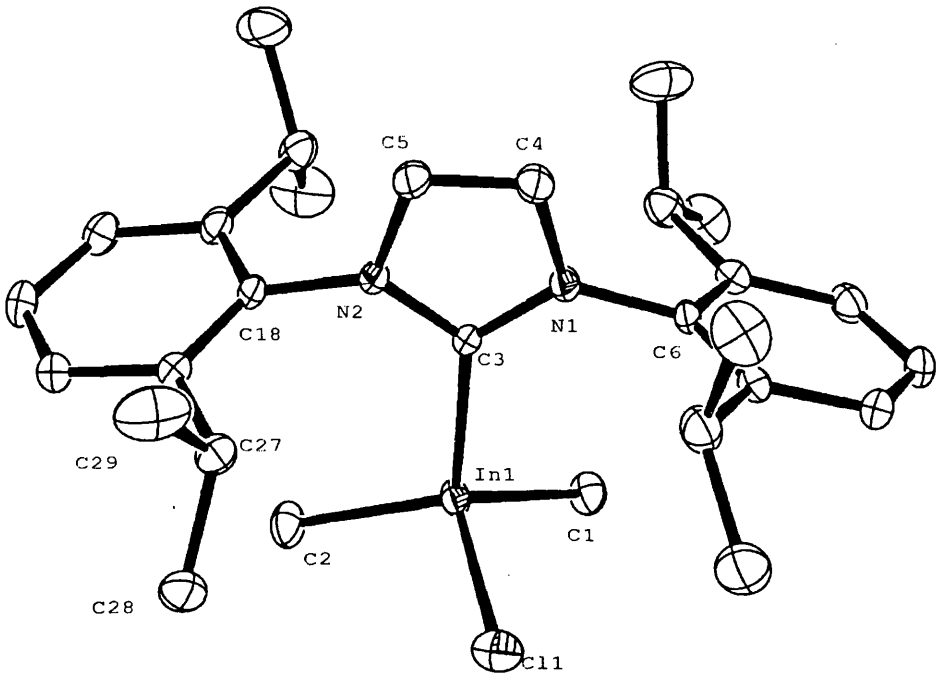

Figure 30 : Molecular structure of $Me_2ClIn(iPr)$ showing one of the two molecules in the asymmetric unit (ellipsoids drawn at 30% probability level) hydrogen atoms are omitted for clarity

In(1)-C(1)	2.158(3)	N(1)-C(6)	1.454(3)	C(1)-In(1)-C(2)	119.17(13)	N(2)-C(3)-N(1)	103.7(2)
In(1)-C(2)	2.174(3)	N(2)-C(3)	1.358(3)	C(1)-In(1)-C(3)	109.91(12)	C(3)-N(1)-C(6)	126.5(2)
In(1)-C(3)	2.273(3)	N(2)-C(5)	1.391(4)	C(2)-In(1)-C(3)	112.54(11)	C(3)-N(2)-C(18)	126.0(2)
In(1)-Cl(1)	2.4046(10)	N(2)-C(18)	1.446(3)	C(1)-In(1)-Cl(1)	108.36(10)	N(2)-C(3)-In(1)	126.32(19)
N(1)-C(3)	1.361(3)	C(4)-C(5)	1.346(4)	C(2)-In(1)-Cl(1)	107.65(11)	N(1)-C(3)-In(1)	129.80(19)
N(1)-C(4)	1.391(4)			C(3)-In(1)-Cl(1)	96.73(7)		

Table 2 : Selected bond lengths (Å) and angles (°) for **(8)**

tetrahedral arrangement and instead the single chloride ligand lies essentially orthogonal to the carbene ligand, [C(1)-In-(Cl(1) = 96.73(7)°] although with a less compressed angle than observed in **(7)**. Comparison of bond lengths and angles of **(8)** with those of **(7)** is shown in Table 3.

	Bond lengths (Å) and Bond angles(°)	
	(7)	**(8)**
In(1)-C(1)	2.267(2)	2.273(3)
In(1)-Cl(1)	2.481(1)	2.405(1)
In(1)-C(4)	2.156(2)	2.158(3)
In(1)-C(5)	2.166(2)	2.174(3)
C(1)-N(1)	1.352(3)	1.358(3)
N(1)-C(2)	1.387(3)	1.391(4)
N(1)-C(1)-N(2)	104.6(2)	103.7(2)
C(1)-N(1)-C(2)	111.1(2)	111.5(2)
C(1)-In(1)-Cl(1)	91.45(5)	96.73(7)

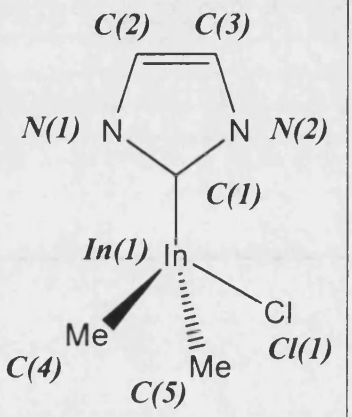

Table 3 : Comparison of some bond lengths and angles of **(7)** and **(8)**

The data shows that the geometry about the indium and in the 5-membered ring in the two compounds is very similar, the exceptions being the indium-chloride bond which is shorter in **(8)** and the less compressed C(1)-In(1)-Cl(1) bond angle in **(8)**.

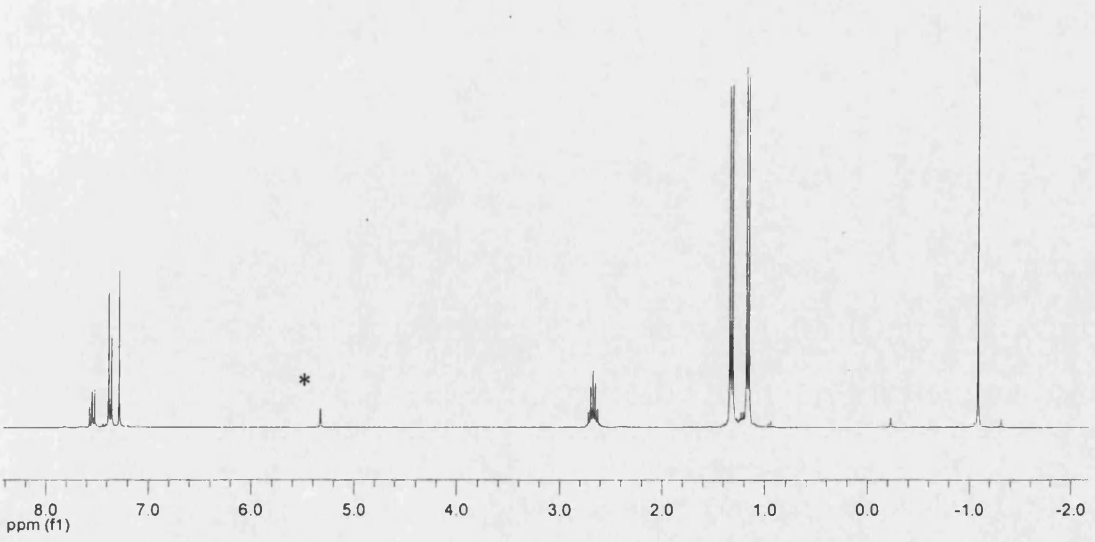

Figure 31 : The ^{1}H NMR spectrum of **(8)** (* = residual solvent)

The ^{1}H spectrum of complex **(8)** is shown in Figure 31. The aromatic protons appear as a 2H integral triplet at 7.54ppm and a 4H integral doublet at 7.37ppm. The olefin protons appear as a singlet at 7.28ppm while a virtual septet (doublet of quartets) is observed for the four CH protons of the isopropyl groups at 2.67ppm. The prochiral methyl substituents of the isopropyl groups appear as a two 12H integral doublets, at 1.33 and 1.17ppm. The two indium methyl groups are equivalent by ^{1}H spectroscopy and appear at -1.08ppm. The $C_{carbene}$ resonance for **(8)** appears in the expected range at 179.7ppm in the $^{13}C\{^{1}H\}$ NMR spectrum. In the solid state **(8)** contains a C_s plane of symmetry, as in **(7)**. The plane is perpendicular to the heterocyclic ring and contains the $C_{carbene}$-indium bond. The symmetry in the solid state can account for some of the equivalency seen in the molecule.

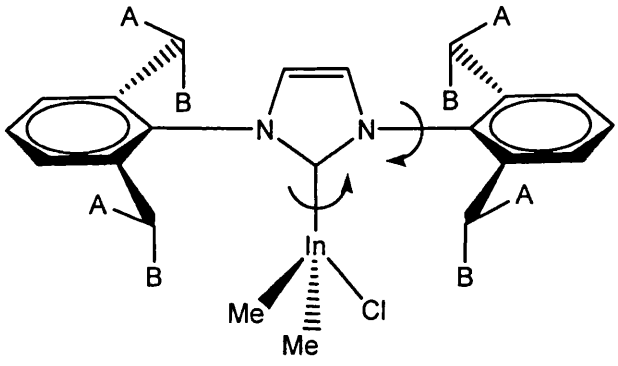

Figure 32 : Bond rotation in **(8)**

Figure 32 shows a diagram of **(8)** where the methyls of the isopropyl substituents which are equivalent in solution are labelled A and B. In order for two doublets to appear for the isopropyl groups, the four methyls labelled A must be equivalent, while the four methyls labelled B must also be equivalent but inequivalent to A. This can only occur by rotation around the In-$C_{carbene}$ bond. This rotation was still observed when the sample was cooled to 203K (-70°C) as two doublets remained at this

temperature. The ^{1}H NMR spectroscopic data also shows that rotation around the N-C bond of the amino subsituents is restricted as has been observed for $Br_3In(iPr)$.[52] If rotation were not restricted then A and B would be equivalent by rotation. If this were the case then one 24H integral doublet resonance would be observed for the 8 methyls.

3.2.3 Synthesis of $Me_2BrIn(iMes)$, (9)

It was considered interesting what effect replacing the chloride in **(7)** with a bromide might have on the structure of the molecule. Therefore trimethylindium was reacted with (iMes)Br (which has been previously reported),[59] in toluene at room temperature in the same manner as for the synthesis of **(7)**. As soon as the reagents were combined in solution, gas evolution was observed. As expected, a ^{1}H NMR scale reaction showed the gas to be methane by the appearance of a singlet resonance at 0.20ppm in CD_2Cl_2. The reaction was complete after 2 hours to give $Me_2BrIn(iMes)$ **(9)** in good yield (75%) (Figure 33). Recrystallisation of the compound in toluene gave crystals suitable for X-ray crystallography. The solid state structure is shown in Figure 34.

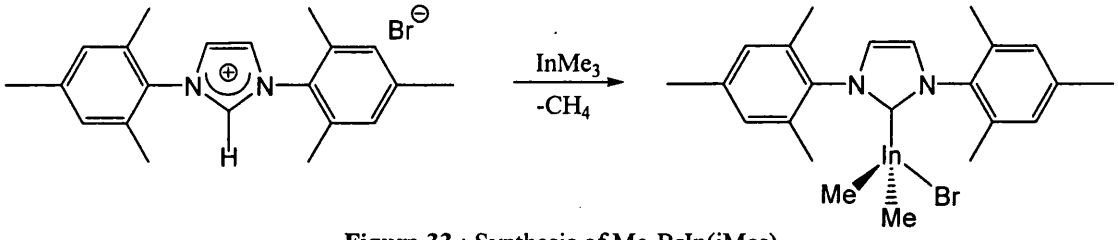

Figure 33 : Synthesis of $Me_2BrIn(iMes)$

One molecule appears in the asymmetric unit of the crystal structure. Table 4 contains its relevant bond lengths and angles. The N(1)-C(3)-N(2) angle, 104.73(12) is like **(7)** and **(8)** and lies between the bond angles for free imidazole-2-ylidenes [~102°] and imidazolium cations [~108°].[49] Complex **(9)** is monomeric and does not display any intermolecular interactions in the solid state. The indium centre is 4-coordinate and

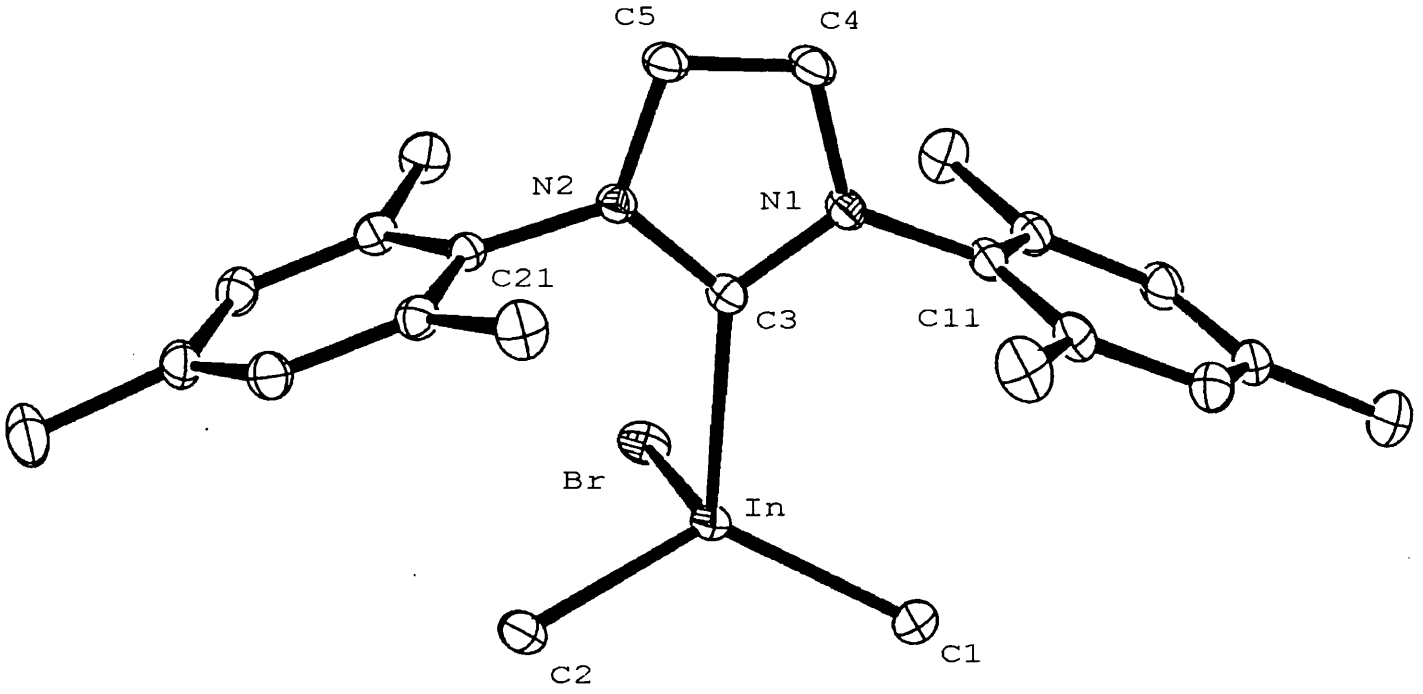

Figure 34 : Molecular structure of the asymmetric unit of $Me_2BrIn(iMes)$ (ellipsoids drawn at 30% probability level) hydrogen atoms are omitted for clarity

In-C(3)	2.2676(14)	N(2)-C(5)	1.3825(18)	C(3)-In-C(1)	112.20(6)	N(1)-C(3)-N(2)	104.73(12)
In-C(1)	2.1602(16)	N(1)-C(4)	1.3837(18)	C(3)-In-C(2)	110.40(6)	C(3)-N(1)-C(4)	110.89(12)
In-C(2)	2.1588(17)	N(1)-C(11)	1.4444(19)	C(3)-In-Br	95.48(4)	C(3)-N(1)-C(11)	124.22(12)
In-Br	2.6198(2)	N(2)-C(21)	1.4466(18)	In-C(3)-N(1)	127.59(10)	N(1)-C(4)-C(5)	106.73(13)
N(1)-C(3)	1.3530(18)	C(4)-C(5)	1.350(2)	C(1)-In-C(2)	124.22(7)		
N(2)-C(3)	1.3516(18)			C(1)-In-Br	104.41(6)		

Table 4 : Selected bond lengths (Å) and angles (°) for **(9)**

like **(7)** the molecule does not adopt a pseudo-tetrahedral arrangement. The bromide ligand lies essentially orthogonal to the carbene ligand [Br-In-C(3) = 95.48(4)] but not to the same extent as the chloride in **(7)** [91.45(5)].

The ^{1}H and $^{13}C\{^{1}H\}$ NMR spectrum shows that the solution behaviour of **(9)** is very similar to that of **(7)**. The ^{1}H NMR spectrum in C_6D_6 shows 5 singlet resonances. The 4H integral aromatic proton resonance appears at 6.73ppm while the 2H integral olefin peak is observed at 5.99ppm. The para-methyl groups of the mesityls appear as a 6H integral resonance at 2.08ppm while the 12 protons of the ortho-methyl groups is observed at 2.04ppm. The metal bound methyl resonance appears as a 6H integral singlet at -0.44ppm. The $^{13}C\{^{1}H\}$ NMR spectrum contains 9 resonances from the $C_{carbene}$ at 177.9ppm to the carbons from the metal bound methyl groups which appear as a resonance furthest upfield at -6.6ppm.

3.2.4 Synthesis of $Me_2ClIn(iMesH_2)$, (10)

It was deemed interesting to determine what difference in properties might be imparted by introduction of an NHC with a saturated backbone. The lack of delocalisation in the 5-membered ring might affect both $C_{carbene}$-In bonding and the geometry around the metal centre. Thus $Me_2ClIn(iMesH_2)$ was synthesised by reaction of $(iMes)H_2$ (which has been previously reported)[14] with $InMe_3$ in toluene (Figure 35).

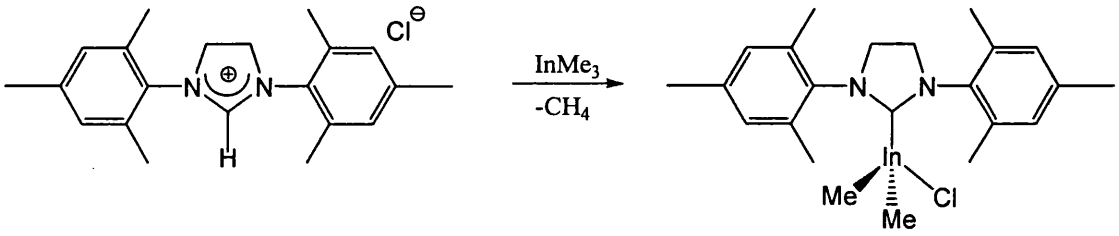

Figure 35 : Synthesis of $Me_2ClIn(iMesH_2)$

The reaction did not go cleanly and only a small amount of complex **(10)** was isolated (yield = 9%) by recrystallisation. The solid state X-ray structure is shown in Figure 36. The asymmetric unit contained one molecule, relevant bond lengths and angles of which are shown in Table 6.

The N-C-N angle of the 5-membered ring in **(10)** is [109.20(12)°] and lies between the value for free ($iMesH_2$) [104.7(3)°] and ($iMesH_2$)Cl [113.1(4)°].[23] These larger angles compared to (iMes) [101.4(2)°] and (iMes)Cl [108.74°] reflect the strain introduced by the longer saturated backbone of the 5-membered ring. Comparison of the solid state structure of **(10)** with **(7)** shows that the bond lengths and geometry of the two molecules are very similar. The Cl-In-$C_{carbene}$ bond angle in **(10)** is 90.33(4)°, an even more compressed angle than the equivalent angle in **(7).**

	Bond lengths (Å) and Bond angles(°)	
	(7)	**(10)**
In(1)-C(1)	2.267(2)	2.281(1)
In(1)-Cl(1)	2.4807(6)	2.4860(5)
In(1)-C(4)	2.156(2)	2.161(1)
In(1)-C(5)	2.166(2)	2.166(1)
C(1)-N(1)	1.352(3)	1.331(18)
N(1)-C(2)	1.387(3)	1.479(2)
C(2)-C(3)	1.341(3)	1.529(2)
Cl(1)-In(1)-C(1)	91.45(5)	90.33(4)
N(1)-C(1)-N(2)	104.64(17)	109.20(12)
C(1)-N(1)-C(2)	111.10(19)	112.46(12)

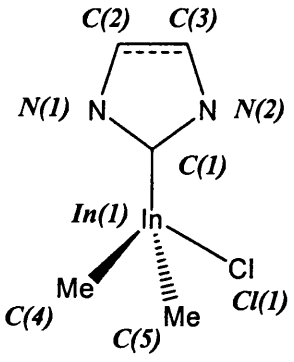

Table 5 : Comparison of some bond lengths and angles of **(7)** and **(10)**

It has been reported that ($iMesH_2$) is a marginally stronger σ-donor than (iMes) and observed that the metal-$C_{carbene}$ bond length using ($iMesH_2$) was statistically shorter than that observed in the (iMes) analogue of Cp*Ru(Cl)($iMesH_2$).[60] Comparison of

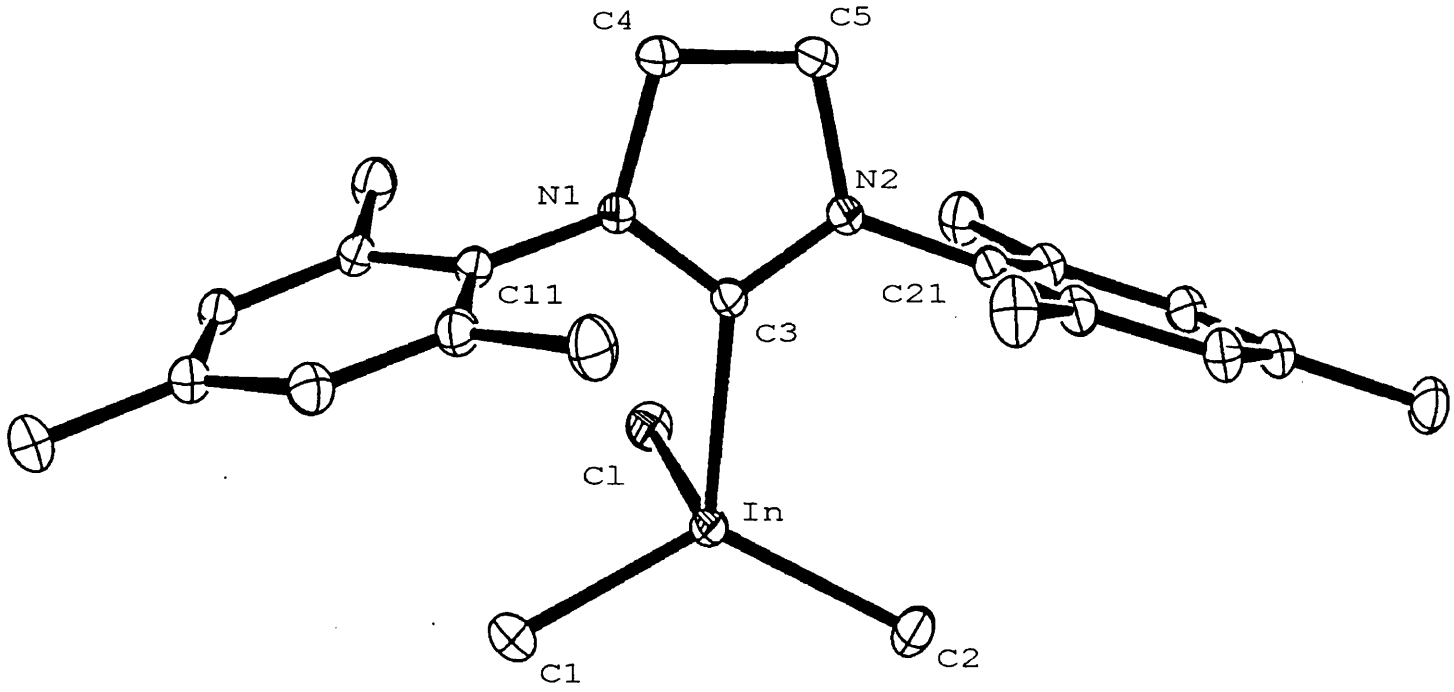

Figure 36 : Molecular structure of the asymmetric unit of $Me_2ClIn(iMesH_2)$ (ellipsoids drawn at 30% probability level) hydrogen atoms are omitted for clarity

In-C(3)	2.2806(14)	N(2)-C(5)	1.479(2)	C(3)-In-C(1)	113.42(7)	N(1)-C(3)-N(2)	109.20(12)
In-C(1)	2.1605(19)	N(1)-C(4)	1.483(2)	C(3)-In-C(2)	112.02(7)	C(3)-N(1)-C(4)	112.46(12)
In-C(2)	2.1664(18)	N(1)-C(11)	1.4412(19)	C(3)-In-Cl	90.33(4)	C(3)-N(1)-C(11)	124.90(13)
In-Cl	2.4860(5)	N(2)-C(21)	1.4416(19)	In-C(3)-N(1)	124.40(10)	N(1)-C(4)-C(5)	102.50(12)
N(1)-C(3)	1.3313(18)	C(4)-C(5)	1.529(2)			C(1)-In-C(2)	123.92(9)
N(2)-C(3)	1.3332(18)					C(1)-In-Cl	103.41(6)

Table 6 : Selected bond lengths (Å) and angles (°) for **(10)**

the $C_{carbene}$-In bond in **(7)** and **(10)** demonstrates that the binding of the two ligands to indium is very similar and in fact after accounting for error, the difference is very small.

Unlike that found for **(7)**, the 5-membered NHC ring is not planar in **(10)** because of the introduction of the saturated backbone. The sp^3 hybridisation at carbons C(2) and C(3) forces the C(2)-C(3) bond to be tilted out of the plane by 7.4°. The ^1H NMR spectrum proves this does not affect the symmetry of the molecule in solution and 5 singlet resonances are observed. Furthest downfield is the 4H integral aromatic resonance at 6.74ppm. This is followed by a singlet 4H integral resonance of the saturated backbone of the 5-membered NHC ring at 2.98ppm. The *para*-methyl substituents of the mesityl rings appear as a 6H integral singlet at 2.24ppm while the 12 protons of the ortho-methyl substituents are observed as a singlet at 2.07ppm. Furthest upfield is a 6H integral singlet observed at -0.58ppm for the two metal bound methyl groups. In the solid state, a C_s symmetry plane exists which lies orthogonal to the heterocyclic ring and contains the $C_{carbene}$-indium bond. This ^1H NMR spectroscopic data shows the behaviour of **(10)** to be similar to that of **(7)**.

Because it proved difficult to synthesise **(10)**, no further work was done with the system or with the carbene ($iMesH_2$).[14]

3.2.5 Synthesis of $Me_3In(iMes)$, (11)

Trimethylindium was reacted with free (iMes) in toluene at ambient temperature for 2 hours. Removal of the solvent *in vacuo* followed by dissolution of the solid in minimum Et_2O and its storage at -20°C gave clear and colourless crystals.

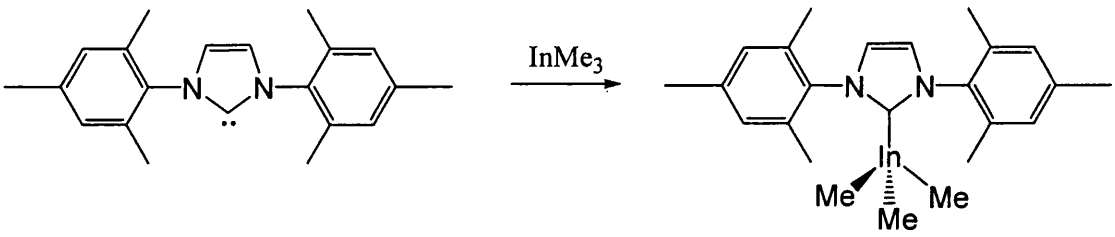

Figure 37 : Synthesis of $Me_3In(iMes)$

The reaction that occurs is shown in Figure 37 while the X-ray structure of the complex is shown in Figure 38. The asymmetric unit contains only half of the molecule, the other half was generated crystallographically. Table 7 shows relevant bond lengths and angles. The N(1)-C(3)-N(2) bond angle of **(11)** [103.65(16)°] is similar to that observed for **(7)-(9)**. Complex **(11)** is monomeric in the solid state and no close intermolecular contacts to the metal are observed (within 3.6Å). The geometry at the 4–coordinate indium centre is pseudo tetrahedral (where the $C_{carbene}$-In-C_{methyl} angles are 106.62(8), 103.29(5) and 103.29(5)°).

The ^1H NMR spectrum shows 5 singlet resonances. Furthest downfield is the 2H integral olefin resonance at 7.12ppm. This is followed by the 4H integral aromatic resonance at 7.05ppm. The para-methyl substituents of the mesityl rings appear as a 6H integral singlet at 2.38ppm while the 12 protons of the ortho-methyl substituents are observed as a singlet at 2.08ppm. Furthest upfield is a 9H integral singlet observed at -1.26ppm for the three metal bound methyl groups. In the $^{13}C\{^1H\}$ NMR spectrum

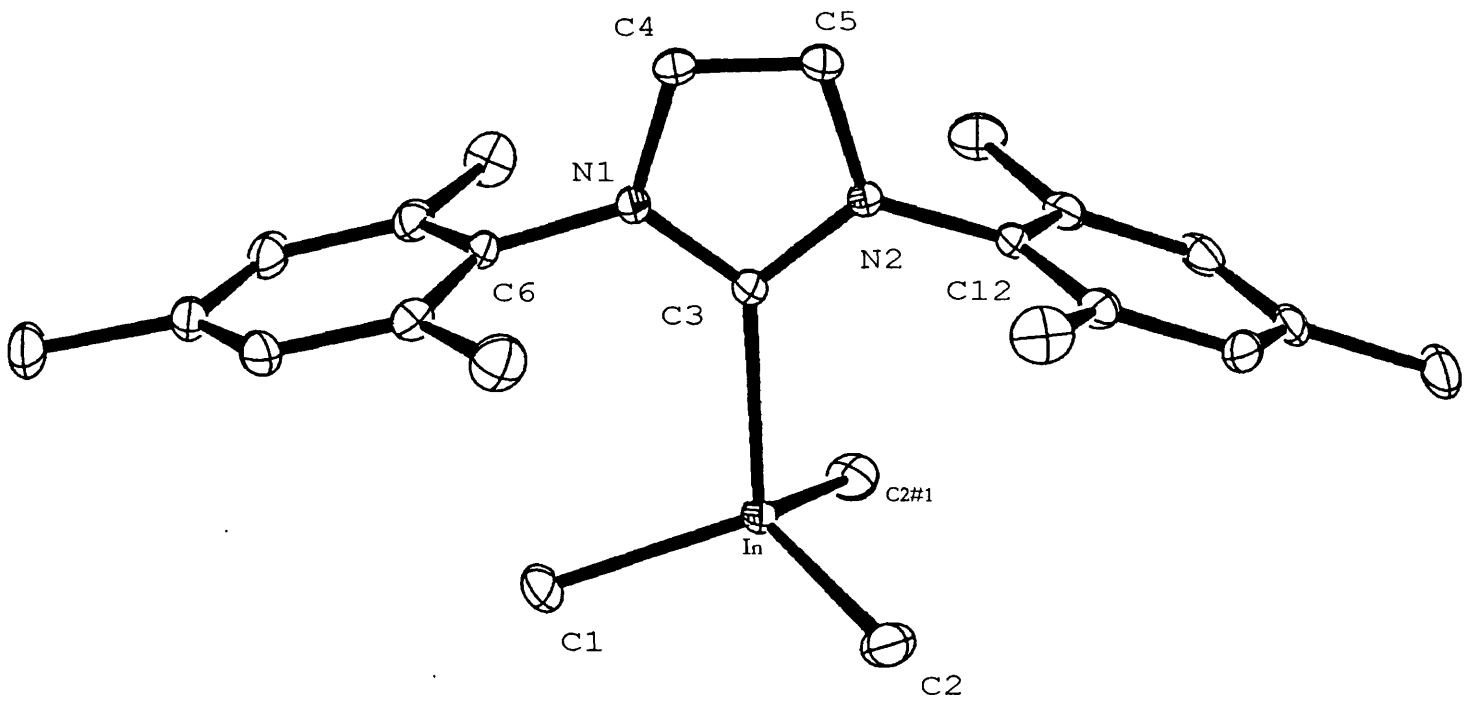

Figure 38 : Molecular structure of $Me_3In(iMes)$ (ellipsoids drawn at 30% probability level) hydrogen atoms are omitted for clarity

In-C(3)	2.3100(18)	N(2)-C(5)	1.391(2)	C(3)-In-C(1)	106.62(8)	N(1)-C(3)-N(2)	103.65(16)
In-C(1)	2.175(2)	N(1)-C(4)	1.385(3)	C(3)-In-C(2)	103.29(5)	C(3)-N(1)-C(4)	111.55(17)
In-C(2)	2.1887(17)	N(1)-C(6)	1.450(3)	In-C(3)-N(1)	130.13(13)	C(3)-N(1)-C(6)	122.90(17)
N(1)-C(3)	1.355(2)	N(2)-C(12)	1.442(2)	C(1)-In-C(2)	112.78(6)	N(1)-C(4)-C(5)	107.08(17)
N(2)-C(3)	1.363(2)	C(4)-C(5)	1.340(3)				

Table 7 : Selected bond lengths (Å) and angles (°) for **(11)**

the $C_{carbene}$ peak appears at 183.0ppm (peak width at ½ height = 1.9Hz) while the metal bound methyl resonance appears at -11.8ppm (peak width at ½ height = 9.0Hz). The resonance of the metal bound carbon of the methyl groups is significantly broader than the resonance of the $C_{carbene}$.

An alternative synthesis for complex **(11)** was developed avoiding the use of the expensive and pyrophoric trimethylindium. Instead, the cheaper and more readily available compound indium trichloride was used. Methylation of indium trichloride using methyllithium to generate $InMe_3$ *in situ* followed by addition of (iMes) gave complex **(11)** in a slightly lower yield (59%) than that observed from the synthesis involving $InMe_3$ (72%).

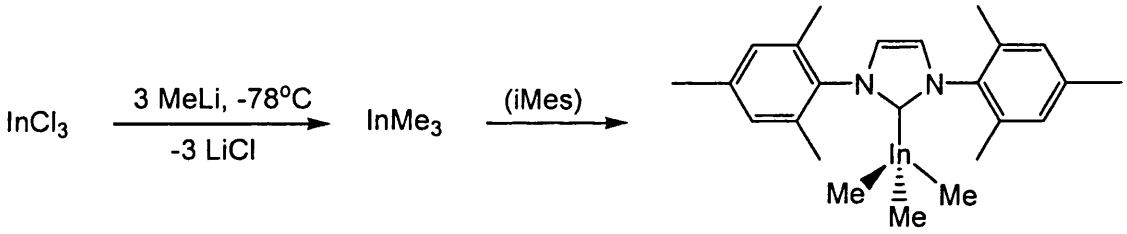

Figure 39 : Alternative synthesis of **(11)** via $InCl_3$

3.2.6 Synthesis of $Me_3In(CN(Pr^i)C_2Me_2NPr^i)$, (12)

Trimethylindium was reacted with the free carbene ($CN(Pr^i)C_2Me_2NPr^i$) in toluene at ambient temperature for 2 hours (Figure 40). Removal of the solvent *in vacuo* yielded a white oily solid. Crystals suitable for single crystal X-ray diffraction could not be obtained.

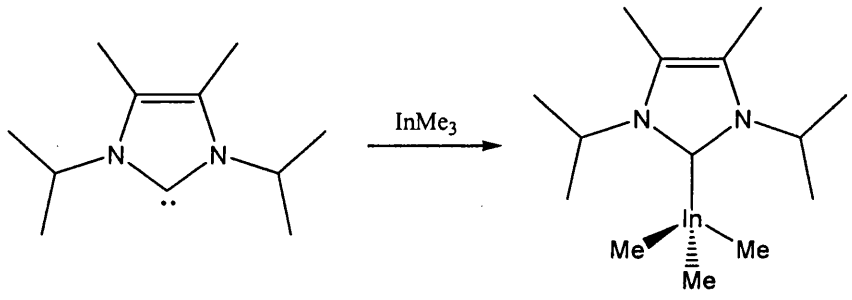

Figure 40 : Synthesis of $Me_3In(CN(Pr^i)C_2Me_2NPr^i)$, **(12)**

In the ^{1}H NMR spectrum four resonances are observed. Furthest downfield is a 2H integral virtual septet from the CH of the isopropylamino groups at 5.15ppm while the 6H integral singlet for the two methyl groups bound to the olefin carbons is observed at 1.56ppm. A 12H integral doublet is observed at 1.09ppm for the methyl substituents of the two isopropyl groups and furthest upfield a 9H integral singlet is observed at 0.02ppm for the three metal-bound methyl groups. The $^{13}C\{^1H\}$ spectroscopic data shows 6 resonances for the 6 different carbon environments. The $C_{carbene}$ resonance is observed at 180.1ppm and the resonance for the three metal-bound methyl groups is observed at -5.6ppm. The four proton resonances and 6 carbon resonances are consistent with rotation about the $C_{carbene}$-In bond.

3.2.7 Synthesis of $Me_2(OTf)In(iMes)$, (13)

Reaction of a stoichiometric amount of TMS(OTf) with $Me_2(Cl)In$-iMes, **(7)** in dichloromethane gave the monotriflate complex $Me_2(OTf)In(iMes)$, **(13)** (Figure 41). This was a rapid reaction, and ^{1}H NMR spectroscopy showed it to be complete after 2 minutes. The by-product of the reaction was identified as chlorotrimethylsilane, TMS(Cl) by the presence of a ^{1}H singlet resonance at 0.51ppm in CD_2Cl_2 (integrating to 9 protons). The solvent and TMS(Cl) were removed *in vacuo*, and the compound was recrystallised using a dichloromethane/hexane layer and stored at -20°C to yield clear and colourless crystals suitable for crystallographic studies.

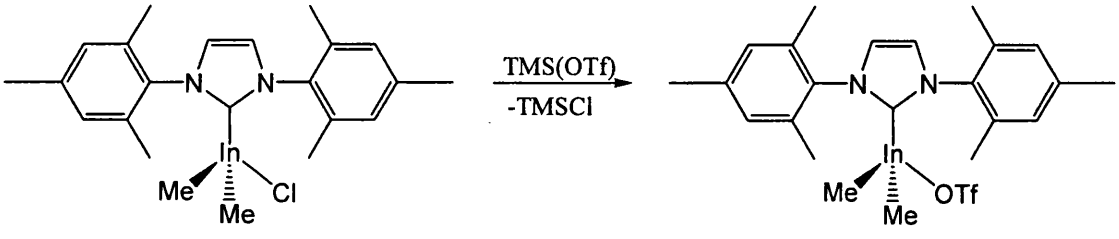

Figure 41 : Synthesis of $Me_2(OTf)In(iMes)$ via reaction of (7) with TMS(OTf)

An alternative route to **(13)** was also found using compound **(11)** instead of **(7)**. Reaction of one equivalent of H(OTf), with $Me_3In(iMes)$ resulted in methane elimination (Figure 42). Methane was identified by its resonance at 0.20ppm by following the reaction by ^1H spectroscopy in CD_2Cl_2. The complex was recrystallised in the same manner as above to yield spectroscopically identical material.

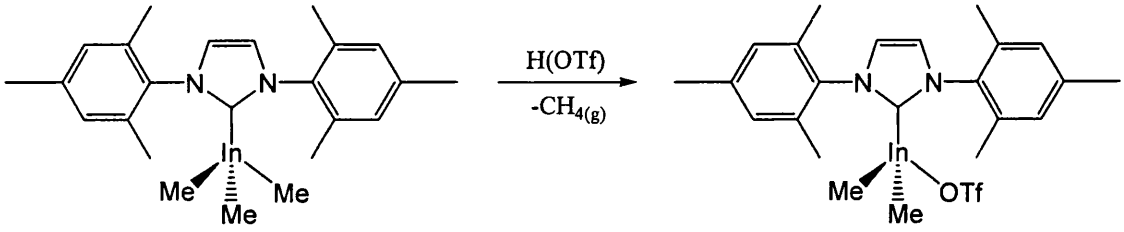

Figure 42 : Synthesis of **(13)**, $Me_2(OTf)In(iMes)$ via reaction of **(11)** with HOTf

The solid state structure of **(13)** is shown in Figure 43. A molecule of co-crystallised solvent (dichloromethane) is not shown. Table 8 shows relevant bond lengths and angles for the complex. The N(1)-C(3)-N(2) bond angle of **(13)** [104.15(18)°] is similar to those of other reported complexes. The extended solid state structure shows that the compound is a one-dimensional coordination polymer where the indium metal centre is 5-coordinate. The arrangement of ligands around the metal centre gives the indium a distorted trigonal-bipyramidal geometry. The oxygens of the triflate ligands [O(1) and O(2#)] occupy the apical positions [O(1)-In-O(2#) 168.57(6)°] while the metal bound methyl groups and the $C_{carbene}$ occupy the equatorial positions. The indium methyls are in the plane of the 5-membered NHC ring and have a C(1)-In-C(2) angle of 135.03(10)°. The $C_{carbene}$-In-O(1) bond angle is compressed from 90° at 80.07(8)° while the $C_{carbene}$-In-O(2)# bond angle is also compressed from 90° at 88.59(7)°.

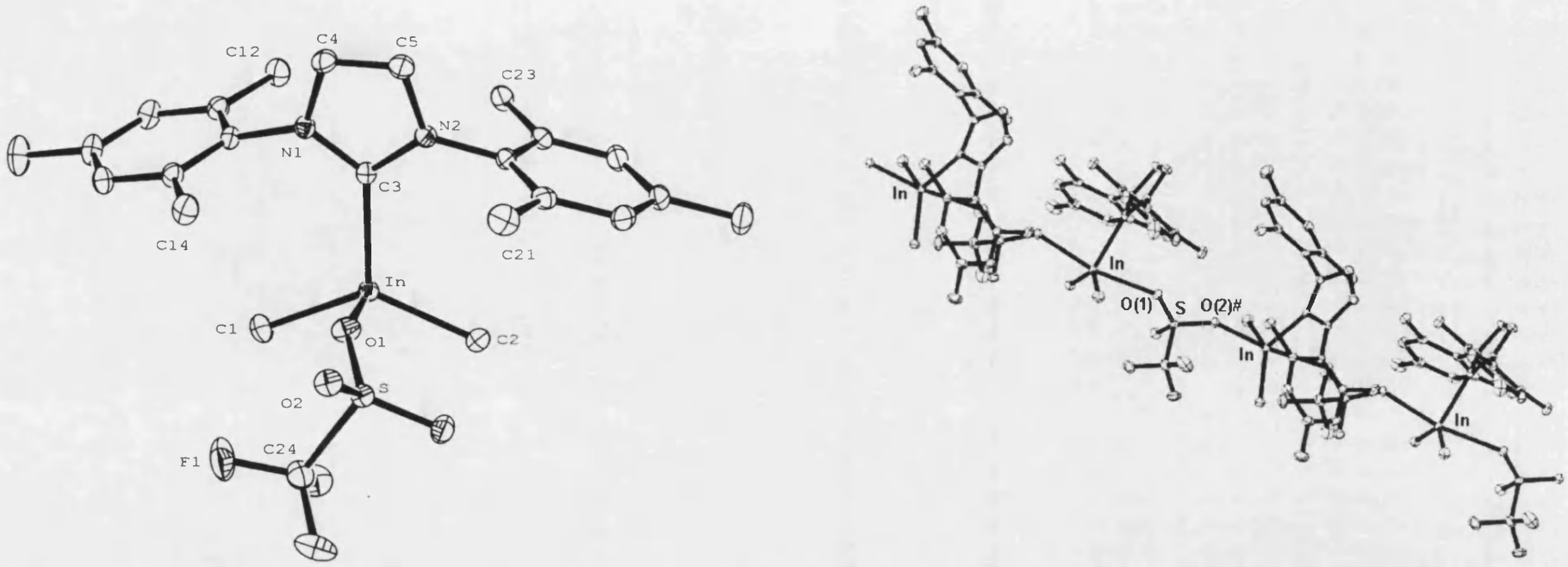

Figure 43 : Molecular atructure of the asymmetric unit of $Me_2(OTf)In(iMes)$ and its extended one-dimensional coordination polymer (ellipsoids drawn at 30% probability level) hydrogen atoms are omitted for clarity

In-C(3)	2.264(2)	N(2)-C(5)	1.384(3)	C(3)-In-C(1)	112.87(9)	N(1)-C(3)-N(2)	104.15(18)
In-C(1)	2.143(2)	N(1)-C(4)	1.385(3)	C(3)-In-C(2)	111.69(8)	C(3)-N(1)-C(4)	111.36(18)
In-C(2)	2.141(2)	N(1)-C(6)	1.453(3)	C(3)-In-O(1)	80.07(7)	C(3)-N(1)-C(6)	125.99(19)
In-O(1)	2.5876(18)	C(4)-C(5)	1.341(3)	In-C(3)-N(1)	128.67(15)	N(1)-C(4)-C(5)	106.6(2)
N(1)-C(3)	1.351(3)	In-O(2)#	2.4617(16)	C(1)-In-C(2)	135.03(10)	O(1)-In-O(2)#	168.57(6)
N(2)-C(3)	1.357(3)			C(1)-In-O(1)	92.13(8)	C(3)-In-O(2)#	88.59(7)

Table 8 : Selected bond lengths (Å) and angles (°) for **(13)**

The ^{1}H NMR spectrum of **(13)** shows 5 singlet resonances in CD_2Cl_2. Furthest downfield is the olefin singlet at 7.28ppm. A 4H integral singlet is observed for the aromatic protons on the mesityl groups at 7.08ppm. The 6H integral singlet for the meta-substituted methyls of the mesityl groups appears at 2.38ppm while the 12H integral singlet for the ortho-substituted methyls appears at 2.09. The most upfield resonance is the metal bound methyl groups which are observed as a 6H integral singlet resonance below zero at -0.83ppm. The $^{13}C\{^{1}H\}$ NMR spectrum shows 10 carbon resonances. The $C_{carbene}$ peak is observed at 176.2ppm and the metal bound methyl carbons appear at -7.1ppm. The carbon of the triflate CF_3 groups appears as a quartet at 120.1ppm [J = 319Hz] due to the carbon coupling to the three fluorine atoms [^{19}F(100%) I = $^{1}/_{2}$]. The ^{19}F NMR spectrum shows a singlet at -78.7ppm. 5 proton resonances and 10 carbon resonances are observed for the compound due to the time averaged mirror plane of the molecule in solution. Its solution behaviour appears to be similar to that of **(7)** suggesting the coordination polymer observed in the solid state does not persist once the compound is in solution.

3.2.8 Synthesis of $Me(OTf)_2In(iMes)$, (14)

Attempts to synthesise the bistriflate complex $Me(OTf)_2In(iMes)$, **(14)** were successful via two different routes. Firstly the monotriflate complex **(13)** was reacted with a stoichiometric amount of H(OTf) (Figure 44). This resulted in methane elimination observed by ^{1}H NMR spectroscopy.

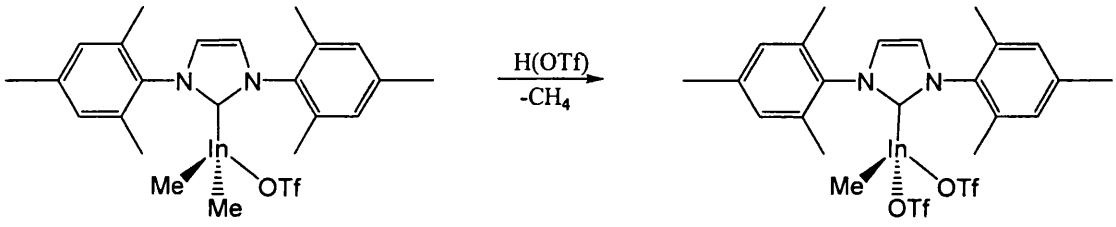

Figure 44 : Synthesis of $Me(OTf)_2In(iMes)$

Compound **(14)** can also be readily synthesised from compounds **(7)** and **(12)** (Figure 45), because both of these reactions involve production of the monotriflate compound **(13)** before this goes onto react further to become the bistriflate species **(14)**.

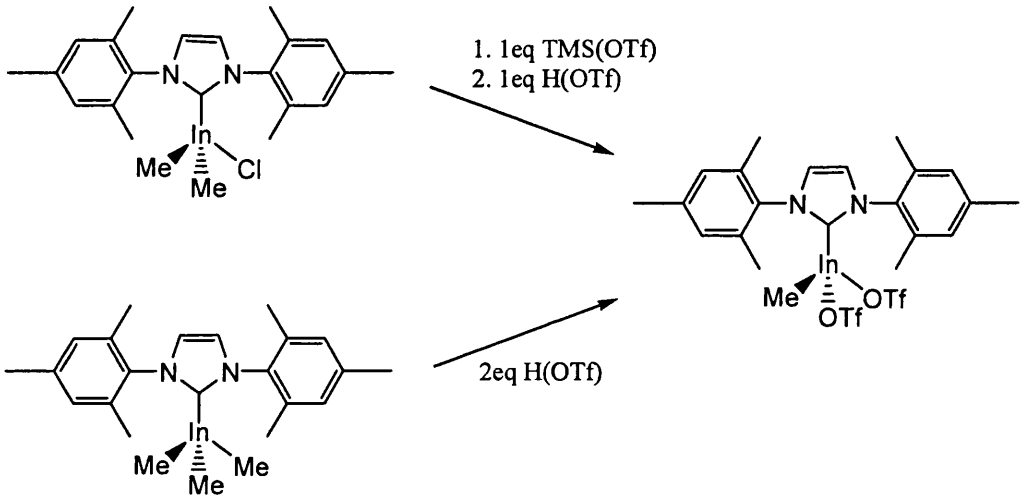

Figure 45 : The two routes to $Me(OTf)_2In(iMes)$

A CH_2Cl_2/hexane layer yielded crystals suitable for X-ray crystallography studies and the asymmetric unit of the solid state data is shown in Figure 46. A disordered molecule of co-crystallised solvent (dichloromethane) which is present in the lattice is not shown. Table 9 shows relevant bond lengths and angles for the complex. Complex **(14)** is dimeric in the solid state and no other close intermolecular contacts are observed. The indium is 5-coordinate and the geometry around the metal centre is a distorted trigonal-bipyramid. The oxygens of the triflate ligands that directly bind to the indium in the asymmetric unit [O(1) and O(4)] are in the apical positions and the O(1)-In-O(4) angle is 160.34(5)°. The metal methyl group, the $C_{carbene}$ and the oxygen of the third triflate from an adjacent molecule [O(3)] occupy the equatorial positions. The dimer is formed through two of the triflate ligands which form a In(1)-O-S-O-In(2)-O-S-O-In(1) 8-membered ring. Each of the triflates not involved in dimerisation has a shorter indium-oxygen bond length [In-O(4) = 2.2506(12)Å] than those that

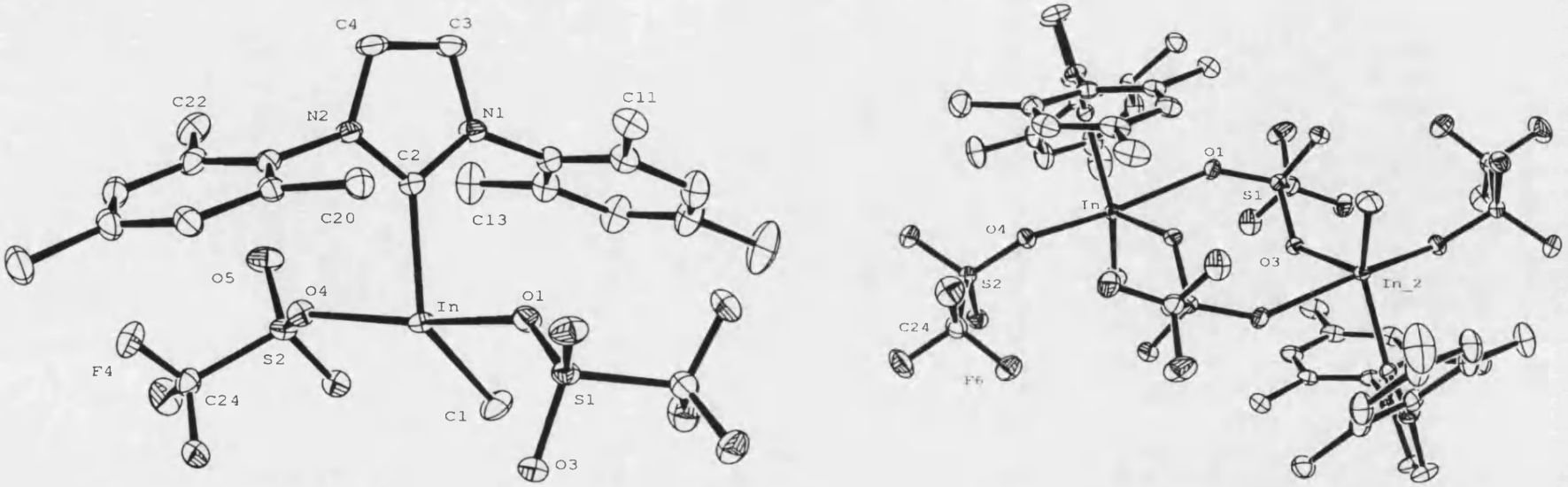

Figure 46 : Molecular structure of the asymmetric unit of $Me(OTf)_2In(iMes)$ and its dimer in the solid state (ellipsoids drawn at 30% probability level) hydrogen atoms are omitted for clarity

In-C(2)	2.1823(16)	N(2)-C(4)	1.383(2)	C(2)-In-C(1)	138.02(8)	N(1)-C(2)-N(2)	105.47(14)
In-C(1)	2.1153(19)	O(1)-S(1)	1.4464(12)	C(2)-In-O(1)	84.28(5)	C(2)-N(1)-C(3)	110.56(14)
In-O(1)	2.4292(12)	O(4)-S(2)	1.4710(13)	C(2)-In-O(4)	87.00(5)	In-O(4)-S(2)	133.10(8)
In-O(4)	2.2506(12)			In-C(2)-N(1)	122.44(11)	In-O(1)-S(1)	143.16(8)
N(1)-C(2)	1.349(2)			O(1)-In-O(4)	160.34(5)		
				O(1)-In-C(1)	92.35(7)		

Table 9 : Selected bond lengths (Å) and angles (°) for **(14)**

bridge the two indium centres to form the dimer [In-O(1) = 2.4292(12)Å]. The $C_{carbene}$-In-O(1) bond angle is compressed below 90° at 84.28(5)° while the $C_{carbene}$-In-O(2) angle is less compressed at 88.00(5)°.

The ^{1}H NMR spectrum of **(14)**, like **(13)**, shows 5 singlet resonances in CD_2Cl_2. Furthest downfield is the 2H integral olefin singlet at 7.39ppm. A singlet is observed for the four aromatic protons on the mesityl groups at 7.10ppm. The singlet for the meta-substituted methyl groups appears at 2.39ppm while the 12H integral singlet for the ortho-substituted methyls appears at 2.13ppm. The most upfield resonance is the metal bound methyl group which is observed as a 3H integral singlet resonance at -0.41ppm. The $^{13}C\{^{1}H\}$ NMR spectrum shows 10 carbon resonances. The $C_{carbene}$ peak is observed at 168.7ppm, this is the furthest upfield shift so far observed for the $C_{carbene}$ in any of the compounds. The metal bound methyl carbon appears at -5.0 [2.1ppm further downfield than the analogous resonance in the **(13)**] illustrating the increased Lewis acidity of the indium metal centre (see section 3.3.2). The carbon of the CF_3 groups, as in **(13)**, appears as a quartet at 119.3ppm due to the coupling to the three fluorine atoms [J = 318Hz]. The ^{19}F NMR spectrum shows one singlet resonance at -77.8ppm. In the solid state the molecule is a dimer with a centre of inversion. From the NMR spectra it cannot be ascertained if the complex is monomeric or dimeric in solution. Only one ^{19}F NMR environment exists suggesting that a fluxional process may be occurring on the NMR timescale because 2 different triflate environments occur in the solid state.

It was found from initial synthetic experiments that TMS(OTf) is an effective reagent for substitution of chlorides but not methyl groups, while H(OTf) conversely is

effective for substitution of methyls but not chlorides. Preliminary results also showed that use of fresh TMS(OTf) was crucial due to the fact that older TMS(OTf) becomes contaminated with moisture resulting in H(OTf) formation. Experiments with TMS(OTf) contaminated with trace amounts of water showed that reaction of 1 equivalent with **(7)** gave two compounds: **(13)** (via halide abstraction) and what is presumed to have been Me(Cl)(OTf)In(iMes) (via protonolysis) (Figure 47) which was observed in the ^{1}H NMR spectrum although it was not isolated. The resonances observed for the compound were a 2H integral singlet at 7.37ppm for the olefin protons, a 4H integral singlet at 7.10ppm from the aromatic protons, 6H and 12H integral singlets at 2.39ppm and 2.14ppm for the mesityl methyl groups and the 3H integral for the metal bound methyl at -0.49ppm.

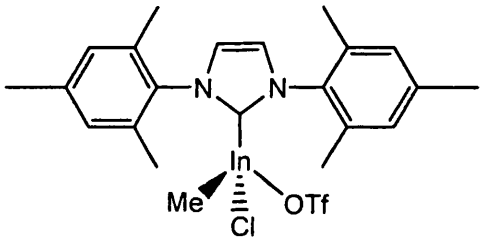

Figure 47 : Structure of Me(Cl)(OTf)In(iMes) formed *in situ*

3.2.9 Synthesis of $Me_2(NTf_2)In(iMes)$, (15)

Gas phase acidity measurements have shown trifluoromethanesulfonimde, $H(NTf_2)$ to be a stronger acid than H(OTf).[61] This means it should coordinate more weakly to the indium centre and increase the Lewis acidity of the metal centre, hopefully making an indium triflamide complex a better Lewis acid catalyst than its triflate analogue. Because triflation of the trismethyl complex **(11)** with one or two equivalents of H(OTf) resulted in a clean reaction generating the monotriflate complex, **(13)** and the bistriflate complex, **(14)** respectively, it was postulated that it should be possible to introduce triflamide ligands via the same method. Therefore $Me_3In(iMes)$, **(11)** was

reacted directly with a stoichiometric amount of the $H(NTf_2)$ in CH_2Cl_2 (Figure 48). Gas evolution was observed, and this was shown to be methane (0.20ppm) by following the reaction by ^1H NMR spectroscopy in CD_2Cl_2. The NMR data showed the reaction was complete in under 2 minutes. The solvent was removed in vacuo to yield a white solid. Recrystallisation in DCM/hexane at -20°C yielded a crop of clear and colourless crystals of complex **(15)**, $Me_2(NTf_2)In(iMes)$ suitable for X-ray diffraction (yield = 85%).

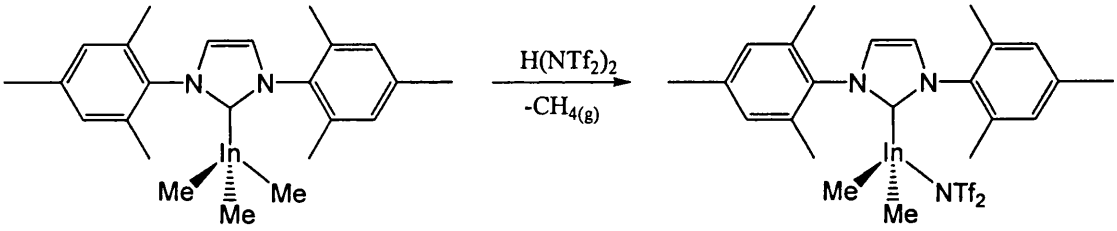

Figure 48 : Synthesis of $Me_2(NTf_2)In(iMes)$

The asymmetric unit of **(15)** is shown in Figure 49. Table 10 shows relevant bond lengths and angles. The solid state structure shows that the compound is a kinked one-dimensional coordination polymer where the indium metal centre is 5-coordinate, similarly to **(13)**. The arrangement of ligands around the metal centre gives the indium a trigonal-bipyramidal geometry. The oxygens of the triflamide ligands [O(1) and O(4) occupy the apical positions [O(1)-In-O(4) = 174.05(10)°] where the $C_{carbene}$-In-O(1) bond angle of 88.32(9)° and the $C_{carbene}$-In-O(4) bond angle of 91.34(11) show no significant distortion. The metal bound carbons of the methyl groups and the $C_{carbene}$ [C(1), C(2) and C(3) respectively] occupy the equatorial positions. The angle between the methyl groups [C(1)-In-C(2)] is 136.51(15)° while the $C_{carbene}$-In-C_{Me} angle for each of the methyl groups is ~112° [C(3)-In-C(1) = 111.85(13)°, C(3)-In-C(2) = 111.62(14)°]. The metal bound methyl groups are not in the plane of the 5-

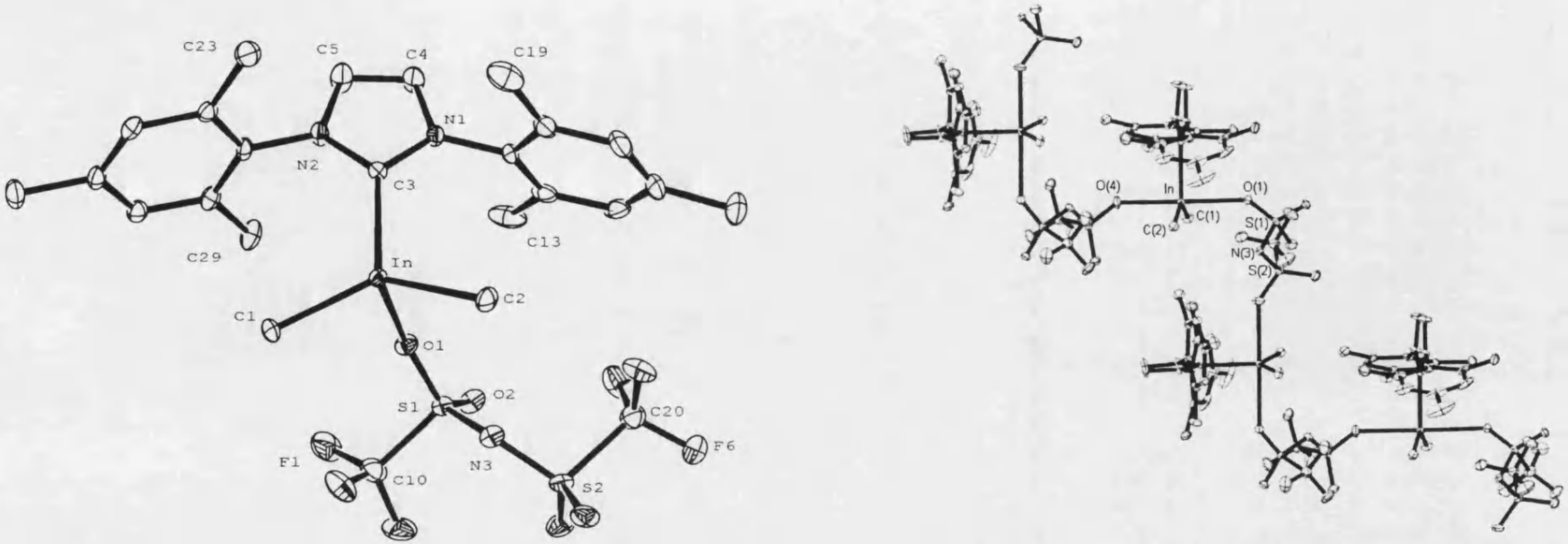

Figure 49 : Molecular structure of the asymmetric unit of $Me_2(NTf_2)In(iMes)$ and its one dimensional coordination polymer in the solid state (ellipsoids drawn at 30% probability level) hydrogen atoms are omitted for clarity

In-C(2)	2.134(3)	N(2)-C(3)	1.343(4)	C(3)-In-C(1)	111.85(13)	C(1)-In-O(1)	87.23(13)
In-C(1)	2.138(3)	N(2)-C(5)	1.386(5)	C(3)-In-C(2)	111.62(14)	N(1)-C(3)-N(2)	104.5(3)
In-C(3)	2.269(3)	S(1)-N(3)	1.569(3)	C(3)-In-O(1)	88.32(9)	N(1)-C(4)-C(5)	106.3(3)
In-O(1)	2.593(3)	S(2)-N(3)	1.575(3)	C(3)-In-O(4)	91.34(11)	S(1)-N(3)-S(2)	125.1(2)
In-O(4)	2.522(3)			C(1)-In-C(2)	136.51(15)	O(1)-S(1)-N(3)	107.98(17)
				O(1)-In-O(4)	174.05(10)	N(3)-S(2)-C(20)	104.22(19)
				C(1)-In-C(2)	136.51(15)		

Table 10 : Selected bond lengths (Å) and angles (°) for **(15)**

membered NHC ring which is rotated by 18° away from the C(2)-In-C(l) plane. This is probably a result of packing forces. The indium-oxygen bond lengths are not equidistant [In-O(1) = 2.593(3)Å, InO(4) = 2.522(3)] again this is probably a result of packing arrangement. Interestingly, although the nitrogen of the triflamide ligand is deprotonated, it does not bind to the metal through this nitrogen although formally it is now two coordinate. Instead it binds through one of its S=O oxygen atoms two bonds away from the nitrogen. This type of binding has been observed for other metal triflamides.[62,63] The N-S bonds lengths [S(1)-N(3) = 1.569(3)Å, S(2)-N(3) = 1.575(3)] lie between the average values reported for N-S single [1.604Å] and N=S double bonds [154.4Å].[64] This suggests a degree of delocalisation of the negative charge formally on the nitrogen.

The ^{1}H NMR spectrum for **(15)** shows 5 singlet resonances. Furthest upfield is the 2H integral olefin resonance at 7.30ppm, neighbouring this is the 4H integral aromatic proton resonance at 7.09ppm. The mesityl methyl substituents appear as a 6H integral singlet at 2.38 and a 12H integral singlet at 2.09ppm. Furthest upfield is the 6H integral singlet resonance attributed to the metal bound methyl groups at -0.72ppm. The $^{13}C\{^{1}H\}$ NMR spectrum, as expected, shows 10 resonances. The $C_{carbene}$ resonance is furthest downfield at 175.5ppm while the carbons of the methyl groups directly bound to the metal centre furthest upfield at -5.7ppm. The ^{19}F NMR spectrum shows one singlet resonance at -79.0ppm. This NMR spectroscopic data is similar to that of **(13)**. As expected because of the triflamide's weaker coordinating ability to the metal in comparison to the triflate, the $^{13}C\{^{1}H\}$ resonance for the metal bound methyl has been shifted further downfield by 1.4ppm in comparison to **(13)**, suggesting the enhanced Lewis acidity at the indium metal centre.

3.2.10 Synthesis of $Me(NTf_2)_2In(iMes)$, (16)

Complex **(11)** was reacted with 2 equivalents of $H(NTf_2)$ (Figure 50) causing rapid evolution of methane gas observed as a singlet resonance in CD_2Cl_2 at 0.20ppm in the ^1H NMR spectrum (the reaction was complete in less than two minutes). The solvent was removed in vacuo to yield a white solid. Recrystallisation in DCM/hexane at -20°C yielded a crop of clear and colourless crystals of complex **(16)**, suitable for X-ray crystallography studies (Yield 84%).

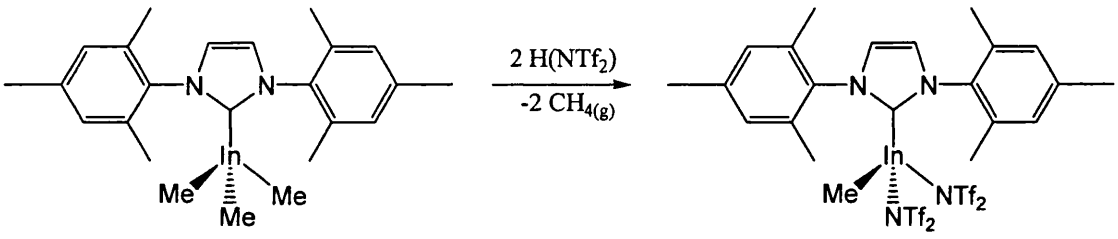

Figure 50 : Synthesis of $Me(NTf_2)_2In(iMes)$

The asymmetric unit of the solid state structure is shown in Figure 51, while Table 11 shows relevant bond lengths and angles. The molecule is monomeric in the solid state with no close intermolecular contacts. This is because the second equivalent of triflamide binds with the indium at two positions through its oxygens to make it 5-coordinate. For this reason no one dimensional coordination polymer or discrete dimer is observed in the solid state. This type of triflamide binding to metals at two positions through its oxygen atoms has been previously observed.[62,63] The 5-coordinate indium adopts a distorted trigonal bipyramidal arrangement where two of the oxygens on separate triflamide ligands [O(1) and O(5)] occupy the apical positions and the $C_{carbene}$, $C_{Me\text{-}In}$ and the remaining bound oxygen from the triflamide coordinated at two positions [C(1), C(2) and O(3)], occupy the equatorial positions.

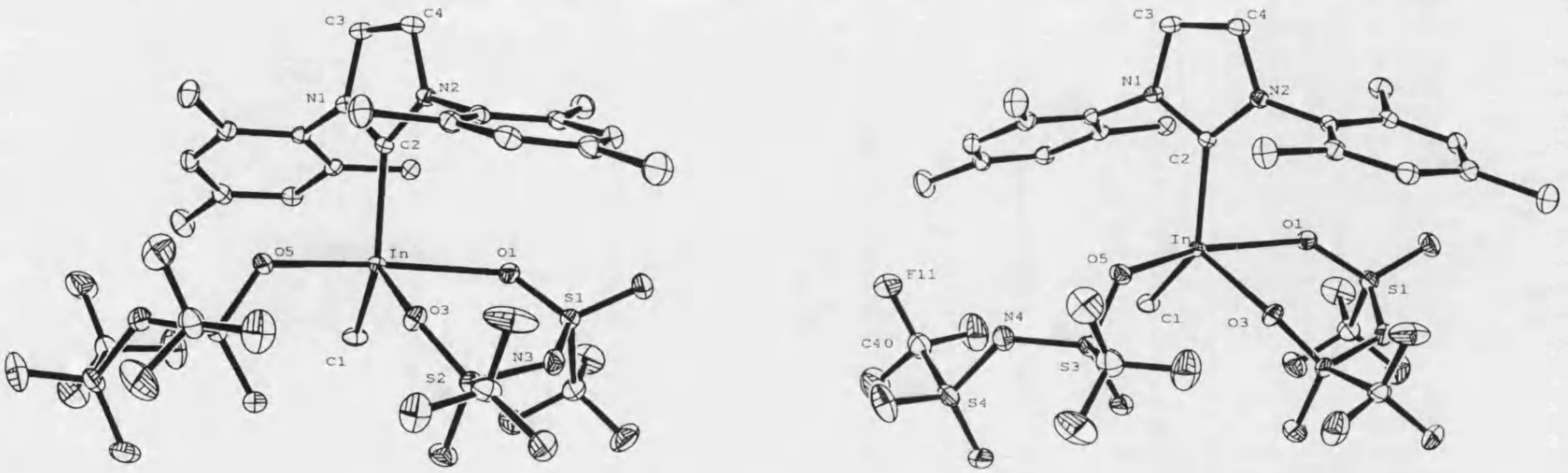

Figure 51 : Molecular structure of the asymmetric unit of $Me(NTf_2)_2In(iMes)$ from two different angles in the solid state (ellipsoids drawn at 30% probability level) hydrogen atoms are omitted for clarity

In-C(2)	2.170(2)	N(2)-C(2)	1.343(3)	C(2)-In-C(1)	138.55(9)	O(1)-In-O(3)	75.13(6)
In-C(1)	2.114(2)	N(2)-C(4)	1.383(3)	C(2)-In-O(1)	90.54(7)	N(1)-C(2)-N(2)	105.95(18)
In-O(1)	2.4152(16)	S(1)-N(3)	1.568(2)	C(2)-In-O(3)	107.08(7)	N(1)-C(3)-C(4)	106.15(19)
In-O(3)	2.2047(15)	S(2)-N(3)	1.559(2)	C(2)-In-O(5)	89.69(7)	S(1)-N(3)-S(2)	124.45(13)
In-O(5)	2.2957(15)			C(1)-In-O(3)	114.13(8)	In(1)-O(5)-S(3)	125.04(9)
				O(1)-In-O(5)	155.48(6)	S(3)-N(4)-S(4)	126.12(15)

Table 11 : Selected bond lengths (Å) and angles (°) for **(16)**

The ^{1}H NMR spectrum for **(16)** shows 5 singlet resonances, furthest upfield is the 2H integral olefin resonance at 7.53ppm and adjacent to it is the 4H integral aromatic proton resonance at 7.15ppm. The mesityl methyl substituents appear as a 6H integral singlet at 2.40 and a 12H integral singlet at 2.14ppm. Furthest upfield is the 3H integral singlet resonance attributed to the metal bound methyl groups at -0.04ppm. The $^{13}C\{^{1}H\}$ NMR spectrum as expected shows 10 resonances from the $C_{carbene}$ furthest downfield at 166.8ppm to the carbons of the methyl groups directly bound to the metal centre furthest upfield at -3.1ppm. The ^{19}F NMR spectrum shows one singlet resonance at -78.6ppm. Comparison of the $^{13}C\{^{1}H\}$ chemical shift of metal bound methyl resonance of **(16)** [-3.1ppm] with the corresponding resonances in **(14)** [-5.0ppm] and **(15)** [-5.7ppm] suggests that the Lewis acidity of the metal centre is highest in **(16)**, as expected.

Attempts to synthesise both the tris-triflate and tris-triflamide compounds were unsuccessful. Reactions of both **(11)** with 3 equivalents of the required acids resulted in only **(14)** and **(16)** in each case, while direct reaction of $In(OTf)_3$ and $In(NTf_2)_3$ with (iMes) was also unsuccessful.

3.3 Discussion

A range of indium(III) NHC complexes have been synthesised and structurally and spectroscopically chracterised. This section will involve in depth discussion of their solution and solid state structures.

3.3.1 Observation of the $C_{carbene}$ by $^{13}C\{^1H\}$ NMR Spectroscopy

The difficulty in observing the $C_{carbene}$ resonance in the $^{13}C\{^1H\}$ NMR spectrum for all previously reported indium carbene complexes has been documented [e.g. $Cl_3In(iMes)$].[1] This has been explained by the interaction of the $C_{carbene}$ with the quadrupolar indium nuclei (^{115}In, 95% I = $^9/_2$ and ^{113}In, 5% I = $^9/_2$) which broadens the resonance to such an extent it is not observed.[47,52,54,58] So why is it that the $C_{carbene}$ resonance in complexes **[(7)-(16)]** is clearly observed?

Perhaps this may be explained by first understanding the coupling mechanism through which quadrupolar broadening occurs. Spin-spin (T_2) relaxation is a through bond phenomenon and its timeframe is dependent on the molecular tumbling time of the molecules in solution.[65] The faster the T_2 relaxation, the broader the peaks appear in the spectrum. The nature of quadrupolar nuclei means any coupling of nuclei with spin I = $^1/_2$ to a nuclei with spin of I > $^1/_2$ results in faster relaxation, causing peak broadening. In the case of $Cl_3In(iMes)$, it is reported that this relaxation is so fast that the resonance of $C_{carbene}$ is so broad it is not observed.[1] As spin-spin coupling occurs through bonds, it is transmitted through the electron density between the bonded atoms. If the bond is ionic, a node in electron density exists between the two bonded atoms unlike in a covalent bond where no such node exists. This node stops the coupling and thus the peaks are not broadened. However if covalent character remains, but in a reduced capacity due to increased bond length, the coupling to the

quadrupolar nuclei is weaker thus peak broadening is reduced. Atoms in Molecules (AIM) calculations by G. D. Ruggerio at the University of Bath suggest that the In-$C_{carbene}$ bond in **(7)** is predominantly ionic (In^+ C^-) while examination of the peak broadening (Table 13) observed across the range of complexes **(7)-(16)** shows that the $C_{carbene}$ resonances in the $^{13}C\{^1H\}$ NMR spectrum do exhibit slight broadening. This is apparent when comparing one of the CH_3 resonances (C_{Me}) of the mesityl rings (a peak representative of the other resonances in the spectra where quadrupolar coupling does not occur).

	Peak width at ½ height (Hz)			**Bond Length (Å)**	
	$C_{In\text{-}Me}$	**$C_{carbene}$**	**C_{Me}**	**In-C_{Me}**	**In-$C_{carbene}$**
(11)	9.3	1.9	1.6	2.175(2)	2.312(1)
(8)	10.5	2.2	1.6	2.158(3)	2.273(3)
(7)	9.0	2.5	1.6	2.156(2)	2.267(2)
(15)	9.0	2.5	1.6	2.134(3)	2.269(3)
(16)	9.0	4.3	1.6	2.114(2)	2.170(2)

Table 12 : Peak width at ½ height correlated with bond length for complexes **(7)**, **(8)**, **(11)**, **(15)** and **(16)**

Table 12 shows that there is a clear correlation between the shortening of the In-$C_{carbene}$ bond length and the increased broadening of the $C_{carbene}$ resonance in the $^{13}C\{^1H\}$ NMR spectra. Cl_3In-(iMes), however has a bond length of 2.200(7)Å which falls between those of compounds **(7)** and **(16)**, and thus in this argument its $C_{carbene}$ resonance should appear broadened with a peak width at ½ height lying between 2.5 and 4.3Hz. This is not the case suggesting another process must be responsible for it being unobserveable in its $^{13}C\{^1H\}$ NMR spectrum. This could be caused by an exchange process on the NMR timescale and is discussed later. Table 12 also shows

that the $C_{In\text{-}Me}$ resonances exhibit extensive broadening and this can probably be attributed to the reduced length of the In-C_{Me} bonds in comparison to the In-$C_{carbene}$ bonds [~O.12Å shorter] which suggests that they have increased covalent character.

3.3.2 Measuring the Lewis Acidity at the Metal Centre

The ^{1}H and $^{13}C\{^{1}H\}$ NMR spectroscopic and solid state data give a measure of the comparable Lewis acidity of the complexes. Table 13 shows the correlation of reduced $C_{carbene}$-In and $C_{In\text{-}Me}$ bond lengths with increased downfield shift of the metal bound methyl groups in both the ^{1}H and $^{13}C\{^{1}H\}$ NMR spectra. This can be readily explained by considering the stabilisation of the indium metal centre. In **(11)**, three methyl groups are bound to the metal centre. The inductive effect pushes electron density from the methyls toward the metal, stabilising the indium and as a result it froms a weaker bond to the carbene. In fact out of all our complexes, it is **(11)** which has the furthest downfield $C_{carbene}$ resonance and the furthest upfield indium methyl resonance in the $^{13}C\{^{1}H\}$ and ^{1}H NMR spectra.

	Chemical Shift (ppm)			**Bond Length (Å)**	
	^{1}H $C_{In\text{-}Me}$	$^{13}C\{^{1}H\}$ $C_{In\text{-}Me}$	$^{13}C\{^{1}H\}$ $C_{carbene}$	**In-C_{Me}**	**In-$C_{carbene}$**
(11)	-1.26	-11.8	183.0	2.175(2)	2.312(1)
(7)	-1.03	-8.1	177.5	2.156(2)	2.267(2)
(13)	-0.83	-7.1	176.2	2.141(2)	2.264(2)
(15)	-0.72	-5.7	175.5	2.134(3)	2.269(3)
(14)	-0.41	-5.0	168.7	2.115(2)	2.183(2)
(16)	-0.04	-3.1	166.8	2.114(2)	2.170(2)

Table 13 : ^{1}H and $^{13}C\{^{1}H\}$ NMR spectroscopic data of $C_{In\text{-}Me}$ and $C_{carbene}$ and In-$C_{carbene}$ and In-C_{Me} bond lengths of several complexes

Replacement of a methyl with an electronegative chloride as in **(7)** means the chloride draws some electron density away from the metal. To compensate for this loss of electron density, the indium draws more from the remaining methyl groups and also pulls the $C_{carbene}$ closer toward itself. The result is shorter bond lengths, a downfield shift in the proton and carbon resonances of the metal bound methyls and an upfield shift in the $C_{carbene}$ resonance. As more weakly coordinating anions are used to replace the methyl and chloride groups, the trend of reduced bond lengths, downfield shift of methyl resonances and upfield shift of the $C_{carbene}$ resonances continues. As expected it is the bistriflamide complex, **(16)** which shows the shortest In-Me and In-$C_{carbene}$ bonds, the furthest downfield shift of the metal methyl and the furthest upfield shift of the $C_{carbene}$ resonance of all the complexes.

Metal-$C_{carbene}$ bond length and $C_{carbene}$ chemical shift has been previously documented to give a good measure of the covalency of the metal-$C_{carbene}$ bond.[66] Studies with adducts of NHCs with group 2 metals have shown that the heavier the metal in a group, the weaker the metal-$C_{carbene}$ interaction and the more ionic its nature. The solid state data showed that the trend down the group is an increase in the length of the metal-$C_{carbene}$ bond coupled with a decrease in the N-C-N angle in the NHC ring toward the angle observed for the free carbene. $^{13}C\{^1H\}$ NMR spectroscopy meanwhile showed that down the group the resonance for the $C_{carbene}$ shifts downfield approaching the value observed for free carbene.

In the same manner, the data in Table 13 suggests an increase in covalency can be observed by a reduction in the metal-$C_{carbene}$ bond length. This is supported by the

$C_{carbene}$ resonance upfield chemical shift away from the corresponding resonance in (iMes) (216.0ppm in d^8-toluene).

Comparing the N-C-N bond angle in the 5-membered ring of the complexes also gives a measure of the change in ionic/covalent nature of the $C_{carbene}$-In bond.

more covalent

Complex	N-C-N bond angle (°)
(11)	103.65(16)
(7)	104.64(17)
(13)	104.15(18)
(15)	104.5(30)
(14)	105.47(14)
(16)	105.95(18)

Table 14 : Comparison of N-C-N bond angles in complexes **(7)**, **(8)**, **(11)**, **(15)** and **(16)**

Table 14 shows that the N-C-N bond angles of the complexes falls between the normal value for free imidazole-2-ylidenes [~102°] and imidazolium cations [~108°].[49] However **(11)** behaves more like the ionic system depicted in Figure 52 and **(16)** behaves more like the covalent system.

Indium-$C_{carbene}$ bonding: Ionic Covalent

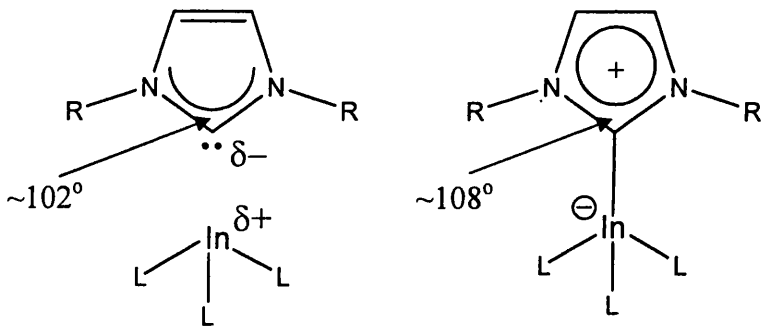

Carbene behaviour: More like free carbene More like imidazolium salt

Figure 52 : Ionic and covalent bonding in indium carbenes

In fact this change in bonding behaviour is also supported by the weak trend in N-C_{olefin} bond length and the strong trend in the resonance of the olefinic protons in the ^1H NMR spectra.

more covalent

Complex	N-C_{olefin} bond length (Å)	^1H NMR H_{olefin} chemical shift
(11)	1.391(2)	7.12
(7)	1.389(3)	7.19
(13)	1.385(3)	7.28
(15)	1.386(5)	7.30
(14)	1.383(2)	7.39
(16)	1.383(3)	7.53

Table 15 : Comparison of N-C_{olefin} bond lengths and the ^1H NMR olefinic chemical shift in complexes **(7)**, **(8)**, **(11)**, **(15)** and **(16)**

As Table 15 shows there is a slight statistical decrease in N-C bond length as In-$C_{carbene}$ covalency increases down the table. This is admittedly a weak trend, but the ^1H NMR spectra of these compounds show a strong trend in downfield chemical shift of the olefin resonance. This agrees with the enhanced delocalisation observed in the 5-membered ring for the imidazolium cation over that of the free carbene (Figure 52).[49] As the covalency in the In-$C_{carbene}$ bond increases, so does the delocalisation in the ring. This delocalisation results in shorter N-C_{olefin} bonds and further deshielding of the olefin backbone as the ring donates more electon density to the $C_{carbene}$ atom as its bond with the metal becomes shorter.

Combining the trends in solid and solution state techniques reported in this section convincingly shows that an increase in Lewis acidity at the metal causes an increase in covalency of the In-$C_{carbene}$ bond and the delocalisation in the NHC ring both of which can be readily observed structurally and spectroscopically.

3.3.3 Solution Equilibria Suggesting Bis-Adduct Formation

Although Jones and co-workers report several bis carbene indium halide adducts,[47] none are reported for the carbenes (iMes) or (iPr). When efforts were made to introduce a second molecule of (iMes) to complex **(7)** some interesting results were observed.

While the reaction of **(7)** with (iMes)Cl showed no reaction after 48 hours, reaction of **(7)** with (iMes) results in an equilibrium in solution. Both the ^{1}H and $^{13}C\{^{1}H\}$ NMR spectra of the reaction mixture in C_6D_6 shows only one set of NHC peaks which were not free carbene or **(7)**. This was the case even when more than one equivalent of extra (iMes) was added.

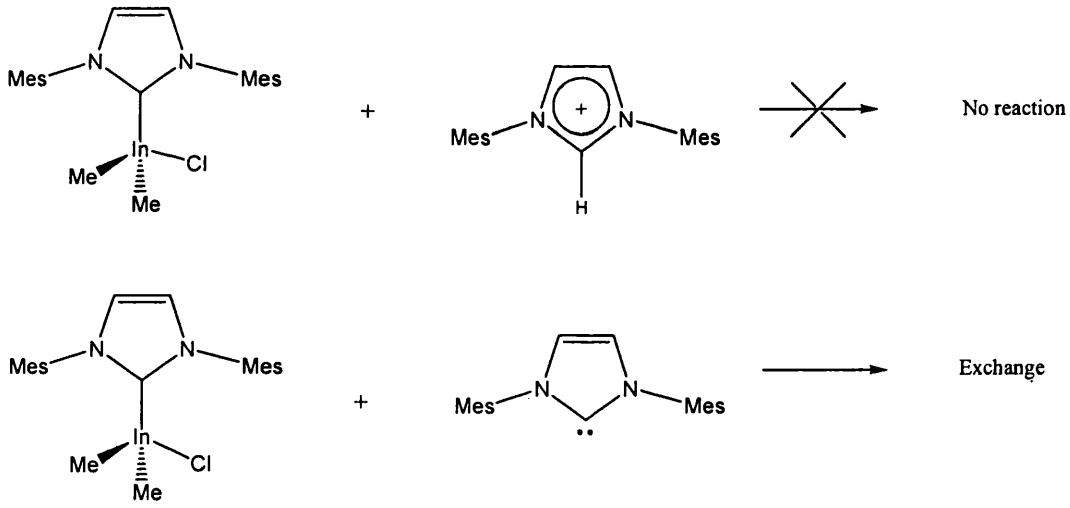

Figure 53 : Reaction of **(7)** with (iMes)Cl and (iMes)

A ^{1}H NMR spectrum of a 1 : 1.5 mixture of **(7)** : (iMes) shows the resonance for the olefin protons at 6.38ppm while in **(7)** it appears at 6.05ppm and for (iMes) at 6.49ppm. Thus the peak lies between the resonances in the two starting materials and is time-averaged. It lies closer to the resonance of (iMes) because 1.5 equivalents of (iMes) are present in the reaction. The singlet observed for the metal methyls remains

unaffected by the exchange process at -0.54ppm, the same shift observed for them in **(7)**. The corresponding ^{1}H NMR spectra are shown in Figure 54. Importantly in the $^{13}C\{^{1}H\}$ NMR spectrum no $C_{carbene}$ resonance for **(7)** or free (iMes) is observed.

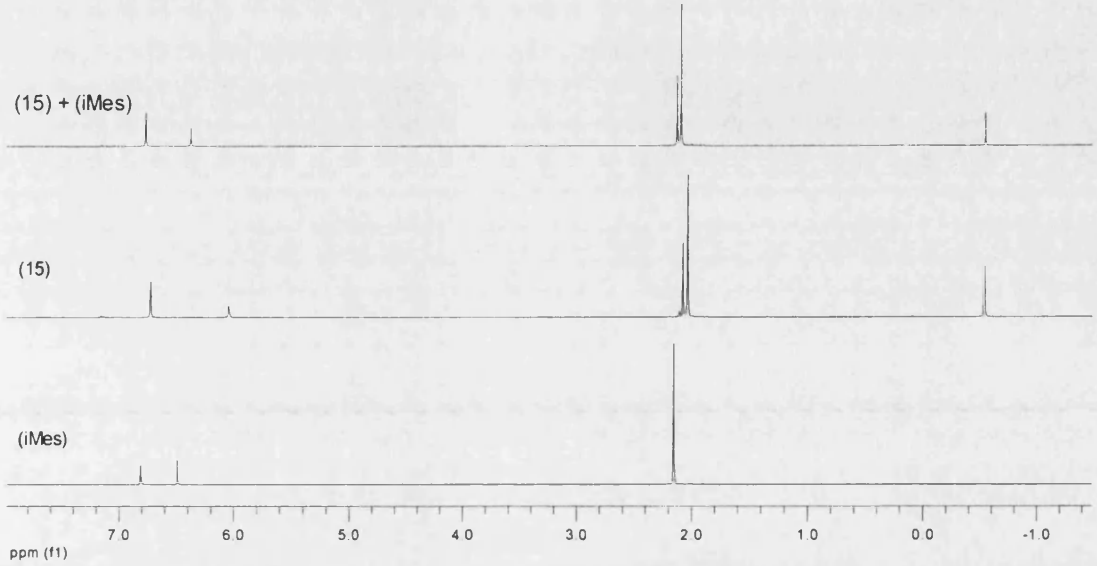

Figure 54 : ^{1}H NMR spectra of the mixture of complex **(7)** and (iMes), complex **(7)**, and (iMes)

The NMR spectra suggest a fluxional process is occurring (Figure 55). This equilibrium is faster than the NMR timescale and this is why only time-averaged peaks are observed in both the ^{1}H and $^{13}C\{^{1}H\}$ NMR spectra.

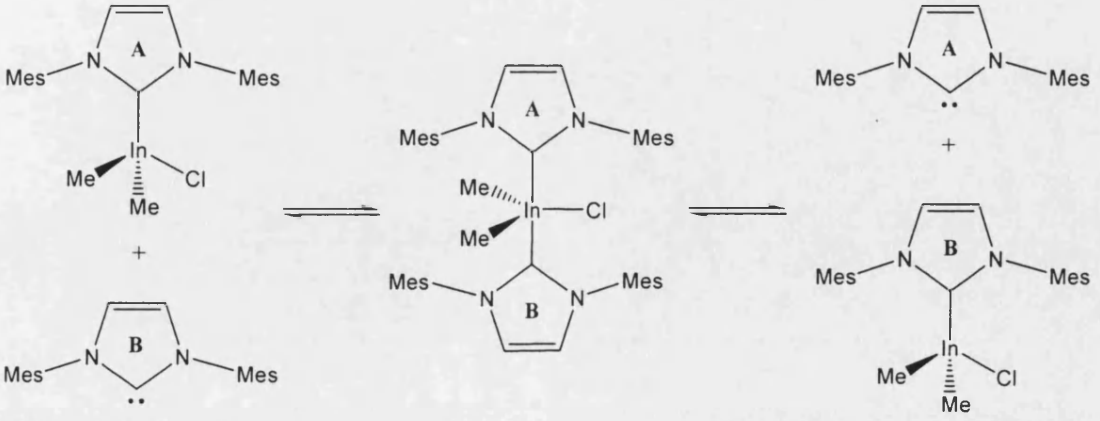

Figure 55 : Equilibium process between **(7)** and (iMes)

A 1:1 mixture of **(7)** : (iMes) dissolved in d_8-toluene was studied at lower temperatures by NMR spectroscopy. At -80°C, **(7)** and free (iMes) are observed in the ^1H NMR spectrum while the $^{13}C\{^1H\}$ NMR spectrum exhibited both the $C_{carbene}$ for (iMes) at 216.0ppm and the $C_{carbene}$ of **(7)** at 175.2ppm. Because only **(7)** and (iMes) were observed by NMR spectroscopy at -80°C, we can be confident that bis-adduct formation, if it occurs, is short-lived. Analogous exchange processes are suggested to occur for **(11)** and **(12)**. It is likely that it is this process that causes the $C_{carbene}$ resonance of Cl_3In(iMes) to be substantially broadened as to make it unobserveable. When the reaction of Cl_3In(iMes) and free (iMes) in a C_6D_6-THF mixture (due to solubility issues) was carried out, a crystalline material crashed out in the NMR tube which was not analyzed but could potentially be the bis adduct. This would agree with documented bis-adduct formation.[54]

Further crossover experiments were carried out to determine how readily the carbene comes away from the indium metal centre in solution. Combination of a 1:1 ratio of compounds **(7)** and **(12)** demonstrated formation of a statistical mixture of 4 complexes. The reaction scheme is shown in Figure 56, while the $C_{carbene}$ region of the $^{13}C\{^1H\}$ NMR spectrum showing the 4 different $C_{carbene}$ peaks attributed to the 4 products is displayed in Figure 57.

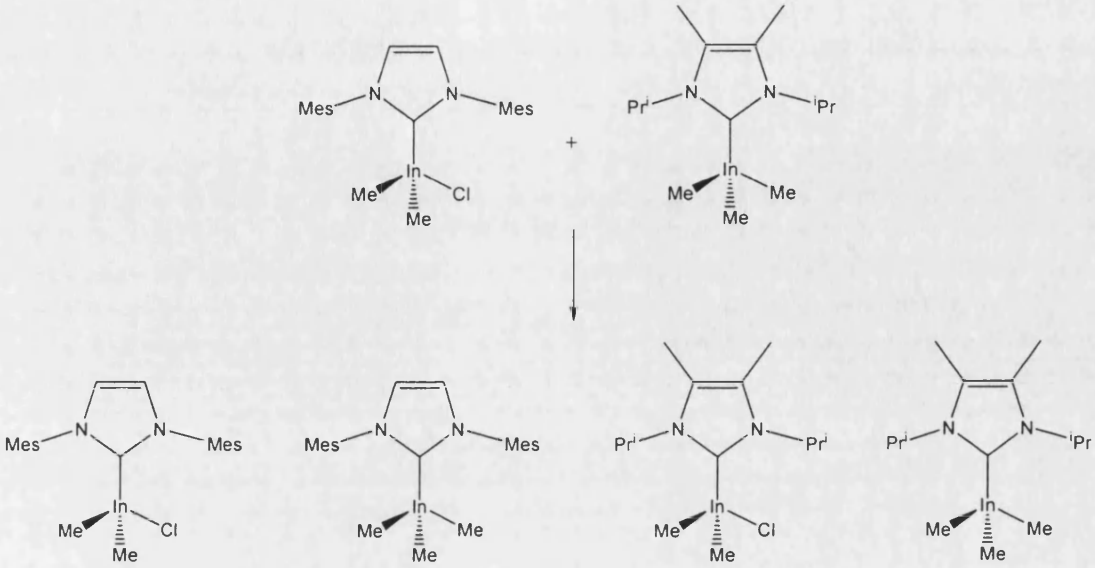

(7) **(11)** **(*)** **(12)**

Figure 56 : Reaction of compounds **(7)** and **(12)**

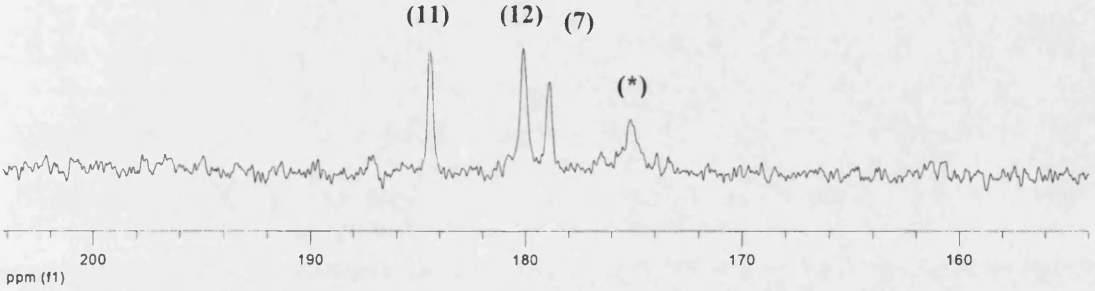

Figure 57 : $^{13}C\{^1H\}$ NMR spectrum showing the 4 $C_{carbene}$ resonances of the 4 compounds

These four compounds present in the mixture (Figure 53) have been reported elsewhere in this chapter where their $C_{carbene}$ resonances are: **(7)** [179.0ppm], **(11)** [184.8ppm] and **(12)** [180.1], while it follows that the fourth compound observed is $Me_2ClIn(CN(^iPr)C_2Me_2{}^iPr)$ (*) and as expected its $C_{carbene}$ resonance appears slightly downfield of **(12)** at 175.1ppm due to the introduction of the electronegative chlorine. This compound was not isolated. This data indicates that the In-$C_{carbene}$ bond is labile on the "chemical" timescale but that exchange is much slower than the NMR

timescale as only 2 $C_{carbene}$ peaks would be observed if the exchange was much faster and possibly none if the exchange occurred on the NMR timescale.

3.3.4 Does a $C_{carbene}$•••Cl interaction exist?

In the solid state, compounds **(7)**, **(8)** and **(10)** show a distorted pseudo-tetrahedral geometry around the 4-coordinate metal centre with compressed $C_{carbene}$-In-Cl bond angles.

Compound	$C_{carbene}$-In-Cl angle (°)
(7)	91.45(5)
(8)	96.73(7)
(10)	90.33(4)

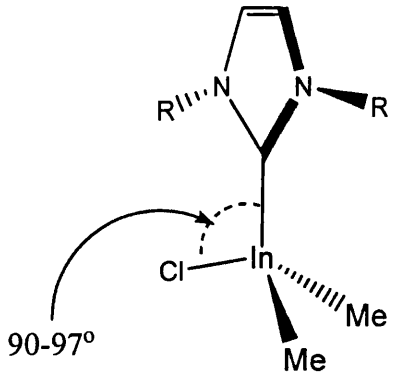

Table 16 : Compressed $C_{carbene}$-In-Cl bond lengths of **(7)**, **(8)** and **(10)**

Two recent papers have also reported a compressed angle $C_{carbene}$-M-Cl for 5-coordinate transition metal bis chloride carbene complexes. It is proposed that the compressed angle is caused by an intramolecular $C_{carbene}$•••Cl interaction.[57,67] For each of these compounds, DFT calculations have shown the geometry distortion around the metal is not caused by crystals packing effects.

In one of these complexes, a 5-coordinate titanium carbene complex,[57] the geometry is distorted from a trigonal bipyramidal arrangement. The angular distortion (away from 90°) observed for the two chlorides in the complex is 6.7°. For this titanium complex, which is discussed in the chapter introduction (Figure 24),[57] it is reported DFT calculations show there is an interaction between the formally vacant $C_{carbene}$

(2p) orbital on the carbene ligand and the chloride by overlap between the chloride lone pairs and the carbenic 2p orbital (Figure 58).

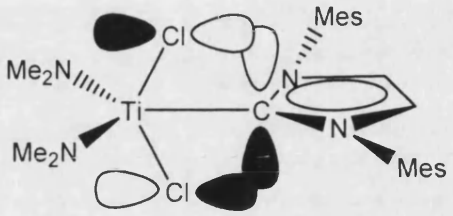

Figure 58 : Proposed orbital $C_{carbene}$•••Cl overlap in $Cl_2(Me_2N)_2Ti(iMes)$

It seems apposite to consider that the reason Arduengo-type carbenes have such stability is due to the substituents in the vicinal positions, having σ-acceptor π-donor character.[6,7] The electron-donating amino- substituents donate electron density back into the $C_{carbene}$ 2p orbital and it is for this reason amino carbenes are such poor π-acceptors because their 2p orbital is effectively already full. ^{53}Cr-NMR spectroscopy of $[LCr(CO)_5]$ complexes where L = NHC have been used to demonstrate their lack of π-acceptor ability.[68] Therefore although the titanium complex is slightly distorted from an ideal trigonal bipyramidal geometry,[57] to suggest DFT calculations for a Ti-NHC that shows only a small distortion in the solid state structure prove a $C_{carbene}$•••Cl interaction exists is contentious.

On the proviso that orbital overlap and ensuing $C_{carbene}$•••Cl interaction observed in the titanium complex was the cause of the observed distortion, the solid state structure of **(7)** was examined. The first suggestion that a $C_{carbene}$•••Cl interaction may exist in the solid state is that of distorted tetrahedral environment where the $C_{carbene}$-In-Cl bond [91.45(5)°] is compressed well below the tetrahedral angle by 18° (a significant increase in the distortion over that observed for the titanium compound). This finding

is supported by the associated $C_{carbene}$•••Cl distance of 3.40Å which lies inside the sum of the van der Waals radii of carbon and chlorine [3.60Å][69] and by the angle at which the carbene sits, canted towards the chlorine by 12.8°. To rule out the distortion of the geometry being simply a packing effect or the approach of another molecule to form a dative In-Cl bond, DFT calculations were carried out. The DFT calculations at the B3lYP/LAN2DZ level of theory did indeed give good agreement with the observed structure for **(7)** (Figure 59, Table 17) demonstrating that packing effects are not responsible for the distortion. The solid state data also shows that no close intermolecular contacts to the indium within 4.1Å are present.

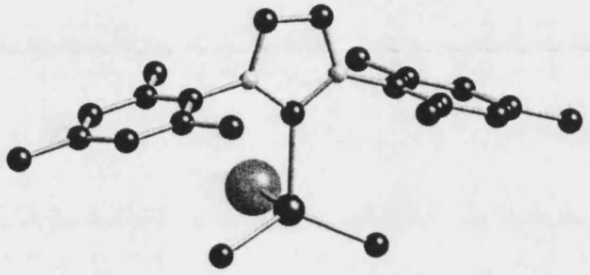

Figure 59 : DFT (B3LYP/LAN2DZ) optimised structure of **(7)**.

	Selected Bond Lengths and Angles	
	Crystal structure	DFT Calculated structure
C(1)-In(1)-Cl(1)	91.45(5)°	93.82°
In(1)-Cl(1)	2.481(1)Å	2.516Å
In(1)-C(1)	2.267(2)Å	2.306Å
C(1)•••Cl(1)	3.403Å	3.525Å

Table 17: Comparison of some crystal structure and DFT calculated bond lengths and angles in **(7)**

If an orbital overlap of the $C_{carbene}$ 2p orbital and a lone pair of the chloride is occurring in similar way to that proposed for the titanium complex then it would occur as shown in Figure 60.

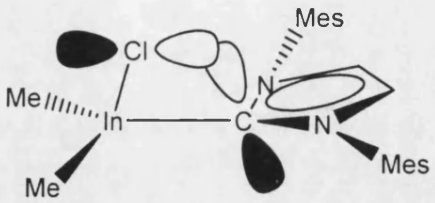

Figure 60 : Proposed $C_{carbene}$•••Cl orbital overlap in **(7)**

If this overlap occurs, one might expect the geometry at the $C_{carbene}$ to alter from an sp^2 geometry toward an sp^3 tetrahedral geometry as the interaction although not a formal bond makes the $C_{carbene}$ move towards 4-coordinate. However the 5-membered ring is canted 12.8° *toward* the chloride instead of away from it as would be expected moving to sp^3. Another consideration is that donation of electron density into the 2p $C_{carbene}$ non-bonding orbital should also increase the $C_{carbene}$-N bond lengths in the 5-membered ring. $H_3In(iMes)$ is used as a comparison because it does not have any chlorides and thus no "interactions" are expected. The 5-membered ring bond lengths and angles if $H_3In(iMes)$ and **(7)** are compared in Table 18.

	Bond lengths (Å) and Bond angles(°)		
	(7)	$H_3In(iMes)$	
In(1)-C(1)	2.267(2)	2.253(5)	
C(1)-N(1)	1.352(3)	1.353(6)	
N(1)-C(2)	1.387(3)	1.390(6)	
N(1)-C(1)-N(2)	104.64(17)	104.5(4)	
C(1)-N(1)-C(2)	111.10(19)	110.9(4)	

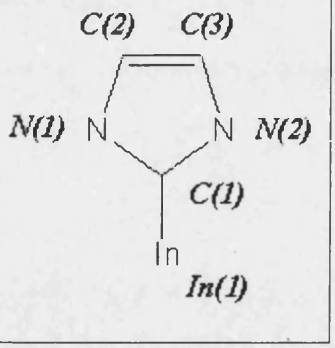

Table 18 : Comparison of relevant bond lengths in **(7)** and $H_3In(iMes)$[1]

The selected bond lengths of the two compounds are the same within errors which suggests the Cl•••$C_{carbene}$ interaction in **(7)** is extremely weak or that it does not occur.

This distortion of the 4-coordinate geometry seen in (7) about the indium centre is not observed in $Cl_3In(iMes)$ but is observed in the closely related dihydride $H_2ClIn(iMes)$ although not to the same extent [$C_{carbene}$-In-Cl = 101.7°] (Figure 61) and in this case no intramolecular interaction is commented on.[1] Although $H_2ClIn(iMes)$ does show a compressed $C_{carbene}$-In-Cl angle it has a different geometry at the indium centre than that observed in (7).

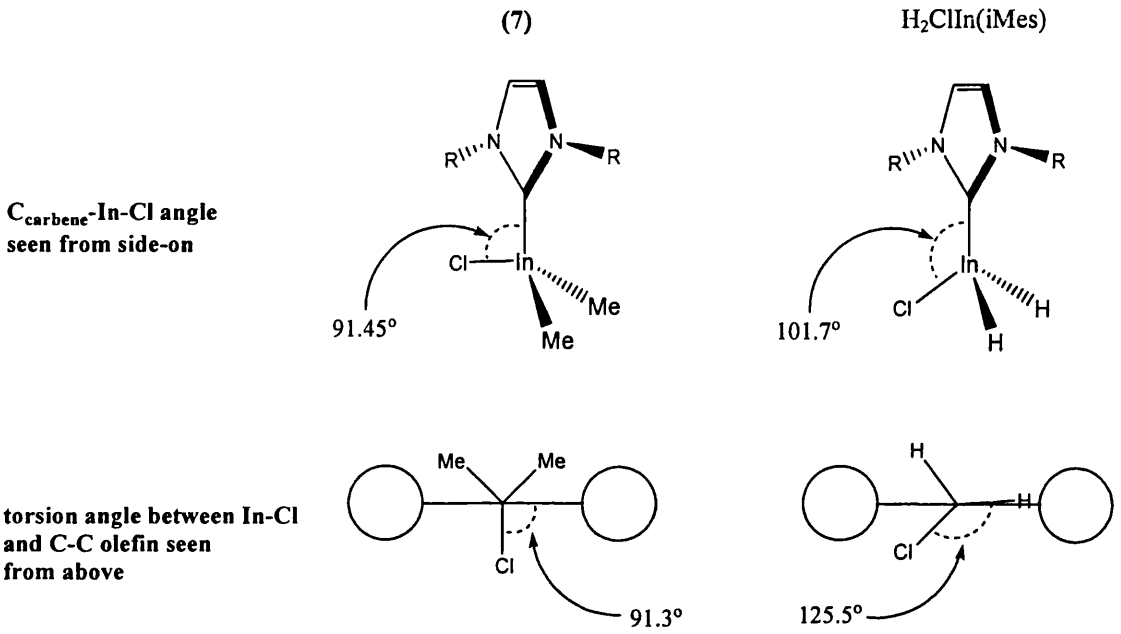

Figure 61 : Compounds (7) and $H_2ClIn(iMes)$ viewed from side on and above concentrating on the $C_{carbene}$-In-Cl angle and the torsion angle between the In-Cl and C-C olefin bonds (from above atoms and bonds are omitted for clarity, the mesityl rings are depicted as circles)

Figure 61 shows that the chloride in $H_2ClIn(iMes)$ does not line up perpendicular to the C-C olefin bond - the position it would be expected to adopt to maximize orbital overlap of a chloride lone pair and the $C_{carbene}$ 2p orbital. The $C_{carbene}$•••Cl distance [3.567Å] does however still lie within the sum of the van der Waals radii of carbon and chlorine [3.60Å].[69] This suggests that an interaction may possibly still exist but supports the argument that it must be extremely weak as the $C_{carbene}$-In bond is not orientated to maximise orbital overlap and yet the arrangement observed is by definition energetically favourable.

The $C_{carbene}$-In-Cl angles in Cl_3In(iMes) are 108.7(2), 112.09(15) and 111.45(15)Å,[1] showing that the geometry around the indium is essentially tetrahedral (ideal tetrahedral angle = 109.3°). This could be because the three chlorides are competing with one another for a close interaction with the $C_{carbene}$ 2p orbital. It is the chloride perpendicular to the C-C olefin bond of the 5-membered NHC ring which shows the slightly compressed angle [108.7(2)].

The weakness of any $C_{carbene}$•••Cl interaction is further demonstrated by the solution behaviour of **(8)**. ^{1}H NMR spectroscopy shows that free rotation around the $C_{carbene}$-In bond in **(8)** occurs rapidly on the NMR timescale even at -70°C. If this interaction was in anyway significant, free rotation around the $C_{carbene}$-In bond would not be expected.

These arguments suggest that the existence of a C•••Cl intramolecular interaction is by no means certain. If this interaction does exist, it is certainly only a weak one. DFT calculations have shown however that the geometrical distortion in **(7)** is definitely not caused by crystal packing effects but it seems unlikely that C•••Cl interactions, if they do exist, are alone responsible.

3.3.5 Are H•••Cl intramolecular interactions responsible?

For this reason, we decided to determine if hydrogen bonding might play some part in the geometrical distortion. A study of the solid state structure of **(7)** after refinement of the hydrogen positions suggest that H•••Cl intramolecular interactions may be present.

The cut-off point for the length of a C-H•••Cl-M hydrogen bond (where M = metal) is a matter of some debate. It was recently reported that the conceptual van der Waals

cut-off criterion can not reliably be applied to establish the presence of weak inter- and intramolecular H•••Cl hydrogen bonding interactions and is perhaps better suited to being analysed by a distance/angle criterion technique.[70] Another recent in depth study of hydrogen bonding of compounds in the Cambridge Structural Database (CSD) reports that a reasonable H•••Cl cut-off distance for C-H•••Cl-M hydrogen bonding interactions is 2.987Å. Accepting any H•••Cl intramolecular distance outside this range of being too long to be an interaction, then the H•••Cl distances observed in **(7)** suggest that hydrogen bonding may be a factor in the observed molecular distortion.

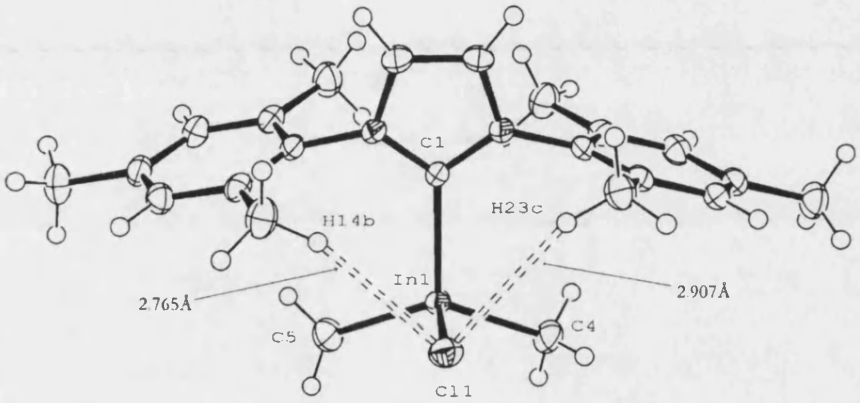

Figure 62 : Asymmetric unit of **(7)** showing the intramolecular H•••Cl hydrogen bonds

The distances between the only two hydrogens significantly close to the chloride [H(14b)•••Cl(1) = 2.765Å, H(23c)•••Cl(1) = 2.907Å] lie inside the aforementioned cut-off point and suggest that there are two intramolecular hydrogen bonding interactions. This suggests that the two C-H•••Cl-M may play an important part in causing the distorted geometry.

The fact that intramolecular hydrogen bonding may be occurring in **(7)** shows that the combination of the distorted geometry around the indium centre and the canting of the

carbene toward the chloride may in fact be caused by H•••Cl hydrogen bonding interactions.

Examination of the crystal structure of $(NMe_2)_2Cl_2Ti(iMes)$ suggests that, although the hydrogens have not been freely refined, there is a distinct possibility that H•••Cl intramolecular hydrogen bonds exist. The two shortest H•••Cl distances to each chloride in the structure are shown in Table 19 and Figure 63.

Cl•••H	Distance (Å)
Cl(1)•••H(12)	2.661
Cl(1)•••H(17)	2.876
Cl(2)•••H(23)	2.674
Cl(2)•••H(6)	2.985

Table 19 : Close Cl•••H intramolecular contacts in $(NMe_2)_2Cl_2Ti(iMes)$

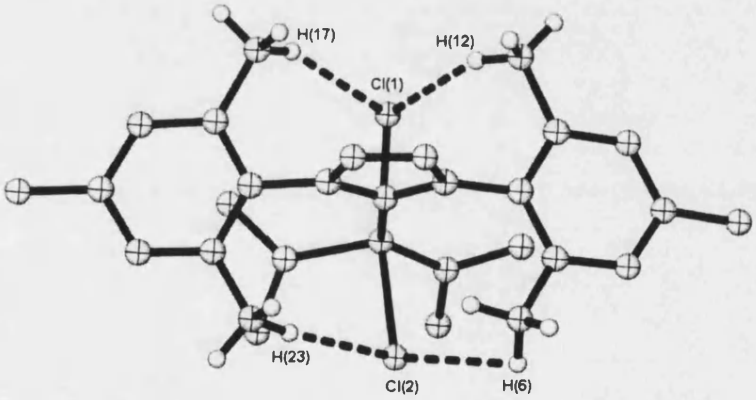

Figure 63 : Close Cl•••H intramolecular contacts in $(NMe_2)_2Cl_2Ti(iMes)$

Compounds **(8)-(10)** also show significantly compressed bond angles from the tetrahedral angle (Table 20). However the hydrogens of these compounds have not been freely refined so it is difficult to say with certainty that hydrogen bonding is occurring unlike in complex **(7)** where the hydrogen positions are known. The two

closest H•••Cl intramolecular distances of complexes **(8)-(10)** are shown in Table 20 with those of **(7)** as a means of comparison.

	H•••Cl distances (Å)		$C_{carbene}$•••X distances (Å)	$C_{carbene}$-In-X angle (°)
(7)	2.765	2.907	3.403	91.45(5)
(8)	3.113	2.975	3.497	96.73(7)
(9)	2.917	3.226	3.625	95.48(4)
(10)	2.732	3.455	3.383	90.33(4)

Table 20 : Close H•••Cl distances and $C_{carbene}$•••Cl distances and $C_{carbene}$-In-X angles in complexes **(7)-(10)** (where X = Br, Cl)

The data shows the general trend that the shorter the H•••Cl distances, the shorter the $C_{carbene}$•••Cl distances, but if one of these is the dominant force in the geometrical distortion how can it be determined? Interestingly it is **(10)** which shows the single shortest H•••Cl distance and $C_{carbene}$•••Cl distance. This is a result of the saturated back bone of the 5-membered ring which due to the two carbons in the backbone being sp^3 hybridised is not planar (see section 3.2.1.4). Because of this different geometry compared to compounds **(7)-(9)**, one side of the saturated backbone is canted further toward the chloride by 8.5° i.e. the C(5)•••Cl distance is 3.443Å and the C(4)•••Cl distance is 3.674Å, this is a difference of 0.23Å. It is the side of the molecule canted further toward the chloride that possesses the shorter H•••Cl contact [2.732Å] to the detriment of the other H•••Cl contact which is so long [3.455Å] it can be ignored. Compound **(10)** has the shortest $C_{carbene}$•••Cl distance and it could be argued that due to the lack of delocalisation in the 5-membered ring in ($iMesH_2$) that less electron density is donated to the 2p orbital of the $C_{carbene}$ by the amino-substituents so it takes more from the lone pairs on the chloride by having a better orbital overlap. It can also be argued that the H•••Cl contact and the $C_{carbene}$•••Cl

distance are shorter only because the sp^3 hybridisation of the carbene backbone forces the ring further towards the chloride. $Cl_3In(iMes)$ and $H_2ClIn(iMes)$ meanwhile, although their hydrogen are not freely refined show no close intramolecular H•••Cl contacts within 2.987Å.

The solid state structures of **(7)-(10)** also show possible intermolecular H•••Cl interactions to one of the olefin protons of a neighbouring molecule.

	H•••X distances (Å)	
	intramolecular	intermolecular
(7)	2.765	2.697
(8)	2.975	2.689
(9)	2.917	2.936
(10)	2.732	2.715

Table 21 : Shortest H•••X intra and inter-molecular distances in complexes **(7)-(10)** (where X = Br, Cl)

These values generally lie slightly inside the shortest intramolecular H•••Cl distances observed for each compound and as Figure 64 shows are positioned below the chloride so might be expected to pull the chloride downward but that is clearly not the case. These close intermolecular contacts may simply be a result of packing effects, but do suggest that presuming intramolecular hydrogen bonding is the cause of the distortion is also ambiguous.

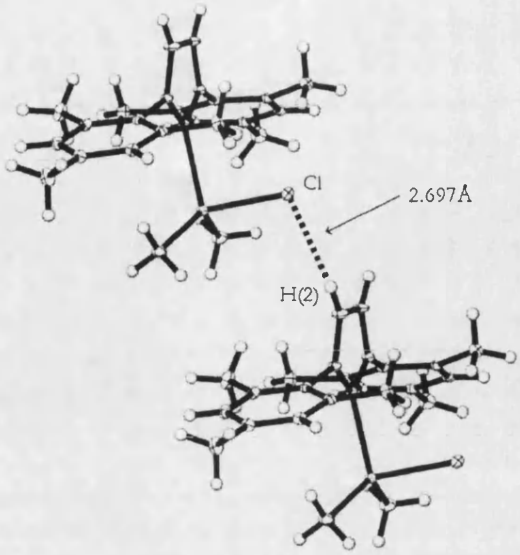

Figure 64 : Intermolecular H•••Cl hydrogen bonding in **(7)**

The complexes $Cl_3In(iMes)$ and $H_2ClIn(iMes)$ also have short H•••Cl intermolecular contacts within 2.987Å shown in Table 22 although the hydrogens here have also not been freely refined.

	Intermolecular H•••Cl contacts (Å)
$Cl_3In(iMes)$	2.797
	2.943
	2.948
$H_2ClIn(iMes)$	2.736
	2.871

Table 22 : Shortest H•••Cl intermolecular distances in $Cl_3In(iMes)$ and $H_2ClIn(iMes)$

The positions of the hydrogens involved here might also be expected to pull the chloride downward but this does not occur here either.

Ultimately, the presence of both H•••Cl and $C_{carbene}$•••Cl interactions cannot at this stage be discounted or proved and the distortion could in fact be a combination of the

two interactions. Evidently the distortion is very weak as shown by the similarity of the solid state structure of **(7)** with H_3In(iMes) and does not persist in solution as observed by the free rotation of the $C_{carbene}$-indium bond by NMR spectroscopy in compound **(8)**.

3.3.6 Mechanism of Reaction of $InMe_3$ with (iMes)Cl

The most likely mechanism for the reaction is shown in Figure 65.

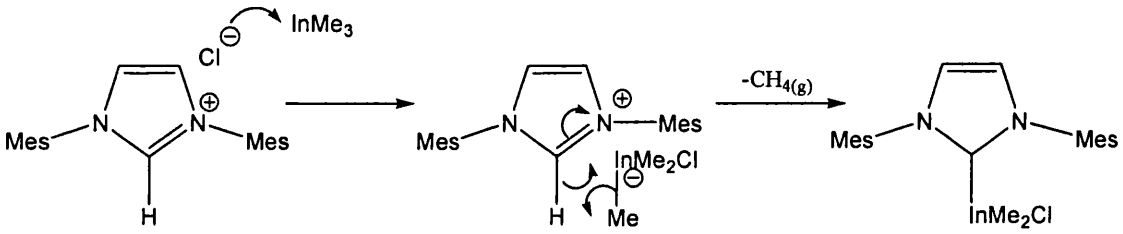

Figure 65 : Possible mechanism for the reaction of $InMe_3$ with (iMes)Cl

Credence is given to this mechanism because of the similarity of the intermediate step with the solid state structure of $[^iPrH]^+[InBr_4]^-$ which has been isolated and reported.[52] It was possible to isolate this compound due to the enhanced stability offered to the metal centre by its bromide ligands. The anion $^-InMe_3Cl$ however is likely to be only short-lived and rapidly abstracts a proton from the carbene and eliminates methane to form **(7)**. This is also supported by tests of the reaction of (iMes)NTf_2 with $InMe_3$ where no reaction is observed. The weak coordinating nature of the triflamide anion means it cannot stabilise the indium in the form as the intermediate $Me_3In(NTf_2)$ so that the acidic proton can be abstracted by protonolysis.

The production of **(13)-(16)** occurs by a simple protonolysis mechanism in the cases where acids are used to introduce the weakly coordinating triflate and triflamide ligands. Where TMS(OTf) is used the the system undergoes chloride abstraction.

3.4 Summary

A range of indium(III) carbene complexes have been synthesised and structurally and spectroscopically characterised. Systematic substitution of both the methyls and chloride with triflate and triflamide ligands has been shown to increase the Lewis acidity of the metal centre by the measure if ^{1}H and $^{13}C\{^{1}H\}$ NMR spectroscopy. A route to these potentially useful compounds has been developed by the synthesis of the air stable pre-cursors **(7)** and **(11)**, whilst reaction of these compounds with the appropriate acid or trimethylsilyl reagent gives complexes **(13)-(16)** in a matter of minutes. At this stage the cause of the distortions observed in the solid state structures of **(7)-(10)** has not been completely resolved, but it is clear that whatever interaction is responsible, it is weak and does not persist in solution. This means it is unlikely to be of importance for the use of these compounds in catalysis.

3.5 References

(1) Abernethy, C. D.; Cole, M. L.; Jones, C. *Organometallics* **2000**, *19*, 4852.
(2) Herrmann, W. A.; Kocher, C. *Angew. Chem.-Int. Edit.* **1997**, *36*, 2163-2187.
(3) Arduengo, A. J. *Accounts Chem. Res.* **1999**, *32*, 913-921.
(4) Herrmann, W. A.; Weskamp, T.; Böhm, V. P. W. *Advances in Organometallic Chemistry and references therein* **2001**, *48*, 1-69.
(5) Clayden, J.; Greeves, N.; Warren, S.; Wothers, P. *Organic Chemistry*; Oxford University Press: Oxford, 2001, Ch. 40.
(6) Wanzlick, H.-W. *Angew. Chem. Int. Ed.* **1962**, *1*, 75.
(7) Wanzlick, H.-W.; Kleiner, H.-J. *Angewandte Chemie* **1961**, *73*, 493.
(8) Wanzlick, H.-W.; Esser, F.; Kleiner, H.-J. *Chemische Berichte* **1963**, *96*, 1208.
(9) Arduengo, A. J.; Harlow, R. L.; Kline, M. *J. Am. Chem. Soc.* **1991**, *113*, 361.
(10) Bourissou, D.; Guerret, O.; Gabbai, F. P.; Bertrand, G. *Chem. Rev.* **2000**, *100*, 39-91.
(11) Hahn, F. E.; Wittenbecher, L.; Le Van, D.; Frohlich, R. *Angew. Chem.-Int. Edit.* **2000**, *39*, 541-+.
(12) Heinemann, C.; Muller, T.; Apeloig, Y.; Schwarz, H. *J. Am. Chem. Soc.* **1996**, *118*, 2023-2038.
(13) Arduengo, A. J.; Dias, H. V. R.; Harlow, R. L.; Kline, M. *J. Am. Chem. Soc.* **1992**, *114*, 5530-5534.
(14) Arduengo, A. J.; Krafczyk, R.; Schmutzler, R.; Craig, H. A.; Goerlich, J. R.; Marshall, W. J.; Unverzagt, M. *Tetrahedron* **1999**, *55*, 14523-14534.
(15) Arduengo, A. J.; Davidson, F.; Dias, H. V. R.; Goerlich, J. R.; Khasnis, D.; Marshall, W. J.; Prakasha, T. K. *J. Am. Chem. Soc.* **1997**, *119*, 12742-12749.
(16) Lee, S.; Hartwig, J. F. *J. Org. Chem.* **2001**, *66*, 3402-3415.
(17) Grundemann, S.; Kovacevic, A.; Albrecht, M.; Faller, J. W.; Crabtree, R. H. *J. Am. Chem. Soc.* **2002**, *124*, 10473-10481.
(18) Furstner, A.; Ackermann, L.; Gabor, B.; Goddard, R.; Lehmann, C. W.; Mynott, R.; Stelzer, F.; Thiel, O. R. *Chem.-Eur. J.* **2001**, *7*, 3236-3253.
(19) Herrmann, W. A.; Kocher, C.; Goossen, L. J.; Artus, G. R. J. *Chem.-Eur. J.* **1996**, *2*, 1627-1636.
(20) Herrmann, W. A.; Elison, M.; Fischer, J.; Kocher, C.; Artus, G. R. J. *Chem.-Eur. J.* **1996**, *2*, 772-780.
(21) Xu, L. J.; Chen, W. P.; Bickley, J. F.; Steiner, A.; Xiao, J. L. *J. Organomet. Chem.* **2000**, *598*, 409-416.
(22) Denk, M. K.; Thadani, A.; Hatano, K.; Lough, A. J. *Angew. Chem. Int. Edit.* **1997**, *36*, 2607-2609.
(23) Arduengo, A. J.; Goerlich, J. R.; Marshall, W. J. *J. Am. Chem. Soc.* **1995**, *117*, 11027-11028.
(24) Alder, R. W.; Blake, M. E.; Bortolotti, C.; Bufali, S.; Butts, C. P.; Linehan, E.; Oliva, J. M.; Orpen, A. G.; Quayle, M. J. *Chem. Commun.* **1999**, 241-242.
(25) Alder, R. W.; Blake, M. E.; Bortolotti, C.; Bufali, S.; Butts, C. P.; Linehan, E.; Oliva, J. M.; Orpen, A. G.; Quayle, M. J. *Chem. Commun.* **1999**, 1049-1049.
(26) Alder, R. W.; Allen, P. R.; Murray, M.; Orpen, A. G. *Angew. Chem. Int. Edit. Engl.* **1996**, *35*, 1121-1123.
(27) Alder, R. W.; Blake, M. E. *Chem. Commun.* **1997**, 1513-1514.
(28) Alder, R. W.; Butts, C. P.; Orpen, A. G. *J. Am. Chem. Soc.* **1998**, *120*, 11526-11527.

(29) Wanzlick, H.-W.; Schönherr, H.-J. *Angew. Chem. Int. Ed.* **1968**, *7*, 141.
(30) Öfele, K. J. *J. Organomet. Chem.* **1968**, *12*, P42.
(31) Arduengo, A. J.; Dias, H. V. R.; Davidson, F.; Harlow, R. L. *J. Organomet. Chem.* **1993**, *462*, 13-18.
(32) Herrmann, W. A.; Runte, O.; Artus, G. *J. Organomet. Chem.* **1995**, *501*, C1-C4.
(33) Oldham, W. J.; Oldham, S. M.; Scott, B. L.; Abney, K. D.; Smith, W. H.; Costa, D. A. *Chem. Commun.* **2001**, 1348-1349.
(34) Arduengo, A. J.; Tamm, M.; McLain, S. J.; Calabrese, J. C.; Davidson, F.; Marshall, W. J. *J. Am. Chem. Soc.* **1994**, *116*, 7927-7928.
(35) Fourmari, P.; de Cointet, P.; Laviron, E. *Bull. Soc. Chim. Fr.* **1968**, 2438.
(36) Chan, B. K. M.; Chan, N. H.; Grimett, M. R. *Aus. J. Chem.* **1977**, *30*, 2005.
(37) Haque, M. R.; Rasmussen, M. *Tetrahedron* **1994**, *50*, 5535-5554.
(38) Grimmett, M. R. *Imidazole and Benzimidazole Synthesis*; Academic Press: London, 1997.
(39) Huang, J. K.; Nolan, S. P. *J. Am. Chem. Soc.* **1999**, *121*, 9889-9890.
(40) Jafarpour, L.; Nolan, S. P. In *Advances in Organometallic Chemistry, Vol. 46*, 2001; Vol. 46.
(41) Jafarpour, L.; Nolan, S. P. *J. Organomet. Chem.* **2001**, *617*, 17-27.
(42) Arduengo, A. J., III *US 5077414* **1991**.
(43) Herrmann, W. A.; Goossen, L. J.; Spiegler, M. *J. Organomet. Chem.* **1997**, *547*, 357-366.
(44) Bohm, V. P. W.; Weskamp, T.; Gstottmayr, C. W. K.; Herrmann, W. A. *Angew. Chem. Int. Edit.* **2000**, *39*, 1602-+.
(45) Herrmann, W. A.; Goossen, L. J.; Kocher, C.; Artus, G. R. J. *Angew. Chem. Int. Edit. Engl.* **1996**, *35*, 2805-2807.
(46) Bildstein, B.; Malaun, M.; Kopacka, H.; Wurst, K.; Mitterbock, M.; Ongania, K. H.; Opromolla, G.; Zanello, P. *Organometallics* **1999**, *18*, 4325-4336.
(47) Black, S. J.; Hibbs, D. E.; Hursthouse, M. B.; Jones, C.; Malik, K. M. A.; Smithies, N. A. *J. Chem. Soc.-Dalton Trans.* **1997**, 4313-4319.
(48) Kuhn, N.; Henkel, G.; Kratz, T.; Kreutzberg, J.; Boese, R.; Maulitz, A. H. *Chem. Ber.-Recl.* **1993**, *126*, 2041-2045.
(49) Arduengo, A. J.; Dias, H. V. R.; Calabrese, J. C.; Davidson, F. *J. Am. Chem. Soc.* **1992**, *114*, 9724-9725.
(50) Li, X. W.; Su, J. R.; Robinson, G. H. *Chem. Commun.* **1996**, 2683-2684.
(51) Kuhn, N.; Kratz, T. *Synthesis* **1993**, 561-562.
(52) Baker, R. J.; Davies, A. J.; Jones, C.; Kloth, M. *J. Organomet. Chem.* **2002**, *656*, 203-210.
(53) Downs, A. J.; Pulham, C. R. *Chem. Soc. Rev.* **1994**, *23*, 175-184.
(54) Hibbs, D. E.; Hursthouse, M. B.; Jones, C.; Smithies, N. A. *Chem. Commun.* **1998**, 869-870.
(55) Baker, R. J.; Cole, M. L.; Jones, C.; Mahon, M. F. *J. Chem. Soc.-Dalton Trans.* **2002**, 1992-1996.
(56) Abernethy, C. D.; Cole, M. L.; Davies, A. J.; Jones, C. *Tetrahedron Lett.* **2000**, *41*, 7567.
(57) Shukla, P.; Johnson, J. A.; Vidovic, D.; Cowley, A. H.; Abernethy, C. D. *Chem. Commun.* **2004**, 360-361.
(58) Francis, M. D.; Hibbs, D. E.; Hursthouse, M. B.; Jones, C.; Smithies, N. A. *J. Chem. Soc.-Dalton Trans.* **1998**, 3249-3254.
(59) Cole, M. L.; Jones, C.; Junk, P. C. *New J. Chem.* **2002**, *26*, 1296-1303.

(60) Hillier, A. C.; Sommer, W. J.; Yong, B. S.; Petersen, J. L.; Cavallo, L.; Nolan, S. P. *Organometallics* **2003**, *22*, 4322-4326.
(61) Koppel, I. A.; Taft, R. W.; Anvia, F.; Zhu, S. Z.; Hu, L. Q.; Sung, K. S.; Desmarteau, D. D.; Yagupolskii, L. M.; Yagupolskii, Y. L.; Ignatev, N. V.; Kondratenko, N. V.; Volkonskii, A. Y.; Vlasov, V. M.; Notario, R.; Maria, P. C. *J. Am. Chem. Soc.* **1994**, *116*, 3047-3057.
(62) Davidson, M. G.; Raithby, P. R.; Johnson, A. L.; Bolton, P. D. *Eur. J. Inorg. Chem.* **2003**, 3445-3452.
(63) Earle, M. J.; Hakala, U.; McAuley, B. J.; Nieuwenhuyzen, M.; Ramani, A.; Seddon, K. R. *Chem. Commun.* **2004**, 1368-1369.
(64) Hoppenheit, R.; Lork, E.; Petersen, J.; Mews, R. *Chem. Commun.* **1997**, 1659-1660.
(65) Friebolin, H. *Basic One- and Two Dimensional NMR Spectroscopy*; 3 ed.; Wiley-VCH: Weinheim, 1998.
(66) Arduengo, A. J.; Davidson, F.; Krafczyk, R.; Marshall, W. J.; Tamm, M. *Organometallics* **1998**, *17*, 3375-3382.
(67) Abernethy, C. D.; Codd, G. M.; Spicer, M. D.; Taylor, M. K. *J. Am. Chem. Soc.* **2003**, *125*, 1128-1129.
(68) Hafner, A.; Hegedus, L. S.; Deweck, G.; Hawkins, B.; Dotz, K. H. *J. Am. Chem. Soc.* **1988**, *110*, 8413-8421.
(69) Bondi, A. *Journal of Physical Chemistry* **1964**, *68*, 441-451.
(70) Aakeroy, C. B.; Evans, T. A.; Seddon, K. R.; Palinko, I. *New J. Chem.* **1999**, *23*, 145-152.

Chapter 4 - Catalyst Screening in Friedel-Crafts Acylations

4.1 Introduction

The complexes synthesised in Chapter 3, especially those with triflate or triflamide ligands, are potential sources of Lewis acidic $[(iMes)InMe]^{2+}$ or $[(iMes)InMe_2]^{+}$ fragments. It was anticipated that such complexes would make effective catalysts for Friedel-Crafts acylation, which are promoted by Lewis acids. $In(OTf)_3$ and $In(NTf)_3$ have been shown to be active in this type of reaction but their low solubility means they are ill-defined and thus the active species in the catalysis is unknown. This introduction will cover background of the Friedel-Crafts acylation reaction and an overview of related metal triflate and triflamide catalysis.

4.1.1 Introduction to Friedel-Crafts Acylations

Since the publication in 1877 of the details of the reaction between arylchloride and benzene in the presence of aluminium trichloride, $AlCl_3$,[1] the scope of what is called a Friedel-Crafts reaction has widened so as to make an exact definition difficult. Substitution, isomerization, elimination, cracking, polymerisation and addition reactions under the effect of Lewis acids are all referred to as Friedel-Crafts reactions. However, to generalise, a Friedel-Crafts reaction involves the following components: [2-6]

1. The substance to be substituted (e.g. an arene or olefin)
2. A reagent to provide the substituent (e.g. acyl or alkyl halide)
3. A catalyst which is usually a Lewis or Brønsted acid
4. A solvent (this can be an excess reagent)
5. The substituted product

6. The by-product generated from the substituent donor

The Friedel-Crafts acylation reaction is one of the oldest reactions for the preparation of ketones by carbon-carbon bond formation. The products are widely used commercially, for example, in the synthesis of anthraquinone dyes,[2] and pharmaceuticals such as the anti-inflammatory drugs Naproxen,[7] Ibuprofen (Figure 1)[8] the anti-cancer drug Tamoxifen,[9] and the anti-hyperlipemic Fenofibrate.[10]

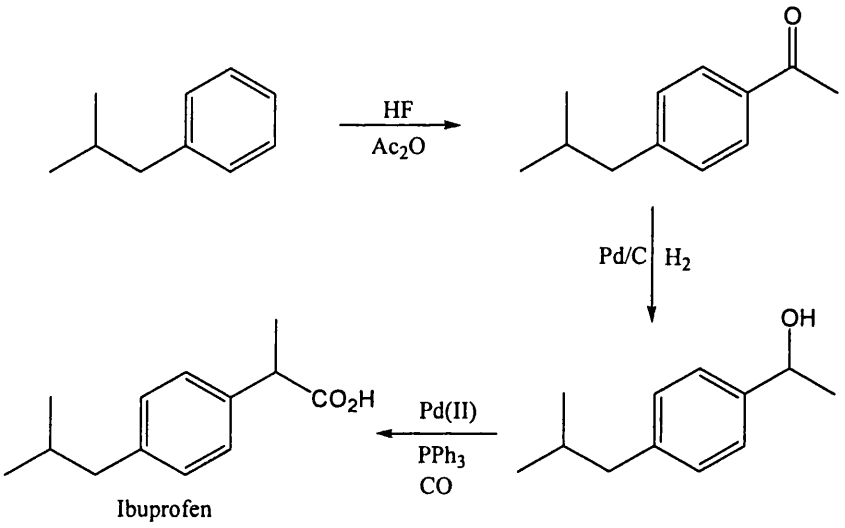

Figure 1 : Synthetic pathway to Ibuprofen

Whilst a general Friedel-Crafts alkylation reaction proceeds in the presence of a catalytic amount of a Lewis acid such as $AlCl_3$ or boron trifluoride, BF_3, acylation reactions require more than a stoichiometric amount of Lewis acid due to their coordination to the product ketones. This leads to an environmentally flawed process with gaseous effluents and mineral wastes. However, this reaction becomes catalytic if the coordination complex of the Lewis acid and the product ketone becomes partially dissociated. This dissociation is Lewis acid and temperature dependent,[2-6] and it is possible to carry out Friedel-Crafts acylation reactions in the presence of a catalytic amount of some Lewis acids at high temperature.[11] However, a temperature

increase usually provokes side reactions. Consequently, the search for more efficient catalysts for this reaction is a current challenge. Indeed even after more than one century of study, the ideal catalyst, which satisfies industrial, economical and safety constraints, and allows the Friedel-Crafts acylation reaction to proceed with a broad range of aromatics and acylating reagents still remains to be discovered.

Catalysts which have been previously reported in this type of reaction include iron chloride ($FeCl_3$), zinc chloride ($ZnCl_2$),[11] zeolites[12-14] and gallium chloride with silver perchlorate ($GaCl_3$-$AgClO_4$)[15] but these systems show activity only in the acylation of activated aromatics. The extension of $FeCl_3$ catalysis to unactivated aromatics has, however, been achieved under microwave conditions,[16,17] and efficient Brønsted acid catalysts are also known including superacidic systems,[18-23] and sulfonic acids.[24-27]

In terms of acylating agents, carboxylic anhydrides are one of the most reactive acyl sources. The use of anhydrides however, has three drawbacks: the relatively limited diversity of commercially available anhydrides when compared with carboxylic acids, the acidic by-product and their inability to acylate unactivated aromatics.[28] Acylation with acid halides derived from the parent acid solves the former problem, whilst a number of efficient acyl donors with neutral by-products have been developed, principally in the field of pH-dependent enzyme-catalysed reactions.[29,30,31] Acid halides also appear to be able to acylate unactivated systems.[28]

Acid chlorides provide the only real viable alternatives to carboxylic anhydrides, although harsher conditions (higher temperature, longer reaction times and increased catalyst loading) are required.[28,32] By this route, a wide range of ketones can be

produced from carboxylic acids after first converting them to the corresponding acid chloride before acylation is carried out.

4.1.2 Metal Triflates as Friedel-Crafts Acylation Catalysts

Since the synthesis of triflic acid, H(OTf) in 1954,[33] its derivatives have been the subject of many studies. Where Friedel-Crafts acylation reactions are concerned two main lines of research have been developed. The first is the search for new acylating agents, such as mixed anhydrides (carboxylic triflic anhydrides or acyl triflates, RCOOTf) in which the triflate moiety (a "super-leaving group") provides a significant activation of the acyl group.[24,25] The second more importantly for the scope of this thesis is the synthesis and study of the catalytic activity of triflates of elements having potential Lewis acidity.

The first use of metal triflates as catalysts for acylation was reported in 1988.[34] Boron, aluminium and gallium triflates were shown to catalyse the benzoylation of toluene in up to 72% yield. However, 50mol% of these highly sensitive and expensive catalysts was required. Transition metal salts such as lanthanide, scandium and copper triflates[35-38] and triflamides[39] have also been developed as catalysts for acylation reactions. Their stability in water has been documented and this enables their recycling through the aqueous phase on work up.[40] Their catalytic activity is limited, however, to the acylation of activated aromatics.

Unactivated aromatics (fluorobenzene, chlorobenzene and dichlorobenzene) have also been benzoylated via catalysis with a gallium triflate analogue. Gallium nonafluorobutanesulfonate [$Ga(ONf)_3$] catalyses the reactions using benzoyl chloride

as the benzoylating agent to give the corresponding ketones in high yield (Figure 2 and Table 1).[41]

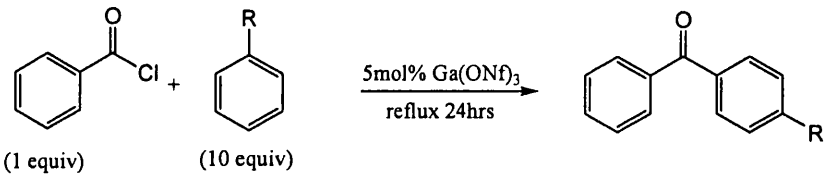

R	Yield (%)
H	90
Me	88
Cl	98
F	91

Figure 2 & Table 1: Acylations with benzoyl chloride catalysed by $Ga(ONf)_3$

4.1.3 Metal Triflamides as Friedel-Crafts Acylation Catalysts

The use of the trifluoromethanesulfonyl (Tf) group as an electron withdrawing substituent on nitrogen substantially increases the acidity of an amine, imine or imide. Compounds incorporating one Tf group such as $CF_3SO_2NH_2$ and $CF_3SO_2N(H)Ph$ exhibit pK_a values of weak acids while two sulfonyl groups on nitrogen drastically increase the acidity of the remaining proton, as shown by $(FSO_2)_2NH$,[42] $(RSO_2)_2NH$[43] (R = aryl) and bis(perfluoroalkylsulfonyl)imides $HN(SO_2R_f)_2$ (R_f = CF_3, C_2F_5 and C_4F_9).[44] It is for this reason that their use as either anions or acids in Lewis acid and Brønsted acid catalysis has proved so successful.

Initially synthesised in 1984,[45] bis(trifluoromethanesulfonyl)amine $H(NTf_2)$ is a good catalyst for C-C bond forming reactions such as Friedel-Crafts, Mukaiyama 1,2 additions and 1,4-additions.[46] Metal salts of $H(NTf_2)$ have also been reported as effective Lewis acid catalysts for Diels-Alder,[47] acetylisation,[48] acetalisation,[49] debenzylation,[50,51] and Friedel-Crafts reactions.[39] Metal triflamides are, in general, more effective Lewis acid catalysts than metal triflates because triflamides are less coordinating and believed to enhance the Lewis acidity at the metal centre. For

example, acylation of anisole to 4-methoxyacetophenone proceeds under much milder conditions when using ytterbium triflamide, $Yb(NTf_2)_3$ compared with ytterbium triflate $Yb(OTf)_3$,[39] while scandium triflamide, $Sc(NTf_2)_3$ is a far superior catalyst than $Sc(OTf)_3$ in the deprotection of benzyl ester to its parent acid (Figure 3).[49]

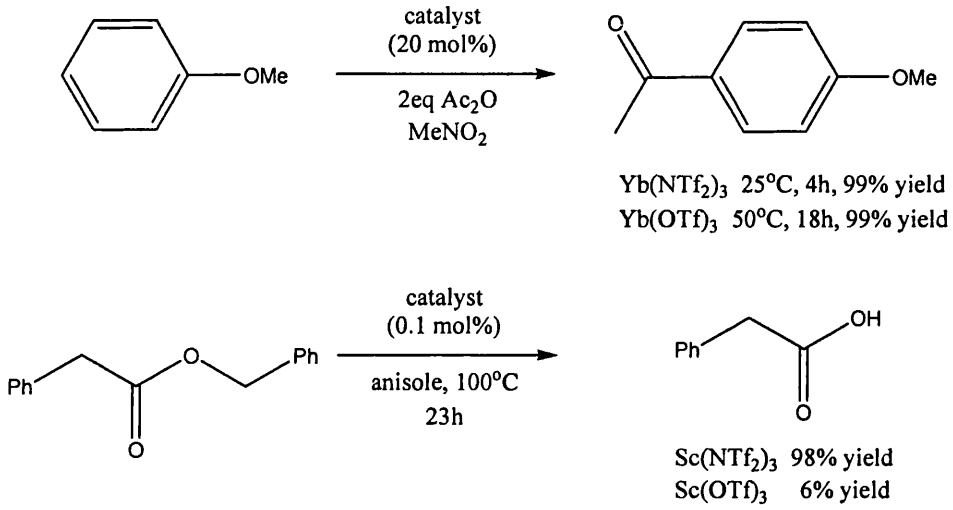

Figure 3 : Demonstrating the advantage of metal triflamides over metal triflates

A range of metal triflamides have also been tested in the benzoylation of toluene with benzoyl chloride at 1mol% catalyst loading and 110°C in the absence of solvent media (Table 2). The metal triflamides of cobalt and zinc, $Co(NTf_2)_2$ and $Zn(NTf_2)_2$ have even been documented to be active in the acylation of chlorobenzene with benzoyl chloride using an ionic liquid as the solvent media. At 130°C over 18 hours 95% and 55% yields were obtained respectively.[52]

Catalyst (1mol%)	Time (h)	Yield (%)
$LiNTf_2$	120	<5
$Mg(NTf_2)$	48	99
$Ca(NTf_2)$	120	<5
$Sr(NTf_2)$	120	31
$Ba(NTf_2)$	120	65
$Mn(NTf_2)$	5	99
$Co(NTf_2)$	3	99
$Ni(NTf_2)$	4	99
$Cu(NTf_2)$	72	99
$Zn(NTf_2)$	48	99
$Sn(NTf_2)$	48	91
$Pb(NTf_2)$	6	95

Table 2 : Reaction of benzoyl chloride (5mmol) with toluene (7.5mmol) by various metal triflamides in the absence of solvent media

However, it is indium(III) systems containing triflate and triflamide ligands that we are most interested in for the scope of this thesis and thus the following section contains a review of the pertinent literature involving these types of system in Friedel-Crafts acylations.

4.1.4 $In(OTf)_3$ and $In(NTf_2)_3$ in Friedel-Crafts Acylations

Excellent results have previously been obtained using $In(OTf)_3$ in the acylation of alcohols, amines and aldehydes as well as aromatics by the Frost group.[53] The efficacy of indium(III) triflamide in this type of reaction has also been studied.[54]

Substrate	Reaction time (mins)	Product	Yield (%)
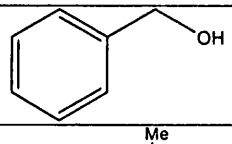	15	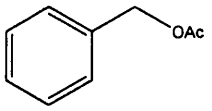	97
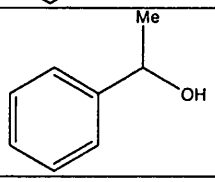	30	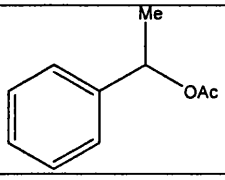	98
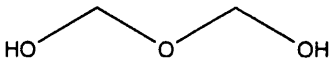	60	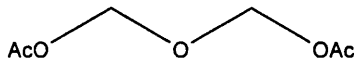	92
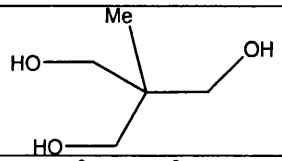	60	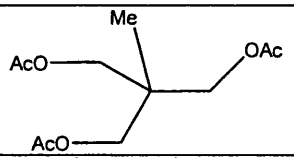	96
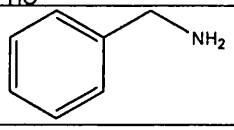	30	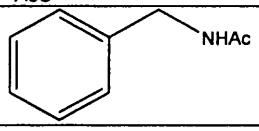	98

Table 3: The 0.1mol% $In(OTf)_3$ catalysed acylations of a range of substrates in acetonitrile

A proposed mechanism for the activation of acetic anhydride by indium(III) salts is shown in Figure 4.[32] Coordination of a lone pair of electrons from the acetic anhydride to the Lewis acidic indium provides enhanced electrophilicity at the carbonyl carbons, resulting in attack from the aromatic nucleophile. The acetate anion abstracts a proton, which results in re-aromatisation to give the product ketone and the by-product acetic acid in a stoichiometric ratio.

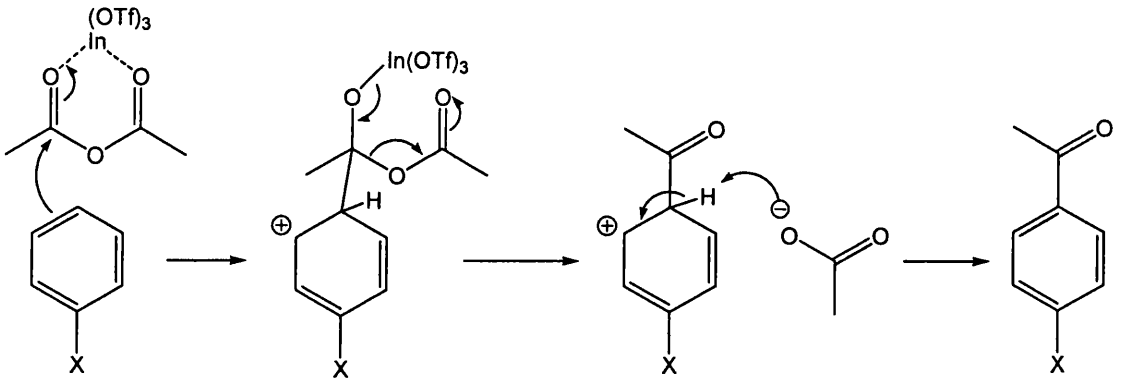

Figure 4 : Possible mechanism for the activation of acetic anhydride (where X = OMe)

4.1.5 Summary and Scope of Chapter

In summary, both $In(OTf)_3$ and $In(NTf)_3$ have been shown to exhibit strong activity in the Lewis acid catalysed Friedel-Crafts acylation of activated aromatics. The mechanisms of reaction during catalysis have not been documented although it has been postulated to occur as shown in section 4.1.4. Given the ill-defined nature of these catalysts the actual reactive species is not known. Use of the soluble, well-defined complexes reported in Chapter 3 (which may act as models) may allow the elucidation of the active species in these reactions.

4.2 Results

4.2.1 Acylations with Acetic Anhydride

The Friedel-Crafts acylation reaction chosen for the preliminary catalyst screening test was the reaction of anisole with acetic anhydride to produce the *para*-substituted 4-methoxyacetophenone and one equivalent of acetic acid as a by-product

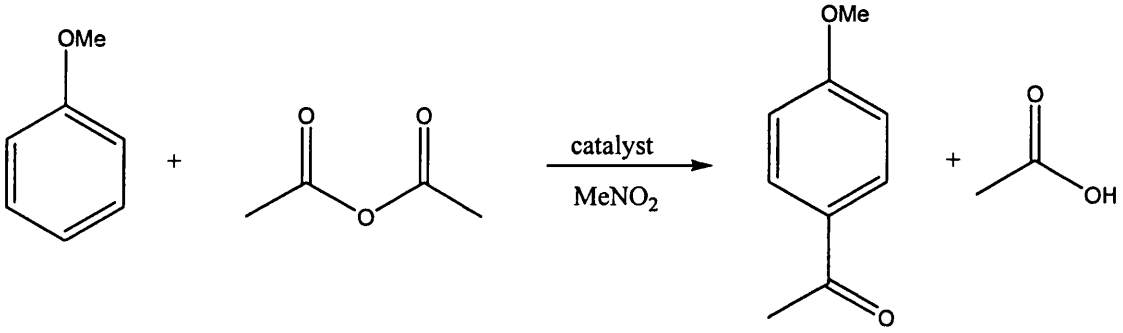

Figure 5 : The catalysed reaction of anisole and acetic anhydride

The conditions for the acylation of activated aromatics employed were developed previously in the Frost group.[32,55] These include a catalyst loading of 5mol%, addition of 1.5 equivalents of acetic anhydride, a temperature of 50°C and nitromethane as the solvent medium.

4.2.2 Preliminary Screening

By carrying out the reactions in d^3-nitromethane and drying and purifying all materials and the solvent before use, it was possible to study the product conversion vs. time behaviour for the acylation of anisole directly by ^1H NMR spectroscopy and obtain accurate reaction completion times. Tests with compounds **(7), (11), (13)** and **(15)** showed no conversion of anisole. However, **(14)** and **(16)** showed good activity in the reaction (Table 3).

compound		activity
(7)	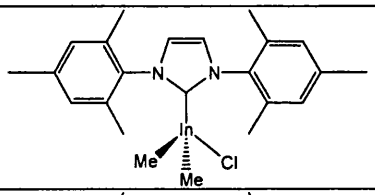	inactive & decomposes
(11)	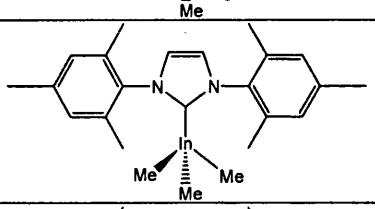	inactive & decomposes
(13)	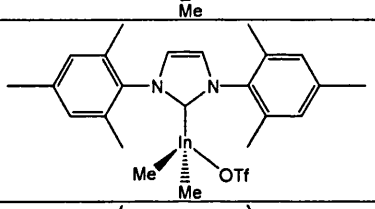	inactive & decomposes
(15)	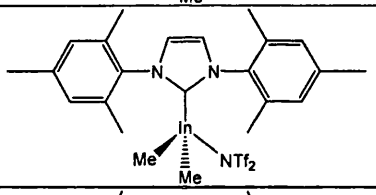	inactive & decomposes
(14)	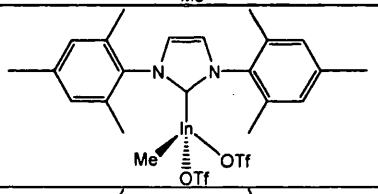	active but has poor solubility
(16)	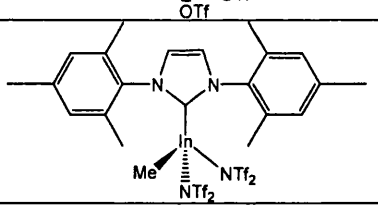	active & new compound generated

Table 3 : Compounds tested and their performance (as determined by ^{1}H NMR spectroscopy)

Catalysis studies with **(7)**, **(11)**, **(13)** and **(15)** showed that the decomposition in each case was induced by the presence of the acylating agent, acetic anhydride alone while no change in the complexes was observed in the presence of anisole. ^{1}H NMR spectroscopy showed that in the presence of acetic anhydride, compounds **(7)**, **(13)** and **(15)** decomposed to give chiefly the protonated carbene imidazolium cation,

$(iMes)^+$, where the partnering anions in each case are at this stage unknown (but will probably be acetate). However in the case of the decomposition of **(11)** in the presence of acetic anhydride that no $(iMes)^+$ is produced. It was also evident that no methane elimination occurred in any of the four decompositions reactions as no peak was observed at 0.20ppm in the ^1H NMR spectra when the reactions were monitored *in situ*. Time constraints have prevented a more detailed analysis of these four reactions, so the identities of the other decomposition products for **(7), (11), (13)** and **(15)** remain undetermined. Most importantly our tests show that **(7), (11), (13)** and **(15)** are completely inactive as catalysts in the reaction.

For the successful reactions involving **(14)** and **(16)** it was possible to accurately analyse the percentage of product conversion. The ratio of anisole to 4-methoxyacetophenone was calculated by integration of the 2H resonance of the 4-methoxyacetophenone product at 7.97ppm and of the 2H resonance of the anisole at 7.31ppm. This allowed the product conversion to be readily determined in each spectrum. Obtaining spectra at 2 or 2.5 minute intervals during the reactions meant the percentage product conversion over time could be resolved.

As the following graph shows using a catalyst loading of 5mol%, addition of 1.5 equivalents of acetic anhydride, a temperature of 50°C and nitromethane, the reaction catalysed by $In(OTf)_3$ (used as a standard) is complete in 22 minutes while using **(16)** it is complete in 30 minutes (Figure 6). Compound **(14)** however shows lower activity and after 5 hours the reaction is still incomplete with only 91% of anisole converted to the 4-methoxyacetophenone product.

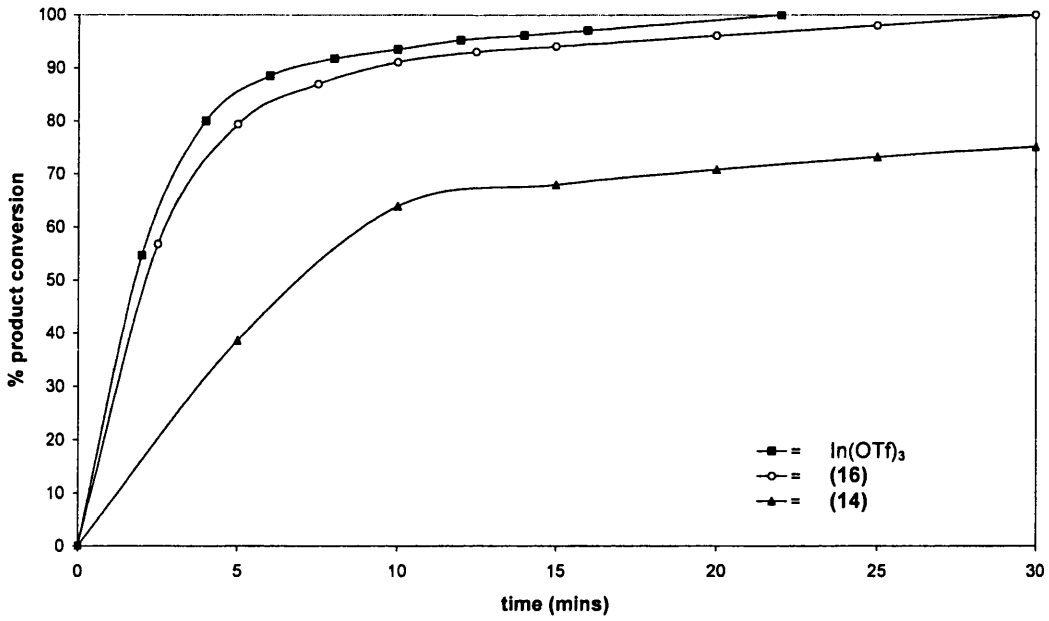

Figure 6 : Graph showing conversion of 4-methoxyacetophenone vs. time for the catalysts $In(OTf)_3$, **(14)** and **(16)**.

It is important to point out that the result for **(14)** may not be accurate due to problems with its isolation. When analytically pure crystals of **(14)** are dried *in vacuo*, the molecule of dichloromethane that co-crystallises in the lattice appears to be removed leaving a white powder which is reluctant to dissolve in dichloromethane or nitromethane. It is possible that this is the reason that the reaction is significantly slower than for **(16)**.

Despite repeated attempts, the data obtained for each catalysis test does not fit a first or second order rate equation. Even under pseudo 1^{st} order conditions where the reaction was repeated using 10 equivalents of anisole and then 10 equivalents of acetic anhydride the data did not fit the rate equation.

4.2.3 Substrate Screening for (16)

Because preliminary tests with **(16)** proved it was the most catalytically active of our complexes, it was tested with a range of aromatic substrates of varying activation using acetic anhydride as the acylating agent. The results are shown in Table 4.

Substrate		Yield (%)	Reaction time (mins)	Product
Furan		100	2	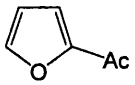
Phenol	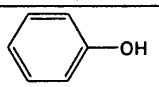	100	2	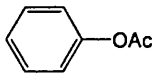
Aniline	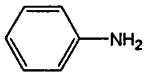	100	2	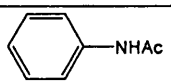
2,3-dimethylanisole	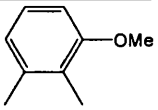	100	16	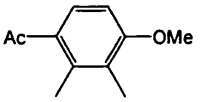
Veratrole	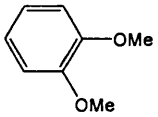	100	20	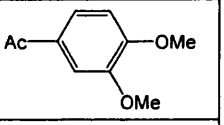
Anisole	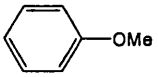	100	30	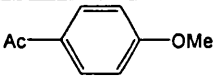
1,4-benzodioxane	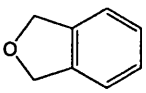	88	40	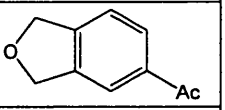
Mesitylene	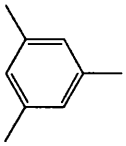	86	300	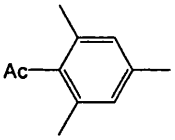

Table 4 : Successful acylation reactions using **(16)**

As the table shows, the acylation reactions of the most activated substrates furan and the alcohol phenol and amine aniline are all complete within two minutes, much faster than that of anisole (30 mins). The acylation reactions of 2,3-dimethylanisole and veratrole, are also completed more rapidly than the acylation of anisole in 16 and 20 minutes respectively. The less activated systems 1,4-benzodioxane reaches 88%

conversion after 40 minutes and stops, while mesitylene reaches 86% conversion respectively after 300 minutes.

Tests with the less activated aromatic systems *m*-xylene, toluene, benzene and bromobenzene however, were unsuccessful and despite increasing the reaction temperature to 80°C for 24 hours no reactions were observed. The catalysis of the acylation of mesitylene, *m*-xylene and toluene however, has been shown to be successful using a 1mol% catalyst loading of $In(OTf)_3$. For toluene harsher conditions were required (the reaction was carried out in refluxing nitromethane and with 10mol% $In(OTf)_3$) but in all three cases a good yield is obtained after a one hour reaction (Table 5).[32] In the case of bromobenzene however, even when $In(OTf)_3$ and harsh reactions conditions are employed for 24 hours the acylation does not occur.

Substrate		Yield (%)	Product
mesitylene	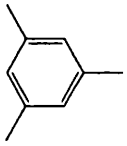	99	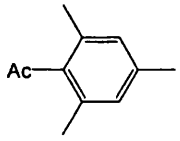
m-xylene	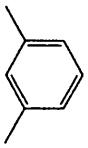	90	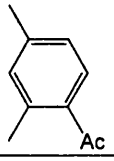
toluene*	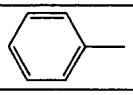	82	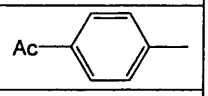
bromobenzene*	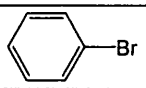	0	no reaction

Table 5 : Acylations using $In(OTf)_3$ (* = reaction carried out at reflux and 10mol% $In(OTf)_3$)

4.2.4 Recycling the Catalyst

While $In(OTf)_3$ can be readily recycled by extraction in the aqueous phase during reaction work-up followed by drying,[32] this is not possible with **(16)** which

decomposes in water to give intractable, unidentifiable products. However, a brief study was undertaken to determine if **(16)** retained its activity after already being used in a catalysis reaction. The acylation of anisole by acetic anhydride using a 5mol% catalyst loading of **(16)** was carried out followed by addition of another 100mol% of anisole and 150mol% more acetic anhydride 24 hours later. As before the reaction was tracked by ^{1}H NMR spectroscopy (Figure 7).

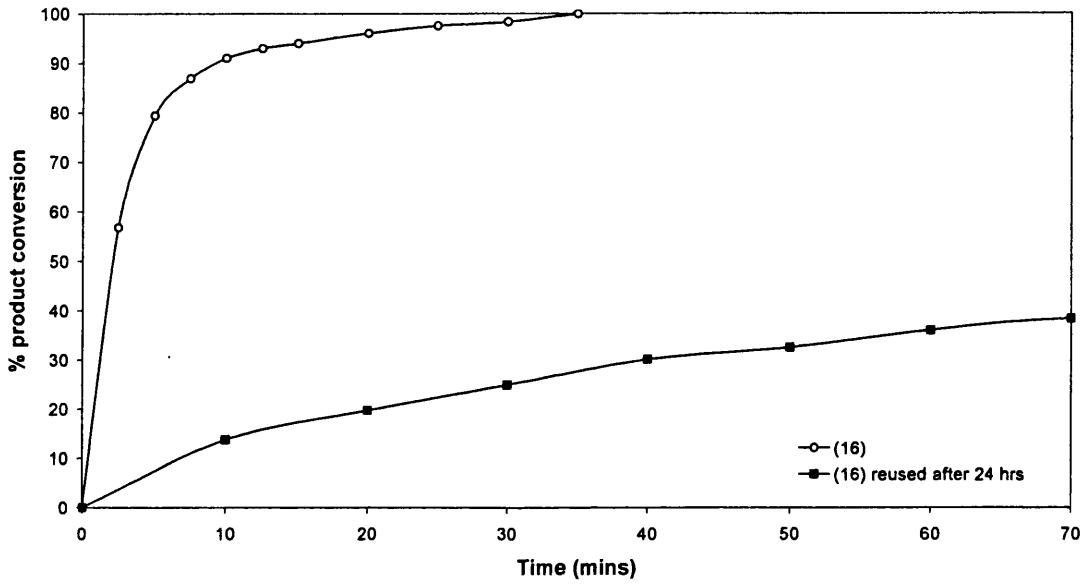

Figure 7 : Graph showing yield of 4-methoxyacetophenone for the first catalysts run using **(16)** and for the second run 24 hours later

Although the data cannot be fitted to a first-order rate equation, it is evident that the speed of conversion is significantly decreased for the second catalysis reaction. In fact the speed of conversion appears similar to that observed after the initial stages of the first catalysis reaction and after 1 hour of the second run, only 36% product conversion is observed.

4.2.5 Behaviour of (16) during catalysis

As well as obtaining accurate reaction yields and completion times, tracking the reaction by ^{1}H NMR spectroscopy also made it possible to follow the behaviour of **(16)** in solution during the catalysis. Study of the ^{1}H NMR spectra during a 5mol% **(16)** catalysed acylation of anisole in d^3-nitromethane at 50°C showed that from the point the catalysis reaction was initiated to the point of reaction completion a new indium carbene complex was present in solution. Observation of the ^{1}H NMR spectra show that this new complex which shall be termed complex **(X)** has the chemical shifts shown in table 6.

resonances	**chemical shifts**
olefin	7.78 (2H)
aromatic	7.19 (4H)
para-mesityl methyls	2.39 (6H)
ortho-mesityl methyls	2.19 (12H)
indium methyl	-0.14 (3H)

Table 6 : The resonances observed attributed to complex **(X)** in the ^{1}H NMR spectra in the **(16)** catalysed reaction of anisole in CD_3NO_2

Studies showed that unlike compounds **(7)**, **(11)**, **(13)** and **(15)** it is only when the three reagents: **(16)**, anisole and acetic anhydride are combined that **(X)** is formed. From the ^{1}H NMR spectroscopy, **(X)** is postulated to consist of a monomethylindium species bound to the carbene. No acidic proton resonance attributed to $(iMes)^+$ is observed suggesting the In-$C_{carbene}$ bond remains intact while the metal bound methyl resonance is observed at -0.14ppm slightly upfield of the respective resonance in **(16)** [+0.07ppm]. The ligands (L^1 and L^2 in Figure 8) are proposed to be either two acetates or a triflamide and an acetate (this is discussed further in section 4.2.3).

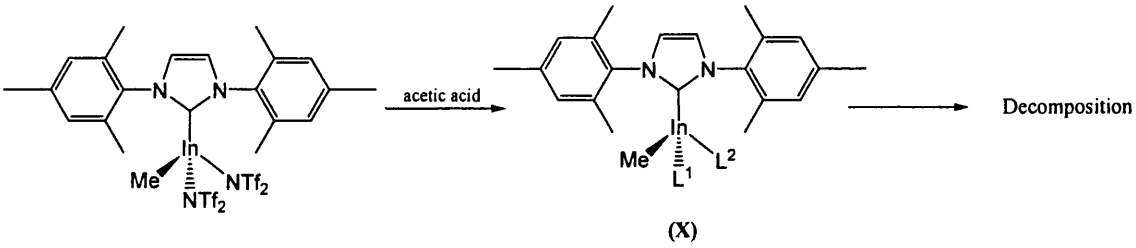

(X)

Figure 8 : Reaction of **(16)** to form **(X)** at the start of a catalysis reaction followed by decomposition (where L^1 = acetate, L^2 = triflamide or acetate)

^{1}H NMR spectroscopy shows that **(X)** starts to decompose extensively once the catalysis is complete. In fact within 2 hours of catalysis completion, the ^{1}H and ^{13}C NMR spectra show the presence of an imidazolium carbene cation (distinguished by its one proton triplet at ~8.6ppm) as well as several unknown unidentifiable decomposition products. Even removal of the solvent *in vacuo* as soon as the catalysis reaction is complete does not stop this decomposition. For this reason a ^{13}C NMR spectrum of **(X)** could not be obtained.

To determine if acetic acid (produced as a by-product in the catalysis reaction) could be responsible for the decomposition, studies of the reaction of **(16)** with acetic acid were carried out. Over two hours, **(16)** decomposed in the presence of the acid. First complex **(X)** was produced; this was followed by decomposition in the same manner as observed in the catalysis reactions to yield a group of unknown compounds and the protonated carbene cation $(iMes)^+$. A brief study of the reaction of **(16)** with sodium acetate also showed decomposition. In this case however, formation of complex **(X)** was not observed suggesting that the presence of acetic acid is vital to generate **(X)** (Figure 8).

4.2.6 $Me_2(CH_3COO)_2In(iMes)$, (17)

An investigation was conducted to ascertain how **(11)** behaves in the presence of acetic acid and to determine if this might yield further information on its behaviour in the presence of acetic anhydride as witnessed during catalysis screening. It was hoped this would also provide information about how acetate coordination to indium might occur. Studies showed that reaction of **(11)** with one to three equivalents of acetic acid resulted in the isolation of only one compound, a bismethyl, bisacetate indium complex coordinated to (iMes), **(17)** (Figure 9).

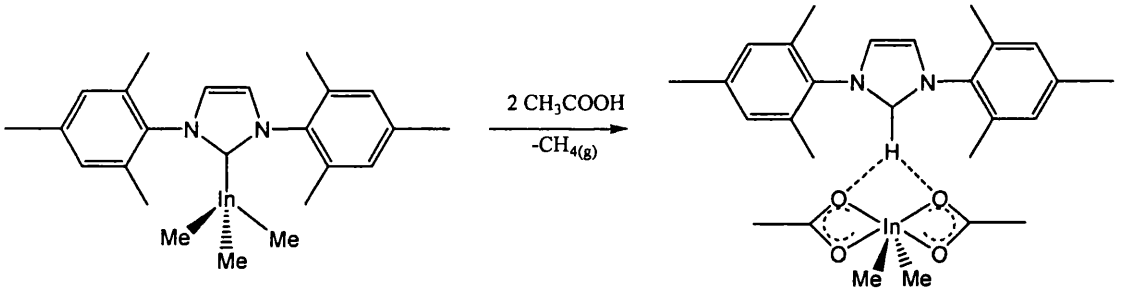

Figure 9 : Synthesis of **(17)** via reaction of **(11)** with two equivalents of acetic acid

The anticipated product had been a bisacetate complex similar to **(16)** where the carbene remains bound to a monomethyl indium species (Figure 10). This reaction, however, does not occur and we suggest instead the introduction of the first equivalent of acetic acid results in methane elimination to form an unstable bismethyl monoacetate indium carbene species. In the presence of a second equivalent of acetic acid, instead of another metal bound methyl substituent being abstracted, the carbene ligand is protonated off the indium centre to form the carbene cation. The second acetate meanwhile coordinates to the metal to form a 6-coordinate bismethyl bisacetate indium(III) anionic species which stabilises the carbene cation to give the air stable complex **(17)**.

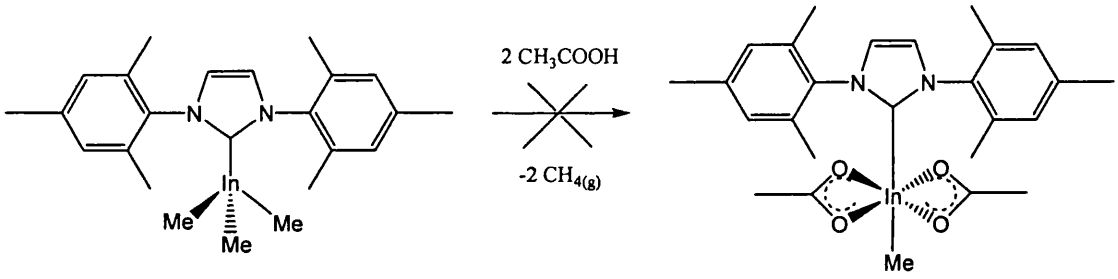

Figure 10 : Expected reaction of **(11)** with two equivalents of acetic acid

The methyl substitution and indium-$C_{carbene}$ bond cleavage occurred by protonolysis. Rapid evolution of methane gas was observed and confirmed by a singlet resonance in CD_2Cl_2 at 0.20ppm (the reaction was complete in five minutes). Complex **(17)** was produced and isolated in reasonable yield (72%) as a clear and colourless crystalline material by layering the dichloromethane reaction mixture with hexane and storing it at -20°C for 3 days. The crystals formed were suitable for X-ray crystallography and the solid state structure of **(17)** is shown in Figure 11 while Table 7 shows relevant bond lengths and angles. Complex **(17)** is monomeric in the solid state and no close intermolecular contacts to the indium (within 3.27Å) are observed. The N(1)-C(7)-N(2) bond angle [108.44°] is typical for imidazolium cations [~108°][56,57] and the carbene has no direct bonding interaction with the indium metal centre although hydrogen bonding between the indium species and the imidazolium cation is present. The molecule has C_2 symmetry and the indium adopts a 6-coordinate geometry with 4 short bonding contacts to the two methyl groups [2.1356(16)Å and 2.1324(17)Å] (which are the same within errors) and two of the oxygens of the acetate ligands [2.2128(10)Å and 2.2080(10)Å] (which are also the same within errors). It has two longer bonds with the remaining two oxygens of each acetate ligand [2.835Å and 2.845Å] lying well within the atomic radii for oxygen and indium [3.40Å].[58] The six coordinate indium(III) species sits directly below the carbene and the two methyl groups are opposite one another and occupy one plane aligned 37.3° out of the plane

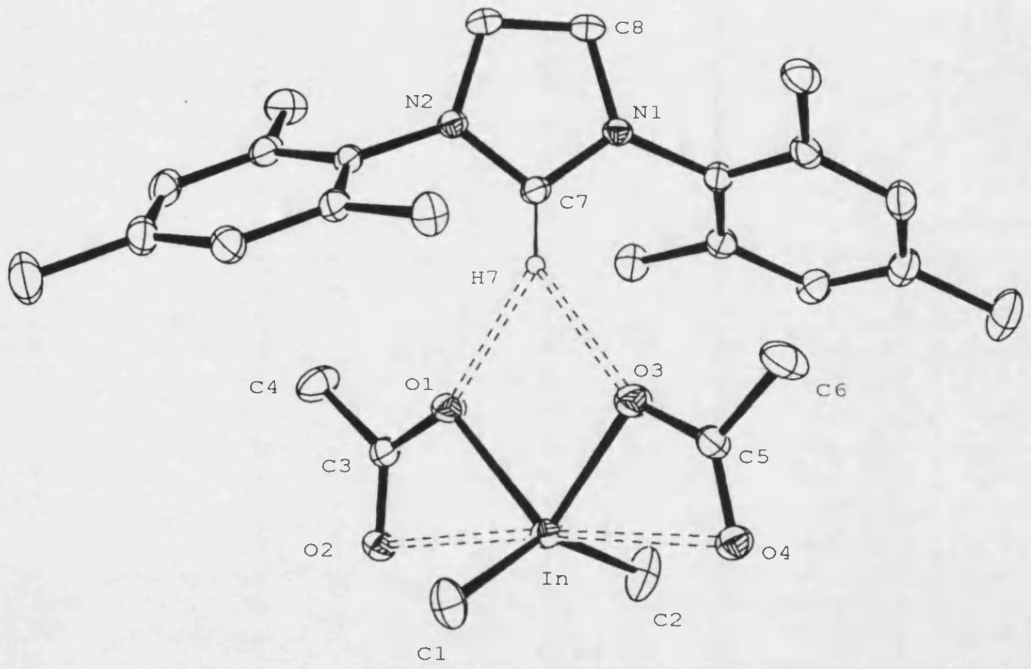

Figure 11 : Molecular structure of $Me_2(COOCH_3)_2In(iMes)$ (ellipsoids drawn at 30% probability level) excluding H(7) hydrogen atoms are omitted for clarity

In-C(1)	2.1356(16)	H(7)-O(1)	2.304	N(1)-C(7)-N(2)	108.44(12)	C(7)-N(1)-C(8)	108.90(11)
In-C(2)	2.1324(17)	H(7)-O(3)	2.328	C(1)-In-C(2)	142.88(9)	O(1)-C(3)-O(2)	123.12(13)
In-O(1)	2.2128(10)	N(1)-C(7)	1.3272(17)	C(1)-In-O(1)	104.39(6)	O(1)-C(3)-C(4)	116.48(13)
In-O(3)	2.2080(10)	N(1)-C(8)	1.3888(17)	C(1)-In-O(2)	90.14	O(2)-C(3)-C(4)	120.40(13)
In-O(2)	2.835	O(1)-C(3)	1.2817(17)	O(1)-In-O(2)	50.24	O(1)-H(7)-O(3)	80.36
In-O(4)	2.845	O(2)-C(3)	1.2380(16)	In-O(1)-H(7)	97.48		

Table 7 : Selected bond lengths (Å) and angles (°) for **(17)**

of the 5-membered heterocyclic ring. The acetate ligands are trans to one another and strongly hydrogen bond with the proton bound to the $C_{imidazolium}$ atom, the O•••H distances [2.304Å and 2.328Å] anchoring the imidazolium in place. Because the methyl groups of the acetate ligand point toward the carbene mesityl groups, the aromatic groups occupy a staggered geometry where they tilt in opposite directions from one another. This configuration minimises the steric repulsions between the methyl substituents of the cation and the acetate methyls of the anion.

In the ^{1}H NMR spectrum the resonance attributed to the acidic proton bound to the $C_{carbene}$ appears as a resonance at 9.94ppm and is a triplet due to ^{4}J coupling (1.4Hz) to the two protons on the olefin backbone of the 5-membered ring. The olefin protons appear as a 2H doublet at 7.65ppm where the multiplicity is caused by ^{4}J coupling (1.4Hz) to the acidic proton. The 4 aromatic protons are observed as a singlet at 7.11ppm. The methyl substituents of the mesityl rings appear as a 6H singlet at 2.39ppm and a 12H singlet at 2.16ppm while the methyl groups of the metal bound acetate ligands appear as a 6H singlet at 1.57ppm. Furthest upfield is the singlet resonance of the two metal bound methyl groups at -0.60ppm. The ^{13}C NMR spectrum of **(17)** shows the 11 carbon environments of the molecule and correlation spectroscopy proves that the quaternary carbons of the acetate ligands appears furthest downfield at 178.0ppm while the C-H peak appears at 139.9ppm the expected region for the C-H of imidazolium cations.[56,57] The acetate methyl resonance is observed at 23.1ppm while the metal bound methyl resonance is observed furthest upfield at -5.8ppm. Tests with **(17)** showed it was completely inactive as a catalyst in the acylation of anisole. Even after 2 weeks, **(17)** and the substrates remained in the solution unchanged.

4.2.7 Lewis vs Brønsted Acidity

It was important to determine the nature of the active species in the catalysis reactions involving **(16)** and see if it behaved as a Lewis or Brønsted acid during the reactions. Because a Brønsted acid is a protic acid by definition, a base will readily neutralise the acid. Therefore, introduction of a suitably hindered base would neutralise any protic acid present but would be too sterically hindered to interact with the Lewis acidic metal centre (as previously documented in some brief mechanistic studies of $Bi(OTf)_3$ and $Yb(OTf)_3$).[28,40] Interestingly introduction of 5mol% of the hindered base 2,6-di-tert-butylpyridine to a **(16)** catalysed acylation reaction shut down the catalysis completely and no product was observed after 24 hours. This was also found to be the case when the hindered base was added to a $In(OTf)_3$ catalysed acylation reaction. This study briefly unequivocally demonstrates that the catalytic process is clearly Brønsted acid promoted and not Lewis acid promoted. The stoichiometric addition of the hindered base to **(16)** shows that no chemical shift change is observed in the two reagents proving no coordination of the base to the indium centre occurs.

Tests were carried out using the protic acids H(OTf) and $H(NTf_2)$, as the catalysts in the absence of any indium reagent. These two acids proved extremely active as catalysts in the reaction and even outperformed $In(OTf)_3$. Figure 12 shows a comparison of the product conversions over time of H(OTf), $H(NTf_2)$, $In(OTf)_3$ and **(16)**.

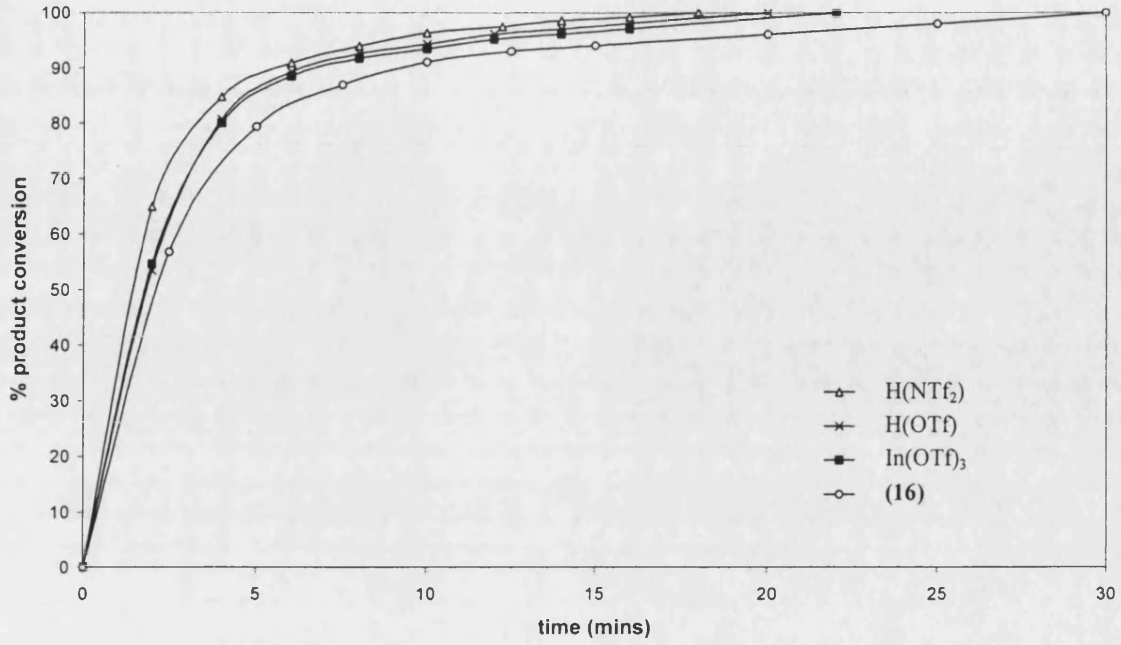

Figure 12 : Graph showing the comparable conversion times of the acylation of anisole catalysed by 5mol% $H(NTf_2)$, H(OTf), $In(OTf)_3$ and **(16)**

As the graph shows, $H(NTf_2)$ gives 100% yield in 18 minutes. This is closely followed by H(OTf) in 20 minutes, $In(OTf)_3$ in 22 minutes and **(16)** in 30 minutes. The plots of product conversion against reaction time for each catalyst show the rates of conversion to be very similar for all four systems. The introduction of hindered base in each case quenches each reaction immediately. From the graph it is clear that the metal is involved in the catalysis as the four different catalysts show different rates.

While H(OTf) and $H(NTf_2)$ have proved to be effective Brønsted acid catalysts in the acylation reactions, interestingly, perchloric, hydrochloric and acetic acid are all inactive as catalysts in the same acylation reactions. Inspection of pK_a values shows they are not as acidic as $H(NTf_2)$ or H(OTf) on the scale H(OTf) (-14) > $HClO_4$ (-10) > HCl (-8) > $H(OCOCH_3)$ (4.7). Unfortunately no pK_a value is available for $H(NTf_2)$, but gas phase acidity measurements have shown the enhanced acidity of $H(NTf_2)$

[ΔG_{acid} = 291.8 kcal/mol] over H(OTf) [ΔG_{acid} = 299.5 kcal/mol].[44] It is clear from these results that a very acidic proton is required for the catalysis to occur.

To ensure that the indium metal centre was not also directly acting as a Lewis acid catalyst in the preliminary stages of the acylation reactions to generate a proton, a further study was also carried out involving the reaction of a 1:1:1:1 ratio of substrate : acylating agent : **(16)** : hindered base. It was expected that if the Lewis acidic indium could coordinate and activate the acetic anhydride in the absence of a highly acidic protic species, then the reaction would still turnover once. However no catalysis reaction was observed by ^{1}H NMR spectroscopy.

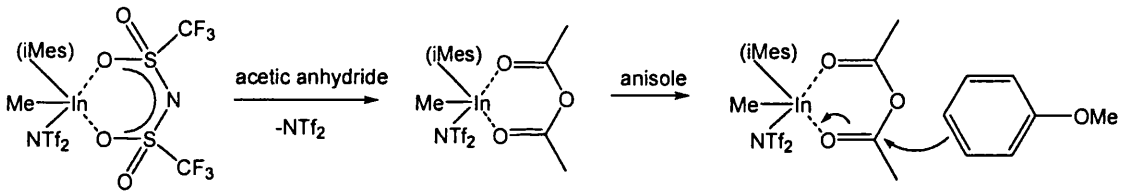

Figure 13 : Possible mechanism if the reaction was directly catalysed by the metal centre

In summation the most important points from our results are:

- The monotriflate/triflamide complexes [**(13)** and **(15)**] and complexes without triflate/triflamide ligands [**(7)**, **(11)**] are not active catalysts.
- The bistriflate/triflamide complexes **(14)** and **(16)** are active catalysts.
- Thus the catalysis reaction requires a strong Lewis acid and/or two vacant sites.
- The low solubility of **(14)** makes tracking its behaviour during catalysis difficult.
- Compound **(X)** is formed immediately in successful catalysis reactions where **(16)** is employed.

- The indium metal centre of **(X)** is unable to catalyse the reaction in the absence of a protic source.
- The catalysis reactions therefore require the generation/presence of a very strong acid to proceed.
- The presence of acetic acid ultimately results in the In-$C_{carbene}$ bond cleavage of **(16)** to form $(iMes)^+$ preventing its reuse or recycling.

4.3 Discussion

4.3.1 Mechanisms of the Reaction

In the case of the catalytically active complexes, our studies in Chapter 3 showed the metal bound methyl group in the monomethyl systems **(14)** and **(16)** could not be removed by introduction of a protic acid. However, in the case of the inactive systems, the bismethyl systems, **(7)**, **(13)** and **(15)**, one of the two metal-bound methyl groups can be readily removed by protonolysis. Tracking the catalysis reactions of **(7)**, **(13)** and **(15)** it was clear that methane elimination did not occur in any of the three reactions as observed by ^1H NMR spectroscopy. It is plausible therefore that these compounds have decomposed in a similar manner to that observed on addition of the second equivalent of acetic acid to **(17)**, which results in cleavage of the In-$C_{carbene}$ bond and $(iMes)^+$ formation. The reaction of compound **(11)** with acetic anhydride remains unclear by ^1H NMR spectroscopy and if time allowed would have been investigated in more detail. Whatever the products of the reaction are in that case, no methane elimination is observed, the In-$C_{carbene}$ bond remains intact and no catalytic activity is observed in the acylation reaction.

4.3.2 Lewis assisted Brønsted acidity

Our studies into the reaction of a 1:1:1:1 ratio of substrate : acylating agent : **(16)** : hindered base showed that the Lewis acidic indium metal centre of **(16)** was not directly responsible for the success of the catalysis reaction.

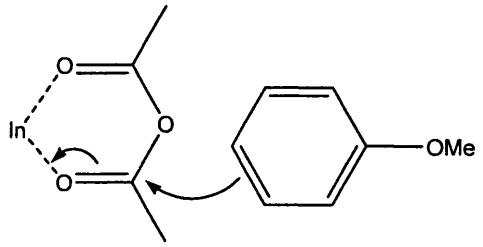

Figure 14 : Possible mechanism if the catalysis was initiated by acetic anhydride coordination to the metal

So if the reaction is not initiated by coordination of the acetic anhydride to the metal centre how does the reaction start? It is clear that compound **(X)** is formed from **(16)** instantaneously in the presence of both acetic anhydride and anisole. Studies have also shown complex **(X)** is formed instantaneously from the direct reaction of **(16)** and acetic acid. In both cases the existence of **(X)** is relatively short-lived and degrades to give principally $(iMes)^+$. In the catalysis run it is important to reiterate that the decomposition of **(X)** starts to occur only once the catalysis reaction is complete. It is likely that this **(X)** is the active species.

It would appear therefore that formation of **(X)** depends on the presence of acetic acid (earlier studies showed that neither a 1:1 mixture of acetic anhydride and **(16)** nor a 1:1 mixture of anisole and **(16)** gave **(X)**). Observation of the ^1H NMR spectrum of the purified acetic anhydride shows however that a residual acetic acid impurity (~1.0%) is present. Thus it is possible that compound **(X)** is formed in the presence of acetic anhydride but only in very small amounts (<1.0%) We postulate that **(X)** exists in one of the two forms shown in Figure 15 where coordination of one or two

molecules of acetic acid to the indium to form a chelate ring would result in a single or double triflamide substitution. The ^{1}H NMR spectra in our earlier studies showed that the proton from the acetic acid does not cause elimination of the single metal bound methyl group. The spectra show the methyl remains coordinated during catalysis and its chemical shift [-0.14ppm] appears slightly upfield of the metal bound methyl resonance in **(16)** [-0.04ppm]. This slight upfield chemical shift suggests that the Lewis acidity at the metal centre has not been significantly affected.

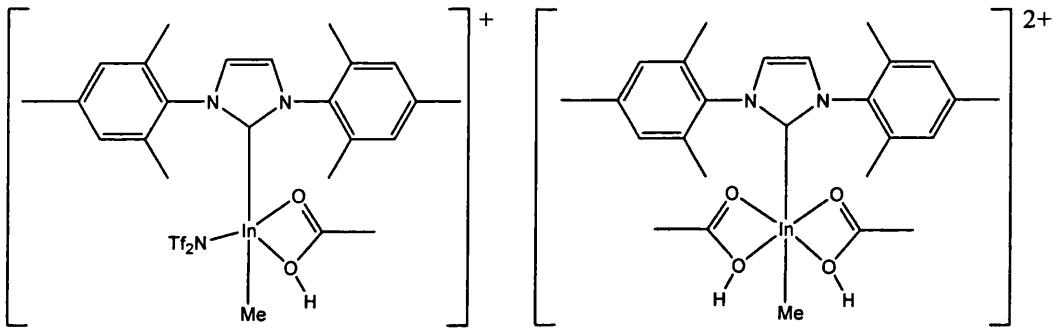

form **(I)** form **(II)**

Figure 15 : Two possible structures for complex **(X)**

For complex **(X)** to exist as form **(I)** or **(II)**, one or both triflamide ligands have to dissociate from the metal. A report involving the catalytic formation of calyx[4]resorcinanes by reaction of resorcinol with acetic acid using $Yb(OTf)_3$ as the catalyst speculates a similar situation exists where a triflate comes away from the metal so acetic acid can bind in its place. This forms a Lewis assisted Brønsted acid (Figure 16).[40]

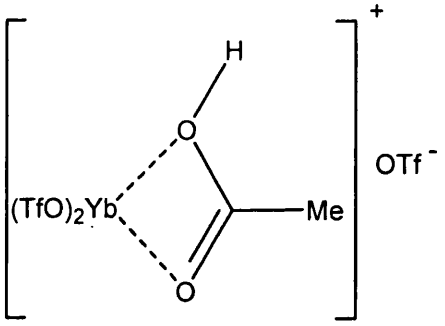

Figure 16 : Formation of a Lewis assisted Brønsted acid from the reaction of $Yb(OTf)_3$ with acetic acid

Coordination of the acid to the metal in our system would result in a marked increase in the Brønsted acidity of the acetic acid and this also means it is likely proton transfer can occur between coordinated acetic acid and free triflate resulting in a rapid equilibrium.[40] Thus it is possible an equilibrium exists for our system where the coordinated acetic acid in **(X)** can lose a proton resulting in $H(NTf_2)$ formation (Figure 17).

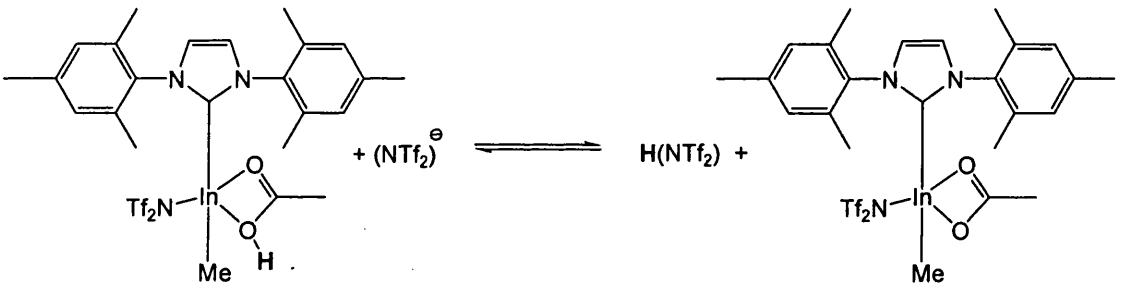

Figure 17 : Postulated equilibrium between complex **(X)** and $H(NTf_2)$ (**H** = proton being transferred)

At the start of the catalysis only a small amount of residual acetic acid impurity (from the acetic anhydride) is present but, once **(X)** and then $H(NTf_2)$ have been generated, the catalysis reaction can turn over rapidly generating more acetic acid by-product, resulting in formation of more of **(X)** until all of the **(16)** present has been converted. Our studies have shown that this is a fast process (complete in less than 2 minutes).

While $H(NTf_2)$ has been shown to be an active catalyst in the acylation reactions, the possibility that **(X)** could also be active cannot be discounted. For this to be the case our studies have shown that the Lewis assisted Brønsted acid would require a similar pK_a to that of H(OTf) [-14], but because **(X)** cannot be isolated, its acidity has not been determined.

The stability of complex **(X)** during the catalysis can perhaps be attributed to its involvement in catalysis. As long as both **(X)** and $H(NTf_2)$ are involved in catalysis the $In\text{-}C_{carbene}$ bond remains intact because the decomposition of **(X)** is sufficiently slow that the Brønsted acids are involved in the kinetically favourable catalytic cycle. Once the catalysis is complete however, intramolecular attack of $In\text{-}C_{carbene}$ bond by the acidic proton of the coordinated acetic acid in **(X)** can cause its cleavage via protonation of the carbene to form $(iMes)^+$.

4.4 Summary

Using predominantly compound **(16)**, which tests showed was our most catalytically active compound, it has been shown that a range of activated aromatic substrates can be readily acylated. The solubility of this system also made it possible to track the behaviour of **(16)** in solution during catalysis reactions via ^1H NMR spectroscopy. From monitoring catalysis reactions and further experimental investigation we were able to determine that the catalysis reactions occur via an acid-catalysed mechanism. Our studies suggest that a Lewis assisted Brønsted acid, complex **(X)** plays an important part in the reaction. Dissociation of a triflamide ligand from the metal centre followed by coordination of acetic acid to form a chelate, enhances the acidity of the acetic acid. The acid is then able to transfer its proton to the triflamide anion to

form $H(NTf)_2$ which is acidic enough to promote catalysis itself. While $H(NTf)_2$ and has been shown to be an effective catalyst in the reaction in the absence of indium due to its high acidity, the acetic acid chelate will also be active if its pKa ~ -14.

4.5 References

(1) Friedel, C.; Crafts, J. M. *Comptes Rendus de l'Académie des Sciences - Series IIC - Chemistry* **1877**, *84*, 1450.
(2) Olah, G. A. *Friedel-Crafts and Related Reactions*; Wiley-Interscience: New York, 1964.
(3) Olah, G. A. *Friedel-Crafts Chemistry*; Wiley-Interscience: New York, 1973.
(4) Heaney, H.; Trost, B. M., Ed.; Pergamon Press: Oxford, 1991; Vol. 2, Chap. 3.2.
(5) Taylor, R. *Electrophilic Aromatic Substitution*; Wiley-Interscience: Chichester, 1990.
(6) Olah, G. A.; Reddy, V. P.; Prakash, G. K. S. *Encyclopedia of Chemical Technology*; 4th ed.; Wiley: New York, 1994.
(7) Lombardino, G. J. *Non-Steroidal Anti-Inflammatory Drugs*; Wiley-Interscience: New York, 1985.
(8) Harrison, I. T.; Lewis, B.; Nelson, P.; Rooks, W.; Roszkowski, A.; Tomolinos, A.; Fried, J. H. *J. Med. Chem.* **1970**, *13*, 203.
(9) Jordan, V. C. *Breast Cancer Res. Tr.* **1983**, *2*, 73.
(10) Willson, T. M.; Brown, P. J.; Sternbach, D. D.; Henke, B. R. *J. Med. Chem.* **2000**, *43*, 527.
(11) Pearson, D. E.; Buehler, C. A. *Synthesis* **1972**, 533.
(12) Cornelis, A.; Gerstmans, A.; Laszlo, P.; Mathy, A.; Zieba, I. *Catal. Lett.* **1990**, *6*, 103-110.
(13) Cornelis, A.; Laszlo, P.; Wang, S. *Tetrahedron Lett.* **1993**, *34*, 3849-3852.
(14) Clark, J. H.; Cullen, S. R.; Barlow, S. J.; Bastock, T. W. *J. Chem. Soc.-Perkin Trans. 2* **1994**, 1117-1130.
(15) Mukaiyama, T.; Ohno, T.; Nishimura, T.; Suda, S.; Kobayashi, S. *Chem. Lett.* **1991**, 1059-1062.
(16) Laporte, C.; Marquie, J.; Laporterie, A.; Desmurs, J. R.; Dubac, J. *Comptes Rendus Acad. Sci. Ser. II C* **1999**, *2*, 455-465.
(17) Marquie, J.; Laporte, C.; Laporterie, A.; Dubac, J.; Desmurs, J. R.; Rogues, N. *Ind. Eng. Chem. Res.* **2000**, *39*, 1124-1131.
(18) Ohta, S.; Kimoto, S. *Tetrahedron Lett.*, *16*, 2279-2282.
(19) Macdowell, D. W. H.; Patrick, T. B. *J. Org. Chem.* **1967**, *32*, 2441.
(20) Poirier, Y. *Bull. Soc. Chim Fr.* **1963**, 1523.
(21) Olah, G. A. *Angew. Chem.-Int. Edit. Engl.* **1993**, *32*, 767-788.
(22) Yato, M.; Ohwada, T.; Shudo, K. *J. Am. Chem. Soc.* **1991**, *113*, 691-692.
(23) Sato, Y.; Yato, M.; Ohwada, T.; Saito, S.; Shudo, K. *J. Am. Chem. Soc.* **1995**, *117*, 3037-3043.
(24) Effenberger, F.; Epple, G. *Angew. Chem.-Int. Edit. Engl.* **1972**, *11*, 300.
(25) Effenberger, F.; Sohn, E.; Epple, G. *Chem. Ber.-Recl.* **1983**, *116*, 1195-1208.
(26) Effenberger, F.; Eberhard, J. K.; Maier, A. H. *J. Am. Chem. Soc.* **1996**, *118*, 12572-12579.
(27) Izumi, J.; Mukaiyama, T. *Chem. Lett.* **1996**, 739-740.
(28) Le Roux, C.; Dubac, J. *Synlett* **2002**, 181-200.
(29) Mukaiyama, T.; Nagaoka, H.; Ohshima, M.; Murakami, M. *Chem. Lett.* **1986**, 165-168.

(30) Ishii, Y.; Takeno, M.; Kawasaki, Y.; Muromachi, A.; Nishiyama, Y.; Sakaguchi, S. *J. Org. Chem.* **1996**, *61*, 3088-3092.
(31) Tashiro, D.; Kawasaki, Y.; Sakaguchi, S.; Ishii, Y. *J. Org. Chem.* **1997**, *62*, 8141-8144.
(32) Hartley, J. P., PhD Thesis, University of Bath, 2002.
(33) Haszeldine, R. N.; Kidd, J. M. *J. Chem. Soc.* **1954**, 4228.
(34) Olah, G. A.; Farooq, O.; Farnia, S. M. F.; Olah, J. A. *J. Am. Chem. Soc.* **1988**, *110*, 2560-2565.
(35) Kawada, A.; Mitamura, S.; Kobayashi, S. *J. Chem. Soc.-Chem. Commun.* **1993**, 1157-1158.
(36) Kawada, A.; Mitamura, S.; Kobayashi, S. *Synlett* **1994**, 545-546.
(37) Kawada, A.; Mitamura, S.; Kobayashi, S. *Chem. Commun.* **1996**, 183-184.
(38) Singh, R. P.; Kamble, R. M.; Chandra, K. L.; Saravanan, P.; Singh, V. K. *Tetrahedron* **2001**, *57*, 241-247.
(39) Mikami, K.; Kotera, O.; Motoyama, Y.; Sakaguchi, H.; Maruta, M. *Synlett* **1996**, 171-172.
(40) Barrett, A. G. M.; Braddock, D. C.; Henschke, J. P.; Walker, E. R. *J. Chem. Soc.-Perkin Trans. 1* **1999**, 873-878.
(41) Matsuo, J.; Odashima, K.; Kobayashi, S. *Synlett* **2000**, 403-405.
(42) Ruff, J. K. *Inorg. Chem.* **1965**, *4*, 1446.
(43) Meussdorffer, J. N.; Niederprum, H. *Chemiker Ztg.* **1972**, *96*, 582.
(44) Koppel, I. A.; Taft, R. W.; Anvia, F.; Zhu, S. Z.; Hu, L. Q.; Sung, K. S.; Desmarteau, D. D.; Yagupolskii, L. M.; Yagupolskii, Y. L.; Ignatev, N. V.; Kondratenko, N. V.; Volkonskii, A. Y.; Vlasov, V. M.; Notario, R.; Maria, P. C. *J. Am. Chem. Soc.* **1994**, *116*, 3047-3057.
(45) Foropoulos, J.; Desmarteau, D. D. *Inorg. Chem.* **1984**, *23*, 3720-3723.
(46) Cossy, J.; Lutz, F.; Alauze, V.; Meyer, C. *Synlett* **2002**, 45-48.
(47) Kobayashi, H.; Nie, J.; Sonoda, T. *Chem. Lett.* **1995**, 307-308.
(48) Ishihara, K.; Kubota, M.; Yamamoto, H. *Synlett* **1996**, 265-&.
(49) Ishihara, K.; Karumi, Y.; Kubota, M.; Yamamoto, H. *Synlett* **1996**, 839-&.
(50) Ishihara, K.; Hiraiwa, Y.; Yamamoto, H. *Synlett* **2000**, 80-82.
(51) Grieco, P. A.; Handy, S. T. *Tetrahedron Lett.* **1997**, *38*, 2645-2648.
(52) Earle, M. J.; Hakala, U.; McAuley, B. J.; Nieuwenhuyzen, M.; Ramani, A.; Seddon, K. R. *Chem. Commun.* **2004**, 1368-1369.
(53) Chauhan, K. K.; Frost, C. G.; Love, I.; Waite, D. *Synlett* **1999**, 1743-1744.
(54) Frost, C. G.; Hartley, J. P.; Griffin, D. *Tetrahedron Lett.* **2002**, *43*, 4789-4791.
(55) Chauhan, K. K., PhD Thesis, University of Bath, 2002.
(56) Arduengo, A. J.; Dias, H. V. R.; Calabrese, J. C.; Davidson, F. *J. Am. Chem. Soc.* **1992**, *114*, 9724-9725.
(57) Arduengo, A. J.; Dias, H. V. R.; Harlow, R. L.; Kline, M. *J. Am. Chem. Soc.* **1992**, *114*, 5530-5534.
(58) Bondi, A. *J. Phys. Chem.* **1964**, *68*, 441-451.
(59) Furstner, A.; Voigtlander, D.; Schrader, W.; Giebel, D.; Reetz, M. T. *Org. Lett.* **2001**, *3*, 417-420.

Chapter 5 - Experimental

5.1 Experimental Techniques

5.1.1 General

All manipulations unless otherwise stated were performed under an argon or nitrogen atmosphere, using standard Schlenk-line and glove-box techniques. Glassware was oven dried at 130°C overnight and flamed under vacuum three times before use. CH_2Cl_2 and MeCN were distilled from CaH_2. Toluene, hexane, diethyl ether and THF were distilled from sodium-benzophenone-ketyl. C_6D_6 was dried over a potassium mirror; CD_2Cl_2 and CD_3NO_2 were distilled under vacuum from CaH_2. Microanalyses were performed by Mr Alan Carver (University of Bath Microanalytical Service) and Mass spectrometry were performed by Mr Chris Cryer (University of Bath Mass Spectrometry Service). Mass spectrometry analyses were carried out on all compounds but for each compound the ions found were not consistent with the molecular ion.

5.1.2 NMR Spectroscopy

^1H, ^{19}F, $^{13}C\{^1H\}$ spectra were recorded on a Bruker Avance 400MHz and Bruker Avance 300MHz spectrometers. Residual protio solvent was used as reference for ^1H NMR spectra (CD_2Cl_2: $\delta = 5.33$, C_6D_6: $\delta = 7.16$, CD_3NO_2: $\delta = 4.33$, $C_6D_5CD_3$: $\delta = 7.09$) and ^{13}C spectra (CD_2Cl_2: $\delta = 54.0$, C_6D_6: $\delta = 128.7$, CD_3NO_2: $\delta = 62.8$, $C_6D_5CD_3$: $\delta = 128.3$). ^{19}F NMR spectra were referenced to external $CFCl_3$. Values are quoted in ppm.

5.1.3 Crystallographic Studies

Crystallographic measurements for all structures were recorded on a Nonius KappaCCD diffractometer with $Mo_{K\alpha}$ radiation (0.71073 Å). Structure solution followed by full-matrix least-squares refinement was performed by using the SHELX suite of programs throughout. Hydrogens were included in calculated positions unless otherwise stated.

5.2 Syntheses and Characterisation

5.2.1 Starting Materials

The Schiff bases 4-phenylaminopent-3-ene-2-one,[4-6] 1-phenyl-4-phenylaminopent-3-ene-2-one,[6] 4-(S-methylbenzyl)aminopent-3-ene-2-one,[7] 4-(2,6-diisopropylphenyl) aminopent-3-ene-2-one,[8] and complex $Me_2Indipp_2nacnac$,[9] were synthesized by published methods. The starting materials (iMes)Cl, free (iMes),[1] (iPr)Cl and free (iPr),[2] $(iMesH_2)Cl$[2] and $(CN(Pr^i)C_2Me_2NPr^i)$[3] were all prepared by previously published methods. All other chemicals were used as purchased from Aldrich, Acros, Avocado, Fisher, Fluka or Strem chemicals.

5.2.2 Syntheses

Satisfactory microanalyses on all indium bis methyl compounds coordinated to Schiff bases and their derivatives were unobtainable, consistently being low in carbon and hydrogen by two methyl groups despite repeated attempts with pure crystalline samples. Satisfactory mass spectrometry data on all compounds reported was unobtainable despite repeated attempts with pure crystalline samples.

$[Me_2In\{N[C_6H_5]C(CH_3)CHC(CH_3)\mu\text{-}O\}]_2$, (1): $InMe_3$ (1.150 g, 7.19 mmol) and $HN[C_6H_5]C(CH_3)CHC{=}O(CH_3)$ (1.145 g, 6.53 mmol) were stirred in 15 ml toluene

for 2 hrs. Methane gas evolution was observed. The solvent was removed *in vacuo*. The product was then dissolved up in hot hexane and stored at 277K. After 3 hrs clear and colourless crystals had formed (1.605 g, 5.03 mmol)

Yield: 78 %.

δ^1H (295K, C_6D_6): 6.96-7.04 (2H, m, *J* cannot be determined, aromatics), 6.86 (1H, tt, ^1J = 7.4Hz, ^2J = 1.4Hz, aromatics), 6.65-6.70 (2H, m, *J* cannot be determined, aromatics), 4.82 (1H, s, CH in chelate ring), 1.97 (3H, s, CH_3), 1.45 (3H, s, CH_3), 0.03 (6H, s, $InMe_2$)

δ^1H (295K, CD_2Cl_2): 7.36 (2H, tt, ^1J = 7.9Hz, ^2J = 1.9Hz, aromatics), 7.19 (1H, tt, ^1J = 7.5Hz, ^2J = 1.4Hz, aromatics), 6.89 (2H, dt, ^1J = 7.3Hz, ^2J = 1.4Hz, aromatics), 4.96 (1H, s, CH in chelate ring), 1.97 (3H, s, CH_3), 1.77 (3H, s, CH_3), -0.23 (6H, s, $InMe_2$)

δ^{13}C{^{1}H} (295K, C_6D_6): 184.9, 171.6, 149.0, 130.4, 125.9, 124.6, 98.3, 28.7, 23.5, -6.0

$Me_2In\{N[C_6H_5]C(CH_3)CHC(C_6H_5)\mu$-O}, (2): $InMe_3$ (120 mg, 0.93 mmol) and $HN[C_6H_5]C(CH_3)CHC{=}O(C_6H_5)$ (200 mg, 0.84 mmol) were stirred in 5 ml toluene for 2 hrs. Methane gas evolution was observed. The solvent was removed *in vacuo*. The product was then dissolved up in hot hexane and stored at 277K. After 4 days clear and pale yellow crystals had formed (230 mg, 0.60 mmol)

Yield: 72 %.

δ^1H (295K, C_6D_6): 7.99 (2H, m, *J* = 7.7Hz, aromatics), 7.10-7.20 (3H, m, *J* cannot be determined, aromatics), 6.98 (2H, t, *J* = 7.7Hz, aromatics), 6.83 (1H, tt, ^1J = 7.4Hz, ^2J = 1.1Hz, aromatics), 6.65 (2H, m, *J* cannot be determined, aromatics), 5.58 (1H, s, CH in chelate ring), 1.49 (3H, s, CH_3), 0.00 (6H, s, $InMe_2$)

δ^1H (298K, CD_2Cl_2): 7.82-7.88 (2H, m, *J* cannot be determined, aromatics), 7.36-7.44 (3H, m, *J* cannot be determined, aromatics), 7.23 (1H, tt ^3J = 7.5Hz, ^4J = 1.2Hz, aromatic), 6.97(2H, m, *J* cannot be determined, aromatics), 5.66 (1H, s, CH in chelate ring), 1.93 (3H, s, CH_3), -0.14 (6H, s, $InMe_2$)

$\delta^{13}C\{^1H\}$ (298K, CD_2Cl_2): 177.9, 172.9, 148.4, 141.6, 130.4, 130.1, 128.6, 127.4, 125.9, 124.1, 95.9, 24.0, -6.9

$\delta^{13}C\{^1H\}$ (295K, C_6D_6): 179.0, 172.8, 148.9, 142.1, 130.9, 130.4, 129.0 128.2, 126.1, 124.4, 96.4, 24.0, -6.1

$[Me_2In\{OC(CH_3)CHC(C_6H_5)\mu\text{-}O\}]_2$, (3): $InMe_3$ (325 mg, 2.03 mmol) and $OC(CH_3)CHC{=}O(C_6H_5)$ (300 mg, 1.85 mmol) were stirred in 10 ml toluene for 2 hrs. Methane gas evolution was observed. The solvent was removed *in vacuo*. The product was then dissolved up in hot hexane and stored at 277K overnight. Colourless crystals formed (396 mg, 1.294 mmol).

Yield: 70 %.

δ^1H (295K, CD_2Cl_2): 7.82-7.88 (2H, m, *J* cannot be determined, aromatics), 7.38-7.53 (3H, m, *J* cannot be determined, aromatics), 5.99 (1H, s, CH in chelate ring), 2.14 (3H, s, CH_3), 0.02 (6H, s, $InMe_2$)

δ^1H (295K, C_6D_6): 7.85 (2H, m, *J* cannot be determined, aromatics), 7.06-7.18 (3H, m, *J* cannot be determined, aromatics), 5.84 (1H, s, CH in chelate ring), 1.84 (3H, s, methyl), 0.10 (6H, s, $InMe_2$)

$\delta^{13}C\{^1H\}$ (295K, CD_2Cl_2): 194.4, 185.6, 140.1, 131.9, 128.8, 127.9, 97.6, 29.4, -4.5

$Me_2In\{N[S\text{-}CH(CH_3)C_5H_6]CHC(C_6H_5)\mu\text{-}O\}$, (4): $InMe_3$ (225 mg, 1.41 mmol) and $HN[S\text{-}CH(CH_3)C_5H_6]CHC{=}O(C_6H_5)$ (340 mg, 1.28 mmol) stirred in 5 ml toluene overnight. Methane gas evolution was observed. The solvent was removed *in vacuo* to yield a yellow oil (503 mg, 1.23 mmol). Attempts to grow crystals suitable for X-ray diffraction were unsuccessful.

Yield: 95 %.

δ^1H (295K, CD_2Cl_2): 7.82-7.85 (2H, m, J = cannot be determined, aromatics), 7.34-7.48 (8H, m, J = cannot be determined, aromatics), 5.56 (1H, s, CH in chelate ring), 5.11 (1H, q, J = 6.7Hz, CH in chiral group), 2.25 (3H, s, CH_3), 1.67 (3H, d, J = 6.7Hz, CH_3 in chiral group), -0.08 (3H, s, InMe), -0.55 (3H, s, InMe)

$\delta^{13}C\{^1H\}$ (295K, CD_2Cl_2): 176.3, 172.3, 142.5, 141.7, 130.1, 129.5, 128.6, 128.5, 128.1, 127.3, 96.7, 58.7, 23.7, 21.5, -4.6, -6.7

$[Cl_2In\{N[o\text{-}C_6H_3(^iPr)_2]C(CH_3)CHC(CH_3)\mu\text{-}O\}]_2{\cdot}C_6H_5CH_3$, (5): The compounds $(Et_2O)_2Li\{N[o\text{-}C_6H_3(^iPr)_2]C(CH_3)CHC(CH_3)\mu\text{-}O\}$ (200 mg, 0.563 mmol) and excess $InCl_3$ (174 mg, 0.789 mmol) were stirred in 5 ml toluene at 130°C for 48 hours. The mixture was filtered via cannula whilst hot and the filtrate was allowed to cool upon which clear and colourless crystals formed (90 mg, 0.062 mmol).

Yield: 36 %.

δ^1H (295K, CD_2Cl_2): δ = 7.14-7.35 (11H, overlapped, aromatics), 5.41 (1H, s, CH in chelate ring), 2.91 (4H, septet, J = 6.8Hz, CH isopropyl), 2.41 (6H, s, methyl), 2.35 (3H, s, tolene methyl), 1.85 (6H, s, methyl), 1.26 (12H, d, J = 6.8Hz, CH_3 isopropyl), 1.14 (12H, d, J = 6.8Hz, CH_3 isopropyl)

$\delta^{13}C\{^1H\}$ (295K, CD_2Cl_2): 181.4, 178.0, 142.1, 140.8, 138.5, 127.5, 128.7, 128.5, 126.0, 125.0, 102.9, 29.0, 28.3, 26.0, 24.7, 24.5

Elemental Analysis: Calcd (%) for $C_{41}H_{52}N_2O_2Cl_4In_2$: C 50.44, H 5.37, N 2.87; found C 49.6, H 5.69, N 2.76

$Me_2ClIn(iMes)$, (7): $InMe_3$ (387 mg, 2.42 mmol) and (iMes)Cl (750 mg, 2.20 mmol) were stirred in 15 ml toluene at ambient temperature overnight. The solvent volume was reduced to half volume and stored at 277K overnight to yield a batch of clear and colourless crystals. The crystals were removed and the remaining solution was re-cooled to 277K for further recrystallisation. This was repeated 3 times (or until no further crystals were formed) (885 mg, 1.82 mmol).

Yield: 83 %.

Alternative synthetic route: A Schlenk was charged with $InCl_3$ (200 mg, 0.90 mmol). THF (15 ml) was added via cannula and stirred at 195K. 1.6 M MeLi in ether (1.7 ml, 2.72 mmol) was added via syringe and the mixture was stirred at 195K for 1hr and then allowed to warm to ambient temperature. The cloudy solution was added via cannula directly to (iMes)Cl (308 mg, 0.90 mmol) and stirred for a further hour to leave a yellow liquid/brown precipitate. The mixture was filtered and the filtrate dried in vacuo, taken in toluene and filtered again. This second filtrate volume was reduced and stored at 277K overnight to yield a batch of pale yellow crystals. This was repeated 3 times (or until no further crystals were formed) (295 mg, 0.61 mmol).

Yield: 67 %

δ^1H (298K, CD_2Cl_2): 7.19 (2H, s, olefin), 7.05 (4H, s, aromatic), 2.37 (6H, s, Me), 2.12 (12H, s, Me), -1.03 (6H, s, In-Me)

δ^1H (298K, C_6D_6): 6.73 (4H, s, aromatic), 6.05 (2H, s, olefin), 2.08 (6H, s, Me), 2.04 (12H, s, Me), -0.54 (6H, s, In-Me)

$\delta^{13}C\{^1H\}$ (298K, CD_2Cl_2): 177.5, 140.5, 136.0, 134.9, 129.8, 124.3, 21.4, 18.0, -8.1

$\delta^{13}C\{^1H\}$ (298K, C_6D_6): 179.0, 140.5, 136.1, 135.5, 130.3, 123.8, 21.7, 18.4, -7.2

Elemental Analysis: Calcd (%) for $C_{23}H_{30}ClInN_2$: C, 56.99; H, 6.24; N, 5.78 Found: C, 57.20; H, 6.21; N, 5.66

$Me_2ClIn(^iPr)$, (8): $InMe_3$ (103 mg, 0.64 mmol) and (^{i}Pr)Cl (200 mg, 0.57 mmol) were stirred in 10 ml toluene at ambient temperature overnight. The solvent volume was reduced to half volume and stored at 277K overnight to yield a batch of clear and colourless crystals. The crystals were removed and the remaining solution was re-cooled to a temperature of 277K for further recrystallisation. This was repeated 3 times (or until no further crystals were formed) (287 mg, 0.50 mmol).

Yield: 86 %

δ^1H (298K, CD_2Cl_2): 7.54 (2H, t, J = 7.5Hz, aromatics), 7.37 (4H, d, J = 7.5Hz, aromatics), 7.28 (2H, s, olefin), 2.67 (4H, septet, J = 6.8Hz, CH isopropyl), 1.33 (12H, d, J = 6.8Hz, CH_3 isopropyl), 1.17 (12H, d, J = 6.8Hz, CH_3 isopropyl), -1.08 (6H, s, $InMe_2$)

δ^1H (203K, CD_2Cl_2): 7.51 (2H, t, J = 7.8Hz, aromatics), 7.37 (4H, d, J = 7.8Hz, aromatics), 7.33 (2H, s, olefin), 2.48 (4H, septet, J = 6.4Hz, CH isopropyl), 1.19 (12H, d, J = 6.4Hz, CH_3 isopropyl), 1.08 (12H, d, J = 6.4Hz, CH_3 isopropyl), -1.32 (6H, s, $InMe_2$)

$\delta^{13}C\{^1H\}$ (298K, CD_2Cl_2): 179.7, 146.5, 134.8, 131.3, 125.6, 124.7, 29.2, 26.0, 23.4, -7.4

Elemental Analysis: Calcd (%) for $C_{29}H_{42}ClInN_2$: C, 61.22; H, 7.44; N, 4.92; Found: C, 60.6; H, 7.36; N, 4.75

$Me_2BrIn(iMes)$, (9): $InMe_3$ (50 mg, 0.31 mmol) and (iMes)Br (110 mg, 0.29 mmol) were stirred in 15 ml toluene at ambient temperature overnight. The solvent volume was reduced to half volume and the solution stored at 277K overnight to yield a batch of clear and colourless crystals. The crystals were removed and the remaining solution was returned to a temperature of 277K for further recrystallisation. This was repeated 3 times (or until no further crystals were formed) (113 mg, 0.21 mmol)

Yield: 75%.

δ^1H (298K, C_6D_6): 6.73 (4H, s, aromatic), 5.99 (2H, s, olefin), 2.08 (6H, s, Me), 2.04 (12H, s, Me), -0.44 (6H, s, In-Me)

$\delta^{13}C\{^1H\}$ (298K, C_6D_6): 177.9, 140.6, 136.1, 135.4, 130.3, 123.7, 21.7, 18.6, -6.6

Elemental Analysis: Calcd (%) for $C_{23}H_{30}BrInN_2$: C, 52.20; H, 5.71; N, 5.29 Found C, 51.8; H, 5.72; N, 5.57

$Me_2ClIn(iMesH_2)$, (10): $InMe_3$ (52 mg, 0.325 mmol) and ($iMesH_2$)Cl (100 mg, 0.29 mmol) were stirred in 5 ml toluene at ambient temperature overnight. The solvent volume was reduced to half volume the solution was stored at 277K overnight to yield a batch of clear and colourless crystals. (15 mg, 0.03 mmol)

Yield: 9 %.

δ^1H (298K, C_6D_6): 6.74 (4H, s, aromatics), 2.98 (4H, s, saturated backbone), 2.24 (6H, s, *p*-Me), 2.07 (12H, s, *o*-Me), -0.58 (6H, s, $InMe_2$)

Elemental Analysis: Calcd (%) for $C_{23}H_{32}ClInN_2$: C, 56.75; H, 6.63; N, 5.75 Found C, 56.87; H, 6.70; N, 5.66

Me_3In(iMes), (11): $InMe_3$ (209 mg, 1.31 mmol) and free (iMes) (400 mg, 1.31 mmol) were stirred in 15 ml toluene at ambient temperature overnight. The solvent was removed in vacuo. The compound was recrystallised from miniumum Et_2O and stored at 253K overnight to yield a batch of clear and colourless crystals. The crystals were removed and the remaining solution was returned to a temperature of 253K for further recrystallisation. This was repeated 3 times (or until no further crystals were formed) (438 mg, 0.94 mmol).

Yield: 72%.

Alternative synthetic route: A Schlenk was charged with $InCl_3$ (200 mg, 0.90 mmol). THF (15 ml) was added via cannula and the mixture was stirred at 195K. 1.6 M MeLi in ether (1.7 ml, 2.72 mmol) was added via syringe and the mixture was stirred at 195K for 1hr and then allowed to warm to ambient temperature. The cloudy solution was added via cannula directly to a Schlenk charged with free (iMes) (277 mg, 0.90 mmol) and this was stirred for a further hour to leave a brown liquid/brown precipitate. The mixture was filtered and the filtrate dried in vacuo, taken in Et_2O and filtered again. This second brown filtrate volume was reduced and stored at 253K overnight to yield a batch of colourless crystals. This was repeated 3 times (or until no further crystals were formed) (248mg, 0.53mmol).

Yield: 59%

δ^1H (298K, CD_2Cl_2): 7.12 (2H, s, olefin), 7.05 (4H, s, aromatic), 2.38 (6H, s, Me), 2.08 (12H, s, Me), -1.26 (9H In-Me)

δ^1H (298K, C_6D_6): 6.77 (4H, s, aromatic), 6.04 (2H, s, olefin), 2.10 (6H, s, Me), 1.99 (12H, s, Me), -0.53 (9H In-Me)

δ^1H (298K, toluene-d^8): 6.74 (4H, s, aromatic), 6.10 (2H, s, olefin), 2.10 (6H, s, Me), 1.98 (12H, s, Me), -0.68 (9H In-Me)

$\delta^{13}C\{^1H\}$ (298K, CD_2Cl_2): 183.0, 139.8, 135.9, 135.8, 129.5, 123.7, 21.4, 17.9, -11.8

$\delta^{13}C\{^1H\}$ (298K, C_6D_6): 184.8, 140.0, 136.2, 136.0, 130.1, 123.2, 21.7, 18.3, -10.3

$\delta^{13}C\{^1H\}$ (298K, C_6D_6): 184.8, 139.7, 136.0, 135.7, 129.8, 122.9, 21.4, 18.0, -10.5

Elemental Analysis: Calcd (%) for $C_{24}H_{33}InN_2$: C, 62.08; H, 7.16; N, 6.03 Found: C, 61.8; H, 7.05; N, 6.00

$Me_3In(CN(^iPr)C_2Me_2{}^iPr)$, (12): $InMe_3$ (200 mg, 1.25 mmol) and $(CN(^iPr)C_2Me_2{}^iPr)$ (225 mg, 1.25 mmol) were stirred in 10 ml toluene at ambient temperature overnight. The solvent was removed in vacuo to yield a white crystalline solid. Attempts to grow crystals suitable for X-ray diffraction were unsuccessful (383 mg, 1.125 mmol).

Yield: 90 %

δ^1H (298K, C_6D_6): 5.15 (2H, septet, J = 7.1Hz, $CH_{isopropyl}$), 1.56 (6H, s, Me), 1.09 (12H, d, J = 7.1Hz, $CH_{3isopropyl}$), 0.02 (9H, s, In-Me)

$\delta^{13}C\{^1H\}$ (298K, C_6D_6): 180.1, 126.0, 53.3, 22.6, 10.6, -5.6

Elemental Analysis: Calcd (%) for $C_{14}H_{29}InN_2$: C, 49.43; H, 8.59; N, 8.23 Found: C, 49.21; H, 8.47; N, 8.15

$Me_2(OTf)In(iMes)$, (13): A Young's tube was charged with $Me_2ClIn(iMes)$ (50 mg, 0.11 mmol) and CH_2Cl_2 (5ml) added via cannula. TMS(OTf) (20 μl, 0.11 mmol) was added via syringe at ambient temperature. The reaction mixture was stirred for 5 minutes. The solvent was removed in vacuo to yield a white solid. The compound was recrystallised from CH_2Cl_2 and hexane and stored at 253K overnight to yield a batch of clear and colourless crystals (41 mg, 0.069 mmol).

Yield: 58 %

Alternative synthetic route: A Young's tube was charged with $Me_3In(iMes)$ (50 mg, 0.11 mmol) and CH_2Cl_2 (5 ml) was added via cannula. H(OTf) (9.5 μl, 0.11 mmol) was added via syringe at ambient temperature. The reaction mixture was stirred for 5 minutes. The solvent volume was reduced in vacuo and layered with hexane and stored at 253K overnight to yield a crop of clear and colourless crystals. (35 mg, 0.06 mmol)

Yield: 55 %

δ^1H (298K, CD_2Cl_2): 7.28 (2H, s, olefin), 7.08 (4H, s, aromatic), 2.38 (6H, s, CH_3), 2.09 (12H, s, CH_3), -0.83 (6H, s, In-CH_3)

$\delta^{13}C\{^1H\}$ (298K, CD_2Cl_2): 176.2, 141.0, 135.7, 134.4, 130.0, 124.9, 120.1 (319Hz, q, CF_3), 21.4, 17.6, -7.1

$\delta^{19}F$ (298K, CD_2Cl_2): -78.7

Elemental Analysis: Calcd (%) for $C_{24}H_{30}F_3InN_2O_3S{\cdot}CH_2Cl_2$: C, 43.94; H, 4.72; N, 4.10 Found C, 43.74; H, 4.58; N, 4.03

$Me(OTf)_2In(iMes)$, (14): A Young's tube was charged with $Me_2ClIn(iMes)$ (50 mg, 0.10 mmol) and CH_2Cl_2 (5 ml) was added via cannula. TMS(OTf) (19 μl, 0.10 mmol) was added via syringe at ambient temperature and the reaction mixture was stirred for

5 minutes. H(OTf) (9 μl, 0.10 mmol) was then added via syringe. Gas evolution was observed and the reaction mixture was stirred for a further 5 minutes. Solvent was removed in vacuo to yield a white solid. The compound was recrystallised from CH_2Cl_2 and hexane and stored at 253K overnight to yield a batch of clear and colourless crystals (49 mg, 0.067 mmol)

Yield: 65 %

Alternative synthetic route: A Young's tube was charged with $Me_3In(iMes)$ (50 mg, 0.11 mmol) and CH_2Cl_2 (5 ml) was added via cannula. H(OTf) (19 μl, 0.22 mmol) was added via syringe at ambient temperature. The reaction mixture was stirred for 5 minutes. The solvent volume was reduced in vacuo and layered with hexane and stored at 253K overnight to yield a crop of clear and colourless crystals. (47 mg, 0.065 mmol)

Yield: 60%

δ^1H (298K, CD_2Cl_2): 7.39 (2H, s, olefin), 7.10 (4H, s, aromatic), 2.39 (6H, s, CH_3), 2.13 (12H, s, CH_3), -0.41 (3H, s, In-CH_3)

$\delta^{13}C\{^1H\}$ (298K, CD_2Cl_2): 168.7, 142.1, 135.6, 132.8, 130.4, 126.3, 119.3 (318Hz, q, CF_3), 21.4, 17.7, -5.0

$\delta^{19}F$ (298K, CD_2Cl_2): –77.8

Elemental Analysis: Calcd (%) for $C_{24}H_{27}F_6InN_2O_6S_2 \cdot CH_2Cl_2$: C, 39.36; H, 3.72; N, 3.82 Found: C, 39.20; H, 4.04; N, 3.79

$Me_2(NTf_2)In(iMes)$, (15): A Young's tube was charged with $Me_3In(iMes)$ (50 mg, 0.11 mmol) and $H(NTf_2)$ (30 mg, 0.11 mmol). CH_2Cl_2 (5 ml) was added via cannula and the reaction mixture was stirred for 10 minutes releasing methane gas. The

solution was layered with hexane and stored at 253K overnight to yield a batch of clear and colourless crystals (66 mg, 0.091 mmol)

Yield: 85 %

δ^1H (298K, CD_2Cl_2): 7.30 (2H, s, olefin), 7.09 (4H, s, aromatic), 2.38 (6H, s, CH_3), 2.09 (12H, s, CH_3), -0.72 (6H, s, In-CH_3)

$\delta^{13}C\{^1H\}$ (298K, CD_2Cl_2): 175.5, 141.3, 135.5, 134.1, 130.1, 125.2, 119.9 (321Hz, q, CF_3), 21.4, 17.6, -5.7

δ^{19}F (298K, CD_2Cl_2): –79.0

Elemental Analysis: Calcd (%) for $C_{25}H_{30}F_6InN_3O_4S_2$: C, 41.16; H, 4.15; N, 5.76 Found: C, 40.90; H, 4.23; N, 5.66

Me(NTf$_2$)$_2$In(iMes), (16): A Young's tube was charged with Me_3In(iMes) (50 mg, 0.11 mmol) and H(NTf$_2$) (60 mg, 0.22 mmol). CH_2Cl_2 (5 ml) was added via cannula and the reaction mixture was stirred for 10 minutes releasing methane gas. The solution was layered with hexane and stored at 253K overnight to yield a batch of clear and colourless crystals (90 mg, 0.090 mmol)

Yield: 84 %

δ^1H (298K, CD_2Cl_2): 7.53 (2H, s, olefin), 7.15 (4H, s, aromatic), 2.40 (6H, s, CH_3), 2.14 (12H, s, CH_3), -0.04 (3H, s, In-CH_3);

δ^1H (298K, CD_3NO_2): 7.88 (2H, s, olefin), 7.24 (4H, s, aromatic), 2.42 (6H, s, CH_3), 2.20 (12H, s, CH_3), 0.07 (3H, s, In-CH_3);

$\delta^{13}C\{^1H\}$ (298K, CD_2Cl_2): 166.8, 142.9, 135.4, 132.0, 130.8, 126.6, 119.4 (320Hz, q, CF_3), 21.4, 17.6, -3.1;

δ^{19}F (298K, CD_2Cl_2): –78.6

Elemental Analysis: Calcd (%) for $C_{26}H_{27}F_{12}InN_4O_8S_4$: C, 31.40; H, 2.74; N, 5.63 Found: C, 31.20; H, 2.76; N, 5.56

$Me_2(CH_3COO)_2In(iMes)$, (17): A Young's tube was charged with $Me_3In(iMes)$ (100 mg, 0.215 mmol) and acetic acid (25 μl, 0.43 mmol). CH_2Cl_2 (5 ml) was added via cannula and the reaction mixture was stirred for 20 minutes releasing methane gas. The solution was layered with hexane and stored at 253K for several days to yield a batch of clear and colourless crystals (88 mg, 0.16 mmol)

Yield: 72 %

δ^1H (298K, CD_2Cl_2): 9.94 (1H, t, J = 1.4Hz, (iMesH)) 7.65 (2H, d, J = 1.4Hz, olefin), 7.11 (4H, s, aromatic), 2.39 (6H, s, CH_3), 2.16 (12H, s, CH_3), 1.57 (6H, s, CO_2CH_3), -0.60 (6H, s, In-CH_3)

δ^1H (298K, CD_3NO_2): 7.83 (2H, s, olefin) 7.19 (4H, s, aromatic), 2.40 (6H, s, CH_3), 2.21 (12H, s, CH_3), 1.69 (6H, s, CO_2CH_3), -0.52 (6H, s, In-CH_3)

$\delta^{13}C\{^1H\}$ (75.5MHz, CD_2Cl_2): 178.0, 142.3, 139.9, 134.7, 131.1, 130.5, 125.3, 23.1, 21.4, 17.8, -5.8

Elemental Analysis: Calcd (%) for $C_{27}H_{39}InN_2O_4$: C, 56.85; H, 6.89; N, 4.91 Found: C, 57.0; H, 6.49; N, 4.96

(iMesH)NTf_2, (18): A Schlenk was charged with $Li(NTf_2)$ (200 mg, 0.70 mmol) and (iMes)Cl (237 mg, 0.70 mmol). CH_2Cl_2 (5 ml) was added via cannula and the reaction mixture was stirred for 24 hours resulting in LiCl precipitation. The solution was separated by cannula filtration and the solvent was removed in vacuo to yield pale yellow crystals (358 mg, 0.60 mmol)

Yield: 87 %

δ^1H (298K, CD_3NO_2): 8.78 (1H, t, J = 1.4Hz, (iMesH)), 7.81 (2H, d, J = 1.4Hz, olefin), 7.20 (4H, s, aromatic), 2.41 (6H, s, CH_3), 2.22 (12H, s, CH_3)

$\delta^{13}C\{^1H\}$ (75.5MHz, CD_3NO_2): 143.3, 138.3, 136.1, 132.1, 131.0, 126.5, 121.3 (321Hz, q, CF_3), 21.2, 17.5

Elemental Analysis: Calcd (%) for $C_{23}H_{25}N_3O_4S_2F_6$: C, 47.17; H, 4.30; N, 7.18 Found: C, 47.7; H, 4.40; N, 7.22

5.2.3 Reaction Monitoring Experiments

5.2.3.1 General Procedure for The Monitoring of The Reaction between Anisole and Acetic Anhydride

5 mg of compound **(16)** (5 mol%, 5.0 μmol) was dissolved in 0.8 ml CD_3NO_2 in a Young's NMR tube. To this solution, 11μl of anisole (100 mol%, 0.10 mmol) was added. The NMR spectrometer probe was then heated to 50°C and a ^1H NMR spectrum of the sample acquired. 14μl of acetic anhydride (150 mol%, 1.51 mmol) was then added. The Young's NMR tube was then shaken and returned to the NMR spectrometer probe. Measurements were then taken at timed intervals. The disappearance of the peaks centred at δ = 7.31 (2H), 6.97 (1H), 6.95 (2H), 3.83 (3H) due to anisole were monitored along with the growth of the peaks centred at δ = 7.97 (2H), 7.03 (2H), 3.91 (3H), 2.55(3H) due to 4-methxoyacetophenone. The ratio of anisole to 4-methoxyacetophenone was calculated by integration of the 2H resonance of the 4-methoxyacetophenone product at 7.97 ppm and of the 2H resonance of the anisole at 7.31 ppm. This allowed the product conversion to be readily determined in each spectrum. This technique was also used for the acylation of anisole where 5mol% of $In(OTf)_3$, H(OTf), $H(NTf_2)$ and **(14)** were used to catalyse the reaction.

5.2.3.2 General Procedure for the Monitoring of the Reaction between Other Organic Substrates and Acetic Anhydride Catalysed by (16)

The same procedure was used as previously for the different organic substrates. The ratio of product : starting material was determined in the same manner as above but was dependent on the chemical shifts of the resonances of the substrate and the product. Table 1 shows the chosen resonances used to calculate the percentage product conversion for each substrate and its acylated product.

	^{1}H NMR chemical shift (δ) of resonances in CD_3NO_2 used for percentage product conversion calculations	
Substrate	**Starting Material**	**Product**
furan	6.45 (2H)	6.64 (1H)
phenol	7.24 (2H	7.43 (2H)
aniline	7.13 (2H)	7.33 (2H)
2,3-dimethylanisole	7.03 (1H)	7.61 (1H)
veratrole	6.94 (4H)	7.54 (1H)
anisole	7.31 (2H)	7.97 (2H)
1,4-benzodioxane	6.84 (4H)	7.50 (2H)
mesitylene	6.81 (3H)	6.89 (2H)

Table 1 : The chemical shifts of a chosen resonance from both the substrate and the product used for percentage product conversion calculations

5.2.3.3 Studies of the Acylation of Anisole in the Presence of Hindered Base

5 mg of compound **(16)** (5 mol%, 5.0 μmol) was dissolved in 0.8 ml CD_3NO_2 in a Young's NMR tube. To this solution was added 1.2 μl 2,6-di-tert-butylpyridine (5 mol%, 5.0 μmol). The Young's NMR tube was shaken and 11μl of anisole (100 mol%, 0.10 mmol) was added. The NMR spectrometer probe was then heated to 50°C and a ^{1}H NMR spectrum of the sample acquired. 14 μl of acetic anhydride (150

mol%, 1.51 mmol) was then added. The Young's NMR tube was then shaken and returned to the NMR spectrometer probe. Measurements were then taken at timed intervals. No product was observed.

5.2.3.4 Studies of the Acylation of Anisole Using a Statistical Mixture (1:1:1:1) of (16) : Hindered base : Anisole : Acetic anhydride

46 mg of compound **(16)** (100 mol%, 46 μmol) was dissolved in 0.8 ml CD_3NO_2 in a Young's NMR tube. To this solution was added 10.5 μl 2,6-di-tert-butylpyridine (100mol%, 46 μmol). The Young's NMR tube was shaken and 5.5 μl of anisole (100mol%, 46 μmol) was added. The NMR spectrometer probe was then heated to 50°C and a ^1H NMR spectrum of the sample acquired. 7 μl of acetic anhydride (100mol%, 46 μmol) was then added. The Young's NMR tube was then shaken and returned to the NMR spectrometer probe. Measurements were then taken at timed intervals. No 4-methoxyacetophenone product was observed.

5.3 References

(1) Arduengo, A. J.; Dias, H. V. R.; Harlow, R. L.; Kline, M. *J. Am. Chem. Soc.* **1992**, *114*, 5530-5534.

(2) Arduengo, A. J.; Krafczyk, R.; Schmutzler, R.; Craig, H. A.; Goerlich, J. R.; Marshall, W. J.; Unverzagt, M. *Tetrahedron* **1999**, *55*, 14523-14534.

(3) Kuhn, N.; Kratz, T. *Synthesis* **1993**, 561-562.

(4) Roberts, E.; Turner, E. E. *J. Chem. Soc.* **1927**, 1832-1857.

(5) Martin, D. F.; Janusonis, G. A.; Martin, B. M. *J. Am. Chem. Soc.* **1961**, *83*, 73-75.

(6) Singh, R. V.; Tandon, J. P. *J. Prakt. Chem.* **1979**, *321*, 151-158.

(7) Cimarelli, C.; Palmieri, G. *Tetrahedron* **1998**, *54*, 915-926.

(8) Parks, J. E.; Holm, R. H. *Inorg. Chem.* **1968**, *37*, 2317.

(9) Stender, M.; Eichler, B. E.; Hardman, N. J.; Power, P. P.; Prust, J.; Noltemeyer, M.; Roesky, H. W. *Inorg. Chem.* **2001**, *40*, 2794-2799 and references therein.

Appendix A

Crystal Data and Structure Refinement Tables for all Compounds

Table 1 : Crystal data and structure refinement for compound **(1)**

Identification code	compound **(1)**
Empirical formula	$C_{26}\ H_{36}\ In_2\ N_2\ O_2$
Formula weight	319.10
Temperature	150(2) K
Wavelength	0.71073 Å
Crystal system	monoclinic
Space group	C2/c
Unit cell dimensions	a = 16.9940(2)Å $\alpha = 90^\circ$
	b = 8.60500(10)Å $\beta = 106.0840(10)^\circ$
	c = 19.1720(2)Å $\gamma = 90^\circ$
Volume	2693.84(5) $Å^3$
Z	4
Calculated density	1.574 Mg/m^3
Absorption coefficient	1.735 mm^{-1}
F(000)	1280
Crystal size	0.25 x 0.25 x 0.20 mm
Theta range for data collection	3.69 to 30.03°
Limiting indices	-23<=h<=23, -11<=k<=12, -24<=l<=26
Reflections collected	25524
Independent reflections	3904 [R(int) = 0.0329]
Completeness to theta	30.03 99.1 %
Max. and min. transmission	0.7229 and 0.6709
Refinement method	Full-matrix least-squares on F^2
Data / restraints / parameters	3904 / 0 / 148
Goodness-of-fit on F^2	1.075
Final R indices [I>2σ(I)]	$R_1 = 0.0215$, $wR_2 = 0.0470$
R indices (all data)	$R_1 = 0.0232$, $wR_2 = 0.0479$
Extinction coefficient	0.00166(12)
Largest diff. peak and hole	1.060 and -1.136 $e.Å^{-3}$

Table 2 : Crystal data and structure refinement for compound **(2)**

Identification code	compound **(2)**
Empirical formula	C_{18} H_{20} In N O
Formula weight	381.17
Temperature	150(2) K
Wavelength	0.71073 Å
Crystal system	triclinic
Space group	P $\bar{1}$
Unit cell dimensions	a = 9.86100(10)Å α = 91.61°
	b = 9.95100(10)Å β = 92.0750(10)°
	c = 18.2430(2)Å γ = 109.5650(10)°
Volume	1684.12(3)Å^3
Z	4
Calculated density	1.503 Mg/m^3
Absorption coefficient	1.402 mm^{-1}
F(000)	768
Crystal size	0.33 x 0.13 x 0.13 mm
Theta range for data collection	3.57 to 30.06°
Limiting indices	-13<=h<=13, -14<=k<=14, -25<=l<=25
Reflections collected	33364
Independent reflections	9731 [R(int) = 0.0406]
Completeness to theta	30.06 98.7 %
Max. and min. transmission	0.8388 and 0.6548
Refinement method	Full-matrix least-squares on F^2
Data / restraints / parameters	9731 / 0 / 385
Goodness-of-fit on F^2	1.057
Final R indices [I>2σ(I)]	R_1 = 0.0275, wR_2 = 0.0644
R indices (all data)	R_1 = 0.0350, wR_2 = 0.0681
Extinction coefficient	0.0071(4)
Largest diff. peak and hole	1.059 and -1.068 e.Å^{-3}

Table 3 : Crystal data and structure refinement for compound **(3)**

Identification code	compound **(3)**
Empirical formula	C_{12} H_{15} In O_2
Formula weight	306.06
Temperature	150(2) K
Wavelength	0.71073 Å
Crystal system	triclinic
Space group	P $\bar{1}$
Unit cell dimensions	a = 6.9360(3)Å α = 91.433(2)°
	b = 8.1140(4)Å β = 102.447(2)°
	c = 11.3220(5)Å γ = 99.738(2)°
Volume	611.99(5)Å^3
Z	2
Calculated density	1.661 Mg/m^3
Absorption coefficient	1.909 mm^{-1}
F(000)	304
Crystal size	0.50 x 0.38 x 0.15 mm
Theta range for data collection	3.62 to 30.08°
Limiting indices	-9<=h<=9, -11<=k<=11, -15<=l<=15
Reflections collected	8318
Independent reflections	3436 [R(int) = 0.0806]
Completeness to theta	30.08 95.2 %
Max. and min. transmission	0.7627 and 0.4486
Refinement method	Full-matrix least-squares on F^2
Data / restraints / parameters	3436 / 0 / 137
Goodness-of-fit on F^2	1.146
Final R indices [I>2σ(I)]	R_1 = 0.0908, wR_2 = 0.2699
R indices (all data)	R_1 = 0.0971, wR_2 = 0.2745
Extinction coefficient	0.15(2)
Largest diff. peak and hole	5.513 and -2.160 e.Å^{-3}

Table 4 : Crystal data and structure refinement for compound **(5)**

Identification code	compound **(5)**
Empirical formula	$C_{34}\ H_{40}\ Cl_4\ In_2\ N_2\ O_2 \bullet C_6H_5CH_3$
Formula weight	980.32
Temperature	150(2) K
Wavelength	0.71073Å
Crystal system	triclinic
Space group	P $\bar{1}$
Unit cell dimensions	a = 10.7770(2)Å alpha = 67.4680(10)°
	b = 14.8210(2)Å beta = 88.2390(10)°
	c = 15.4900(3)Å gamma = 74.3970(10)°
Volume	2193.79(7)Å^3
Z	2
Calculated density	1.484 Mg/m^3
Absorption coefficient	1.329 mm^{-1}
F(000)	996
Crystal size	0.40 x 0.30 x 0.15 mm
Theta range for data collection	3.60 to 27.50°
Limiting indices	-13<=h<=13, -19<=k<=19, -20<=l<=20
Reflections collected	37024
Independent reflections	9946 [R(int) = 0.0368]
Completeness to theta	27.50 99.0 %
Max. and min. transmission	0.8255 and 0.6184
Refinement method	Full-matrix least-squares on F^2
Data / restraints / parameters	9946 / 0 / 473
Goodness-of-fit on F^2	1.125
Final R indices [I>2σ(I)]	R_1 = 0.0309, wR_2 = 0.0734
R indices (all data)	R_1 = 0.0413, wR_2 = 0.0770
Largest diff. peak and hole	0.852 and -0.913 e.Å^{-3}

Table 5 : Crystal data and structure refinement for compound **(6)**

Identification code	compound **(6)**
Empirical formula	$C_{30}\ H_{43}\ F_3\ N_2\ O_3\ S$
Formula weight	568.72
Temperature	150(2) K
Wavelength	0.71073 Å
Crystal system	monoclinic
Space group	P $2_1/n$
Unit cell dimensions	a = 10.15300(10)Å $\alpha = 90^\circ$
	b = 27.4410(4)Å $\beta = 98.0750(10)^\circ$
	c = 11.5030(2)Å $\gamma = 90^\circ$
Volume	3173.06(8) $Å^3$
Z	4
Calculated density	1.191 Mg/m^3
Absorption coefficient	0.151 mm^{-1}
F(000)	1216
Crystal size	0.65 x 0.45 x 0.10 mm
Theta range for data collection	2.91 to 30.03°
Limiting indices	-14<=h<=14, -38<=k<=38, -16<=l<=16
Reflections collected	38501
Independent reflections	9105 [R(int) = 0.0532]
Completeness to theta	30.03 98.1 %
Max. and min. transmission	0.9851 and 0.9084
Refinement method	Full-matrix least-squares on F^2
Data / restraints / parameters	9105 / 0 / 352
Goodness-of-fit on F^2	1.038
Final R indices [I>2σ(I)]	$R_1 = 0.0471$, $wR_2 = 0.1189$
R indices (all data)	$R_1 = 0.0710$, $wR_2 = 0.1316$
Largest diff. peak and hole	0.294 and -0.325 $e.Å^{-3}$

Table 6 : Crystal data and structure refinement for compound **(7)**

Identification code	compound **(7)**
Empirical formula	$C_{23}H_{30}ClInN_2$
Formula weight	484.76
Temperature	150(2) K
Wavelength	0.71073 Å
Crystal system	triclinic
Space group	P-1
Unit cell dimensions	a = 8.2890(1)Å α = 68.725(1)°
	b = 11.0870(1)Å β = 86.534(1)°
	c = 13.6710(2)Å γ = 75.138(1)°
Volume	1130.84(2) $Å^3$
Z	2
Density (calculated)	1.424 Mg/m^3
Absorption coefficient	1.173 mm^{-1}
F(000)	496
Crystal size	0.13 x 0.10 x 0.10 mm
Theta range for data collection	4.00 to 27.66°
Index ranges	-10<=h<=10; -14<=k<=14; -17<=l<=17
Reflections collected	16860
Independent reflections	5183 [R(int) = 0.0450]
Reflections observed (>2σ)	4708
Data Completeness	0.982
Absorption correction	None
Refinement method	Full-matrix least-squares on F^2
Data / restraints / parameters	5183 / 0 / 253
Goodness-of-fit on F^2	1.067
Final R indices [I>2σ(I)]	R^1 = 0.0279 wR_2 = 0.0651
R indices (all data)	R^1 = 0.0349 wR_2 = 0.0685
Largest diff. peak and hole	0.860 and -1.101 $eÅ^{-3}$

Table 7 : Crystal data and structure refinement for compound **(8)**

Identification code	compound **(8)**
Empirical formula	C_{29} H_{42} Cl In N_2
Formula weight	568.92
Temperature	150(2) K
Wavelength	0.71073Å
Crystal system	monoclinic
Space group	P $2_1/a$
Unit cell dimensions	a = 16.86500(10)Å $\alpha = 90^o$
	b = 19.5420(2)Å $\beta = 109.3930(4)^o$
	c = 19.0080(2)Å $\gamma = 90^o$
Volume	5909.14(9)$Å^3$
Z	8
Calculated density	1.279 Mg/m^3
Absorption coefficient	0.908 mm^{-1}
F(000)	2368
Crystal size	0.38 x 0.25 x 0.05 mm
Theta range for data collection	3.56 to 30.03°
Limiting indices	-23<=h<=23, -27<=k<=26, -26<=l<=26
Reflections collected	130040
Independent reflections	17218 [R(int) = 0.0717]
Completeness to theta	30.03 99.6 %
Max. and min. transmission	0.9560 and 0.7241
Refinement method	Full-matrix least-squares on F^2
Data / restraints / parameters	17218 / 0 / 595
Goodness-of-fit on F^2	1.036
Final R indices [I>2σ(I)]	R1 = 0.0475, wR2 = 0.1111
R indices (all data)	R1 = 0.0880, wR2 = 0.1269
Largest diff. peak and hole	1.594 and -1.708 e.$Å^{-3}$

Table 8 : Crystal data and structure refinement for compound **(9)**

Identification code	compound **(9)**
Empirical formula	C_{23} H_{30} Br In N_2
Formula weight	529.22
Temperature	150(2) K
Wavelength	0.71073 Å
Crystal system	monoclinic
Space group	P $2_1/c$
Unit cell dimensions	a = 8.27500(10)Å $\alpha = 90^o$
	b = 15.3940(2)Å $\beta = 92.9630(10)^o$
	c = 18.6610(2)Å $\gamma = 90^o$
Volume	2373.96(5) $Å^3$
Z	4
Calculated density	1.481 Mg/m^3
Absorption coefficient	2.688 mm^{-1}
F(000)	1064
Crystal size	0.25 x 0.25 x 0.20 mm
Theta range for data collection	4.20 to 36.30°
Limiting indices	-13<=h<=13, -25<=k<=25, -30<=l<=31
Reflections collected	48626
Independent reflections	11434 [R(int) = 0.0427]
Completeness to theta	36.30 99.6 %
Max. and min. transmission	0.6155 and 0.5530
Refinement method	Full-matrix least-squares on F^2
Data / restraints / parameters	11434 / 0 / 253
Goodness-of-fit on F^2	1.012
Final R indices [I>2σ(I)]	$R_1 = 0.0322$, $wR_2 = 0.0753$
R indices (all data)	$R_1 = 0.0520$, $wR_2 = 0.0827$
Extinction coefficient	0.0058(3)
Largest diff. peak and hole	1.034 and -1.366 $e.Å^{-3}$

Table 9 : Crystal data and structure refinement for compound **(10)**

Identification code	compound **(10)**
Empirical formula	C_{23} H_{32} Cl In N_2
Formula weight	486.78
Temperature	150(2) K
Wavelength	0.71073 Å
Crystal system	triclinic
Space group	P $\bar{1}$
Unit cell dimensions	a = 8.3090(1)Å α = 67.424(1)°
	b = 11.3720(2)Å β = 84.481(1)°
	c = 13.7910(2)Å γ = 71.647(1)°
Volume	1141.60(3) $Å^3$
Z	2
Calculated density	1.416 Mg/m^3
Absorption coefficient	1.162 mm^{-1}
F(000)	500
Crystal size	0.30 x 0.25 x 0.15 mm
Theta range for data collection	3.73 to 36.30°
Limiting indices	-13<=h<=13, -18<=k<=18, -22<=l<=22
Reflections collected	30396
Independent reflections	10733 [R(int) = 0.0547]
Completeness to theta	36.30 97.2 %
Max. and min. transmission	0.8450 and 0.7219
Refinement method	Full-matrix least-squares on F^2
Data / restraints / parameters	10733 / 0 / 244
Goodness-of-fit on F^2	1.051
Final R indices [I>2σ(I)]	R_1 = 0.0404, wR_2 = 0.1085
R indices (all data)	R_1 = 0.0468, wR_2 = 0.1133
Largest diff. peak and hole	0.994 and -1.793 $e.Å^{-3}$

Table 10 : Crystal data and structure refinement for compound **(11)**

Identification code	compound **(11)**
Empirical formula	C_{24} H_{33} In N_2
Formula weight	464.34
Temperature	150(2) K
Wavelength	0.71073 Å
Crystal system	orthorhombic
Space group	P c 2_1 n (nonstandard setting of P n a 2_1)
Unit cell dimensions	a = 8.21300(10)Å $\alpha = 90^o$
	b = 12.32300(10)Å $\beta = 90^o$
	c = 23.1350(2)Å $\gamma = 90^o$
Volume	2341.47(4) $Å^3$
Z	4
Calculated density	1.317 Mg/m^3
Absorption coefficient	1.019 mm^{-1}
F(000)	960
Crystal size	0.68 x 0.38 x 0.10 mm
Theta range for data collection	3.46 to 27.54°
Limiting indices	-10<=h<=10, -15<=k<=15, -30<=l<=30
Reflections collected	32572
Independent reflections	2797 [R(int) = 0.0338]
Completeness to theta	27.54 99.1 %
Max. and min. transmission	0.9049 and 0.5441
Refinement method	Full-matrix least-squares on F^2
Data / restraints / parameters	2797 / 0 / 163
Goodness-of-fit on F^2	1.110
Final R indices [I>2σ(I)]	R_1 = 0.0205, wR_2 = 0.0522
R indices (all data)	R_1 = 0.0221, wR_2 = 0.0533
Largest diff. peak and hole	0.459 and -0.454 e.$Å^{-3}$

Table 11 : Crystal data and structure refinement for compound **(13)**

Identification code	compound **(13)**
Empirical formula	$C_{23}\ H_{30}\ F_3\ In\ N_2\ O_3\ S \bullet CH_2Cl_2$
Formula weight	683.31
Temperature	150(2) K
Wavelength	0.71073 Å
Crystal system	monoclinic
Space group	P 2_1/c
Unit cell dimensions	a = 9.06100(10)Å $\alpha = 90^o$
	b = 22.3800(3)Å $\beta = 100.9230(10)^o$
	c = 14.7900(2)Å $\gamma = 90^o$
Volume	2944.86(6)Å^3
Z	4
Calculated density	1.541 Mg/m^3
Absorption coefficient	1.102 mm^{-1}
F(000)	1384
Crystal size	0.50 x 0.15 x 0.08 mm
Theta range for data collection	3.07 to 27.38°
Limiting indices	-11<=h<=11, -28<=k<=28, -19<=l<=19
Reflections collected	49531
Independent reflections	6651 [R(int) = 0.0596]
Completeness to theta	27.38 99.5 %
Max. and min. transmission	0.9170 and 0.6087
Refinement method	Full-matrix least-squares on F^2
Data / restraints / parameters	6651 / 0 / 342
Goodness-of-fit on F^2	1.038
Final R indices [I>2σ(I)]	R_1 = 0.0302, wR_2 = 0.0709
R indices (all data)	R_1 = 0.0466, wR_2 = 0.0784
Largest diff. peak and hole	0.433 and -0.655 e.Å^{-3}

Table 12 : Crystal data and structure refinement for compound **(14)**

Identification code	compound **(14)**
Empirical formula	$C_{23}\ H_{27}\ F_6\ In\ N_2\ O_6\ S_2 \bullet CH_2Cl_2$
Formula weight	817.34
Temperature	150(2) K
Wavelength	0.71073 Å
Crystal system	triclinic
Space group	$P\ \bar{1}$
Unit cell dimensions	$a = 9.42300(10)Å \quad \alpha = 85.3780(10)^o$
	$b = 12.5040(2)Å \quad \beta = 83.6180(10)^o$
	$c = 14.5090(2)Å \quad \gamma = 83.1720(10)^o$
Volume	$1682.95(4)Å^3$
Z	2
Calculated density	$1.613\ Mg/m^3$
Absorption coefficient	$1.058\ mm^{-1}$
F(000)	820
Crystal size	0.25 x 0.25 x 0.25 mm
Theta range for data collection	3.49 to 30.09^o
Limiting indices	-13<=h<=13, -17<=k<=17, -20<=l<=20
Reflections collected	30330
Independent reflections	9809 [R(int) = 0.0340]
Completeness to theta	30.09 99.1 %
Refinement method	Full-matrix least-squares on F^2
Data / restraints / parameters	9809 / 12 / 465
Goodness-of-fit on F^2	1.032
Final R indices [$I>2\sigma(I)$]	$R_1 = 0.0277$, $wR_2 = 0.0638$
R indices (all data)	$R_1 = 0.0345$, $wR_2 = 0.0671$
Largest diff. peak and hole	0.394 and $-0.548\ e.Å^{-3}$

Table 13 : Crystal data and structure refinement for compound **(15)**

Identification code	compound **(15)**
Empirical formula	$C_{25}\ H_{30}\ F_6\ In\ N_3\ O_4\ S_2$
Formula weight	729.46
Temperature	150(2) K
Wavelength	0.71073 Å
Crystal system	orthorhombic
Space group	$P\ 2_1\ 2_1\ 2_1$
Unit cell dimensions	a = 11.6000(2)Å $\alpha = 90^o$
	b = 12.8070(2)Å $\beta = 90^o$
	c = 21.3390(2)Å $\gamma = 90^o$
Volume	3170.15(8)Å^3
Z	4
Calculated density	1.528 Mg/m^3
Absorption coefficient	0.946 mm^{-1}
F(000)	1472
Crystal size	0.88 x 0.32 x 0.22 mm
Theta range for data collection	3.32 to 27.50°
Limiting indices	-15<=h<=15, -16<=k<=16, -27<=l<=27
Reflections collected	23215
Independent reflections	6595 [R(int) = 0.0667]
Completeness to theta	27.50 94.5 %
Max. and min. transmission	0.8189 and 0.4898
Refinement method	Full-matrix least-squares on F^2
Data / restraints / parameters	6595 / 0 / 378
Goodness-of-fit on F^2	1.048
Final R indices [I>2σ(I)]	R_1 = 0.0354, wR_2= 0.0950
R indices (all data)	R_1= 0.0371, wR_2 = 0.0963
Absolute structure parameter	-0.02(2)
Largest diff. peak and hole	1.498 and -1.277 e.Å^{-3}

Table 14 : Crystal data and structure refinement for compound **(16)**

Identification code	compound **(16)**
Empirical formula	$C_{26}\ H_{27}\ F_{12}\ In\ N_4\ O_8\ S_4$
Formula weight	994.57
Temperature	150(2) K
Wavelength	0.71073 Å
Crystal system	monoclinic
Space group	P $2_1/n$
Unit cell dimensions	a = 15.4880(2) Å $\alpha = 90^o$
	b = 15.7670(2) Å $\beta = 108.1890(10)^o$
	c = 16.3360(2) Å $\gamma = 90^o$
Volume	3789.90(8)Å^3
Z	4
Calculated density	1.729 Mg/m^3
Absorption coefficient	0.948 mm^{-1}
F(000)	1968
Crystal size	0.63 x 0.50 x 0.25 mm
Theta range for data collection	3.64 to 27.48°
Limiting indices	-20<=h<=20, -20<=k<=20, -20<=l<=21
Reflections collected	59467
Independent reflections	8639 [R(int) = 0.0612]
Completeness to theta	27.48 99.4 %
Max. and min. transmission	0.7976 and 0.5866
Refinement method	Full-matrix least-squares on F^2
Data / restraints / parameters	8639 / 0 / 503
Goodness-of-fit on F^2	1.056
Final R indices [I>2σ(I)]	R_1 = 0.0318, wR_2 = 0.0757
R indices (all data)	R_1 = 0.0419, wR_2 = 0.0822
Largest diff. peak and hole	0.846 and -1.105 e.Å^{-3}

Table 15 : Crystal data and structure refinement for compound **(17)**

Identification code	compound **(17)**
Empirical formula	$C_{27}\ H_{37}\ In\ N_2\ O_4$
Formula weight	568.41
Temperature	150(2) K
Wavelength	0.71073 Å
Crystal system	monoclinic
Space group	P $2_1/n$
Unit cell dimensions	a = 11.41000(10)Å $\alpha = 90^o$
	b = 17.7920(2)Å $\beta = 108.94^o$
	c = 14.99200(10)Å $\gamma = 90^o$
Volume	2878.75(5)$Å^3$
Z	4
Calculated density	1.311 Mg/m^3
Absorption coefficient	0.852 mm^{-1}
F(000)	1176
Crystal size	0.40 x 0.22 x 0.15 mm
Theta range for data collection	2.97 to 27.51°
Limiting indices	-14<=h<=14, -22<=k<=23, -19<=l<=19
Reflections collected	41476
Independent reflections	6575 [R(int) = 0.0316]
Completeness to theta	27.51 99.2 %
Max. and min. transmission	0.8828 and 0.7268
Refinement method	Full-matrix least-squares on F^2
Data / restraints / parameters	6575 / 0 / 317
Goodness-of-fit on F^2	1.056
Final R indices [I>2σ(I)]	$R_1 = 0.0220$, $wR_2 = 0.0590$
R indices (all data)	$R_1 = 0.0266$, $wR_2 = 0.0619$
Largest diff. peak and hole	0.372 and -0.624 $e.Å^{-3}$

Appendix B

Publications

Silver Phosphanes Partnered with Carborane Monoanions: Synthesis, Structures and Use as Highly Active Lewis Acid Catalysts in Hetero-Diels-Alder Reaction.
Patmore, N. J.; Hague, C.; Cotgreave, J. H.; Mahon, M. F.; Frost, C. G.; Weller, A. S.
Chem. Eur. J. **2002**, 8, 2088

Well-defined Indium(III) *N*-Heterocyclic Carbene Complexes with Triflate Ligands: Structural Models for the $In(OTf)_3$ Catalyst.
Cotgreave, J. H.; Colclough, D.; Kociok-Köhn, G.; Ruggerio, G.; Frost. C. G.; Weller, A. S. *J. Chem. Soc., Dalton Trans.* **2004**, 1519

Silver Phosphanes Partnered with Carborane Monoanions: Synthesis, Structures and Use as Highly Active Lewis Acid Catalysts in a Hetero-Diels–Alder Reaction

Nathan J. Patmore, Catherine Hague, Jamie H. Cotgreave, Mary F. Mahon, Christopher G. Frost,* and Andrew S. Weller*[a]

Abstract: Four Lewis acidic silver phosphane complexes partnered with $[1\text{-}closo\text{-}CB_{11}H_{12}]^-$ and $[1\text{-}closo\text{-}CB_{11}H_6Br_6]^-$ have been synthesised and studied by solution NMR and solid-state X-ray diffraction techniques. In the complex $[Ag(PPh_3)(CB_{11}H_{12})]$ (**1**), the silver is coordinated with the carborane by two stronger 3c–2e B–H–Ag bonds, one weaker B–H–Ag interaction and a very weak $Ag\cdots C_{arene}$ contact in the solid state. In solution, the carborane remains closely connected with the $\{Ag(PPh_3)\}^+$ fragment, as evidenced by ^{11}B chemical shifts. Complex **2** $[Ag(PPh_3)_2(CB_{11}H_{12})]_2$ adopts a dimeric motif in the solid state, each carborane bridging two Ag centres. In solution at low temperature, two distinct complexes are observed that are suggested to be monomeric $[Ag(PPh_3)_2][CB_{11}H_{12}]$ and dimeric $[Ag(PPh_3)_2(CB_{11}H_{12})]_2$. With the more weakly coordinating anion $[CB_{11}H_6Br_6]^-$ and one phosphane, complex **3** $[Ag(PPh_3)(CB_{11}H_6Br_6)]$ is isolated. Complex **4**, $[Ag(PPh_3)_2(CB_{11}H_6Br_6)]$, has been characterised spectroscopically. All of the complexes have been assessed as Lewis acids in the hetero-Diels–Alder reaction of *N*-benzylideneaniline with Danishefsky's diene. Exceptionally low catalyst loadings for this Lewis acid catalysed reaction are required (0.1 mol%) coupled with turnover frequencies of $4000\,h^{-1}$ (quantitative conversion to product after 15 minutes using **3** at room temperature). Moreover, the reaction does not occur in rigorously dry solvent as addition of a substoichiometric amount of water (50 mol%) is necessary for turnover of the catalyst. It is suggested that a Lewis assisted Brønsted acid is formed between the water and the silver. The effect of changing the counterion to $[BF_4]^-$, $[OTf]^-$ and $[ClO_4]^-$ has also been studied. Significant decreases in reaction rate and final product yield are observed on changing the anion from $[CB_{11}H_6Br_6]^-$, thus demonstrating the utility of weakly coordinating carborane anions in organic synthesis.

Keywords: carboranes · cluster compounds · cycloaddition · homogeneous catalysis · silver

Introduction

Monoanionic carborane anions based around $[closo\text{-}1\text{-}CB_{11}H_{12}]^-$ (**A**, see Scheme 1) are among the most inert and least coordinating anions currently known.[1, 2] The high chemical stability and low nucleophilicity of these ions means that they have been used to stabilise exotic cationic species, which are not isolatable with other, more coordinating, anions.[3–6] Such anions also have the potential to act as partners with cationic Lewis acidic transition metal complexes that take part in various catalytic processes. Somewhat surprisingly, given the almost ubiquitous use of $[B(C_6F_5)_4]^-$ and derivatives in such applications, there are only a few reports of anions such as **A** or related compounds utilised in catalytic processes,[7–10] despite their potential advantages over perfluorinated borates.[11, 12]

The coordination chemistry of cationic silver(I) phosphane complexes (combined with a range of anions) has been studied in some detail,[13–16] to the point that useful structural predications may be made on the basis of spectroscopic data.[17] Silver phosphanes *exo*-coordinated to polyhedral boranes are rarer,[18] but recent work, particularly from Stone et al.[19–21] has established this area. Related complexes in which *exo*-coordinated silver is bound to ligands other than phosphane,[22–25] or arene solvent molecules[26–29] or where the silver is partnered with halogeno-substituted carboranes[27, 30–33] are also known.

One of us has a current interest in the synthesis, structures and reactivity of Lewis acidic transition metal complexes partnered with anion **A** and derivatives.[24, 25] Concurrently, there is also interest in Lewis acid catalysis using silver(I) salts as effective promoters of a wide-range of organic transformations including allylation, aldol, ene and glycosylation

[a] Dr. C. G. Frost, Dr. A. S. Weller, N. J. Patmore, C. Hague
J. H. Cotgreave, Dr. M. F. Mahon
Department of Chemistry, University of Bath
Bath, BA27AY (UK)
Fax: (+44) 1225-826231
E-mail: c.g.frost@bath.ac.uk, a.s.weller@bath.ac.uk

0947-6539/02/0809-2088 $ 20.00+.50/0 *Chem. Eur. J.* **2002**, *8*, No. 9

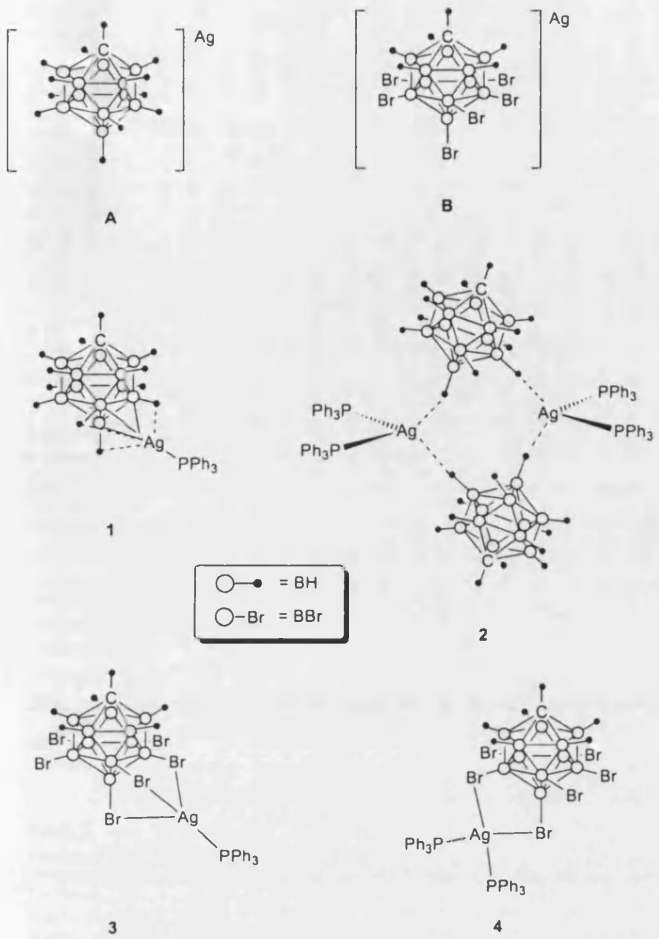

Scheme 1. Structures **A** and **B** and **1**–**4**.

reactions.[34] Of particular note is the use of silver(I) BINAP ([1,1′-binaphthalene]-2,2′-diylbis(diphenylphosphane)) complexes in asymmetric aldol reactions,[35–38] Mukaiyama aldol reactions,[39] asymmetric allylations[40] and hetero-Diels–Alder reactions.[41] It is well established that these reactions are accelerated by other Lewis acids (for example: Ti, B, Al, Sn complexes). However, many of these established catalysts are sensitive to air, water and product inhibition and consequently are used at a low substrate/catalyst ratio. The use of silver(I) phosphane complexes can provide a practical solution, with many precatalysts being stable in air and retaining activity in the presence of reaction product. Nevertheless, the best examples from the literature routinely employ high catalytic loadings (5–10 mol%) to achieve competitive rates and product yields. We are thus interested in developing silver(I) Lewis acids complexed with carborane anions in anticipation that the weakly coordinating nature of the anions will reveal enhanced activity for these systems. The hetero-Diels–Alder reaction is one of the most useful methods for the synthesis of bioactive heterocycles. Hence we chose to test our new complexes in this challenging reaction with the intention of identifying structure–activity relationships when the coordination sphere of the silver (number of phosphanes, anion) is systematically changed.

We report here the synthesis and solution and solid-state structural investigations for complexes of the formula $[Ag(PPh_3)_n(CB_{11}H_6Y_6)]$ ($n = 1, 2$; Y = H, Br) and their use as active catalysts in the hetero-Diels–Alder reactions of *N*-benzylideneaniline with Danishefsky's diene. Aspects of this work have been communicated previously.[42]

Results and Discussion

Synthesis and structures: Silver(I) salts of monoanionic carborane anions are readily prepared and are air stable and useful synthons for subsequent reactions. For example, they can be used in silver salt metathesis reactions to introduce a carborane anion into a metal's coordination sphere[23, 25, 29, 43, 44] or to generate synthetically useful salts.[28] In addition they often have significant solubility in aromatic solvents compared with other cations, facilitating more complete characterisation of the cation/anion pair. In principle, they also provide a useful starting point for the investigation of silver(I) complexes of the general formula $[Ag(L)_n(CB_{11}H_6Y_6)]$ (L = two electron donor; Y = H, halogen) as simple addition of the required ligand (L) results in complex formation.

Addition of slightly less than one equivalent (to avoid formation of **2**, vide infra) of PPh_3 to a suspension of $Ag[CB_{11}H_{12}]$ in CH_2Cl_2 results in the formation of $[Ag(PPh_3)(CB_{11}H_{12})]$, **1**, as an analytically pure solid in good isolated yield after recrystallisation (Tables 1 and 2). The solid-state structure of **1** is presented in Figure 1. The $\{AgPPh_3\}^+$ fragment interacts with the carborane anion through the three {BH} units that form the B(12)–B(7)–B(8) polyhedral face, a coordination motif seen previously in $[(Cp^*)ZrMe_2\text{-}\eta^3\text{-}(CB_{11}H_{12})]$.[10] The silver phosphane fragment does not sit over the centre of this face but is more localised towards B(8) and the corresponding Ag–B bond lengths reflect this: Ag(1)–B(8) 2.504(1) Å, Ag(1)–B(12) 2.569(3) Å, Ag(1)–B(7) 2.619(2) Å. These bond lengths are broadly similar to those previously reported for the related complex $[2,2,2\text{-}(CO)_3\text{-}2\text{-}PPh_3\text{-}7,12\text{-}\{Ag(PPh_3)\}\text{-}closo\text{-}2,1\text{-}MoCB_{10}H_9]$[20, 21] (2.552(4) Å and 2.589(4) Å), in which the Ag centre is bound dihapto by the cage and is the only other *closo*-polyhedral borane structure reported with an *exo*-$\{AgPR_3\}$ fragment, although there are others reported with ligands other than phosphane,[22] with Ag–metal bonds[21] and with *endo* coordination of a silver fragment.[18] The location of the silver phosphane fragment in relation to the B(8)–B(12) bond is such that the silver atom adopts a planar coordination motif with respect to P(1), B(8) and B(12) with the sum of relevant angles around Ag(1) 359.7°. P(1) essentially lies on the same plane formed by Ag(1), B(8) and B(12) (max deviation from plane 0.083 Å for P(1)), resulting in an apparent vacant coordination site *transoid* to H(7). Inspection of the extended lattice packing diagram shows that there are no Ag···H–B intermolecular interactions directed towards this vacant site.[18, 20] However, there is a long intermolecular interaction (3.348 Å) between Ag(1) and C(35)′ of a phenyl ring in a symmetry related molecule (Figure 2), and the arene carbon approaches the silver from the reverse of the trigonal

  0947-6539/02/0809-2089 $ 20.00+.50/0

Table 1. Crystal data and structure refinement for **1**, **2** and **3**.

	1	**2**	**3**
empirical formula	$C_{19}H_{27}AgB_{11}P$	$C_{74}H_{84}Ag_2B_{22}P_4$	$C_{19}H_{21}AgB_{11}Br_6P$
M_r	513.16	1550.85	986.57
T [K]	150(2)	170(2)	150(2)
λ [Å]	0.71073	0.71069	0.71073
crystal system	triclinic	triclinic	monoclinic
space group	$P\bar{1}$	$P\bar{1}$	$P2_1/c$
a [Å]	10.282(2)	11.6963(2)	8.89500(10)
b [Å]	10.988(2)	13.1668(2)	24.4140(4)
c [Å]	11.308(2)	14.1393(2)	14.4170(3)
α [°]	76.22(3)	96.8860(6)	90
β [°]	75.25(3)	106.8980(7)	102.0720(10)
γ [°]	75.61(3)	110.5370(8)	90
V [Å^3]	1175.7(4)	1890.30(5)	3061.60(9)
Z	2	1	4
ρ_{calcd} [mg m^{-3}]	1.450	1.362	2.140
μ [mm^{-1}]	0.932	0.646	8.554
F(000)	516	792	1848
crystal size [mm]	0.20 × 0.20 × 0.10	0.25 × 0.20 × 0.17	0.10 × 0.10 × 0.05
θ range [°]	2.96 to 27.50	3.38 to 27.50	3.71 to 27.88
reflections collected	20702	22570	23164
independent reflections	5374 [R(int) = 0.0387]	8605 [R(int) = 0.0250]	7253 [R(int) = 0.0519]
reflections observed ($>2\sigma$)	4538	7964	5880
max and min transmission	0.9126 and 0.8355	1.027, 0.981	0.66 and 0.47
data/restraints/parameters	5374/0/302	8605/2/478	7253/0/349
goodness of fit on F^2	1.018	1.050	1.041
final R indices [$I > 2\sigma$(I)]	$R_1 = 0.0316$ $wR_2 = 0.0757$	$R_1 = 0.0289$ $wR_2 = 0.0738$	$R_1 = 0.0358$ $wR_2 = 0.0783$
R indices (all data)	$R_1 = 0.0417$ $wR_2 = 0.0813$	$R_1 = 0.0323$ $wR_2 = 0.0763$	$R_1 = 0.0521$ $wR_2 = 0.0855$
largest diff. peak and hole [e Å^{-3}]	0.544 and −0.923	1.727 and −0.584	1.081 and −1.181

Table 2. Selected bond lengths [Å] and angles [°] for the new compounds **1**–**3**.

Compound **1**			
Ag(1)–P(1)	2.3625(7)	P(1)–Ag(1)–B(7)	142.11(6)
Ag(1)–B(7)	2.619(3)	P(1)–Ag(1)–B(8)	158.23(6)
Ag(1)–B(8)	2.504(3)	P(1)–Ag(1)–B(12)	160.32(6)
Ag(1)–B(12)	2.569(3)	B(12)–Ag(1)–B(8)	41.26(8)
Ag(1)–H(7)	2.36(2)	B(12)–Ag(1)–B(7)	40.37(8)
Ag(1)–H(8)	2.14(2)	B(7)–Ag(1)–B(8)	40.98(8)
Ag(1)–H(12)	2.26(2)		
Compound **2**			
Ag(1)–P(1)	2.4698(3)	Ag(1)–H(12)′	2.17(2)
Ag(1)–P(2)	2.4741(3)	Ag(1)–H(7)	2.51(2)
Ag(1)–B(7)	3.494(2)	P(1)–Ag(1)–P(2)	130.90(1)
Ag(1)–B(12)′	2.892(2)	B(7)–Ag(1)–B(12)′	72.4(6)
Compound **3**			
Ag(1)–P(1)	2.4032(10)	P(1)–Ag(1)–Br(7)	117.44(3)
Ag(1)–Br(7)	2.8710(5)	P(1)–Ag(1)–Br(8)	155.55(3)
Ag(1)–Br(8)	2.6963(5)	P(1)–Ag(1)–Br(12)	93.31(3)
Ag(1)–Br(12)	3.0953(5)	P(1)–Ag(1)–Br(11)′	157.15(1)
Ag(1)–Br(11)′	3.4901(5)	Br(7)–Ag(1)–Br(8)	87.471(14)

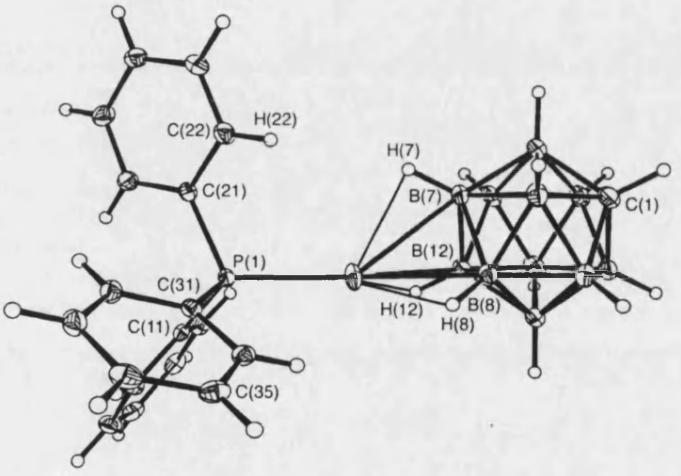

Figure 1. Molecular structure of complex **1**, showing the atom-numbering scheme. Thermal ellipsoids are drawn at the 50% probability level.

plane formed by B(8), B(12), Ag(1) and P(1). Although this distance is very long compared with other reported silver–arene bond lengths found in the solid-state structure of Ag carboranes (ca. 2.5–2.6 Å), we suggest that it may be significant, given the observed orientation of the silver phosphane fragment with respect to the cage. Indeed, gas-phase DFT calculations on **1** show that the silver adopts the expected tetrahedral geometry when there are no intermolecular interactions,[45] while comparable weak silver–arene contacts have been previously identified.[46, 47] The Ag(1)–P(1) distance, at 2.3625(7) Å, is at the shorter end of the range reported for $[Ag(PPh_3)L]$ or $[Ag(PPh_3)]X$ (X = counterion or two-electron ligand (L)) molecules[14, 16] suggesting a relatively strong AgP bond.

In solution, the $^1H\{^{11}B\}$ NMR spectrum of **1** shows a 1:1 ratio of phosphane to carborane anion. Resonances due to {BH} groups are observed at $\delta = 2.25$ and $\delta = 1.85$ in the ratio 1:10 (the latter is a 5+5 coincidence), with no high-field resonances potentially indicative of M–H–B interactions observed.[48] That only two {BH} resonances are observed suggests that the $\{AgPPh_3\}$ fragment is fluxional over the surface of the cage and affords time-averaged C_{5V} symmetry in solution. This facile process is evidenced by no significant change observed in the spectrum when recorded at −90 °C.

0947-6539/02/0809-2090 $ 20.00+.50/0 *Chem. Eur. J.* **2002**, *8*, No. 9

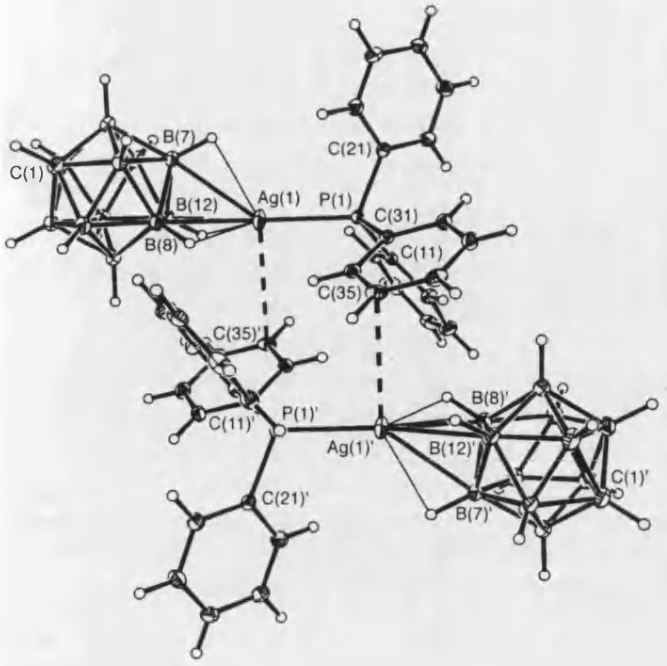

Figure 2. Dimeric unit formed in the extended lattice by Ag···C_{arene} contacts (Ag–C(35)' 3.348 Å). Atom labelling and other details as in Figure 1.

Related metallaboranes with *exo*-coordinated {$AgPPh_3$} fragments are also highly fluxional in solution.[20, 21] We were initially surprised to observe that the $^{11}B\{^1H\}$ NMR spectrum shows that both the antipodal [B(12)] and lower pentagonal belt [B(7)–(11)] borons undergo a significant upfield shift on complexation with the {$AgPPh_3$} fragment when compared with $Ag[CB_{11}H_{12}]$ (Figure 3), while there is no significant shift in the {BH} resonances observed in the $^1H\{^{11}B\}$ NMR spectrum. This was unexpected as coordination of an *exo*-metal fragment results in significant upfield shifts of the *exo*-metal coordinated {BH} units in *both* the ^1H and ^{11}B NMR spectra in other systems.[25, 44] Specifically, in the $^{11}B\{^1H\}$ NMR spectrum, resonances are observed at $\delta = -10.3$, $\delta = -11.2$ and $\delta = -12.0$ in the ratio 1:5:5. This dichotomy between ^1H and ^{11}B chemical shifts may be indicative of the cage-silver bonding predominantly originating from Ag–B interactions,[49] with a reduced contribution (or perhaps a more electrostatic interaction) from the cage hydrogens. It is noteworthy that AgH interactions can be observed by ^1H NMR spectroscopy in certain cases and show both significant chemical shifts and AgH coupling constants,[50] neither of which are observed for complex **1**, or previously in related Ag cage compounds.[19–21]

Given that only the antipodal [B(12)] and lower pentagonal belt [B(7)–B(11)] boron atoms appear significantly perturbed in the ^{11}B NMR spectrum on coordination of the {$AgPPh_3$} fragment, we suggest a mechanism to explain the observed fluxionality that incorporates the metal phosphane precessing around the five triangular faces formed between B(7)–B(11) and B(12). This mechanism is similar to that previously observed for the movement of $\{Rh(cod)\}^+$[44] or $\{Pt(t\mathrm{Bu}_2\mathrm{P}(\mathrm{CH}_2)_3\mathrm{P}t\mathrm{Bu}_2)\}^+$[51] over the surface of [*closo*-$CB_{11}H_{12}]^-$. In the $^{31}P\{^1H\}$ NMR spectrum of **1**, a peak centred at $\delta = 18.70$ is observed as a pair of concentric doublets, due to ^{109}AgP and ^{107}AgP coupling, having an average value for $J(AgP)_{average}$ of 743 Hz. This large value is consistent with the strong AgP bond seen in the solid state and is also indicative of a low-coordinate silver phosphane species;[13] this suggests the observed solution and solid-state structures of **1** are similar.

Addition of two equivalents of PPh_3 to $Ag[CB_{11}H_{12}]$ gives complex **2**, having the empirical formula $[Ag(PPh_3)_2(CB_{11}H_{12})]$, which has been characterised by solution NMR spectroscopy and in the solid state by X-ray diffraction. The extra PPh_3 ligand has the effect of disturbing the silver-cage bonding from **1**, so that a dimeric, centrosymmteric, $[Ag(PPh_3)_2(CB_{11}H_{12})]_2$ unit is now observed (Figure 4), in which each carborane unit bridges two silver centres. Each cage interacts with the two silver centres through one shorter (Ag(1)–H(12)' 2.17(2) Å, Ag(1)–B(12)' 2.892(2) Å) and one longer (Ag(1)–H(7) 2.51(2) Å, Ag(1)–B(7) 3.494(2) Å) Ag···H–B interaction. This bonding mode to the two silver centres by the antipodal [B(12)] and a single lower pentagonal belt [B(7)] vertex is similar to that observed in the extended solid-state structure of $[Mo(Cp)(CO)_3I \cdot Ag(CB_{11}H_{12})]_2$.[24] Dimeric and tetrameric silver carborane complexes with cages other than $[CB_{11}H_{12}]^-$ have also been previously reported.[18, 20–22] As expected on moving to a higher coordination number in going from **1** to **2**, the Ag–P bond lengths are relatively longer in the latter complex (Ag(1)–P(1) 2.4698(3) Å, Ag(1)–P(2) 2.4741(3) Å). The P(1)–Ag(1)–P(2) angle of 130.90(1)° is similar to that observed in the three-coordinate complex $[Ag(PPh_3)_2(NCMe)][BF_4]$ (129.37(2)°).[14]

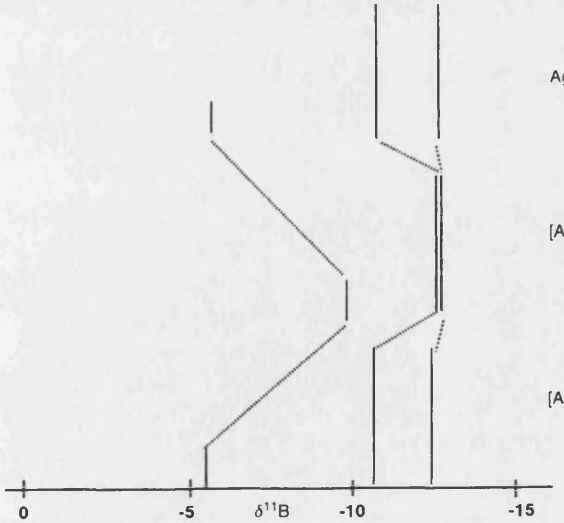

Figure 3. ^{11}B NMR chemical shift "stick" diagram comparing complexes **1** and **2** (solutions in CD_2Cl_2) with $Ag[CB_{11}H_{12}]$ (solution in [D_6]acetone).

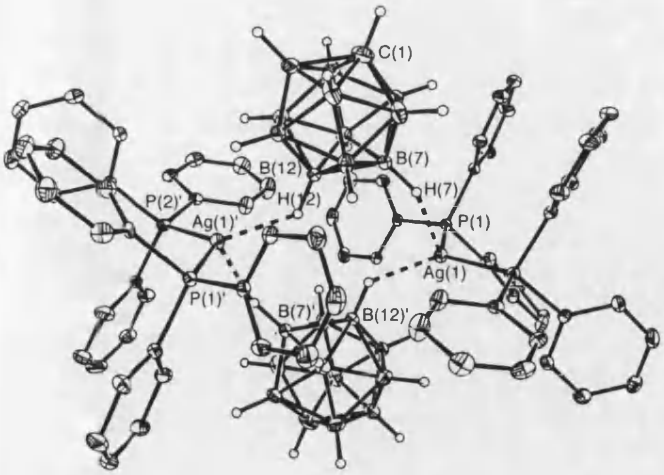

Figure 4. Molecular structure of complex **2**, showing the atom-numbering scheme. Phenyl hydrogen atoms are omitted for clarity. Thermal ellipsoids are drawn at the 50% probability level.

In solution at room temperature in **2**, the carborane does not interact significantly with the metal centre. This is evidenced in the ^{11}B NMR spectrum, which does not show any appreciable perturbation from that found for $Ag[CB_{11}H_{12}]$, with three resonances observed at $\delta = -5.1$, -10.6 and -12.6 in the ratio 1:5:5 (Figure 3). These data reflect the significantly weaker Ag···H–B interactions apparent in **2**, relative to **1**, in the solid state. In the room-temperature $^{31}P\{^1H\}$ NMR spectrum of **2**, a single broad resonance centred at $\delta = 14.8$ is observed, suggesting that the phosphane ligands are undergoing an exchange process. Progressive cooling affords two broad singlets at $\delta = 15.4$ and $\delta = 13.2$ at 0 °C, which gradually sharpen into two sets of doublets at -60 °C, of approximately equal proportions, centred at $\delta = 13.7$ ($J(AgP) = 333$ Hz) and $\delta = 13.6$. The latter resonance is further observed as a pair of concentric doublets, showing coupling to both ^{109}Ag and ^{107}Ag ($J(AgP)_{average} = 519$ Hz). These changes in the NMR spectrum on cooling are consonant with the presence of two different complexes in solution at low temperature, which interconvert at ambient temperature. The species that reveals the larger AgP coupling constant has a value very similar to that reported for two-coordinate $[Ag(PPh_3)_2][BF_4]$ ($J(AgP) = 530$ Hz),[14] while the alternative species has a coupling constant intermediate between the three-coordinate $[Ag(PPh_3)_2Br]$ ($J(AgP) = 385$ Hz)[15] and four-coordinate $[Ag(PPh_3)_4][PF_6]$ ($J(^{107}AgP) = 224$ Hz)[13] silver phosphane complexes. On the basis of these observations, we tentatively suggest that, at low temperature an approximate 1:1 mixture consisting of the two-coordinate, ion-pair separated, species $[Ag(PPh_3)_2][CB_{11}H_{12}]$ and the dimeric $[Ag(PPh_3)_2(CB_{11}H_{12})]_2$ is formed. No evidence for the disproportionation of **2** to form $[Ag(PPh_3)][CB_{11}H_{12}]$ and $[Ag(PPh_3)_3][CB_{11}H_{12}]$ was seen in the low-temperature $^{31}P\{^1H\}$ NMR spectrum.[13] The low-temperature $^{11}B\{^1H\}$ NMR spectrum exhibits two broad peaks at $\delta = -5.8$ (1B) and $\delta = -11.6$(10B), essentially unshifted from room-temperature values.

The coordination chemistry of the anion [*closo*-$CB_{11}H_{12}]^-$ can be usefully compared with that of [*closo*-$CB_{11}H_6Br_6]^-$, in which the six lower hydrogen atoms in the cage are replaced with bromines, and it is considered to be significantly more weakly coordinating than $[CB_{11}H_{12}]^-$. While there are now a significant number of solid-state structural investigations on the silver salts of perhalogenated anions,[27, 30–33] there are few studies in which both the solution and solid-state structures of their transition metal complexes have been investigated. Addition of one equivalent of PPh_3 to a suspension of $Ag[CB_{11}H_6Br_6]$ in CH_2Cl_2 affords the new complex $[Ag(PPh_3)(CB_{11}H_6Br_6)]$ (**3**). The solid-state structure of **3** is presented in Figure 5. On first inspection, the silver(I) centre is coordinated with the carborane anion through two shorter (2.6963(5) Å and 2.8710(5) Å) Ag–Br interactions and one longer one (3.0953(5) Å), all of which fall comfortably within the sum of the van der Waals radii for silver and bromine. These bond lengths are of similar values to those previously reported for silver complexes of $[CB_{11}H_6Br_6]^-$[31] and dibromoalkane complexes of silver.[52] The silver phosphane bond length (2.4032(10) Å) is slightly longer than that found in **1**. The phosphane phenyl groups adopt a relatively uncommon C_{2v} arrangement, a result of one phenyl group (C(2)–C(7)) twisting to minimise interactions with Br(12). Given that the silver is formally 4-connected in the asymmetric unit, the fact that it appears to adopt a *pseudo*trigonal planar, as opposed to a tetrahedral coordination motif (sum of relevant angles around Ag(1) is 360.5°) was on first inspection puzzling to us. However, similar to **1**, the packing diagram (Figure 6) reveals a long interaction (3.4901(5) Å) between Ag(1) and Br(11)′ on a symmetry related cage in the lattice; this bromine atom approaches Ag(1) approximately *trans* to Br(12) (Br(12)–Ag(1)–Br(11)′ 157.15(1)°). Although this distance is long, the coordination motif around the silver suggests that it is significant in the solid state. This interaction completes the coordination sphere at the silver centre. It also results in phenyl groups on symmetry related phosphanes having a close approach in the lattice (Figure 6), and the Ag(1)–P(1) vector being canted from lying equidistant between Br(7)

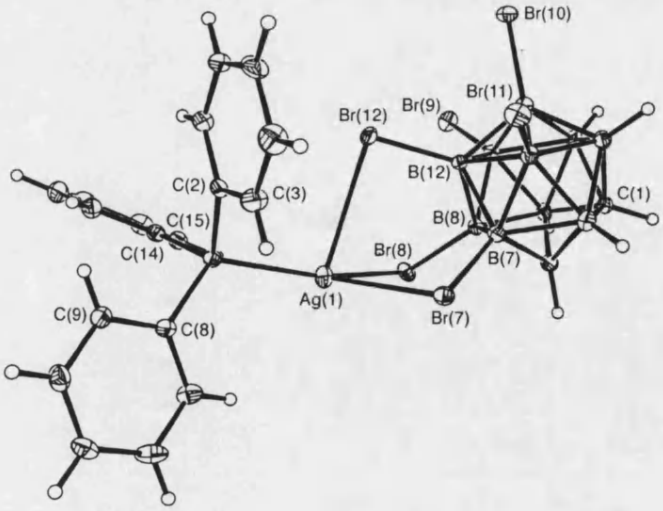

Figure 5. Molecular structure of complex **3**, showing the atom-numbering scheme. Thermal ellipsoids are drawn at the 50% probability level.

0947-6539/02/0809-2092 $ 20.00+.50/0 *Chem. Eur. J.* **2002**, *8*, No. 9

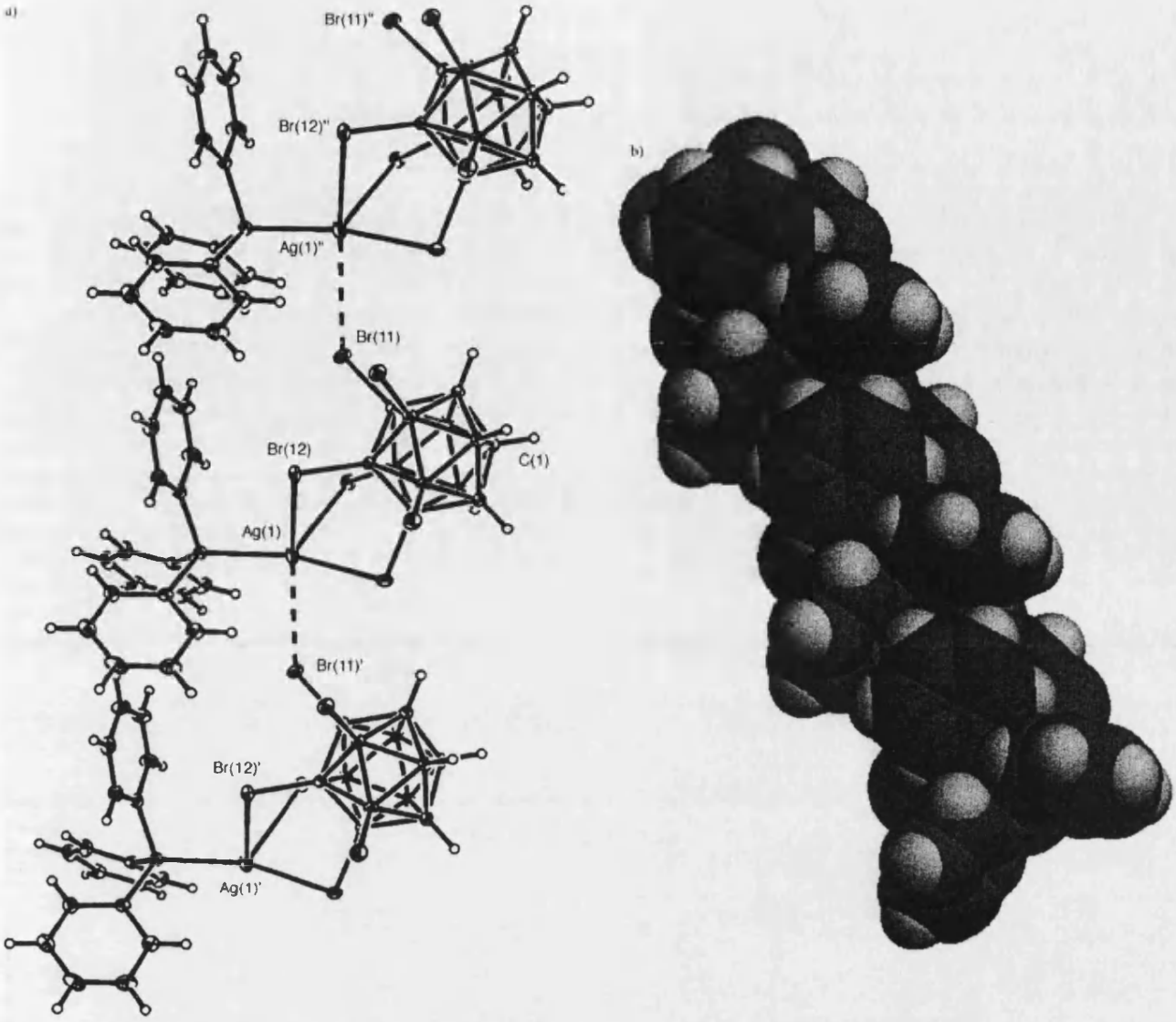

Figure 6. Extended solid-state structure apparent in complex **3**: a) showing weak axial Ag···Br interactions; b) space-filling diagram showing orientation of phenyl groups in the solid state.

and Br(8) (P(1)–Ag(1)–Br(8) 155.55(3)°, P(1)–Ag(1)–Br(7) 117.44(3)°).

In solution, C_{5v} symmetry is observed for the cage anion in the ^{11}B NMR spectrum, which shows that the $\{AgPPh_3\}^+$ fragment does not retain a rigid coordination motif with respect to the cage. The $^{31}P\{^1H\}$ NMR spectrum of **3** is similar to that of **1** with a resonance centred at $\delta = 16.52$ is observed as a concentric pair of doublets, $J(AgP)_{average} = 715$ Hz, suggesting that similar structures are adopted in solution for both complexes. This value is slightly smaller than that observed for **1**, in line with the slightly longer Ag–P bond observed in the solid state for **3** compared with complex **1**.[17]

Addition of two equivalents of PPh_3 to $Ag[CB_{11}H_6Br_6]$ results in the isolation of a white solid having the empirical formula $[Ag(PPh_3)_2(CB_{11}H_6Br_6)]$ (**4**). Despite repeated attempts, crystals suitable for X-ray diffraction could not be obtained, so characterisation of complex **4** was limited to NMR spectroscopy and microanalysis. In solution at room temperature, the $^{31}P\{^1H\}$ NMR spectrum of **4** has a broad singlet at $\delta = 12.9$, showing that the phosphane ligands are undergoing exchange under ambient conditions. The corresponding $^1H\{^{11}B\}$ NMR spectrum shows a 2:1 ratio of phosphane to cage, with no signals observed at high field. The low-temperature (–80 °C) $^{31}P\{^1H\}$ NMR spectrum shows that one species is present at this temperature, due to two concentric doublets centred around $\delta = 8.1$. The magnitude of the AgP coupling constant ($J(AgP)_{average} = 240$ Hz) is very small and of the same order of that associated with $[Ag(PPh_3)_4]^+$.[13] To account for this, a low-temperature limiting structure that has a sp^3 hybridised silver(I) centre is suggested, in which the hexabromo carborane anion is coordinated to the silver by two of the bromines on the cage. That there is a more intimate contact between the halogenated cage and silver in **4** compared with the silver-cage contact

in **2** is further reflected in the relative catalytic activities of these two compounds, which will be presented later. While we have taken measures to use pure samples (recrystallised material used exclusively for NMR and catalysis experiments), we cannot completely rule out the presence of small amounts of free PPh_3 in **2** and **4**, which would lead to rapid phosphane exchange at room temperature.[13]

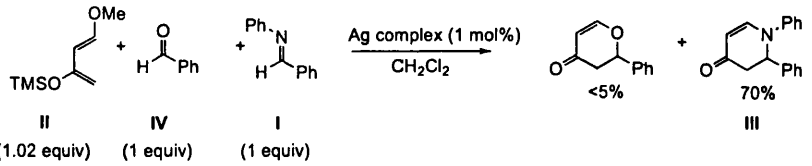

Scheme 3. Activation of imines in the presence of aldehydes by silver complex **3**.

Catalysis: We have investigated the reaction between *N*-benzylideneaniline (**I**) and Danishefsky's diene (**II**) (Scheme 2) with the silver complexes **1** to **4**. Importantly, in the absence of any catalyst there was only a trace (less than 5%) of product after 24 hours at room temperature. Initial experiments using freshly distilled reagent grade solvents revealed that the addition of 1 mol% of silver complex promoted the efficient formation of the product (**III**) in less than one hour at room temperature (Table 3). On the bench under these conditions, complexes **1** to **4** were significantly more active than $[Ag(PPh_3)(OTf)]$ and $[Ag(PPh_3)(BF_4)]$ whilst $[Ag(PPh_3)(ClO_4)]$ was of comparable activity. Remarkably, the catalyst loading could be lowered to 0.1 mol% of complex **3** and the reaction was still complete in less than thirty minutes to afford an isolated yield of 99% product (> 2000 turnovers $hour^{-1}$).

Table 3. Yields of compound **III**. Catalyst (1 mol%); imine **I** (1.1 mmol); Danishefsky's diene (**II**) (1.65 mmol). Yields reported are after reaction for 60 minutes at room temperature and workup (see Experimental Section for full details).

	Complex	Isolated yield of **III** [%]
1	$[Ag(PPh_3)(BF_4)]$	35
2	$[Ag(PPh_3)(OTf)]$	70
3	$[Ag(PPh_3)(ClO_4)]$	90
4	$[Ag(PPh_3)(CB_{11}H_{12})]$ (**1**)	98
5	$[Ag(PPh_3)_2(CB_{11}H_{12})]$ (**2**)	99
6	$[Ag(PPh_3)(CB_{11}H_6Br_6)]$ (**3**)	99
7	$[Ag(PPh_3)_2(CB_{11}H_6Br_6)]$ (**4**)	85

A competition experiment illustrated that silver complex **3** could preferentially activate imines in the presence of aldehydes (Scheme 3). When Danishefsky's diene (**II**) was added to a 1:1 mixture of benzaldehyde (**IV**) and imine (**I**) in the presence of 1 mol% of **3**, the product arising from the reaction, after 15 minutes at room temperature, was isolated in 70% yield whilst the aldehyde adduct was produced in only 5% yield. According to the classification system suggested by Kobayashi et al.,[53] the silver catalyst is thus an A-2 Lewis acid (active, imine selective).

Prompted by these results we decided to follow the reactions by ^1H NMR spectroscopy, using catalyst loadings of 0.1 mol%, in the anticipation of uncovering structure–activity relationships involving counterion and/or phosphane ligands. This initially resulted in the unexpected observation that the reaction between diene **II** and imine **I** did not proceed (no reaction after ca. two hours at room temperature) when in the NMR tube, using rigorously dried solvent (CD_2Cl_2 vacuum distilled from CaH_2). However, addition of a substoichiometric amount of water (ca. 50 mol%, 1 μL, unoptimised) to these solutions resulted in rapid initiation of the reaction. This is an example of a water-accelerated Lewis acid catalysed reaction; such reactions, in which water is an important partner, are being increasingly appreciated.[54] Pertinent to this observation, modest yield enhancements on addition of stoichiometric amounts of water to a hetero-Diels–Alder reaction catalysed by lanthanide trifluoromethanesulfonylamides[55] have been reported previously. Currently, we are unsure about the exact role of the water in the reaction. It is likely, however, that a polarised, silver-bound, water molecule acts as a Lewis assisted Brønsted acid, similar to that in lanthanide salt catalysed aromatic electrophilic substitutions.[56] It is also similar to the role metal-coordinated water is suggested to play in certain catalytic processes.[57] In support of this, preliminary DFT calculations on the model system $[Ag(Me_3P)(OH_2)(MeNH{=}CHMe)]^+$ indicate that a coordinated water molecule plays an important function in the silver promoted [2+4] addition of imine to diene. A putative intermediate in this process is shown in Scheme 4, in which the water molecule forms a hydrogen bond with the nitrogen atom.[45] This proposed intermediate accounts for both the observed dependence on trace amounts of water in this reaction and the strong counterion effect observed (vide infra), with both the Lewis assisted Brønsted acidity (OH···N hydrogen bond) and the need for a vacant site (alkene coordination) playing important roles. Experimentally, what is clear is that trace

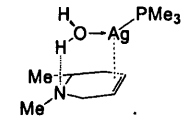

Scheme 4. Proposed intermediate structure.

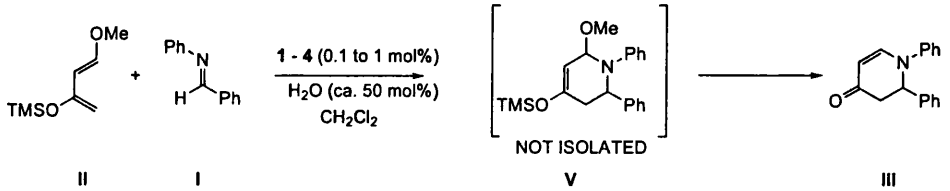

Scheme 2. Reaction between *N*-benzylideneaniline (**I**) and Danishefsky's diene (**II**) with the silver complexes **1**–**4**.

0947-6539/02/0809-2094 $ 20.00+.50/0 *Chem. Eur. J.* **2002**, *8*, No. 9

amounts of water are needed for this reaction to proceed, which is probably made available to the reaction, when at the bench, by adventitious water.

That a silver-bound water molecule is strongly implicated as a catalytic proton source in these reactions is demonstrated by the following control experiments. Addition of just water to a mixture of **I** and **II** affords no product, while under the standard conditions used for catalysis addition of the hindered base 2,6-di-*tert*-butyl-4-methylpyridine suppressed the reaction completely.[56] Moreover, water need not be the unique proton source. The reaction is easily repeated replacing an alcohol (methanol, 20 mol%) for water, resulting in essentially identical product yields and reaction times.

The results of these NMR experiments, in which water is added, are shown in Figure 7 for the new complexes **1** through **4** and for comparison the complexes $[Ag(PPh_3)(BF_4)]$, $[Ag(PPh_3)(ClO_4)]$[58] and $[Ag(PPh_3)(OTf)]$.[16] All of these experiments were carried out at 0.1 mol% catalyst loading with 50 mol% added water in solutions in CD_2Cl_2, with the diene in 1.5 molar excess. The final products in the NMR tube are a consistent mixture of intermediate **V** and final product **III** (ca. 90:10 ratio), which on workup gives only the final product. The reactions were monitored by selected peaks due to intermediate **V** and the final product (see Experimental Section). No hydrolysis of the imine to benzaldehyde was observed under the conditions used, while the consumption of imine **I** in each run followed the same time-dependent profile (although inversed) as the increase in **V** and **III**.

It is clear from Figure 7 that complex **3** gives the fastest rate of catalysis, complete conversion being apparent after 15 minutes. This equates to a turnover frequency (TOF) of 4000 $hour^{-1}$, which is excellent for a Lewis acid catalysed reaction of this type. Complex **1**, although a slower catalyst than **3**, also yields complete conversion of the imine after $\approx$40 minutes. Not unsurprisingly the monophosphane complexes, $[Ag(PPh_3)(ClO_4)]$ and $[Ag(PPh_3)(OTf)]$, which contain more nucleophilic counterions, are less active than **1** and **3**. The addition of an extra PPh_3 ligand would be expected to both reduce the Lewis acidity of the metal centre while also adding more steric bulk and blocking a potential vacant site. It is not unexpected then, that complexes **2** and **4** are significantly poorer catalysts than any of the monophosphane complexes. Interestingly the relative reaction rates for the bisphosphane complexes **2** and **4** are reversed from those seen for the monophosphane/carborane complexes. Complex **2**, which incorporates the $[CB_{11}H_{12}]$ anion, catalyses the reaction significantly faster than **4**. Although this is perhaps counter-intuitive given the relative coordinating abilities of these two anions, when the solution structures at $-60\,^{\circ}C$ are compared (vide supra), complex **4** shows a considerably smaller value for J(AgP), suggesting a silver centre that has a higher formal coordination number in **4** than in **2**. This implies that the $[CB_{11}H_6Br_6]^-$ anion interacts significantly with the metal centre at this temperature in **4**. Although we do not have the solid-state structure of **4** to hand,[59] this correlation between the magnitude of J(AgP) at low temperature and the relative rates of **2** and **4** is compelling. This difference in rate is also reflected in the relative product yields on the bench after one hour (entries 5 and 7 in Table 3).

The catalyst $[Ag(PPh_3)(BF_4)]$ ceases to function after only a few minutes of activity, giving only modest yields of cycloaddition product in both the NMR and the bench-top experiments (Figure 7 and Table 3, entry 1). We suggest that under the conditions used for catalysis (0.1 mol% catalyst, 50 mol% water), rapid (<2 minutes) silver(I) mediated hydrolysis of the $[BF_4]^-$ anion occurs to afford an oxyborate anion that binds strongly with the metal centre, shutting down the catalytic cycle dramatically. In support of this, hydrolysis of $[BF_4]^-$ to afford coordinated oxyborates has been reported previously.[60, 61]

Conclusion

The preparation of the four silver(I) phosphane complexes partnered with the carborane anions [*closo*-$CB_{11}H_{12}$] and

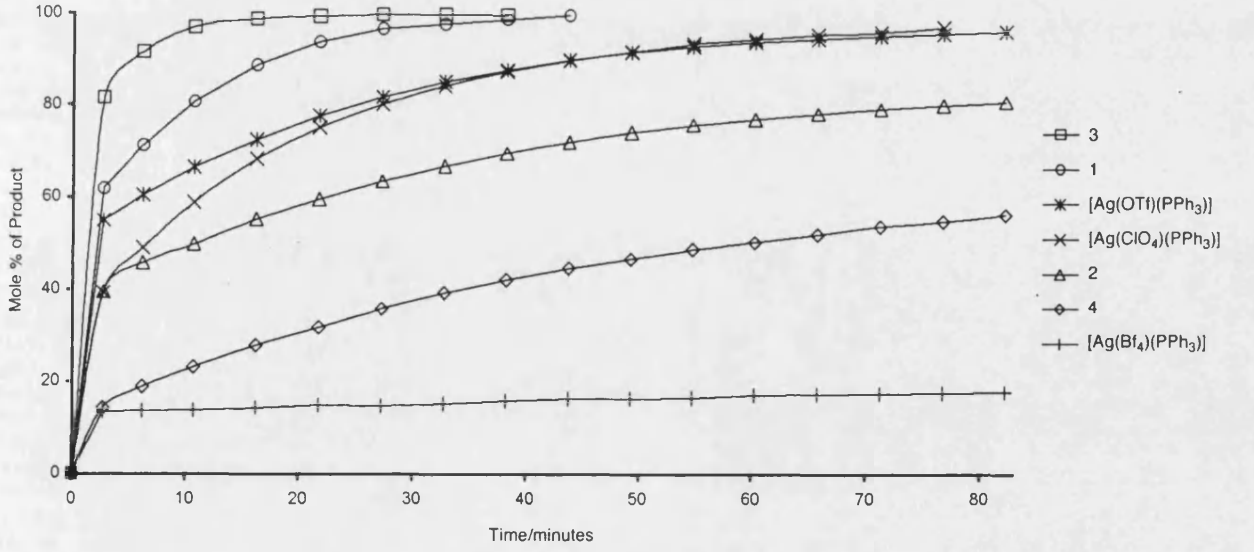

Figure 7. Chart showing relative rates of reaction between **I** and **II** by using 0.1 mol% of catalysts **1**–**4** and $[Ag(PPh_3)(Y)]$ [Y = OTf, BF_4, ClO_4] and 50 mol% added H_2O at room temperature in CD_2Cl_2. See text for other details.

[*closo*-$CB_{11}H_6Br_6$] has allowed a study to be made of the relationship between solid and solution structures and performance as partners to cationic Lewis acids of these anions in an organic transformation. Not unsurprisingly, given the now well-documented[4, 5] inertness coupled with the low nucleophilicity of the hexahalageno anions and the precedent for pronounced counterion effects in Lewis acid catalysed cycloadditions,[62-64] the monophosphane complex **3** is a significantly better catalyst than both **1** and all of the other systems examined. In addition, compound **3** (and presumably the others, although not tested) is selective for imines and can be used at significantly lower catalyst loadings than previously reported for Lewis acid catalysed hetero-Diels–Alder reactions.

To us, the surprising result is that the relative ordering in rate of catalysis between [$CB_{11}H_{12}$] and [$CB_{11}H_6Br_6$] is reversed when two phosphanes are coordinated to the silver centre. Although this was unexpected, it is pleasing that a gross correlation exists between observable NMR properties in solution (magnitude of J(AgP)) and the catalytic activity. Thus, complexes **1** and **3**, which have large AgP coupling constants, are better catalysts than **2** and **4**, with the latter complex exhibiting the poorest performance and the lowest coupling constant by far (albeit measured at low temperature). Overall this suggests that when considering catalyst performance in these, and related systems, the influence of counterion and ligands are not independent and need to be considered together. It is however encouraging that useful catalyst performance indicators may be gleaned from simple NMR experiments, which could help in the identification of promising catalytic systems. To this end, we are currently investigating the applicability of complexes such as **3** in other Lewis acid catalysed reactions and will report on these in due course.

Experimental Section

General: All manipulations were carried out under an argon atmosphere by using standard Schlenk line or dry box techniques. CH_2Cl_2 was distilled from CaH_2 and hexane was distilled from sodium. Solution NMR spectra were measured on Varian 400 MHz and Bruker Advance 300 MHz FT-NMR spectrometers in solutions in CD_2Cl_2. Residual protio solvent was used as a reference (CD_2Cl_2, $\delta = 5.33$) in ^{1}H NMR, $BF_3 \cdot OEt_2$ (external) in ^{11}B NMR and 85% H_3PO_4 (external) for ^{31}P NMR spectra. Coupling constants are given in Hz. Elemental analyses were performed in-house at the Department of Chemistry. The complexes Ag[$CB_{11}H_{12}$][26] and Ag[$CB_{11}H_6Br_6$][13] were prepared by the published literature routes or variations thereof. All other chemicals were used as purchased from Aldrich.

Preparations

[$Ag(PPh_3)(CB_{11}H_{12})$] (*1*): PPh_3 (0.163 g, 0.650 mmol) was dissolved in CH_2Cl_2 (10 mL) and added dropwise to a Schlenk flask charged with Ag[$CB_{11}H_{12}$] (0.155 g, 0.591 mmol), in the dark and with stirring. This solution was stirred overnight and then cannula filtered. The solvent was removed in vacuo to leave a pale yellow solid. Colourless crystals suitable for an X-ray diffraction study were grown by redissolving the product up in minimum CH_2Cl_2, layering with hexane, then placing the sample in a freezer overnight at −30 °C (0.281 g, 92% yield).

^{1}H{^{11}B} (22 °C): $\delta = 7.52-7.29$ (m, 15H; C_6H_5), 2.55 (brs, 1H; CH_{cage}), 2.25 (brs, 1H; BH), 1.85 (10H; 5+5 coincidence, BH); selected ^{1}H{^{11}B} (−90 °C): $\delta = 2.59$ (brs, 1H; CH_{cage}), 2.34 (brs, 1H; BH), 1.94 (5H; BH), 1.76 (5H; BH); ^{11}B{^{1}H} (22 °C): $\delta = -10.3$ (shbr, 1B), −11.2 (br, 5B), −12.0 (5B); ^{11}B $\delta = -10.3$ (d, 5+1 coincidence, J(HB) = 118 Hz), −12.0 (d, J(HB) = 110 Hz, 5B); ^{31}P{^{1}H} (22 °C): $\delta = 18.70$ (dd, $J(Ag^{109}P) = 795$, $J(Ag^{107}P) = 691$ Hz, 1P); IR (KBr): $\tilde{\nu} = 2565$ (vs, BH), 2517 (shs, BH), 2372 cm^{-1} (m, BH); elemental analysis calcd (%) for $C_{19}H_{27}B_{11}AgP$: C 44.5, H 5.30; found: C 44.3, H 5.19.

[$Ag(PPh_3)_2(CB_{11}H_{12})$] (*2*): Ag[$CB_{11}H_{12}$] (0.075 g, 0.299 mmol) and PPh_3 (0.158 g, 0.602 mmol) were stirred together in CH_2Cl_2 (15 mL) in the dark for 1 hour. This solution was filtered and hexane (20 mL) added to the filtrate to induce crystallisation. The colourless product was isolated by decanting off the solvent and drying in vacuo (0.204 g, 88% yield). Crystals suitable for an X-ray diffraction study were grown by redissolving a portion of the solid product in a minimum of CH_2Cl_2, layering with hexanes and then placing in a freezer overnight at −30 °C to yield white crystals.

^{1}H{^{11}B} (22 °C): $\delta = 7.45-7.18$ (m, 30H; C_6H_5), 2.21 (brs, 1H; CH_{cage}), 1.85 (brs, 1H; BH_a), 1.58 (brs, 10H; 5+5 coincidence, BH); ^{11}B{^{1}H} (CD_2Cl_2, 22 °C): $\delta = -5.1$ (brs, 1B), −10.6 (brs, 5B), −12.6 (brs, 5B); ^{11}B (22 °C): $\delta = -5.1$ (d, J(HB) = 128 Hz, 1B), −10.6 (d, J (HB) = 138 Hz, 5B), −12.6 (d, J(HB) = 158 Hz, 5B); ^{31}P{^{1}H} (CD_2Cl_2, 22 °C): $\delta = 14.8$ (s, br); ^{31}P{^{1}H} (−60 °C): $\delta = 13.7$ (brd, J(AgP) = 333 Hz), 13.6 (dd, $J(Ag^{109}P) = 554$, $J(Ag^{107}P) = 483$ Hz); IR (KBr): 2544 (vs, BH), 2442 (m, BH), 2396 cm^{-1} (m, BH); elemental analysis calcd (%) for $C_{37}H_{42}B_{11}AgP_2$: C 57.3, H 5.46; found: C 57.2, H 5.53.

[$Ag(PPh_3)(CB_{11}H_6Br_6)$] (*3*): PPh_3 (0.062 g, 0.236 mmol) was dissolved in CH_2Cl_2 (10 mL) and added dropwise to a Schlenk flask charged with Ag[$CB_{11}H_6Br_6$] (0.200 g, 0.276 mmol) in the dark and with stirring. The resulting solution was stirred overnight and filtered. The supernatent solvent was removed in vacuo to leave a clear oil. Crystals suitable for an X-ray diffraction study were grown by redissolving the product up in minimum CH_2Cl_2, layering with hexane, then placing the sample in a freezer overnight at −30 °C (0.194 g, 83% yield).

^{1}H{^{11}B}: $\delta = 7.52-7.22$ (m, 15H; C_6H_5), 2.73 (brs, 1H; CH_{cage}), 2.43 (5H; BH); ^{11}B: $\delta = -2.1$ (brs, 1B, B), −6.6 (brs, 5B, BBr), −16.9 (d, J(HB) = 157 Hz, 5B, BH); ^{31}P{^{1}H}: $\delta = 16.52$ (d of d, $J(Ag^{109}P) = 766$, $J(Ag^{107}P) = 664$ Hz, 1P); IR (KBr): 2608 (vs, BH), 2593 cm^{-1} (s, BH); elemental analysis calcd (%) for $C_{19}H_{21}B_{11}AgPBr_6$: C 23.1, H 2.12; found: C 22.6, H 2.17.

[$Ag(PPh_3)_2(CB_{11}H_6Br_6)$] (*4*): The compounds Ag[$CB_{11}H_6Br_6$] (0.250 g, 0.345 mmol) and PPh_3 (0.181 g, 0.690 mmol) were stirred together in CH_2Cl_2 (20 mL) in the dark for 1 hour. The solution formed was filtered and solvent removed in vacuo to leave a white solid. This solid was redissolved in minimum CH_2Cl_2, layered with hexane and placed in a freezer overnight at −30 °C to afford a colourless microcrystalline powder (0.246 g, 57%).

^{1}H{^{11}B}: $\delta = 7.45-6.87$ (m, 30H; C_6H_5), 2.45 (brs, 1H; CH_{cage}), 2.21 (brs, 5H); ^{11}B: $\delta = 1.3$ (brs, 1B, B), −6.8 (s, 5B), −17.2 (d, J(HB) = 166 Hz, 5B); ^{31}P{^{1}H} (22 °C): $\delta = 8.1$ (brs); ^{31}P{^{1}H} (−80 °C): $\delta = 8.06$ (dd, $J(^{109}AgP) = 256$, ^{107}J(AgP) = 223 Hz); IR (KBr): 2956 (vs, BH), 2587 cm^{-1} (s, BH); elemental analysis calcd (%) for $C_{37}H_{36}B_{11}AgP_2Br_6$: C 35.7, H 2.89; found: C 35.5, H 3.01.

General experimental procedure for catalytic studies: The imine **I** (0.200 g, 1.1 mmol) in dichloromethane (1.5 mL) at room temperature was added to a stirring solution of freshly recrystallised catalyst (1 mol%) in dichloromethane (3.5 mL). The reaction mixture was allowed to stir for 5 minutes then Danishefsky's diene (**II**) (320 μL, 1.65 mmol) was added dropwise. After 60 minutes, the reaction was quenched with aqueous sodium hydrogen carbonate and extracted with ethyl acetate. The crude product was purified by chromatography on silica gel (hexane/ethyl acetate 4:1) to afford the product **III**.

^{1}H NMR: $\delta = 7.67$ (dd, J(HH) = 1, 7 Hz, 1H), 7.35–6.99 (m, 10H), 5.27 (dd, J(HH) = 1, 7 Hz, 2H), 3.29 (dd, J(HH) = 7, 16 Hz, 1H), 2.77 (ddd, J(HH) = 1, 3, 16 Hz, 1H).

General procedure for NMR tube reactions: Solutions of catalyst were typically prepared by dissolving the compound (1 mg) in CD_2Cl_2 (1 mL) with the use of an ultrasound bath to ensure complete catalyst dissolution, although, by eye, the solids seemed to have dissolved completely. The relevant quantity of catalyst solution to give a 0.1 mol% catalyst concentration (i.e. 0.00011 mmol of catalyst) was taken from this standard solution and placed in an NMR tube previously charged with *N*-benzylideneaniline (20 mg, 0.11 mmol). Danishefsky's diene (32 μL, 0.17 mmol) and water (1 μL, 0.056 mmol) were added to the NMR tube, which was then shaken

  0947-6539/02/0809-2096 $ 20.00+.50/0 *Chem. Eur. J.* **2002**, *8*, No. 9

vigorously before being placed in the NMR spectrometer and measurements were taken at timed intervals. The disappearance of the peak at δ = 8.51 due to PhN=C*H*Ph was monitored, along with the growth of the peaks centred at $\delta = 6.64$ and $\delta = 6.54$ [3H total, intermediate **V**] and $\delta = 5.27$ [1H total, final product **III**]. A plot for each catalyst, of time verses consumption of **I** and time verses total concentrations of **V** and **III** showed essentially the same profile. Repeat runs for all the catalysts tested showed the same time-dependent profiles.

Intermediate **V**: ^{1}H NMR: $\delta = 7.56$ (d, J(HH) = 13 Hz, 1H), 7.42–7.40 (m, 2H), 7.28–7.23 (m, 1H), 7.10–7.01 (m, 3H), 6.64 (m, 1H), 6.54 (m, 2H), 5.58 (d, J(HH) = 12 Hz, 1H), 4.86 (q, J(HH) = 6 Hz, 1H), 4.71 (d, J(HH) = 6 Hz, 1H), 3.68 (s, 3H), 2.94 (dd, J(HH) = 6 Hz, 22H), 0.144 (s, 9H).

X-ray crystallography: The crystal structure data for compounds **1**–**3** were collected on a Nonius KappaCCD. Structure solution followed by full-matrix least-squares refinement was performed by using the SHELX suite of programs throughout.[65] Hydrogens were included at calculated positions throughout, with the exception of H7 and H12 in compound **2**. These latter hydrogens were readily located in the penultimate difference Fourier map and refined at a fixed distance 1.12 Å from parent atoms B(7) and B(12), respectively. Plots were produced by using ORTEX.[66]

CCDC-171721 (**1**), 171769 (**2**) and 168828 (**3**) contain the supplementary crystallographic data for this paper. These data can be obtained free of charge via www.ccdc.cam.ac.uk/conts/retrieving.html (or from the Cambridge Crystallographic Data Centre, 12 Union Road, Cambridge CB21EZ, UK; fax: (+44)1223-336-033; or e-mail: deposit@ccdc.cam.ac.uk).

Acknowledgements

A.S.W. thanks the Royal Society for a University Research Fellowship and equipment grant. The University of Bath is also thanked for financial support (studentships to N.J.P. and C.H.). C.G.F. thanks Astra-Zeneca for generous support from their strategic research fund. The use of the Cambridge Structural Database at Daresbury service is acknowledged. The EPSRC/JERI are acknowledged for funding for the diffractometer.

[1] C. A. Reed, *Acc. Chem. Res.* **1998**, *31*, 133.
[2] S. H. Strauss, *Chem. Rev.* **1993**, *93*, 927.
[3] I. Zharov, B. T. King, Z. Havlast, A. Pardi, J. Michl, *J. Am. Chem. Soc.* **2000**, *122*, 10253.
[4] C. A. Reed, N. L. P. Fackler, K. C. Kim, D. Stasko, D. R. Evans, P. D. W. Boyd, C. E. F. Rickard, *J. Am. Chem. Soc.* **1999**, *121*, 6314.
[5] C. A. Reed, K. C. Kim, R. D. Bolskar, L. J. Mueller, *Science* **2000**, *289*, 101.
[6] A. J. Lupinetti, M. D. Havighurst, S. M. Miller, O. P. Anderson, S. H. Strauss, *J. Am. Chem. Soc.* **1999**, *121*, 11920.
[7] H. W. Turner, European Patent Application 277003, **1988**; [*Chem. Abstr.* **1988**, *110*, 58291].
[8] G. G. Hlatky, R. R. Eckman, H. W. Turner, *Organometallics* **1992**, *11*, 1413.
[9] G. G. Hlatky, H. W. Turner, R. R. Eckman, *J. Am. Chem. Soc.* **1989**, *111*, 2728.
[10] D. J. Crowther, S. L. Borkowsky, D. Swenson, T. Y. Meyer, R. F. Jordan, *Organometallics* **1993**, *12*, 2897.
[11] W. V. Konze, B. L. Scott, G. J. Kubas, *Chem. Commun.* **1999**, 1807.
[12] J. Powell, A. Lough, T. Saeed, *J. Chem. Soc. Dalton Trans.* **1997**, 4137.
[13] E. L. Muetterties, C. W. Alegranti, *J. Am. Chem. Soc.* **1972**, *94*, 6386.
[14] R. E. Bachmann, D. F. Andretta, *Inorg. Chem.* **1998**, *37*, 5657.
[15] G. A. Bowmaker, Effendy J. V. Hanna, P. C. Healy, B. W. Skelton, A. H. White, *J. Chem. Soc. Dalton Trans.* **1993**, 1387.
[16] M. Bardají, O. Crespo, A. Laguna, A. K. Fischer, *Inorg. Chim. Acta.* **2000**, *304*, 7.
[17] G. A. Bowmaker, J. V. Hanna, C. E. F. Rickard, A. S. Lipton, *Dalton Trans.* **2001**, 20.
[18] H. M. Colquohoun, T. J. Greenhough, M. G. H. Wallbridge, *J. Chem. Soc. Chem. Commun.* **1980**, 192.
[19] D. D. Ellis, P. A. Jellis, F. G. A. Stone, *Organometallics* **1999**, *18*, 4982.
[20] D. D. Ellis, A. Franken, P. A. Jellis, J. A. Kautz, F. G. A. Stone, *Dalton Trans.* **2000**, 2509.
[21] D. D. Ellis, J. C. Jeffery, P. A. Jelliss, J. A. Kautz, F. G. A. Stone, *Inorg. Chem.* **2001**, *40*, 2041.
[22] Y.-W. Park, J. Kim, Y. Do, *Inorg. Chem.* **1994**, *33*, 1.
[23] D. J. Liston, C. A. Reed, C. W. Eigenbrot, W. R. Scheidt, *Inorg. Chem.* **1987**, *26*, 2739.
[24] N. J. Patmore, J. W. Steed, A. S. Weller, *Chem. Commun.* **2000**, 1055.
[25] N. J. Patmore, M. F. Mahon, J. W. Steed, A. S. Weller, *Dalton Trans.* **2001**, 277.
[26] K. Shelly, D. C. Finster, Y. J. Lee, W. R. Scheidt, C. A. Reed, *J. Am. Chem. Soc.* **1985**, *107*, 5955.
[27] S. V. Ivanov, A. J. Lupinetti, S. M. Miller, O. P. Anderson, K. A. Solnstev, S. H. Strauss, *Inorg. Chem.* **1995**, *34*, 6419.
[28] Z. W. Xie, T. Jelinek, R. Bau, C. A. Reed, *J. Am. Chem. Soc.* **1994**, *116*, 1907.
[29] S. V. Ivanov, J. J. Rockwell, S. M. Miller, O. P. Anderson, K. A. Solntsev, S. H. Strauss, *Inorg. Chem.* **1996**, *35*, 7882.
[30] C.-W. Tsang, Q. Yang, E. T.-P. Sze, T. C. W. Mak, D. T. W. Chan, Z. Xie, *Inorg. Chem.* **2000**, *39*, 5851.
[31] Z. Xie, B.-M. Wu, T. C. W. Mak, J. Manning, C. A. Reed, *J. Chem. Soc. Dalton Trans.* **1997**, 1213.
[32] Z. Xie, R. Bau, C. A. Reed, *Angew. Chem.* **1994**, *106*, 2566; *Angew. Chem. Int. Ed. Engl.* **1994**, *33*, 2433.
[33] T. Jelinek, P. Baldwin, W. R. Scheidt, C. A. Reed, *Inorg. Chem.* **1993**, *32*, 1982.
[34] A. Yanagisawa in *Lewis Acids in Organic Synthesis* (Ed.: H. Yamamoto), Wiley-VCH, Weinheim, **2000**.
[35] T. Hayashi, M. Sawamura, Y. Ito, *Tetrahedron* **1999**, *48*, 1992.
[36] A. Togni, S. D. Pastor, *J. Org. Chem.* **1990**, *55*, 1649.
[37] A. Yanagisawa, H. Nakashima, A. Ishiba, H. Yamamoto, *J. Am. Chem. Soc.* **1996**, *118*, 4723.
[38] A. Yanagisawa, Y. Nakatuska, K. Asakawa, H. Kageyama, H. Yamamoto, *Synlett* **2001**, 69.
[39] M. Ohkouchi, D. Masui, M. Yamaguchi, T. Yamagishi, *J. Mol. Catal. A* **2001**, *170*, 1.
[40] A. Yanagisawa, Y. Matsumoto, H. Nakashima, K. Asakawa, H. Yamamoto, *J. Am. Chem. Soc.* **1997**, *119*, 9319.
[41] S. Yoo, S. Saaby, R. G. Hazell, K. A. Jørgensen, *Chem. Eur. J.* **2000**, *6*, 2435.
[42] C. Hague, N. J. Patmore, C. G. Frost, M. F. Mahon, A. S. Weller, *Chem. Commun.* **2001**, 2286.
[43] D. J. Liston, Y. J. Lee, W. R. Scheidt, C. A. Reed, *J. Am. Chem. Soc.* **1989**, *111*, 6643.
[44] A. S. Weller, M. F. Mahon, J. W. Steed, *J. Organomet. Chem.* **2000**, *614–615*, 113.
[45] G. D. Ruggiero, A. S. Weller, I. H. Williams, unpublished results.
[46] H.-P. Wu, C. Janiak, G. Rheinwald, H. Lang, *J. Chem. Soc. Dalton Trans.* **1999**, 183.
[47] C. Kleina, E. Graf, M. W. Hosseini, A. D. Cian, J. Fischer, *Chem. Commun.* **2000**, 239.
[48] S. A. Brew, F. G. A. Stone, *Adv. Organomet. Chem.* **1993**, *35*, 135.
[49] A. S. Weller, T. P. Fehlner, *Organometallics* **1999**, *18*, 447.
[50] H. Brunner, D. Mijolovic, B. Wrackmeyer, B. Nuber, *J. Organomet. Chem.* **1999**, *579*, 298.
[51] G. S. Mhinzi, S. A. Litster, A. D. Redhouse, J. L. Spencer, *J. Chem. Soc. Dalton Trans.* **1991**, 2769.
[52] D. M. V. Seggen, P. K. Hurlburt, O. P. Anderson, S. H. Strauss, *Inorg. Chem.* **1995**, *34*, 3453.
[53] H. Kobayashi, T. Busujima, S. Nagayama, *Chem. Eur. J.* **2000**, *6*, 3491.
[54] S. Ribe, P. Wipf, *Chem. Commun.* **2001**, 299.
[55] K. Mikami, O. Kotera, Y. Motoyama, H. Sakaguchi, *Synlett* **1995**, 975.
[56] A. G. M. Barrett, D. C. Braddock, J. P. Henschke, E. R. Walker, *Perkin Trans. 1* **1999**, 873.
[57] N.-M. Kao, C. P. Grey, K. Pitchumai, P. H. Lakshminarasimhan, V. Ramamurthy, *J. Phys. Chem.* **1998**, *102*, 5627.
[58] T. G. M. H. Dikkhoff, R. G. Goel, E. L. Muetterties, C. W. Alegranti, *Inorg. Chim. Acta* **1980**, *44*, L72.
[59] Note added in proof: After the manuscript was submitted the solid-state structure of compound **4** was determined and it shows a monomeric $\{Ag(PPh_3)_2\}^+$ fragment bound to one $[CB_{11}H_6Br_6]$ cage

by two lower pentagonal belt bromine atoms, consistent with the structure proposed from the low-temperature $^{31}P\{^1H\}$ NMR spectrum.

[60] C. J. d. Reijer, M. Wörle, P. S. Pregosin, *Organometallics* **2000**, *19*, 309.

[61] G. Brauers, F. J. Feher, M. Green, J. K. Hogg, A. G. Orpen, *J. Chem. Soc. Dalton Trans.* **1996**, 3387.

[62] A. Lightfoot, O. Schinder, A. Pfaltz, *Angew. Chem.* **1998**, *110*, 3047; *Angew. Chem. Int. Ed.* **1998**, *37*, 2897.

[63] E. P. Kündig, C. M. Saudan, G. Bernardinelli, *Angew. Chem.* **1999**, *111*, 1298; *Angew. Chem. Int. Ed.* **1999**, *38*, 1220.

[64] D. A. Evans, J. A. Murry, P. v. Matt, R. D. Norcross, S. J. Miller, *Angew. Chem.* **1995**, *107*, 864; *Angew. Chem. Int. Ed. Engl.* **1995**, *34*, 798.

[65] G. M. Sheldrick, SHELX-97. Program for Refinement of Crystal Structures, University of Göttingen, Göttingen (Germany), **1997**.

[66] P. McArdle, *J. Appl. Crystallogr.* **1995**, *28*, 65.

Received: October 15, 2001 [F3613]

  0947-6539/02/0809-2098 $ 20.00+.50/0

COMMUNICATION

Dalton
www.rsc.org/dalton

Well-defined indium(III) *N*-heterocyclic carbene complexes with triflate ligands: Structural models for the $In(OTf)_3$ catalyst †

Jamie H. Cotgreave,[a] David Colclough,[b] Gabriele Kociok-Köhn,[a] Giuseppe Ruggiero,[a] Christopher G. Frost *[a] and Andrew S. Weller *[a]

[a] *Department of Chemistry, University of Bath, Bath, BA2 7AY*

[b] *GlaxoSmithKline, Old Powder Mills, Leigh, Nr Tonbridge, Kent, TN11 9AN.*

E-mail: c.g.frost@bath.ac.uk; a.s.weller@bath.ac.uk

Received 19th March 2004, Accepted 8th April 2004

First published as an Advance Article on the web 16th April 2004

Reaction of 1,3-dimesitylimidazolium chloride [IMesH]Cl with $InMe_3$ results in (IMes)$InMe_2Cl$, which on treatment with one equivalent of TMS-OTf affords (IMes)$InMe_2$(OTf), which can be converted to the bistriflate complex (IMes)In(Me)$(OTf)_2$ on addition of HOTf.

Indium(III) salts have received considerable attention as Lewis acids in recent years.[1-3] Their stability to coordinating functional groups present in organic substrates makes them excellent catalysts for a wide variety of transformations. For transformations mediated by Lewis acids, $In(OTf)_3$ (OTf = triflate) is a particularly efficient catalyst.[1] Surprisingly, given their use in organic synthesis, there is only one structurally characterised example of an indium(III)-triflate complex.[4] Indium(III) hydride and halide complexes of *N*-heterocyclic carbenes have been reported by Jones, formed by addition of 'free' IMes carbene to InH_3 or InX_3 precursors; and are noteworthy for their thermal stability.[5-7] We report here an alternative, and convenient, synthetic route to indium(III) *N*-heterocyclic carbene complexes using an air-stable imidazolium chloride salt precursor and subsequent formation and structural characterisation of an indium bistriflate carbene complex. The corresponding monotriflate complex is also reported. These two complexes represent structural models for the poorly defined catalyst $In(OTf)_3$.

Reaction of [IMesH]Cl with one equivalent of $InMe_3$ affords air stable (but moisture sensitive) (IMes)$InMe_2Cl$, **1**, in essentially quantitative yield (Scheme 1). Compound **1** was fully characterised by NMR spectroscopy,‡ microanalysis and X-ray crystallography§ (Fig. 1).

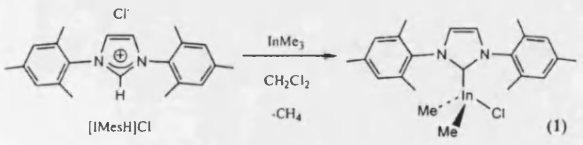

Scheme 1

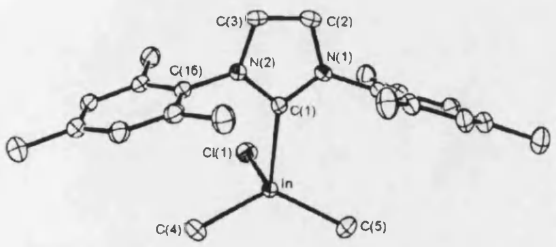

Fig. 1 Solid-state structure of **1**. Hydrogen atoms are omitted for clarity. Selected bond lengths (Å) and angles (°): In–C(1) 2.267(2), In–C(4) 2.166(2), In–C(5) 2.156(2), In–Cl(1) 2.4807(6), C(1)–In–Cl(1) 91.45(5), C(1)–In–C(4) 112.95(9), C(1)–In–C(5) 108.28(7).

† Electronic supplementary information (ESI) available: Full experimental data for the new compounds. See http://www.rsc.org/suppdata/dt/b4/b404179h/

Complex **1** is monomeric in the solid-state with no close [<4.1 Å] intermolecular contacts. The indium centre is four coordinate, but does not adopt the pseudo-tetrahedral arrangement as found in (IMes)$InCl_3$.[5] Instead, the single chloride ligand lies orthogonal to the carbene ligand, [C(1)–In–Cl(1) 91.45(5)°]. This compressed angle suggests the possibility of a weak $C_{carbene} \cdots Cl$ interaction. That the associated $C_{carbene} \cdots Cl$ distance (3.40 Å) also lies just inside the van der Waals radii of carbon and chlorine (3.60 Å) and the carbene ligand is canted towards Cl(1) by 12.8°, gives further weight to the presence of a weak $C_{carbene} \cdots Cl$ interaction. Such interactions have been noted recently in high valent vanadium(V)[8] and titanium(IV)[9] complexes, but not previously for indium. The closely related dihydride, (IMes)InH_2Cl,[5] has been reported by Jones and although no close $C_{carbene} \cdots Cl$ interactions were commented on, it was noted that the C–In–Cl angle was compressed from tetrahedral [101.7°]. Optimisation of **1** at the B3LYP/LAN2DZ level of theory gave good agreement with the observed structure of **1** (Fig. 2†), demonstrating that the solid-state structure is not dominated by crystal packing effects. We have also prepared equivalent complexes with a bromide ligand {starting from [IMesH]Br} or other carbenes [*e.g.* H_2IMes], and these also show similar acute $C_{carbene}$–In–X angles in the solid-state.

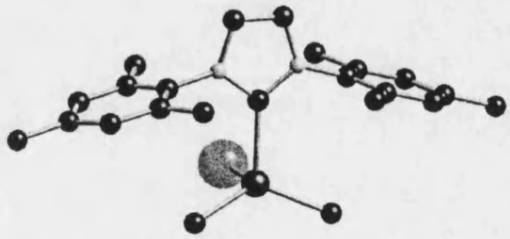

Fig. 2 DFT (B3LYP/LAN2DZ) optimised structure of **1**. Selected calculated distances (Å) and angles (°): $C_{carbene}$–In–Cl 93.82, In–Cl 2.516, In–$C_{carbene}$ 2.306, Cl–$C_{carbene}$ 3.525, $C_{carbene} \cdots Cl$ 3.525.

Complex **1** is a good starting point for the synthesis of indium-triflate complexes. Thus, treatment of **1** with one equivalent of TMS–OTf (trimethylsilyl triflate) results in the clean formation of the monotriflate species (IMes)$InMe_2$(OTf), complex **2** and the concomitant release of Me_3SiCl (by NMR spectroscopy) (Scheme 2). Complex **2** was fully characterised by NMR spectroscopy‡ and single crystal X-ray crystallography (Fig. 3).§

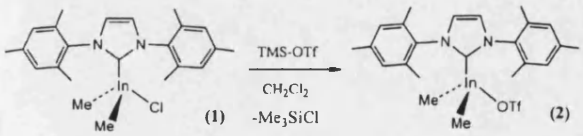

Scheme 2

DOI: 10.1039/b404179h

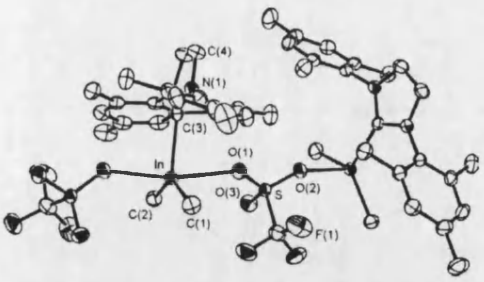

Fig. 3 Solid-state structure of **2**, showing the extended structure in the lattice along the *c* axis. Hydrogen atoms are omitted for clarity. Selected bond lengths (Å) and angles(°): In–C(1) 2.143(2), In–C(2) 2.141(2), In–C(3) 2.264(2), In–O(1) 2.588(2), In–O(2)′ 2.462(2), C(1)–In–C(2) 135.0(1), C(2)–In–C(3) 111.7(1), C(1)–In–C(3) 112.9(1), C(3)–In–O(2)′ 88.59(7), C(3)–In–O(1) 80.07(7), O(2)′–In–O(1) 168.57(6).

In the solid-state complex **2** adopts a trigonal bipyramidal structure with respect to indium, complexed with one IMes, two methyl and two triflate ligands, one of the latter arising from an adjacent molecule in the lattice, overall resulting in a one-dimensional co-ordination polymer. In solution, this extended structure is unlikely to persist, given that **2** shows good solubility in CH_2Cl_2. Possible structures could be monomeric or dimeric (similar to that found for **3** in the solid-state, *vide infra*). The ^{1}H NMR spectrum of **2**‡ shows the expected signals for IMes and methyl ligands while the ^{19}F NMR spectrum shows one triflate environment (δ^{19}F −78.7 ppm).

Addition of a further equivalent of TMS–OTf to **2** does not result in further substitution by triflate to afford a bis triflate complex. Instead this can be accessed by addition of one equivalent of HOTf to **2** (or direct addition of two equivalents of HOTf to (IMes)InMe$_3$ [10]) resulting in the clean formation of (IMes)InMe(OTf)$_2$, **3**, which has been fully characterised by NMR spectroscopy,‡ microanalysis and X-ray crystallography.§

The structure of **3** is presented in Fig. 4, and this demonstrates that the complex forms a centrosymmetric dimer in the solid-state, with the IMes ligands orientated mutually *anti*, and one terminal and one bridging triflate ligand. The indium centre is in an approximate trigonal bipyramidal coordination environment with the methyl, IMes and one OTf ligand occupying the equatorial positions. The In–$C_{carbene}$ distance [In–C(2) 2.183(2) Å] is the shortest of the three compounds reported here, reflecting the formal dicationic nature of the metal centre in **3** (Scheme 3). It is also shorter than equivalent distances in previously reported complexes with indium-IMes motifs.[5,6]

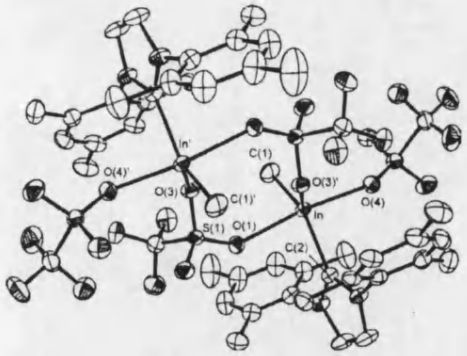

Fig. 4 Solid-state structure of **3**. Hydrogen atoms are omitted for clarity. Selected bond lengths (Å) and angles (°): In–C(1) 2.115(2), In–C(2) 2.183(2), In–O(1) 2.429(1), In–O(3)′ 2.185(1), In–O(4) 2.250(2), C(2)–In–C(1) 138.0(1), C(2)–In–O(1) 84.3(1), C(2)–In–O(3)′ 106.5(1), C(2)–In–O(4) 88.0(1).

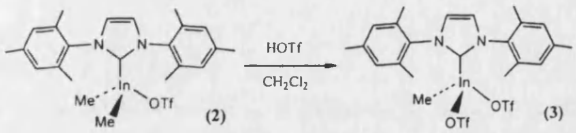

Scheme 3

In solution, only one triflate environment is observed (δ^{19}F −77.8 ppm), suggesting rapid exchange at room temperature.

In conclusion, we have demonstrated that indium(III) *N*-heterocyclic carbene complexes can be conveniently prepared from an air-stable imidazolium chloride salt precursor. Mono- and bis-triflate indium carbene complexes have also been prepared. These represent rare examples of structurally characterised indium-triflates, which are models for the well known, but ill-defined, In(OTf)$_3$ catalyst. Future publications will address the use of these complexes in Lewis-acid catalysis.[10]

We acknowledge the Royal Society (A. S. W.) and the EPSRC (J. H. C.) for funding this work. Mr M. J. Ingleson is thanked for collecting some of the X-ray data.

Notes and references

‡ Spectroscopic data for the new complexes (CD_2Cl_2, 298 K). **1** δ^1H (400MHz): 7.19 (2H, s, olefin), 7.05 (4H, s, aromatic), 2.37 (6H, s, CH_3), 2.12 (12H, s, CH_3), −1.03 (6H, s, In–CH_3). δ^{13}C{^{1}H}(75.5MHz): 177.5 ($C_{carbene}$), 140.5, 136.0, 134.9, 129.8, 124.3, 21.4, 18.0, −8.1 (In–CH_3). **2** δ^1H (400MHz): 7.29 (2H, s, olefin), 7.09 (4H, s, aromatic), 2.39 (6H, s, CH_3), 2.09 (12H, s, CH_3), −0.80 (6H, s, In–CH_3); δ^{13}C{^{1}H} (75.5MHz): 176.2 ($C_{carbene}$), 141.0, 135.7, 134.4, 130.0, 124.9, 120.1 (319Hz, q, CF_3), 21.4, 17.6, −7.1 (In–CH_3); δ^{19}F (376.5MHz): −78.7. **3** δ^1H (400MHz): 7.39 (2H, s, olefin), 7.10 (4H, s, aromatic), 2.39 (6H, s, CH_3), 2.13 (12H, s, CH_3), −0.41 (3H, s, In–CH_3); δ^{13}C{^{1}H} (75.5MHz): δ^{13}C{^{1}H} 168.7 ($C_{carbene}$), 142.1, 135.6, 132.8, 130.4, 126.3, 119.3 (318Hz, q, CF_3), 21.4, 17.7, −5.0 (In–CH_3); δ^{19}F (376.5MHz) δ −77.8.†

§ Crystallographic data. Intensity data were collected at 150 K on a Nonius Kappa CCD, using graphite monochromated MoKα radiation (λ = 0.71073 Å). **1**: $C_{23}H_{30}ClInN_2$, M = 484.76, $P\bar{1}$, a = 8.2890(1), b = 11.0870(1), c = 13.6710(2) Å, α = 68.725(1), β = 86.534(1), γ = 75.138(1)°, V = 1130.84(2) Å^3, Z = 2, μ = 1.424 mm^{-1}, unique reflections = 5183 [R(int) = 0.0450], R_1 = 0.0279, wR_2 = 0.0651 [$I > 2\sigma(I)$]. **2**: $C_{24}H_{30}F_3InN_2O_3S{\cdot}CH_2Cl_2$, M = 683.31, monoclinic, $P2_1/c$, a = 9.06100(10), b = 22.3800(3), c = 14.7900(2) Å, α = 90, β = 100.9230(10), γ = 90°, V = 2944.86(6) Å^3, Z = 4, μ = 1.541 mm^{-1}, unique reflections = 6651 [R(int) = 0.0596], R_1 = 0.0302, wR_2 = 0.0709 [$I > 2\sigma(I)$]. **3**: $C_{24}H_{27}F_6InN_2O_6S_2{\cdot}CH_2Cl_2$, M = 817.34, triclinic, $P\bar{1}$, a = 9.42300(10), b = 12.5040(2), c = 14.5090(2) Å, α = 85.3780(10), β = 83.6180(10), γ = 83.1720(10)°, V = 1682.95(4) Å^3, Z = 2, μ = 1.613 mm^{-1}, unique relections = 9809 [R(int) = 0.0340], R_1 = 0.0277, wR_2 = 0.0638 [$I > 2\sigma(I)$]. CCDC reference numbers 234195 (**1**), 234197 (**2**), 234196 (**3**). See http://www.rsc.org/suppdata/dt/b4/b404179h/ for crystallographic data in CIF format.

1 C. G. Frost and J. Hartley, *Mini-Rev. Org. Chem.*, 2004, **1**, 1.
2 C. G. Frost and K. K. Chauhan, *J. Chem. Soc., Perkin Trans. 1*, 2000, 3015.
3 P. Cintas, *Synlett*, 1995, 1087.
4 R. A. Fischer, H. Sussek, A. Miehr, H. Pritzkow and E. Herdtweck, *J. Organometallic Chem.*, 1997, **548**, 73. An In(I)–OTf complex has recently been reported: C. L. B. Macdonald, A. M. Corrente, C. G. Andrews, A. Taylor and B. D. Ellis, *Chem. Commun.*, 2004, 250.
5 C. D. Abernethy, M. L. Cole and C. Jones, *Organometallics*, 2000, **19**, 4852.
6 R. J. Baker, A. J. Davies, C. Jones and M. Koth, *J. Organomet. Chem.*, 2002, **656**, 203.
7 M. D. Francis, D. E. Hibbs, M. B. Hursthouse, C. Jones and N. A. Smithies, *Dalton Trans.*, 1998, 3249.
8 C. D. Abernethy, G. M. Codd, M. D. Spicer and M. K. Taylor, *J. Am. Chem. Soc.*, 2003, **125**, 1128.
9 P. Shulka, J. A. Johnson, D. Vidovic, A. H. Cowley and C. D. Abernethy, *Chem. Commun.*, 2004, 360.
10 J. H. Cotgreave, C. G. Frost and A. S. Weller, in preparation.